



Michigan Technological University
Create the Future Digital Commons @ Michigan Tech

Dissertations, Master's Theses and Master's
Reports - Open

Dissertations, Master's Theses and Master's
Reports

2011

Characterization of thermal and mechanical properties of polypropylene-based composites for fuel cell bipolar plates and development of educational tools in hydrogen and fuel cell technologies

Daniel López Gaxiola
Michigan Technological University

Follow this and additional works at: <https://digitalcommons.mtu.edu/etds>


 Part of the [Chemical Engineering Commons](#)

Copyright 2011 Daniel López Gaxiola

Recommended Citation

Gaxiola, Daniel López, "Characterization of thermal and mechanical properties of polypropylene-based composites for fuel cell bipolar plates and development of educational tools in hydrogen and fuel cell technologies", Dissertation, Michigan Technological University, 2011.
<https://doi.org/10.37099/mtu.dc.etds/1>

Follow this and additional works at: <https://digitalcommons.mtu.edu/etds>

 Part of the [Chemical Engineering Commons](#)

CHARACTERIZATION OF THERMAL AND MECHANICAL PROPERTIES OF POLYPROPYLENE-BASED
COMPOSITES FOR FUEL CELL BIPOLAR PLATES AND DEVELOPMENT OF EDUCATIONAL TOOLS
IN HYDROGEN AND FUEL CELL TECHNOLOGIES

by:

Daniel López Gaxiola

A DISSERTATION

Submitted in partial fulfillment of the requirements for the degree of

DOCTOR OF PHILOSOPHY

(Chemical Engineering)

MICHIGAN TECHNOLOGICAL UNIVERSITY

2011

© 2011 Daniel López Gaxiola

This dissertation, "Characterization of Thermal and Mechanical Properties of Polypropylene-based Composites for Fuel Cell Bipolar Plates and Development of Educational Tools in Hydrogen and Fuel Cell Technologies," is hereby approved in partial fulfillment of the requirements for the degree of DOCTOR OF PHILOSOPHY IN CHEMICAL ENGINEERING.

Department of Chemical Engineering

Signatures:

Dissertation Co-Advisor _____
Dr. Jason M. Keith

Dissertation Co-Advisor _____
Dr. Julia A. King

Department Chair _____
Dr. Surendra K. Kawatra

Date _____

Table of Contents

List of Figures	x
List of Tables	xiii
Acknowledgements	xv
List of Abbreviations	xvii
Abstract	xviii
Chapter 1: Introduction	1
1.1 Motivation	1
1.2 Energy and Transportation	2
1.3 Hydrogen as an Energy Carrier.	3
1.4 Fuel Cells	4
1.5 Research Objectives	5
Chapter 2: Background.	8
2.1 Introduction	8
2.2 Fuel Cells	8
2.2.1 Fuel Cell Advantages	11
2.2.2 Proton Exchange Membrane Fuel Cells.	12
2.2.2.1 Gas Diffusion Layer	13
2.2.2.2 Electrolyte Membrane	14
2.2.2.3 Catalyst layers	15
2.2.2.4 Bipolar Plates	15
2.2.2.4.1 Composite Bipolar Plates	16
2.3 Thermal Conductivity Background	17
2.4 Mechanical Properties Background	20
2.4.1 Tensile Modulus	20
2.4.2 Flexural Modulus.	21
2.4.3 Factors Affecting Tensile Modulus	22

2.5 Active Learning	23
2.5.1 Problem–Based Learning	24
Chapter 3: Materials and Fabrication Methods	26
3.1 Introduction	26
3.2 Matrix Material	26
3.2.1 Semi-Crystalline Homopolymer Polypropylene Resin H7012-35RN	26
3.3 Filler Materials	27
3.3.1 Carbon Black	27
3.3.2 Synthetic Graphite	29
3.3.3 Hyperion Fibril Carbon Nanotubes	31
3.4 Formulation Naming Convention	32
3.5 Fabrication Methods	34
3.5.1 Extrusion	34
3.5.2 Drying	39
3.5.3 Injection Molding	39
3.5.4 Compression Molding	42
Chapter 4: Test Methods	45
4.1 Synthetic Graphite Length, Aspect Ratio, and Orientation Test Method	45
4.2 Field Emission Scanning Electron Microscope (FESEM) Test Method	46
4.3 Thermal Conductivity: Guarded Heat Flow Meter Test Method	46
4.4 Thermal Conductivity: Nanoflash Method	47
4.4.1 NETZSCH LFA 447 Nanoflash™ Apparatus	47
4.4.2 Heat Capacity Theory	53
4.4.3 Thermal Diffusivity Theory	54
4.5 Mechanical Properties Testing	58
4.5.1 Flexural Test Method	58
4.5.2 Tensile Test Method	60
4.5.3 Nanoscratch testing	62

Chapter 5: Experimental Results for Thermal Conductivity Tests Using the Nanoflash Method	68
5.1 Introduction	68
5.2 Synthetic Graphite Length, Aspect Ratio and Orientation Results	69
5.3 Field Emission Scanning Electron Microscope (FESEM) Results	69
5.4 Nanoflash Through-Plane Thermal Conductivity Results	70
5.4.1 Through-Plane Thermal Conductivity Results for Single-Filler Formulations.	70
5.4.2 Factorial Design Analysis	74
5.5 In-Plane Thermal Conductivity Results	77
5.6 Conclusions.	80
Chapter 6: Thermal Conductivity Modeling	81
6.1 Introduction	81
6.2 Thermal Conductivity Modeling Background	81
6.2.1 Through-Plane Thermal Conductivity Modeling	81
6.2.2 In-Plane Thermal Conductivity Modeling	84
6.2.3 Multiple Filler Thermal Conductivity Modeling	85
6.3 Through-Plane Thermal Conductivity Modeling Results for Single-Filler Formulations	86
6.3.1 Guarded Heat Flow Meter Method	86
6.3.2 Flash Method	90
6.4 In-Plane Thermal Conductivity Modeling Results for Single-Filler Formulations	92
6.5 Modeling Results for Multiple-Filler Formulations	95
6.6 Conclusions	97
Chapter 7: Experimental Results for Mechanical Properties Tests	98
7.1 Introduction.	98
7.2 Synthetic Graphite Length, Aspect Ratio and Orientation Results	98
7.3 Flexural Test Results	98
7.3.1 Flexural Test Results for Single-Filler Formulations	99

7.3.2 Flexural Test Results for Multiple-Filler Formulations	102
7.3.3 Comparison of Flexural Results for Polypropylene and Liquid Crystal Polymer Composites.	103
7.4 Tensile Test Results	104
7.4.1 Tensile Test Results for Single-Filler Formulations	104
7.4.2 Tensile Test Results for Multiple-Filler Formulations	108
7.4.3 Comparison of Tensile Results for Polypropylene and Liquid Crystal Polymer Composites	109
7.5 Comparison of Nanoscratch Test Results for Polypropylene and Liquid Crystal Polymer Composites	110
7.6 Conclusions	112
Chapter 8: Tensile Modulus Modeling	113
8.1 Introduction	113
8.2 Tensile Modulus Modeling Background	113
8.2.1 Rule of Mixtures and Inverse Rule of Mixtures	113
8.2.2 Halpin–Tsai Models	114
8.2.3 Nielsen’s Model	115
8.3 Tensile Modulus Modeling Results	117
8.3.1 Basic and Halpin–Tsai Models Results	118
8.3.2 Nielsen Model Results	119
8.4 Conclusions	121
Chapter 9: Development of Educational Tools in Hydrogen and Fuel Cell Technologies	122
9.1 Introduction	122
9.2 Educational Approaches	123
9.2.1 Traditional Teaching Methodologies	123
9.2.2 Problem–based Learning	124
9.2.3 Active Learning vs. Passive Learning	125
9.3 Learning Styles	127
9.4 Hydrogen and Fuel Cell Education Curriculum	129

9.4.1 Educational Goals	130
9.4.2 Description of Hydrogen and Fuel Cell Curriculum at Michigan Technological University	131
9.5 Preliminary Module Assessment	145
9.6 Conclusions	151
Chapter 10: Summary and Future Work Recommendations	152
10.1 Introduction	152
10.2 Thermal Conductivity Testing	153
10.3 Thermal Conductivity Modeling	154
10.4 Testing of Mechanical Properties	155
10.5 Tensile Modulus Modeling	156
10.6 Development of Hydrogen and Fuel Cell Technology Curriculum	156
10.7 Future Work Recommendations	157
References	159
Appendix A: Through-plane thermal conductivity results using the Flash Method	170
Appendix B: In-plane thermal conductivity results using the Flash Method	192
Appendix C: Flexural strength test results	211
Appendix D: Tensile strength test results	275
Appendix E: List of Problem Modules Developed as Supplementary Material for the Textbook “Elementary Principles of Chemical Processes”, Third Edition, by R. M. Felder and R. W. Rousseau	308
Appendix F: List of Problem Modules Developed as Supplementary Material for the Textbook “Transport Processes and Separation Process Principles (Includes Unit Operations)”, Fourth Edition, by C. J. Geankoplis	312
Appendix G: Permission Letters	316

List of Figures

Figure 2.1 Fuel Cell Experiment performed by William Grove in 1839	9
Figure 2.2 Typical Polarization and Power Curves of a Proton–Exchange Membrane Fuel Cell	10
Figure 2.3 Schematic of a Proton Exchange Membrane Fuel Cell	13
Figure 2.4 Schematic representation of the lattice thermal conductivity in a two–dimensional array. a) Two–dimensional array of atoms b) Impurity atom (point defect). c) Displaced atom (lattice vibration)	20
Figure 2.5 Determination of Elastic Modulus using Stress-Strain Curve	21
Figure 3.1 Chemical Structure for Polypropylene	26
Figure 3.2 Ketjenblack EC-600 JD Primary Aggregate	28
Figure 3.3 Photomicrograph of Thermocarb TC-300 Synthetic Graphite (Courtesy of Asbury Carbons)	30
Figure 3.4 American Leistritz Extruder Corporation Model ZSE 27	36
Figure 3.5 Schenck AccuRate Flexwall Feeder	37
Figure 3.6 Schenck AccuRate Conisteel Feeder	37
Figure 3.7 Water Bath	38
Figure 3.8 ConAir pelletizer Model 20402HP-14A	38
Figure 3.9 Bry Air Drying Oven System	39
Figure 3.10 Niigata Injection Molding Machine Model NE85UA ₄	40
Figure 3.11 Four-Cavity Mold Used in Injection Molding	41
Figure 3.12 Wabash Model V75H-18-CLX Compression Molding Press	44
Figure 4.1 Holometrix Model TCA-300 Thermal Conductivity	46
Figure 4.2 Schematic of Through-Plane Thermal Conductivity Test Method	47
Figure 4.3 NETZSCH LFA 447 Nanoflash™ Apparatus	48
Figure 4.4 NETZSCH LFA 447 Nanoflash™ system (Courtesy of NETZSCH)	48
Figure 4.5 Through-plane measurement for Nanoflash instrument	50
Figure 4.6 Nanoflash sample holder	51
Figure 4.7 Preparation of test specimens for in-plane thermal conductivity	52

Figure 4.8 Temperature response of rear surface under adiabatic conditions	57
Figure 4.9 Temperature response under nonadiabatic conditions for varying values of the heat loss parameter L	57
Figure 4.10 Three-Point Bend Test Method for Flexural Properties Measurement	58
Figure 4.11 Instru-Met Sintech Screw Driven Mechanical Testing Machine set for 3-Point Bend Flexural Properties Testing	59
Figure 4.12 Typical Flexural Stress–Strain Curve for a Polypropylene Sample	59
Figure 4.13 Instru-Met Sintech Screw Driven Mechanical Testing Machine set for Tensile Properties Testing	61
Figure 4.14 Typical Tensile Stress–Strain Curve for a Polypropylene Sample	61
Figure 4.15 (a) Portion of Flexural Bar from where Nanoscratch Specimens were cut. (b) Sample Arrangement for Nanoscratch Testing	63
Figure 4.16 Polishing Apparatus for Nanoscratch Sample Preparation	63
Figure 4.17 10-Sample Holder Used in the Polishing Apparatus	64
Figure 4.18 MTS Nano Indenter XP Used for Nanoscratch Testing	65
Figure 4.19 Scratch Direction Used in the Tests with the Berkovich Indenter	65
Figure 4.20 Olympus BX60 Reflected Light Microscope	67
Figure 5.1 Field Emission Scanning Electron Microscope Photomicrograph of CB/SG/CNT in Polypropylene composite	70
Figure 5.2 Single Filler Nanoflash Through-Plane Thermal Conductivity Results for CB/PP and CNT/PP composites	71
Figure 5.3 Single Filler Nanoflash Through-Plane Thermal Conductivity Results for SG/PP composites	72
Figure 5.4 Single Filler Nanoflash In-Plane Thermal Conductivity Results for CB/PP and CNT/PP composites	78
Figure 5.5 Single Filler Nanoflash In-Plane Thermal Conductivity Results for SG/PP composites	79
Figure 6.1 Experimental and theoretical through-plane thermal conductivities for CB/PP composites for the Guarded Heat Flow Meter	88
Figure 6.2 Experimental and theoretical through-plane thermal conductivities for CNT/PP composites for the Guarded Heat Flow Meter Method	89
Figure 6.3 Experimental and theoretical through-plane thermal conductivities for SG/PP composites for the Guarded Heat Flow Meter.	89
Figure 6.4 Experimental and theoretical through-plane thermal conductivities for CB/PP	

composites for the Flash Method	91
Figure 6.5 Experimental and theoretical through-plane thermal conductivities for CNT/PP composites for the Flash Method	91
Figure 6.6 Experimental and theoretical through-plane thermal conductivities for SG/PP composites for the Flash Method	92
Figure 6.7 Experimental and theoretical through-plane thermal conductivities for CB/PP composites for the Flash Method	93
Figure 6.8 Experimental and theoretical through-plane thermal conductivities for CNT/PP composites for the Flash Method	94
Figure 6.9 Experimental and theoretical through-plane thermal conductivities for SG/PP composites for the Flash Method	94
Figure 7.1 Single-Filler Flexural Modulus Results for CB/PP, SG/PP, CNT/PP, CB/Vectra and SG/Vectra Composites	100
Figure 7.2 Single-Filler Ultimate Flexural Strength Results for CB/PP, SG/PP, CNT/PP, CB/Vectra and SG/Vectra Composites	101
Figure 7.3 Strain at Ultimate Flexural Strength Results for Single-Filler Polypropylene-Based Formulations	102
Figure 7.4 Typical Tensile Stress–Strain Plots for Pure Polypropylene (Initial Portion), Polypropylene with 6 wt.% Carbon Black, Polypropylene with 20 wt.% Synthetic Graphite, and Polypropylene with 6 wt.% Carbon Nanotubes	105
Figure 7.5 Single-Filler Tensile Modulus Results for CB/PP, SG/PP, CNT/PP, CB/Vectra and SG/Vectra Composites	106
Figure 7.6 Single-Filler Ultimate Tensile Strength Results for CB/PP, SG/PP, CNT/PP, CB/Vectra and SG/Vectra Composites	107
Figure 7.7 Strain at Ultimate Tensile Strength Results for Single-Filler Polypropylene-Based Formulations	108
Figure 7.8 Displacement Normal to the Surface Under a Constant Force of 40 mN for Composites Containing 20 wt.% of Synthetic Graphite Particles in Polypropylene . .	111
Figure 8.1 Tensile modulus modeling for carbon black in polypropylene. From lowest to highest, the models are Inverse Rule of Mixtures, Halpin-Tsai Oriented Fiber, 2D Halpin-Tsai, 3D Halpin-Tsai, Nielsen, and Modified Nielsen	119
Figure 8.2 Tensile modulus modeling for synthetic graphite in polypropylene. From lowest to highest, the models at 55 vol.% are Inverse Rule of Mixtures, 3D Halpin-Tsai, 2D Halpin-Tsai, Halpin-Tsai Oriented Fiber, Modified Nielsen, and Nielsen	120
Figure 8.3 Tensile modulus modeling for carbon nanotubes in polypropylene. From lowest to highest, the models at are Inverse Rule of Mixtures, Nielsen, Modified Nielsen, 3D Halpin-Tsai, 2D Halpin-Tsai, and Halpin-Tsai Oriented Fiber	120

List of Tables

Table 1.1 Transportation Sector Energy Consumption in U.S. (Quadrillion BTU) (5)	3
Table 1.2 Comparison of Total U.S. and Transportation Sector CO ₂ Emissions (Million Metric Tons) (5)	3
Table 1.3 Technical Targets for Bipolar Plates for 2015 (9)	6
Table 2.1 Advantages and applications of different types of fuel cell (8)	11
Table 2.2 Specific modulus and strength of common materials (47)	23
Table 3.1 Properties of Dow H7012-35RN Polypropylene Resin/Molded Parts (71)	27
Table 3.2 Properties of Akzo Nobel Ketjenblack EC-600 JD (78)	29
Table 3.3 Properties of Thermocarb TC-300 Synthetic Graphite (80,81)	30
Table 3.4 Sieve analysis of Thermocarb TC-300 Synthetic Graphite (80,81)	31
Table 3.5 Properties of Hyperion FIBRIL™ Carbon Nanotubes (85)	32
Table 3.6 Single Filler Loading Levels in Polypropylene	35
Table 3.7 Multiple Filler Loading Levels in Factorial Design Formulation	35
Table 4.1 Properties for reference materials for Thermal Conductivity measurements . .	55
Table 4.2 Polishing procedure for preparing Nanoscratch test specimens	64
Table 5.1. Single Filler Loading Levels in Polypropylene and Nanoflash Thermal Conductivity Results	73
Table 5.2 Filler Loadings in Factorial Design Formulations	75
Table 5.3 Filler Loadings in Factorial Design Formulations and Thermal Conductivity Results	75
Table 5.4 Factorial Design Analysis for Through-plane Thermal Conductivity (W/m·K) . .	77
Table 6.1 Typical A values for different filler shapes and orientation (128)	83
Table 6.2 Maximum Packing Fraction ϕ_m of common filler types (128)	84
Table 6.3 Experimental and Modeling Results of Through–Plane Thermal Conductivity using the Flash Method	96
Table 7.1 Crest Factors for Penetration in Polymer Composites (31)	112
Table 9.1 Components of Hydrogen Technology Minor (16 Credits Total)	135
Table 9.2 Required and Elective Courses for earning Graduate Certificate in Hybrid	

Electric Vehicle Engineering	137
Table 9.3 Problem modules developed as part of the Hydrogen and Fuel Cells education project for different engineering programs (187)	138

Acknowledgements

First of all I thank God and the Lady of Guadalupe for letting me have this opportunity to get a better professional training and for giving me strength to overcome all obstacles and help me learn from them.

I would like to express my sincere gratitude to my advisors Dr. Jason M. Keith and Dr. Julia A. King. Thanks to them and their knowledge I could enjoy and complete this educational experience. I also thank my committee members: Dr. Tony Rogers and Dr. Gretchen Hein for their contributions to the development of my research project. A special thank goes to Dr. Ibrahim Miskioglu for his help with the experimental and modeling work developed in this project.

I would like to acknowledge the different companies that provided support for this research project and the Department of Energy for funding this project through the Award numbers DE-FG36-08GO18108 and DE-FG36-08GO88104.

I would especially like to thank my family and friends that are in Mexico: my mom Loly, for her unconditional support every day, my dad Arnoldo, my siblings Alejandra and Mario Alberto and especially my youngest brother Arnoldo for his jokes and comic relief, and my friends Lucas Rosas and Dalia Cejudo for great moments during my life and visits to Mexico.

I want to thank fellow students who helped me in conducting experiments and the development of my research, including Mike Via, Beth Johnson and Na Mo.

A special thank goes to the members of NOSOTROS Latin–American Student Organization Rosa Flores, Julio Rivera, Ezequiel Medici, Anieri Morales, Alessia Uboni and Rocío Jimenez who helped me feel close to my country Mexico and my culture through various events and trips during my stay at Michigan Tech.

Finally, I would like to thank my friends for their support throughout my years at Tech: Cho Hui Lim, Di Huang and Felix Adom for sharing great times and personal experiences which helped me to deal with stressful situations during this life experience.

Table of Abbreviations

AFC	Alkaline Fuel Cell
CB	Carbon Black
CHP	Combined Heat and Power
CNT	Carbon Nanotubes
DMFC	Direct Methanol Fuel Cell
DOE	Department of Energy
EERE	Energy Efficiency and Renewable Energy
FESEM	Field Emission Scanning Electron Microscope
GDL	Gas Diffusion Layer
LCP	Liquid Crystal Polymer
MCFC	Molten Carbonate Fuel Cell
MEA	Membrane Electrode Assembly
PAFC	Phosphoric Acid Fuel Cell
PBL	Problem-Based Learning
PEMFC	Proton Exchange Membrane Fuel Cell
PP	Polypropylene
SG	Synthetic Graphite
SOFC	Solid Oxide Fuel Cell

Abstract

In this project we developed conductive thermoplastic resins by adding varying amounts of three different carbon fillers: carbon black (CB), synthetic graphite (SG) and multi-walled carbon nanotubes (CNT) to a polypropylene matrix for application as fuel cell bipolar plates. This component of fuel cells provides mechanical support to the stack, circulates the gases that participate in the electrochemical reaction within the fuel cell and allows for removal of the excess heat from the system.

The materials fabricated in this work were tested to determine their mechanical and thermal properties. These materials were produced by adding varying amounts of single carbon fillers to a polypropylene matrix (2.5 to 15 wt.% Ketjenblack EC-600 JD carbon black, 10 to 80 wt.% Asbury Carbons' Thermocarb TC-300 synthetic graphite, and 2.5 to 15 wt.% of Hyperion Catalysis International's FIBRILTM multi-walled carbon nanotubes) In addition, composite materials containing combinations of these three fillers were produced.

The thermal conductivity results showed an increase in both through-plane and in-plane thermal conductivities, with the largest increase observed for synthetic graphite. The Department of Energy (DOE) had previously set a thermal conductivity goal of 20 W/m·K, which was surpassed by formulations containing 75 wt.% and 80 wt.% SG, yielding in-plane thermal conductivity values of 24.4 W/m·K and 33.6 W/m·K, respectively. In addition, composites containing 2.5 wt.% CB, 65 wt.% SG, and 6 wt.% CNT in PP had an in-plane thermal conductivity of 37 W/m·K.

Flexural and tensile tests were conducted. All composite formulations exceeded the flexural strength target of 25 MPa set by DOE. The tensile and flexural modulus of the composites increased with higher concentration of carbon fillers. Carbon black and synthetic graphite caused a decrease in the tensile and flexural strengths of the composites. However, carbon nanotubes increased the composite tensile and flexural strengths.

Mathematical models were applied to estimate through-plane and in-plane thermal conductivities of single and multiple filler formulations, and tensile modulus of single-filler formulations. For thermal conductivity, Nielsen's model yielded accurate thermal conductivity values when compared to experimental results obtained through the Flash method. For prediction of tensile modulus Nielsen's model yielded the smallest error between the predicted and experimental values.

The second part of this project consisted of the development of a curriculum in Fuel Cell and Hydrogen Technologies to address different educational barriers identified by the Department of Energy. By the creation of new courses and enterprise programs in the areas of fuel cells and the use of hydrogen as an energy carrier, we introduced engineering students to the new technologies, policies and challenges present with this alternative energy. Feedback provided by students participating in these courses and enterprise programs indicate positive acceptance of the different educational tools. Results obtained from a survey applied to students after participating in these courses showed an increase in the knowledge and awareness of energy fundamentals, which indicates the modules developed in this project are effective in introducing students to alternative energy sources.

Chapter 1: Introduction

Today in the United States and much of the world, transportation has great influence on socio-economic aspects such as health, education, employment and culture, as well as in human relations. This has caused transportation to become an absolute necessity.

Because of this necessity, the increase in the use of means of transportation in the United States has led to a dependence on imported oil. Therefore, the government has driven certain environmental regulations and has promoted investment in research and development of new technologies and energy sources for the transportation sector. The aim of these new technologies is to reduce oil dependence and the amount of harmful gases emitted to the environment by vehicles. One of these technologies is the Proton Exchange Membrane Fuel Cell, which as mentioned in subsequent chapters of this dissertation, and represents an alternative that will contribute to a reduction in consumption of fossil fuels and environmental damage.

1.1 Motivation

During the 20th century, the development of new energy sources and improving existing technologies were the most important challenges for researchers in the fields of chemical engineering to achieve energy production efficiently. In the future, based on global energy demand, availability of renewable energy sources such as hydrogen, and other demographic and environmental factors such as climate change are essential to the development of economically viable technologies.

The world population is expected to reach approximately 10 billion by year 2050. According to the International Energy Outlook, the total world consumption of marketed energy will increase 49% from 2007 to 2035, reaching more than twice the current levels by 2050

(1,2). However, the energy consumption per unit of Gross Domestic Product (GDP) will decrease due to the expected increase in energy efficiency (1). Even if new energy technologies will be developed, fossil fuels will continue to be economical and widely available through at least the first half of the 21st century. A rise in the daily oil consumption will increase from 75 million barrels to 114 million barrels by year 2020 will not represent a problem in the availability of oil, since in the past 20 years, the existence of crude oil reserves of about 1 trillion barrels has been proven (1).

1.2 Energy and Transportation

Different energy alternatives dependent on the world energy demands and the availability of renewable energy sources such as hydrogen will define the future challenges in the fields of energy and transportation. The energy demand for all sectors such as industrial, commercial, home energy use and transportation, is expected to continue growing through 2050 with an expected growth in energy demand estimated to increase from the equivalent to 200 million barrels of oil per day (including energy from coal, natural gas and other sources) to over 300 million barrels per day by year 2020 (1). In Table 1.1 we can see the increase in energy consumption for the last 20 years.

It is expected that the demand for oil will increase by approximately 50% by year 2025. Currently, the amount of imported oil represents more than 55% of the demand of energy in the United States and is estimated to raise by more than 68% by 2025 (3). One of the energy-efficient alternatives in the near-term is the use of hybrid electric vehicles (4).

Over the next 20 years, a significant growth in renewable energy technologies is expected. It is estimated that in the following 20 years, wind and solar energies will account for the energy equivalent to only 1 million barrels of oil per day out of 300 million (1). However, after year 2020,

Table 1.1
Transportation Sector Energy Consumption in U.S. (Quadrillion BTU) (5)

Year	Natural Gas	Petroleum	Biomass	Total
1990	0.680	21.6	0.060	22.4
1995	0.724	23.0	0.113	23.8
2000	0.672	25.7	0.135	26.5
2005	0.624	27.3	0.339	27.9
2009	0.687	25.3	0.922	27.0

depending on the advances in science and technology, such as the development of cost-effective catalysts, new materials, etc., a more rapid growth in renewable energies may be achieved.

1.3 Hydrogen as an Energy Carrier

Hydrogen is a clean energy carrier which can be produced from natural sources such as solar, wind and geothermal energies, as well as nuclear energy. There are methods for producing hydrogen from coal, natural gas and biomass combined with carbon dioxide sequestration. The use of hydrogen will contribute to reducing the emissions of greenhouse gases and the dependence on imported oil (4). Table 1.2 summarizes the CO₂ emissions for the last 20 years and the percentage correspondent to the transportation sector.

In year 2003, an amount of \$1.2 billion was announced by President Bush through the Hydrogen Fuel Initiative to promote research in hydrogen technology for the following 5 years and overcome challenges hydrogen infrastructure and bring fuel cell vehicles to the market (4).

Table 1.2
Comparison of Total U.S. and Transportation Sector CO₂ Emissions (Million Metric Tons) (5)

Year	Transportation	Total	Percentage
1990	1587	5021	31.6
1995	1682	5303	31.7
2000	1873	5851	32.0
2005	1989	5974	33.3
2008	1851	5405	34.2

The goal set by the Hydrogen Program is to reach a decision on the marketing of vehicles powered by fuel cells and the development of a hydrogen infrastructure by 2015 (4). This is to be achieved through an intensive research program to overcome the technical and economical challenges.

The Department of Energy (DOE) will incorporate different Research and Development activities to a Hydrogen Program. This will be done as indicated in the Hydrogen Posture Plan. Hydrogen production technologies from different sources such as hydrocarbons and renewable resources will be included in this program. In addition, the development of hydrogen infrastructure and the use of fuel cells for stationary and transport applications will be integrated into the Hydrogen Program. Through this program, the DOE will improve research, development and demonstration activities, hence contributing to the achievement of technical milestones towards a hydrogen economy (3).

1.4 Fuel Cells

Proton exchange membrane fuel cells have become important due to their operating conditions such as low temperature and pressure, and simplicity, viability and short start-up times (6).

The first application of fuel cells in space exploration was in the Gemini program in 1964 where a 1-kW fuel cell powered unit was used (7). The potential market for fuel cells is in power generation for residential applications, onsite and distributed electric power generation and transportation.

A proton exchange membrane fuel cell produces electrical power and water and heat as by-products that can be used for combined heat and power applications. Currently, the most important disadvantage of fuel cells is the cost. However, they have the advantages of being more efficient than internal combustion engines, silent and when hydrogen is used as fuel, they

contribute to a reduction in vehicle emissions (8). The topic on proton exchange membrane fuel cells will be developed further in Chapter 2 of this dissertation.

1.5 Research Objectives

This dissertation has the objective of developing and testing of thermal and mechanical properties of carbon–polypropylene composites for fuel cell bipolar plate applications. Since hydrogen and fuel cell technologies represent an alternative to fossil fuels, it is paramount to educate engineering students in topics related to these technologies. Thus, another objective of this project is the development and implementation of educational tools to disseminate information about hydrogen for general educational purposes and to facilitate the process of permitting hydrogen installations.

The experimental goal of this Ph.D. research project is the development, characterization and model of polypropylene-based resins containing single and multiple carbon fillers that modify the properties of the polymer resin to satisfy the requirements set by the DOE for bipolar plates, summarized in Table 1.3 (9). The three carbon fillers used in this project are carbon black, synthetic graphite and carbon nanotubes, which were extruded with a semi-crystalline polypropylene resin. The thermal conductivity and tensile modulus data obtained for the composites was analyzed using different mathematical models to estimate these properties for each composite formulation. The three carbon fillers used in this project were also combined to further improve the properties of the composite materials for use as fuel cell bipolar plates.

Since fuel cell vehicles and infrastructure are still under development, the engineering education portion of this dissertation will focus on the development of educational tools that will help incorporate fuel cell technology in the transportation sector. Some of these educational tools include the implementation of problem modules in the chemical engineering curricula about fuel

Table 1.3
Technical Targets for Bipolar Plates for 2015 (9)

Characteristic	Targets	
	2005	2015
Cost	\$10/kW	\$3/kW
Weight	0.36 kg/kW	< 0.4 kg/kW
H ₂ Permeation Flux	$< 2 \times 10^{-6} \frac{\text{cm}^3}{\text{cm}^2 \cdot \text{s}}$	$< 2 \times 10^{-6} \frac{\text{cm}^3}{\text{cm}^2 \cdot \text{s}}$
Corrosion	$< 1 \mu\text{A}/\text{cm}^2$	$< 1 \mu\text{A}/\text{cm}^2$
Electrical Conductivity	$> 600 \text{ S}/\text{cm}$	$> 100 \text{ S}/\text{cm}$
Resistivity	$< 0.02 \Omega \cdot \text{cm}$	$0.01 \Omega \cdot \text{cm}$
Thermal Conductivity	20 W/m·K	N/A
Flexural Strength	$> 34 \text{ MPa}$	$> 25 \text{ MPa}$
Flexibility	1.5% to 3.5% (deflection at mid span)	3% to 5% (deflection at mid span)

cells and processes for hydrogen production, thus providing students with updated information about this renewable source of energy.

The following is an outline of the chapters to be developed in this dissertation:

Chapter 2–Background: A description of the performance of fuel cells and bipolar plates in fuel cells will be given in this chapter.

Chapter 3–Materials and Fabrication Methods: In this chapter, information will be provided about the polypropylene matrix and carbon fillers used for fabrication of fuel cell bipolar plates.

Chapter 4–Test Methods: This chapter explains the experimental methods used for determining the thermal and mechanical properties of conductive resins for use as bipolar plates.

Chapter 5–Experimental Results for Thermal Conductivity Tests Using the Nanoflash Method: The experimental values obtained using the flash method for through-plane and in-plane thermal conductivities are summarized in this chapter, for formulations with single and multiple carbon fillers in polypropylene.

Chapter 6–Thermal Conductivity Modeling: The background for the mathematical models used to calculate the thermal conductivity of different composite formulations is given in this section.

Chapter 7–Experimental Results for Mechanical Properties Tests: This chapter includes the experimental results obtained from the flexural and tensile tests performed on different composite formulations.

Chapter 8–Tensile Modulus Modeling: This chapter describes the mathematical models used for estimating the tensile modulus of composites containing single carbon fillers in polypropylene.

Chapter 9–Educational Tools for Hydrogen and Fuel Cells Technology: This chapter provides background information about teaching methods and development of educational tools to introduce engineering students to topics about Hydrogen as an Energy Carrier and Fuel Cells.

Chapter 10–Conclusions: The outcomes of the experimental and education sections of this dissertation are summarized in this chapter.

Chapter 2: Background

2.1 Introduction

The increased energy consumption and power requirements have marked the progress in modern human civilizations. Most of the energy requirements since the industrial revolution have been provided by use of fossil fuels. Engines using this type of fuels are responsible for causing local air pollution, thus affecting the health of millions of people. Because of the increase in carbon dioxide concentration in the atmosphere, the global warming due to the emission of greenhouse gases has intensified.

These environmental problems can be addressed by obtaining energy from renewable sources. Different natural resources such as the sunlight, water and wind currents, and hot springs can be converted into useful energy. These energy sources have the advantage of being abundant and there are no operating costs for using them. One of the alternatives that has been investigated is the development of fuel cells. This type of technology has been under development for combined heat and power fuel cells for stationary applications and for potential production of zero-emission vehicles (10).

2.2 Fuel Cells

William Grove performed the first experiment with fuel cells in 1839. Figure 2.1a is showing the experimental setup used by William Grove, used for electrolyzing water into oxygen and hydrogen by flow of an electric current through the wires in an aqueous sulfuric acid solution. After this experiment, he replaced the power supply with an ammeter and noticed that a recombination of hydrogen and oxygen produced a small current through the wires, as shown in Figure 2.1b.

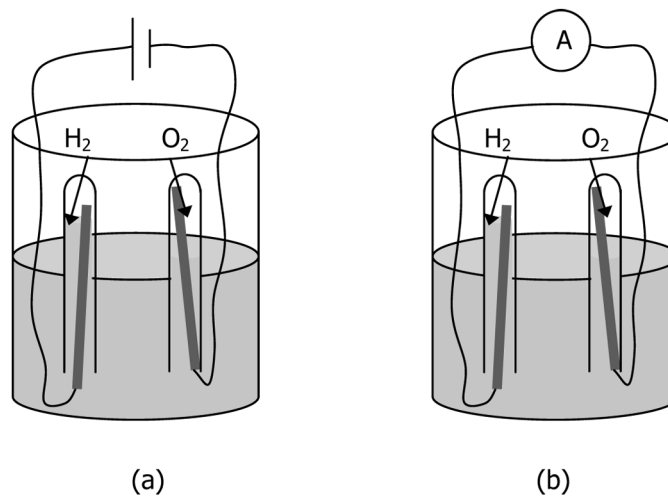


Figure 2.1 Fuel Cell Experiment performed by William Grove in 1839

The fuel cells were invented in the 19th century and the technology was developed in the 20th century. The research and development in the field of fuel cells will lead to power generation in a clean and efficient way for the 21st century. The evolution in fuel cells since the experiment from William Grove has been described with detail in the literature (11-15).

A single fuel cell is the main unit in a fuel cell power source. The performance of a fuel cell system is determined by the behavior of the cell potential as a function of the current density, also known as the polarization curve, shown in Figure 2.2 for a typical fuel cell system. In a fuel cell stack, the variation in the performance of the system will be affected by the following factors (16):

- Scale-up
- Temperature variations between cells.
- Difference in the flow patterns of the reactant gases between cells.
- Water management, i.e. flooding, formation of water droplets in the gas diffusion layers.
- Uneven distribution of the reactant gases in the bipolar plate channels due to an inadequate water management.

The last two of this list of problems with fuel cell systems are more commonly observed in proton exchange membrane fuel cells (PEMFCs), direct methanol fuel cells (DMFCs) and alkaline fuel cells (AFCs). However, the advances in fuel cells engineering and technology have overcome many of these problems, thus achieving almost identical behavior of the polarization curve of a fuel cell stack to that of a single cell (16).

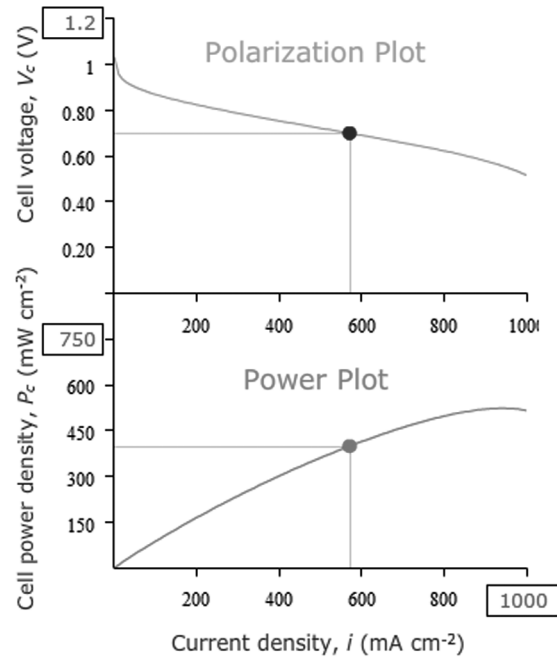


Figure 2.2 Typical Polarization and Power Curves of a Proton–Exchange Membrane Fuel Cell

Fuel Cells can be classified by their operation temperature in low and high temperature fuel cells, the type of ion traveling through the Membrane Electrode Assembly (MEA), etc. The most common system for classifying fuel cells is based on the type of electrolyte. The six major fuel cell technologies present currently are: alkaline (AFC), phosphoric acid (PAFC), polymer electrolyte membrane (PEMFC), molten carbonate (MCFC), solid oxide (SOFC) and direct methanol fuel cells (DMFC) (10). The operating temperatures and power ranges of these types of fuel cells are shown in Table 2.1 (8). Additional information about these types of fuel cells and their operation fundamentals can be found in the literature (6-8,17).

Table 2.1
Advantages and applications of different types of fuel cell (8)

Fuel Cell Type	Power Output Ranges (W)	Applications	Advantages
DMFC	10^0 – 10^2	• Portable electronics equipment.	• Higher energy density than batteries. • Faster recharging
AFC	10^3 – 10^5	• Cars, boats and domestic CHP.	• Potential for zero emissions. • Higher efficiency.
PEMFC	10^0 – 10^5		
PAFC	10^4 – 10^6		
SOFC	10^3 – 10^7	• Distributed power generation, CHP and buses.	• Higher efficiency. • Less pollution • Silent operation
MCFC	10^5 – 10^7		

2.2.1 Fuel Cell Advantages

Fuel cells will continue to produce electricity as long as the fuel and other reactant chemical species are supplied. This property makes them share some characteristics with internal combustion engines. It is also known that fuel cells generate energy by electrochemical reactions, thus showing similar behavior as batteries. In fact, fuel cells combine many of the advantages of both engines and batteries (18).

The fact that fuel cells produce electricity from chemical energy makes them more efficient than internal combustion engines. Another advantage is that most of the components of fuel cells are solid and contain no moving parts, thus making fuel cells long-lasting systems, highly reliable and allowing them to operate silently. In addition, low temperature fuel cells yield potential for zero emissions of CO, CO₂, NO_x and SO_x, and particulate matter. Since the power and capacity of fuel cells are independent (determined by the fuel cell and reservoir sizes, respectively) also the scaling of these two characteristics is independent, a characteristic not observed in batteries. In addition, large batteries scale poorly, whereas fuel cells range from 1-W for portable devices to the megawatt range for power plants. Another advantage of fuel cells with respect to batteries is the possibility of being recharged quicker by refueling, as the latter must be disposed or plugged in for a larger amount of time (18).

2.2.2 Proton Exchange Membrane Fuel Cells

The first PEMFC system was developed by General Electric in the 1960s, which was used by NASA for the first manned space vehicles (8). Figure 2.3 shows a schematic of the electrochemical process occurring inside a PEMFC.

The PEMFCs have received considerable attention for transportation and combined heat and power (CHP) applications because they represent a clean power source for wide power ranges (19).

Instead of releasing thermal energy by the direct combustion of hydrogen and oxygen, PEMFCs generate energy due to the electrochemical reaction between hydrogen and oxygen.

The anode side of the fuel cell is fed with a stream of hydrogen, which will be divided into protons and electrons in the presence of a catalyst layer. The chemical reaction in this section of the fuel cell is represented by:



The protons formed in this reaction permeate through the polymer electrolyte membrane to the cathode chamber of the fuel cell. At the same time, the electrons travel to an external circuit to power an electric load and then return to the cathode side of the MEA. This is how the current output of the fuel cell is created.

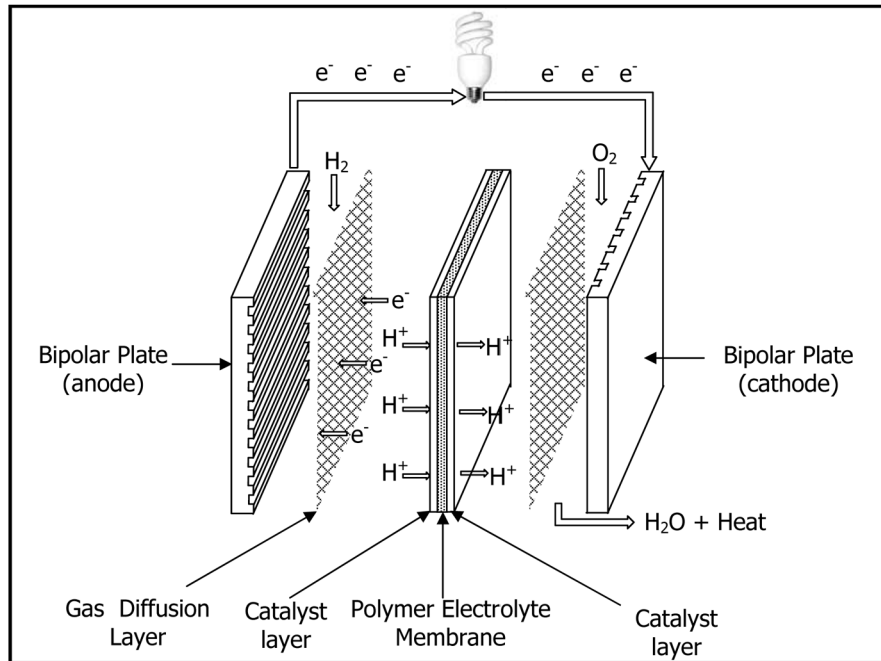
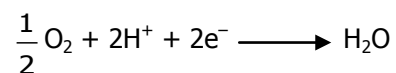
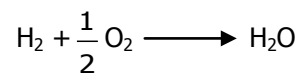


Figure 2.3 Schematic of a Proton Exchange Membrane Fuel Cell

In the channels of the bipolar plate in the cathode chamber, oxygen is being supplied to the fuel cell, which reacts with the protons flowing through the membrane and the electrons returning through the external circuit to produce water. This is a reduction reaction represented by the following stoichiometric equation:



As we can see, the overall reaction taking place in a PEMFC is given by:



2.2.2.1 Gas Diffusion Layer

The gas diffusion layer (GDL) is typically a porous material which may be fabricated with either carbon cloth or carbon paper. The GDL allows reactant gases to pass through it to the catalyst

layer. The transport of electrons to the external circuit is facilitated since the carbon is a conductive material. The carbon material used for fabricating the GDL can be treated with tetrafluoroethylene, thus becoming a hydrophobic material that prevents the GDLs from flooding, while still allowing the gases and steam to flow through the pores of the carbon paper (20).

In addition to these requirements, the gas diffusion layer must have the following characteristics (6):

- Must have good thermal and electrical in both through-plane and in-plane directions.
- The size of the pores of the GDL face adjacent to the catalyst layer must not be too large.
- The GDL must be rigid to support the MEA, while being flexible at the same time to maintain good electrical contacts.

2.2.2.2 Electrolyte Membrane

The polymer electrolyte membrane in a PEMFC must have high proton conductivity, while also acting like a barrier to avoid the fuel mixing with the reactant gases. It must also be made of a material chemically and mechanically stable in the fuel cell operating conditions. Some common materials used as membranes for PEMFCs are perfluorocarbon-sulfonic acid ionomer and Nafion™, the latter being produced by Dupont. The use of a solid electrolyte membrane represents an advantage when compared to systems using a liquid electrolyte (6).

The electrolyte membrane used in PEMFCs is a proton-conducting membrane cast in solid polymer form. Solid electrolyte offers a series of advantages as compared to systems with liquid electrolyte such as AFCs and PAFCs (7).

2.2.2.3 Catalyst layers

Between the gas diffusion layer and the polymer electrolyte membranes is the catalyst layer, where the hydrogen is being split into protons and electrons in the anode chamber and where the water is being produced in the cathode side of the fuel cell. The electrochemical reactions occur in a section of the catalyst layer where the three chemical species (protons, electrons and reactant gases) involved have access.

Current PEMFCs technologies use platinum as the most common material for catalyst layers. The thickness of this layer must be minimized in order to minimize the voltage drops due to the proton transport and permeation of reactant gases in the depth of the catalyst layer (6).

2.2.2.4 Bipolar Plates

Bipolar plates are the component of a PEM fuel cell stack that represent the most significant part by weight, volume and cost (19).

Bipolar plates receive this name since they are conductive plates that act as anode for one cell and as cathode for the adjacent cell. There are different materials used for bipolar plates, such as metal, carbon or conductive polymer composites.

The functions of bipolar plates within a fuel cell are stated below (6):

- They separate reactant gases and the water between cells.
- They provide a conductive medium between the anode and cathode to minimize ohmic losses.
- Bipolar plates have channels engraved for flow of reaction gases.
- They give mechanical support to the fuel cell stack.

- They conduct heat generated by the chemical reaction out of the fuel cell.

To perform these functions, the material used for bipolar plates must have the following characteristics (8):

- Impermeable to reactant gases (hydrogen and oxygen from air in PEMFCs)
- Good electrical conductivity
- A balance between conductivity, strength, size and weight. Weight becomes a priority when fuel cells are to be used for transport and mobile devices.
- Resistance to corrosion
- Easy to manufacture in large quantities
- The distribution of the reactant gases in the channels must be uniform to increase efficiency of the stack.

2.2.2.4.1 Composite Bipolar Plates

Composite bipolar plates represent a good alternative that contributes to the weight, corrosion and cost challenges for this component of fuel cells. A composite bipolar plate is typically made of a polymer matrix to which an electrically and thermally conductive carbon filler(s) is added. For fabrication of composite bipolar plates, there are two types of polymers that can be used as matrix material: thermosetting and thermoplastics. Current technologies use a concentration of a single type of graphite between 70 and 90 wt.% (21). Research performed by our group studied the properties of a thermoplastic polymer with different types of carbon fillers that enhance the electrical, thermal and mechanical properties of the resulting materials (22-35). Thermoplastics have the advantage over thermosetting resins of being recyclable and reusable materials. In addition, the waste material generated from the manufacturing process can be melted and

reused for producing new bipolar plates. Some of the advantages of composite thermoplastic resins over graphitic and metallic bipolar plates are the low cost and weight, higher flexural strength and resistance to corrosion (36).

Development of cost-effective technologies is an important aspect for mass production of bipolar plates for use in fuel cells in the automobile industry. The most common processes used for manufacturing composite bipolar plates are injection and compression molding. The use of injection-molding offers the advantages of automated production, shorter cycle times and excellent product reproducibility (37), whereas composites produced by compression-molding yielded higher thermal and electrical conductivity values (37,38).

2.3 Thermal Conductivity Background

For the design of materials for new applications, heat transfer is an important property to be considered. There are three mechanisms for heat transfer: radiation, convection, and conduction. In this project, we are working with solid materials, where heat conduction is the main mechanism of heat transfer.

The word 'conduction' is associated with the concepts of atomic and molecular activities, as it can be defined as the transfer of energy from particles containing a higher amount of energy to those with lower amounts by interaction between both particles.

The physical explanation of the conduction heat transfer can be done by considering a stagnant fluid with a temperature gradient between different parts of the fluid, e.g., the fluid may be occupying the space between two surfaces at different temperatures. The temperature value of one of the surfaces is associated to the molecules in a given point of the fluid. The translational motion of the fluid molecules and the internal motions of the molecules will determine the energy of the molecules, i.e. higher temperatures are due to higher molecular energies. Hence, the energy transfer to less energetic molecules will occur by the collision of adjacent molecules (39).

The amount of heat transferred by conduction can be quantified using Fourier's Law of Heat Conduction, given in Equation 2.1 (39-42).

$$\dot{q}'' = -k \frac{dT}{dx} \quad (2.1)$$

where:

\dot{q}'' = Heat flux by conduction

k = Thermal conductivity

$\frac{dT}{dx}$ = Temperature gradient in the x-direction

In a solid, heat conduction may be attributed to two different mechanisms: atomic activity in the form of lattice vibrations and translational motion of free electrons. For dielectric materials, the only mechanism through which heat conduction is occurring is by these lattice waves.

The energy of phonons is important in heat conduction, as it has a major influence in the material properties like thermal conductivity, wave transmission and other low-temperature thermodynamic properties (43).

The phonon distribution can be used to explain a heat flow within an insulating material. A heat flow indicates that the phonon distribution in the material is different from that when the material is in thermal equilibrium, corresponding to a state where there is no heat transfer. The thermal conductivity will be then determined by the magnitude of the deviation of the phonon distribution with respect to the equilibrium condition. The difference between these two states can be described in terms of the mean free paths, which in most cases is a function of temperature, frequency and polarization of the phonon mode (41).

The effectiveness of heat transfer by phonons depends on the way phonons are scattered as they move within the material (44). Figure 2.4 is showing two situations where phonon scattering

is occurring. If the distance between defects produced by phonon scattering is longer, it will result in a higher thermal conductivity of the material. This effect can be quantified by Equation 2.2, known as the Debye model, applicable for heat conduction in insulating materials. (45).

$$k = \frac{c \cdot u \cdot \lambda}{3} \quad (2.2)$$

where:

c = Volumetric heat capacity

u = Velocity of sound in the material

λ = Mean free path of phonons in the material

A typically used value in this equation is 5×10^5 cm/s for the speed of sound, which depends on the type of material and is relatively independent of temperature (46). Unlike the speed of sound, the mean free path is affected when temperature changes, with typical values of about 10 nm at room temperature and 10^4 nm near 20K.

In this project, we are studying the thermal properties of carbon-filled polypropylene. Therefore, heat conduction by phonons is the main conduction method in this type of materials. Polymers are dielectric materials so they generally follow the Debye model. The carbon fillers proposed in this study are electrically conductive. However, their thermal conductivity is due to phonon interactions.

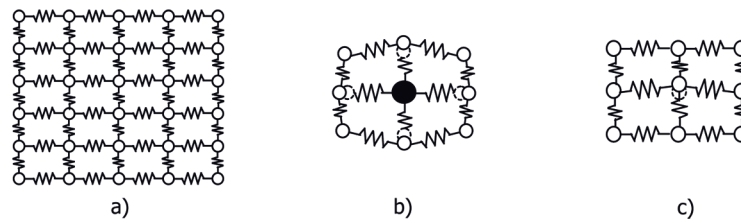


Figure 2.4 Schematic representation of the lattice thermal conductivity in a two-dimensional array. a) Two-dimensional array of atoms b) Impurity atom (point defect). c) Displaced atom (lattice vibration)

2.4 Mechanical Properties Background

Composite materials may be classified into three different classes depending on the type of filler used: particulate-filled materials, which consist of a matrix phase filled with discontinuous filler made of discrete particles, fiber-filled composites, and skeletal or network composites. In this project we studied properties of particulate-filled and fiber-filled composites (47).

Composites filled with fibers are important due to the fact that they can have high strength and stiffness for a given filler concentration. These characteristics can be modified by varying the concentration of a single type of filler in the polymer matrix. As we can see in Table 2.2, the specific strength and modulus (defined as the ratio of the tensile strength and tensile modulus to the density, respectively) for fiber-filled composite materials can surpass the values typically observed for metals. The improvements of a polymer composite when compared to an unfilled polymer are remarkable. Most of the fiber-filled composites are anisotropic, since the fibers are primarily aligned in one direction, giving them the advantage over other materials for different applications by proper design (47).

2.4.1 Tensile Modulus

Tensile Modulus is the measurement of the stiffness of a material. The tensile modulus is defined as the ratio of the stress over the strain, both measured in the longitudinal direction, in the range of the stress where Hooke's Law is valid and is expressed in units of force per unit area. Tensile

modulus is calculated from the linear section of the experimental stress–strain curve created during tensile tests. An example is illustrated in Figure 2.5 with the modulus being approximately 2400 MPa. ASTM Test Method D638 describes the procedure used for tensile testing of plastics (48).

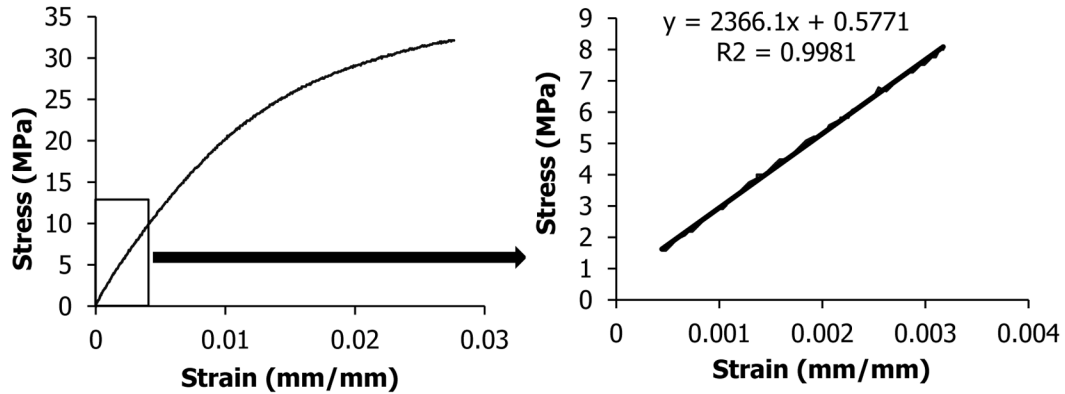


Figure 2.5 Determination of Elastic Modulus using Stress–Strain Curve

2.4.2 Flexural Modulus

The flexural modulus is the ratio of stress to strain in flexural deformation. This property indicates the tendency for a material to bend. Equation 2.3 was used to calculate the flexural modulus from the initial linear portion of the load–deflection curve. Like tensile modulus, is measured in units of force per area. The standard method for determining flexural properties of polymeric materials is described in ASTM Test Method D790 (49).

$$E_b = \frac{L^3 m}{4wd^3} \quad (2.3)$$

where:

E_B = modulus of elasticity in bending, MPa

L = Length of the support span, mm = 48 mm typically

w = Width of test specimen, mm = 12.3 mm typically

d = Depth of test specimen, mm = 3.0 mm typically

m = slope of the initial straight-line portion of the load-deflection curve, N/mm.

The load vs. deflection curve data obtained from the flexural tests is used for calculating the stress vs. strain curve using Equations 2.4 and 2.5 (49).

$$\sigma = \frac{3F \cdot L}{2w \cdot d^2} \quad (2.4)$$

$$\varepsilon = \frac{6D \cdot d}{L^2} \quad (2.5)$$

where:

σ = Stress in the outer fibers at midpoint, MPa

F = Load at a given point on the load-deflection curve, N

ε = Strain in the outer surface, mm/mm

D = Maximum deflection at the center of the test specimen, mm

2.4.3 Factors Affecting Tensile Modulus

The properties of both the fillers and matrix material contribute significantly to the elastic modulus of the resulting materials (50). Carbon may be used as filler in its different forms, ranging from amorphous carbon black to single- or multi-walled carbon nanotube. The modulus of the filler will change depending on the type of carbon used, with values ranging from 827 GPa for carbon black to approximately 1000 GPa for graphite crystals (51,52). Typically, the modulus values of the fillers are higher than that of the matrix material. Hence the lower and upper limits for the composite modulus will be given by the modulus of the matrix and filler, respectively.

Table 2.2
Specific modulus and strength of common materials (47)

Material	Specific modulus $(\frac{\text{lb}_f \cdot \text{in}}{\text{lb}})$	Specific strength $(\frac{\text{lb}_f \cdot \text{in}}{\text{lb}})$
Aluminum	1×10^8	1×10^5
Stainless steel	1.1×10^8	8.8×10^5
Polystyrene	1.1×10^7	1.85×10^5
Epoxy resin	1.1×10^7	2.2×10^5
Uniaxial glass–epoxy composite ($\phi_2 = 0.7$)	9.2×10^7	2.6×10^6
Uniaxial boron–epoxy composite ($\phi_2 = 0.7$)	5.9×10^8	3.7×10^6
Uniaxial graphite–epoxy composite High–modulus fiber ($\phi_2 = 0.6$)	4.9×10^8	2.1×10^6
Uniaxial graphite–epoxy composite High–modulus fiber ($\phi_2 = 0.6$)	3.0×10^8	3.4×10^6

Research work published by different authors has proven that besides the filler and matrix properties, other factors such as the size, shape, orientation, adhesion between the filler and matrix, and material processing techniques will also contribute to the characteristics of the composites (50,52-65).

2.5 Active Learning

As mentioned in the Chapter 1 of this work, in addition to the experimental work to develop new technologies for implementing fuel cells as a new source of energy, it is paramount to train people for careers in the research and development community, thus establishing a connection between the information in hydrogen and fuel cell technologies and the dissemination networks.

Active learning is an important educational tool when teaching engineering topics. Active learning is defined as an instructional method that involves students participation in the learning process. This is done by making students to perform activities that enhance their learning and makes them think about the background related to these activities (66).

The difference between active learning and the traditional forms of lecture where students just listen to the information provided the instructor in class is that active learning includes everything ranging from listening practices that help students to assimilate the information they are being given to writing exercises or group work in which students use the course material to come with solutions to practical situations (66).

Active learning can occur when students are given a question or real-life problem where they are asked to work individually or in groups during a period of time. Then the students share their different approaches to solving these situations with the class (67).

In the past years, active learning has become an important educational tool. Sometimes faculty perceive it as a radical change from traditional lecture formats or question in how it differs from traditional engineering education, e.g., some questions remain about whether traditional engineering courses are considered “active” due to the fact that homework and laboratory assignments are delivered to students (67).

2.5.1 Problem-Based Learning

One example of active learning is Problem-based learning (PBL). This is an instructional method where problems relevant to the lecture are delivered at the beginning of the session, thus used for providing the proper background and motivation for learning the concepts in the following lecture. PBL represents an alternative to motivate students to be self-directed (68).

There are different ways of implementing PBL in a classroom, hence making the assessment of its effectiveness more complex. There are studies trying to compare PBL with traditional teaching techniques. This is difficult as sometimes a point of comparison cannot be made because each of these techniques covers different aspects or educational methods (68).

In meta-studies, to determine the effectiveness of PBL as compared to traditional programs, the common elements in PBL practices will have to produce a ‘greater’ signal than the ‘noise’ caused

by the difference in the implementation of PBL and traditional teaching methods. This variation in PBL practices may yield inconsistent results from meta-studies. Vernon and Blake (69) analyzed 35 meta-studies performed between 1970 and 1992 for medical programs, showing that PBL produced a significant effective size (0.55) in positive attitudes and feedback by the students in these programs. Research work by Albanese and Mitchell (70) stated that the PBL method is preferred by students and faculty members.

Chapter 3: Materials and Fabrication Methods

3.1 Introduction

To manufacture the composites for this study, we used three different carbon fillers and a polymer matrix. The polymer matrix used was Dow's Semi-Crystalline Homopolymer Polypropylene Resin H7012-35RN. The carbon fillers used were Ketjenblack EC-600 JD carbon black from Akzo Nobel, Inc., Asbury Carbons' Thermocarb TC-300 synthetic graphite, and Hyperion Catalysis International's Fibril TM multi-walled carbon nanotubes. The characteristics of each material and additional details will be discussed in the following sections.

3.2 Matrix Material

3.2.1 Semi-Crystalline Homopolymer Polypropylene Resin H7012-35RN

The material selected as polymer matrix for this project was Dow's Semi-Crystalline Homopolymer Polypropylene Resin H7012-35RN. This polypropylene resin contains a nucleating agent which allows shorter molding times, also making it appropriate for injection molding because of its good processability and mold filling. The structure and properties of the polypropylene used in this project are shown in Figure 3.1 and Table 3.1 respectively (71). Since polypropylene is a thermoplastic material, it allows re-melting for other applications, making it a good option for use in bipolar plates by other research groups (72,73).

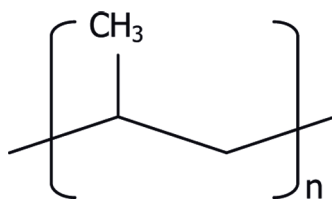


Figure 3.1 Chemical Structure of Polypropylene

Table 3.1
Properties of Dow H7012–35RN Polypropylene Resin/Molded Parts (71)

Resin Properties	
Density (g/cm ³)	0.9
Melt Flow Rate (g/10 min)	35
Melting Point (°C)	163
Glass Transition Temperature (°C)	–6.6
Crystalline Temperature (°C)	127
Molded Parts Properties	
Tensile Strength at Yield, (MPa)	34
Tensile Elongation at Yield, (%)	7
Flexural Modulus, 1% Secant, (MPa)	1,420
Notched Izod Impact @ 23°C , (J/m)	25
Deflection Temperature Under Load @ 0.45 MPa, unannealed, (°C)	110

3.3 Filler Materials

3.3.1 Carbon Black

Carbon black is produced industrially by the thermal decomposition of a hydrocarbon material. Some of the methods used for production of carbon black include the lampblack, gas black, thermal black, acetylene processes. Carbon black can be obtained as a byproduct of the electric arc process and the production of synthesis gas (74,75). The use of carbon black in the rubber industry represents approximately 90% of the total carbon sales, with the major portion of this used in the tire industry. The remaining 10% is used in printing inks and in the plastic industry as pigment and as an electrically conductive filler.

Over 90% of the carbon black currently used, is manufactured by the oil furnace process (74). In this process, the raw materials are hydrocarbons that must be capable of being converted completely to the vapor phase. These materials will be preheated and pumped from the storage tank to the reactor. The reactor feed contains this gas and preheated process air. The reaction is stopped by adding water after the feedstock moves a certain distance from the injection point.

This will cool the carbon black formed and the gas mixture, which will be filtered to separate the carbon black. The bulk density of the carbon is increased by either mixing it in pin mixers with addition of more water or by tumbling in horizontal drums, to form small pellets that are dried in a rotary kiln dryer (75,76). Depending on the final application, carbon black can be sold as powder or pellets (76). The concentration of the raw material, temperature and residence time in the reactor will have an effect on the structure and size of the carbon black produced (77).

The type of carbon black selected for this study was Ketjenblack EC-600 JD from Akzo Nobel Inc. This carbon black has the property of contributing with high electrical conductivity at low concentrations in the resulting composites. This is caused by large area of the high degree of branching of the carbon black, which allows the filler to contact a large amount of polymer, hence raising the electrical conductivity. Ketjenblack EC-600 JD comes in the form of pellets with a size distribution ranging from 100 μ m to 2mm (78). The properties and structure of Ketjenblack EC-600 JD are shown in Table 3.2 and Figure 3.2, respectively.



Figure 3.2 Ketjenblack EC-600 JD Primary Aggregate

Table 3.2
Properties of Akzo Nobel Ketjenblack EC-600 JD (78)

Electrical Resistivity	0.01–0.1 $\Omega\cdot\text{cm}$
Aggregate Size	30–100 nm
Specific Gravity	1.8 g/cm ³
Apparent Bulk Density	100–120 kg/m ³
Ash Content, max	0.1 wt. %
Moisture, max.	0.5 wt. %
BET Surface Area	1250 m ² /g
Pore Volume	480–510 cm ³ /100g

3.3.2 Synthetic Graphite

Carbon materials containing highly graphitizable carbon structures can be treated at high temperatures to produce synthetic graphite. Synthetic graphite is produced from calcined petroleum coke and coal tar pitches. Synthetic graphite manufacturing involves mixing, molding and baking operations before treatment at temperatures between 2500 and 3000°C (79). This treatment at high temperatures allows the phase transformation of amorphous carbon to graphite. Synthetic graphite can be found in different forms, such as flakes, fine powder, irregular grains, etc. (79). The high processing temperatures will allow for the reduction of the concentration of impurities (volatile substances, metal oxides, nitrogen, hydrogen and organic components), which are present in the raw materials. This is the reason why synthetic graphite products have purities of more than 99% (79). Some applications of synthetic graphite include fuel cell bipolar plates, coatings, electrodes, conductive fillers, rubber and plastic compounds, casting, etc. (79).

The synthetic graphite selected for this research work is Asbury Carbons' Thermocarb TC-300, which is a primary synthetic graphite previously sold by Conoco (80,81). Thermocarb TC-300 is obtained from a thermally treated highly aromatic petroleum feedstock. This type of synthetic graphite enhances the thermal and electrical properties of the conductive resins due to its high

thermal and electrical conductivities. The characteristics of this filler are summarized in Tables 3.3 and 3.4 (80,81). Figure 3.3 shows a photomicrograph of Thermocarb TC-300.

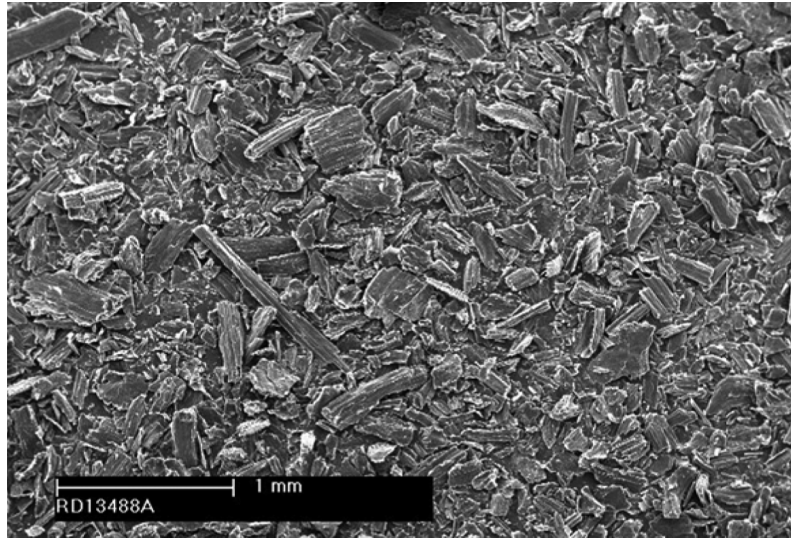


Figure 3.3 Photomicrograph of Thermocarb TC-300 Synthetic Graphite (Courtesy of Asbury Carbons)

Table 3.3
Properties of Thermocarb TC-300 Synthetic Graphite (80,81)

Filler	Thermocarb TC-300 Synthetic Graphite
Carbon Content, wt. %	99.91
Ash, wt. %	<0.1
Sulfur, wt. %	0.004
Density, g/cm ³	2.24
BET Surface Area, m ² /g	1.4
Thermal Conductivity at 23°C, W/m·K	600 in "a" crystallographic direction
Electrical Resistivity of bulk carbon powder at 150 psi, 23°C, parallel to pressing axis, Ω·cm	0.020
Particle Shape	Acicular
Particle Aspect Ratio	1.7

Table 3.4
Sieve analysis of Thermocarb TC-300 Synthetic Graphite (80,81)

Sieve Analysis	wt. %
+600 μm	0.19
+ 500 μm	0.36
+300 μm	5.24
+ 212 μm	12.04
+180 μm	8.25
+150 μm	12.44
+75 μm	34.89
+44 μm	16.17
-44 μm	10.42

3.3.3 Hyperion Fibril Carbon Nanotubes

Carbon nanotubes consist of coaxial cylinders of graphite sheets, ranging from 2 to 50 sheets (82). Properties of carbon nanotubes make them useful in mechanical and electrical applications (82). Multiple methods exist for production of multi-walled carbon nanotubes, such as arc growth, chemical methods, catalytic chemical vapor deposition (CCVD) and chemical vapor deposition (CVD). In this last method, the carbon vaporization may be induced through electric arc discharge, laser ablation, or solar energy (82). When carbon nanotubes are produced industrially by the CVD process, the growth of carbon nanotubes takes place in a fluidized-bed reactor with a capacity of producing 50 kg of carbon per day, with a yield of approximately 80% of carbon nanotubes (83). The catalytic chemical vapor deposition method grows a carbon nanotube by passing a hydrocarbon vapor over a catalyst at a temperature of approximately 1100°C. The process allows high yields to be achieved. However, low concentrations of amorphous carbon are observed when this process is used. One of the disadvantages of the CCVD process for carbon nanotubes production is that the purity of carbon decreases due to the presence of catalyst residues (84). The size, structure and quality of the carbon nanotubes is affected by the hydrocarbon vapor utilized as raw material, temperature and type of catalyst (83).

Carbon nanotubes can be used in applications as semiconductors, medical delivery systems, automobile body panels, paint, tires, and flame retardants in polyethylene and polypropylene (82). One of the reason that makes carbon nanotubes an important focus of study is their good mechanical, electrical and thermal properties (82).

Hyperion Catalysis International's FIBRIL™ multi-walled carbon nanotubes were the third filler selected for this study. It is produced from hydrocarbons with low molecular weight and high purity in a continuous catalyzed reaction occurring in the gas phase. Information provided by the vendor states that the outside diameter of the nanotubes is 10 nm and the length is 10 μm , yielding an aspect ratio (length/diameter) of 1000. The high aspect ratio of this filler allows a great improvement in the thermal and mechanical properties of the composite materials, even at low filler concentrations. This material was obtained from Hyperion Catalysis International in a 20 wt.% FIBRIL™ masterbatch MB3020-01 in polypropylene. Table 3.5 shows the properties of this carbon filler (85).

3.4 Formulation Naming Convention

Each one of the samples produced in this project is assigned a unique identification name and number. Since all the composite samples produced in this work look similar, it is very important to properly label each one of these samples in order to identify which composite formulation is being tested. These labels will indicate the type and concentration of filler used, and the order in which the sample was injection molded. Following is the naming convention used for labeling the samples in this project.

Table 3.5
Properties of Hyperion FIBRIL™ Carbon Nanotubes (85)

Composition	Pure carbon with trace residual of metal oxide catalyst
Diameter	0.01 μm
Length	10 μm
Morphology	8 graphitic sheets wrapped around a hollow 0.005 μm core
Density	2.0 g/cm^3

E w x P y-z-##,

where:

E = Project description (E is for the Department of Energy project)

w = Type of carbon filler (A = carbon black, B = synthetic graphite, and Q = Carbon Nanotubes)

x = Concentration of the carbon filler in the composite, expressed in weight percent.

P = polymer matrix (P corresponding to H7012-35RN Polypropylene resin)

y = Indicates whether the sample is a replicate (none for original, R for first replicate)

z = Specimen type (F for flex bar, T for tensile bar, and TC for thermal conductivity disks)

= Specimen number (Indicating the order in which the sample was produced)

One example for this naming formula is EA7.5P-F-16. This indicates the sample is a flexural test specimen containing 7.5 wt.% carbon black and was the 16th sample injection molded for this formulation. An example for the naming convention for composites containing multiple carbon fillers is EA2.5Q6P-T-21. This label indicates that the sample is a tensile bar containing 2.5 wt.% carbon black and 6 wt.% carbon nanotubes in polypropylene and was the 21st sample from the injection molding machine for this formulation.

Tables 3.6 and 3.7 show the filler concentrations (in wt.% and the corresponding vol.%) in polypropylene for formulations containing single and multiple fillers, respectively, for the composites evaluated in this project.

Some of the samples used for thermal conductivity measurement were obtained from composite plates produced by compression molding. To identify these samples from those produced by

injection molding, the letter 'C' was added after the sample number, e.g., the label 'EA2.5B65Q6P-3C' indicates that this test specimen contains 2.5 wt.% carbon black, 65 wt.% synthetic graphite and 6 wt.% carbon nanotubes and that it was the third conductivity disk cut from a compression molded plate.

3.5 Fabrication Methods

3.5.1 Extrusion

In this project, the matrix and filler materials were used in the same conditions that were provided by the manufacturer. For extruding the samples an American Leistritz Extruder Corporation Model ZSE 27 was used. This extruder is shown in Figure 3.4. This extruder has a 27 mm co-rotating intermeshing twin screw with 10 zones for filler addition and an aspect ratio (length/diameter) of 40. The screw design was chosen to obtain a minimum amount of filler degradation, while still dispersing the fillers well in the polymer. This design is shown elsewhere (86).

The pure polypropylene pellets and the Hyperion FIBRIL™ masterbatch MB3020-01 (containing 20 wt.% carbon nanotubes in polypropylene) were introduced in Zone 1, which is water cooled. For all the composites containing single fillers, synthetic graphite and carbon black were added into the polymer melt at Zone 5. For composites with multiple fillers, the synthetic graphite and carbon black were added to the polymer in zones 5 and 7, respectively. By introducing the fillers at different zones, we can obtain an adequate mix of the large amount of fillers. To control the amount of filler added to the extruder, we used Schenck AccuRate gravimetric feeders. A Schenck AccuRate Flexwall gravimetric feeder was used in Zone 1, shown in Figure 3.5, and Schenck AccuRate Conisteel feeders were used in Zones 5 and 7, shown in Figure 3.6.

Table 3.6
Single Filler Loading Levels in Polypropylene

Filler wt.%	Carbon Black vol.%	Synthetic Graphite vol.%	Carbon Nanotubes vol.%
1.5	N/A	N/A	0.68
2.5	1.3	N/A	1.1
4	2.0	N/A	1.8
5	2.6	N/A	2.3
6	3.1	N/A	2.8
7.5	3.9	N/A	3.52
10	5.3	4.3	4.8
15	8.1	6.6	7.4
20	N/A	9.1	N/A
25	N/A	11.8	N/A
30	N/A	14.7	N/A
35	N/A	17.8	N/A
40	N/A	21.1	N/A
45	N/A	24.7	N/A
50	N/A	28.7	N/A
55	N/A	32.9	N/A
60	N/A	37.6	N/A
65	N/A	42.7	N/A
70	N/A	48.4	N/A
75	N/A	54.7	N/A
80	N/A	61.6	N/A

Table 3.7
Multiple Filler Loading Levels in Factorial Design Formulation

Formulation	Carbon Black		Synthetic Graphite		Carbon Nanotubes	
	wt.%	vol.%	wt.%	vol.%	wt.%	vol.%
No Filler	0	0	0	0	0	0
2.5 CB	2.5	1.3	0	0	0	0
65 SG	0	0	65	42.7	0	0
6 CNT	0	0	0	0	6	2.8
2.5 CB * 65 SG	2.5	2.1	65	43.6	0	0
2.5 CB * 6 CNT	2.5	1.3	0	0	6	2.8
65 SG * 6 CNT	0	0	65	45.2	6	4.7
2.5 CB * 65 SG * 6 CNT	2.5	2.2	65	46.2	6	4.8

The polymer fibers (3 mm in diameter) passing through the extruder enter a water bath and then a ConAir pelletizer Model 20402HP-14A, producing pellets with a length of 3 mm. Figures 3.7 and 3.8 show pictures of the water bath and the pelletizer, respectively. Approximately 10 pounds of pellets for each composite formulation were produced. The extrusion run conditions for all the composite formulations are shown elsewhere (86).



Figure 3.4 American Leistriz Extruder Corporation Model ZSE 27



Figure 3.5 Schenck AccuRate Flexwall Feeder



Figure 3.6 Schenck AccuRate Conisteel Feeder



Figure 3.7 Water Bath



Figure 3.8 ConAir pelletizer Model 20402HP-14A

3.5.2 Drying

After extrusion, the composite pellets were dried using a Bry Air System equipped with a dehumidifying drying oven heated indirectly at a temperature of 80°C for 4 hours. This drying system is shown in Figure 3.9. The water acquired by the polymer in the water bath is removed through this process. Once the polymer is dry, it is stored in moisture barrier bags before being molded.



Figure 3.9 Bry Air Drying Oven System

3.5.3 Injection Molding

The test specimens for testing thermal and mechanical properties were produced using a Niigata injection molding machine, model NE85UA₄ (87). The single screw in this machine has a diameter of 40 mm and an aspect ratio (length/diameter) of 18, with a maximum operating speed of 320 rpm. The maximum injection pressure of this equipment is 22,610 psi, and a maximum clamping force of 82.50 US tons. The screw in this injection molding machine is divided into three sections:

feed, compression, and metering sections with lengths of 396 mm, 180 mm, and 144 mm, respectively (87). A picture of the Niigata injection molding machine is shown in Figure 3.10.

A four-cavity mold (shown in Figure 3.11) was used to produce 3.2 mm thick, 16.5 cm long ASTM Type I tensile bars (end gated), 3.2 mm thick, 6.4 cm diameter disks (end gated) for thermal conductivity testing, and 3.2 mm thick, 12.7 cm long by 1.27 cm wide flex bars (end-gated) (88).



Figure 3.10 Niigata Injection Molding Machine Model NE85UA₄

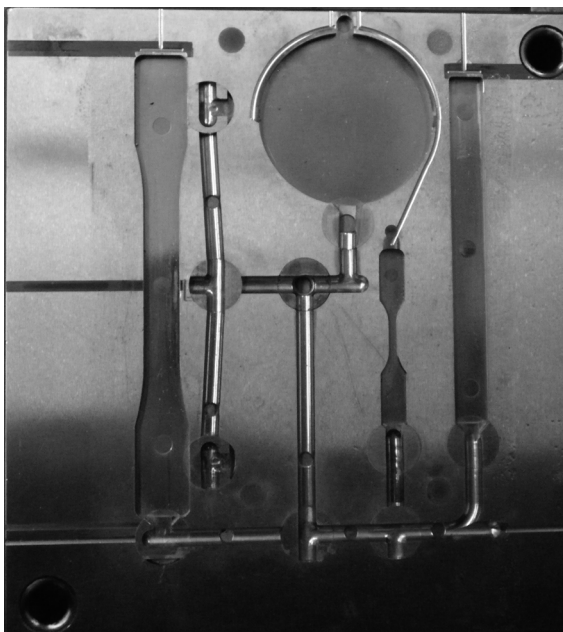


Figure 3.11 Four-Cavity Mold Used in Injection Molding

To begin the injection molding process, the machine was heated to the operating temperature. Then the machine was purged using Dow's semi-crystalline homopolymer polypropylene resin H7012-35RN to remove any contaminants from the previous injection molding process. Approximately four pounds of material yields a set of 25 to 30 flex bars, thermal conductivity disks and Type I tensile bars for each composite formulation. For some formulations, more disks were injection molded. This was due to the high viscosity of the material, which did not allow injection molding tensile and flex bars, especially for materials with high filler concentrations. The conditions for each formulation were kept constant as long as the samples could be molded. Typically, the only parameters modified between formulations were the temperatures, shot size and injection pressure. The samples were then labeled as described in Section 3.4 of this study and stored in Ziploc® bags.

When the required number of samples for a formulation was reached, then the next formulation was added to the hopper. The five samples produced in between formulations were discarded because they are transition material contaminated with the previous formulation. After all the

formulations were molded into specimens, the machine was purged with Dow's semi-crystalline homopolymer polypropylene resin H7012-35RN to remove all the contaminants. When the polymer melt was free from any black material, the injection molding machine was clean and the machine was shut down.

The results from density tests proved that the correct amount of filler was present in each composite formulation. These results are shown elsewhere (86).

3.5.4 Compression Molding

The only composite formulation that was compression molded was the three filler formulation containing 2.5 wt.% Ketjenblack EC-600 JD, 6 wt.% Hyperion FIBRIL™ nanotubes, and 65 wt.% Thermocarb TC-300 in polypropylene semi-crystalline homopolymer resin H7012-35RN. Due to the high viscosity of this material, its composites could only be produced by compression molding. In addition, research by other groups has proven that compression molded composites yielded materials with higher conductivities (89,90). The compression molding press selected for this research work was a Wabash Model V75H-18-CLX. This equipment was used to produce plates with a length of 8.5 inches, a width of 7 inches and thickness of 3.2 mm. A photograph of the Wabash V75H-18-CLX and is shown in Figure 3.12. The procedure for fabricating plates is discussed below.

1. The pellets obtained from the extrusion process were ground up using a coffee grinder. Then the pellets were sifted using a size #65 Taylor mesh sifting tray to collect 222 grams of material with a particle size of less than 208 μm .
2. The temperature of the press platen set was set to 230°C. The platens were then closed to allow the temperature to reach the set point.
3. The 7 inch by 8.5 inch mold was coated with Slide Biodegradable Mold Release, as well as the four shims used to get the desired plate thickness. The top and bottom caul

plates were coated with 10% wt Dynamar 9316 (mold release) from 3M in an acetone solution.

4. To make up the mold, the picture frame mold was placed on top of the protective sheet metal. Then the thinner caul plate was placed with the smooth side up into the picture frame mold. After the caul plate was in the mold, 222 grams of ground material was spread evenly over the plate in the mold. Once the material was in the mold, the thicker caul plate was placed on top with the second piece of protective sheet metal on top.
5. After the platen set point was reached, then the platens were opened and the mold prepared in step four was slid into the press. The guard door was then closed to protect the operators.
6. The platens were closed and a force of 1 ton (34 psi) was applied to the mold for 25 minutes at 230°C.
7. After the 25 minutes, the force was increased from 1 ton to 30 tons (1008 psi) and applied to the mold for an additional 25 minutes at 230°C.
8. The mold was then cooled down to a temperature of 25°C while the force of 30 tons continued to be applied to the mold. This cooling process was done following these steps: water/air was used to cool the platens from 230°C to 177°C, followed by water to cool the plate to 25°C.
9. The mold was removed from the press and then placed on the mold opening device with a piece of metal placed on top of the mold. Then the mold was placed back in the press where 1 ton of force was applied. This caused the compression molded plate to fall out of the picture frame. Everything was removed from the press and cleaned for the next use.

10. After the plates were produced, then the composite disks for thermal conductivity testing are cut out of the compression molded plates.



Figure 3.12 Wabash Model V75H-18-CLX Compression Molding Press

Chapter 4: Test Methods

4.1 Synthetic Graphite Length, Aspect Ratio, and Orientation Test Method

The length and aspect ratio (length/diameter) of synthetic graphite in the composites was determined by the following procedure: first, the polypropylene matrix was dissolved using xylene at 120°C. The filler particles were dispersed on a glass slide and an Olympus SZH10 optical microscope was used to observe the synthetic graphite particles. The microscope is equipped with an Optronics Engineering LX-750 video camera used to obtain images of the filler at a magnification of 70x. The images were collected using Scion Image software Version 1.62, and processed using Adobe Photoshop 5.0 and Image Processing Tool Kit 3.0. The length and aspect ratio of approximately 1000 synthetic graphite particles were determined. Additional details for this test method are shown elsewhere (86).

The orientation of synthetic graphite particles in test specimens for testing tensile and flexural properties was evaluated as follows:

- The samples were cast in epoxy so that the direction of flow in the injection molding process would be observed.
- The samples were polished and observed using an Olympus BX60 reflected light microscope. The samples were observed at a magnification of 200x.
- The images were processed using Adobe Photoshop 5.0 and Image Processing Tool Kit 3.0. Adobe Photoshop 5.0 and the Image Processing Tool Kit version 3.0 were used to process the images.

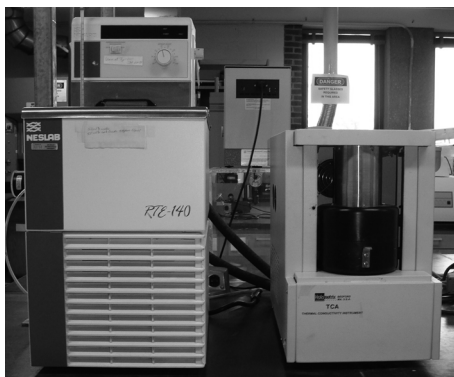
The length and aspect ratio of approximately 1000 synthetic graphite particles were determined. More information about this test method is discussed elsewhere (86).

4.2 Field Emission Scanning Electron Microscope (FESEM) Test Method

The fracture surface of the composite containing the three carbon fillers (2.5 wt.% carbon black, 65 wt.% synthetic graphite, and 6 wt.% carbon nanotubes) was observed with a Hitachi Cold Field Emission Scanning Electron Microscope (FESEM) at 5kV. This method was used to view the smaller fillers (CNT and CB) that could not be seen in the optical microscope.

4.3 Thermal Conductivity: Guarded Heat Flow Meter Test Method

A Holometrix Model TCA-300 Thermal Conductivity Analyzer was used to measure the through-plane thermal conductivity of a 3.2 mm thick, 5 cm diameter disk at a temperature of 55°. This apparatus is shown in Figure 4.1 and follows the ASTM F433 guarded heat flow meter method (91). A temperature of 55°C was selected for the thermal conductivity measurement since it is relatively close to the standard temperature of 25°C, while still allowing a temperature gradient in the apparatus. This test method for measuring through plane conductivity is illustrated in Figure 4.2. The test specimens for this test were disks with a diameter of 5 cm cut from injection molded disks or compression molded plates using a hole saw. A minimum of 4 test specimens were tested for each formulation.



4.1 Holometrix Model TCA-300 Thermal Conductivity

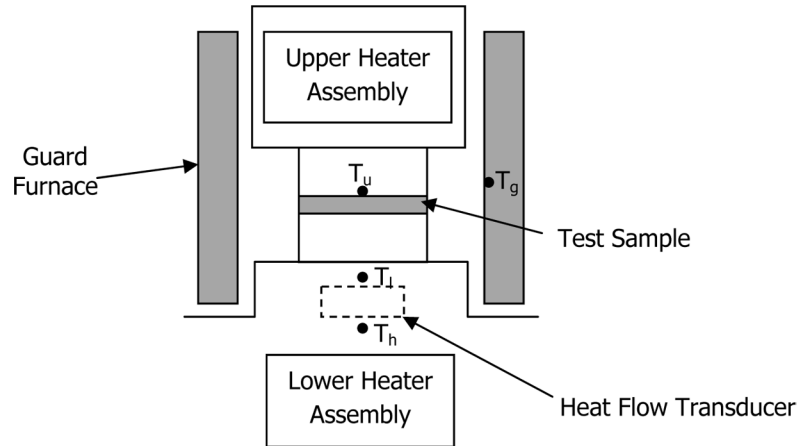


Figure 4.2 Schematic of Through-Plane Thermal Conductivity Test Method (92)

4.4 Thermal Conductivity: Nanoflash Method

4.4.1 NETZSCH LFA 447 Nanoflash™ Apparatus

The NETZSCH LFA 447 Nanoflash™ equipment uses the flash method for measuring the thermal diffusivity of a sample. One major advantage of this device is that it can be used to test a wide range of materials over a large operating range in temperatures (room temperature up to 300°C).

The NETZSCH Nanoflash apparatus can measure the following thermal properties (93):

- Thermal diffusivity α from about 0.01–1000 mm²/s at 3–5% accuracy
- Thermal conductivity λ from about 0.1–2000 W/m–K and 5–7% accuracy
- Specific heat C_p (range unspecified) at 3–7% accuracy.

The operation of this instrument is based upon the following national/international standards: ASTM E–1461 (94). A photograph of this apparatus is shown in Figure 4.3 with a more detailed schematic shown in Figure 4.4.



Figure 4.3 NETZSCH LFA 447 Nanoflash™ Apparatus

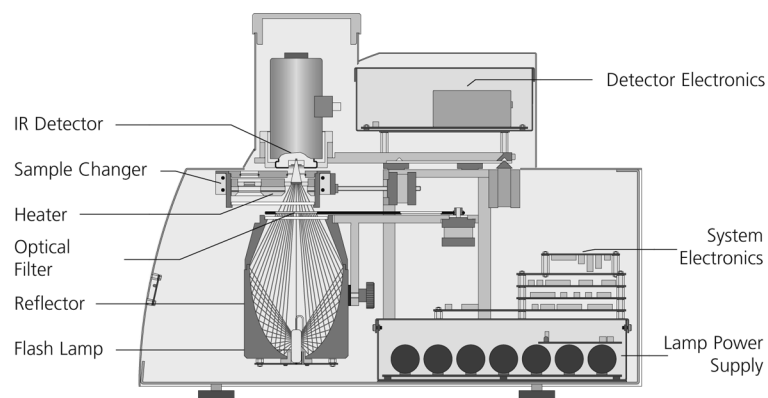


Figure 4.4 NETZSCH LFA 447 Nanoflash™ system (Courtesy of NETZSCH)

A small furnace is enclosed within the sample holder which can heat the samples so that they can be tested over a temperature range from room temperature up to 300°C. A Type K thermocouple is embedded into the sample holder to ensure an accurate temperature before an experiment is conducted. The low heat capacity of the sample holder allows for rapid changes in sample holder temperature. Thus, the Nanoflash apparatus is capable of collecting the temperature-dependent thermal diffusivity in a rapid manner.

A Xenon flash lamp is used to direct a short heat pulse of up to 10 J to the front side of the sample. The energy input to the sample cross-section is uniform at a flux up to 5 J/cm². The heat pulse is in the form of light at a broadband wavelength between 150 and 2000 nm and has a duration of 0.1, 0.28, or 0.5 milliseconds (93). The temperature of the back surface is recorded as a function of time using an infrared detector made of Indium and Antimonide (InSb) which can detect radiation between wavelengths of 2000 and 5000 nm (95). This is a narrow range typically used in infrared detection and thermal imaging in semiconductor materials. When subject to infrared radiation, electric current is generated in the sensor. The signal can be analyzed at frequencies up to 500 kHz. It is noted that the temperature of the detector and other surrounding components are controlled by a liquid nitrogen system. Components of the Nanoflash apparatus are illustrated in Figure 4.4.

The experimental method for testing of the thermal diffusivity of a material is done by applying heat to the front face of the sample, and measuring the temperature on the back face. The time it takes for the temperature of the back face to rise can be used to calculate thermal diffusivity of the sample. The through-plane measurement is illustrated in Figure 4.5 (96). The equipment is sketched in Figure 4.4. In the NETZSCH LFA 447 NanoflashTM system, the sample is aligned between the Xenon Flash Tube assembly and the IR detector.

The operation of the apparatus begins with placement of up to four samples into a test holder, which is shown in Figure 4.6. There are separate holders for testing circular samples with a diameter of 12.7 or 25.4 mm, or a 10 mm square laminate sample holder.

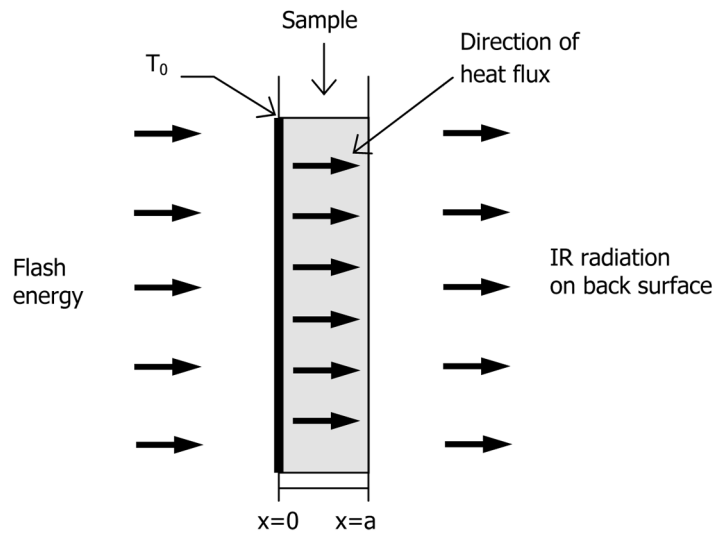


Figure 4.5 Through-plane measurement for Nanoflash instrument

For measurement of through-plane properties, 25.4 mm diameter disks were cut from a 76.2 mm diameter injection molded disk or a compression molded plate, (all 3.3 mm thick). A 25.4 mm diameter sample disk was placed in one of the 25.4 mm round disk holder. A 20.4 mm diameter mask was placed on top of the sample. This assembly was then placed in the 4 sample holder shown in Figure 4.6. For each unknown sample, a reference sample with similar thermal conductivity was placed in the 4 sample holder and run at the same time as the unknown sample. Reference materials include Pyrocera 9606 (3 mm thick), Pyrex 7740 (3 mm thick), and Vespel SP1 (2 mm thick). For all tests, the single layer measurement was used. Each specimen thickness and density was entered before starting a test. The tests were all conducted at 80°C using 304 V, medium pulse width, 100% filter, and 5 shots of the Xenon lamp on one sample. The results from the through-plane measurements included heat capacity, thermal diffusivity, and thermal conductivity at 80°C. The through-plane measurements were performed on 4 different disks for each formulation. In order to determine heat capacity, through plane measurements were performed before any in-plane measurements.

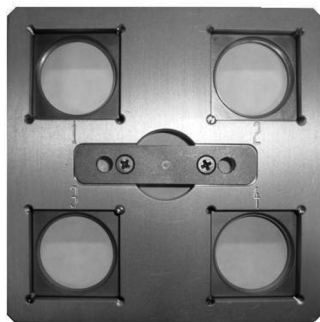
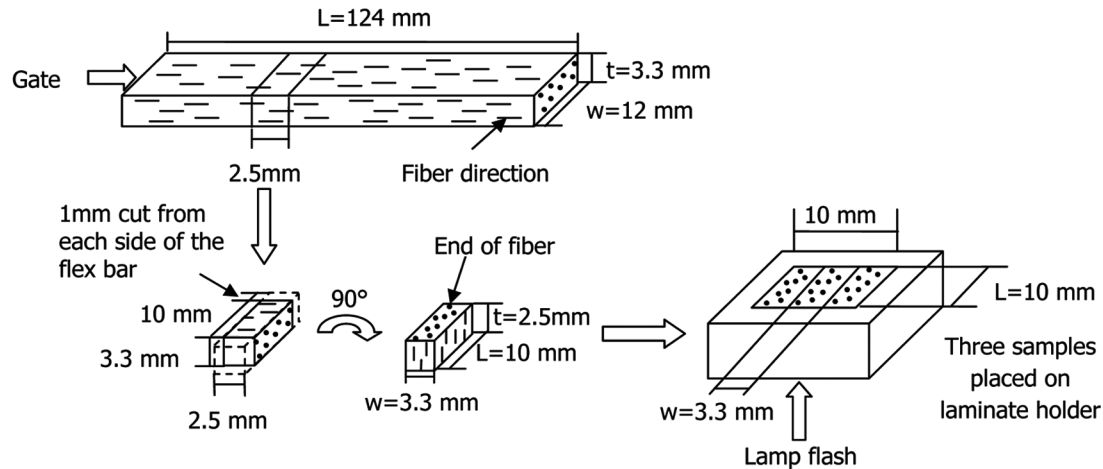


Figure 4.6 Nanoflash sample holder

For the in-plane thermal conductivity tests, 3.3 mm wide, 2.5 mm thick, 10 mm long test specimens were cut from the center of injection molded 3.3 mm thick, 12 mm wide, 124 mm long flexural test bars, as shown in Figure 4.7. In this figure, the typical flow of a fiber is shown to explain alignment.

For each formulation, 3 sets of 3.3 mm wide samples were placed together tightly to ensure no gaps were present between them, in the 10 mm by 10 mm laminate sample holder. A 7.8 mm round diameter mask was placed on top of the sample. This assembly was placed in one slot in the 4 sample holder (see Figure 4.6). To conduct the in plane tests, the single layer measurement was used. Each specimen thickness, density, and heat capacity (also called specific heat) was entered before conducting a test. The tests were conducted at 80°C using 304V, medium pulse width, 100% filter, and 5 shots of the Xenon lamp were conducted on one sample. The results from the in-plane measurements included thermal diffusivity and thermal conductivity at 80°C. The in-plane measurements were performed on 3 different sets of 3 mm wide 'sticks' for each formulation.



where:

w = width

t = thickness

L = length

Figure 4.7 Preparation of test specimens for in-plane thermal conductivity

All samples and reference materials were sprayed with 5 microns of graphite on all surfaces before placing the samples in the holder (93). The graphite allows the sample to absorb a larger amount of energy on the front face and intensifies the signal read on the back face.

First, the temperature at which the conductivity will be measured is set. After reaching the temperature set point, a flash pulse is directed five times at the front face of the sample over a period of time. An Analog/Digital converter amplifies and records a voltage reading for each 'shot of the Xenon lamp' (also called a trial). The energy pulse causes a temperature rise between 0.5 and 2°C on the back face of the sample. In order to maintain the temperature change in certain range, the measurement software allows the adjustment of light filters between the furnace and the flash lamp (96). The Cowan + pulse correction model was always used to analyze the measurement results.

4.4.2 Heat Capacity Theory

The specific heat of a material is defined as the amount of energy required to raise a unit mass of material by one unit of temperature at constant pressure,

$$C_p = \frac{Q}{m\Delta T} \quad (4.1)$$

where:

C_p = specific heat

m = mass

ΔT = change in temperature

Q = energy

The heat capacity of a sample can be measured using a reference sample and comparing the temperature rise of the reference sample to the sample of unknown heat capacity according to Equation 4.2 below. In this test, three different reference materials were used, depending on the sample to analyze. Pyroceram 9606 and Pyrex 7740 disks were used as reference for samples with high thermal conductivities. For samples with low conductivity, the reference was a Vespel SP1 disk. The properties for the reference materials are summarized in Table 4.1 (97-99):

$$C_{p,\text{sample}} = \frac{(mC_p\Delta T)_{\text{ref}}}{(m\Delta T)_{\text{sample}}} = \frac{(mC_p\Delta V)_{\text{ref}} G_{\text{sample}}}{(m\Delta V)_{\text{sample}} G_{\text{ref}}} \quad (4.2)$$

where:

C_p = specific heat

m = mass

ΔT = change in temperature

ΔV = change in voltage

G = amplifier gain

4.4.3 Thermal Diffusivity Theory

There is considerable literature on the flash method for thermal diffusivity (100-103). The usual models consider one-dimensional unsteady state heat conduction in a slab of thickness, a , at an initial temperature of zero. We will consider two limits—adiabatic and nonadiabatic.

In the adiabatic case, Parker et. al. (103) present a detailed theoretical discussion on the flash method for measuring thermal diffusivity. In their work, they extend the analysis of Carslaw and Jaeger (104) for an insulated slab of thickness a subject to a nonuniform initial temperature profile to a case with a step change initial condition due to a flux of radiant energy per unit area, Q over a length, g . The solution to the heat equation with this initial condition is given as:

$$T(x,t) = \frac{Q}{\rho C_p a} \left[1 + 2 \sum_{n=1}^{\infty} \cos\left(\frac{n\pi x}{a}\right) \frac{\sin(n\pi g/a)}{n\pi g/a} \exp\left(-\frac{n^2 \pi^2 \alpha t}{a^2}\right) \right] \quad (4.3)$$

In the limit where g is small at the rear face ($x = a$) we find that:

$$T(a,t) = \frac{Q}{\rho C_p a} \left[1 + 2 \sum_{n=1}^{\infty} (-1)^n \exp\left(-\frac{n^2 \pi^2 \alpha t}{a^2}\right) \right] \quad (4.4)$$

where:

ρ = Density of the material

a = Thickness of test specimen

x = Distance in the direction of heat transfer

t = Time

α = Thermal diffusivity of the material

Table 4.1
Properties for reference materials for Thermal Conductivity measurements

Reference material	Diameter (mm)	Thickness (mm)	Mass (g)	Density (g/cm ³)	Thermal Conductivity (W/m·K)	Specific heat (J/g·K)
Pyroceram 9606	25.38	3.007	3.9707	2.61	3.88	0.731
Pyrex 7740	25.35	2.975	3.3439	2.23	1.15	0.758
Vespel SP1	25.37	2.002	1.4539	1.44	0.35	1.130

It is noted that at time $t = 0$, $T = 0$ and as $t \rightarrow \infty$, $T = \frac{Q}{\rho C_p a}$. Thus, a sketch of a typical

temperature rise curve based upon Equation 4.4 can be seen in Figure 4.8 below, with

$T_{\max} = \frac{Q}{\rho C_p a}$. This graph passes through a temperature equal to half of the adiabatic

temperature rise, $T = \frac{Q}{2\rho C_p a}$ at a time given by:

$$t = \frac{0.1388a^2}{\alpha} \quad (4.5)$$

which can be rearranged to give the thermal diffusivity.

In the nonadiabatic case, at time $t = 0$, the front face is subject to a pulse of energy, $F(t)$. If this pulse is considered instantaneous, the resulting temperature at the back face is given by (102):

$$T(a,t) = 2T_f \sum_{n=1}^{\infty} \frac{\gamma_n^2 (\gamma_n^2 + L^2) \cos(\gamma_n)}{(\gamma_n^2 - L^2)(\gamma_n^2 + L^2 + \frac{\rho C_p a}{k})} \exp\left(-\frac{\gamma_n^2 kt}{\rho C_p a}\right) \quad (4.6)$$

In the above equation, T_f is the final adiabatic sample temperature rise. The thermal diffusivity α ,

has been replaced by $\frac{k}{\rho C_p}$, where k is the sample thermal conductivity, ρ is the sample density,

C_p is the heat capacity, t is time, and L is the Biot number for heat loss, $L = \frac{hk}{a}$, with h

representing a heat transfer coefficient that accounts for the combined effects of radiation, convection, and heat conduction to the surroundings. The values of γ_n are determined by solving the transcendental equation :

$$\tan \gamma_n = \frac{2\gamma_n L}{\gamma_n^2 - L^2} \quad (4.7)$$

The values of T_f , k , and L are adjusted to minimize the error between Equation 4.6 and the experimental data. It is noted that for thin and/or highly conductive samples, the finite width of the flash energy pulse can affect the estimate of thermal conductivity. This is because heating the front surface is not instantaneous relative to the characteristic heat conduction time through the sample. As such, a convolution integral of the pulse shape $F(t)$ and Equation 4.6 is used to give:

$$T_{\text{actual}}(a,t) = \int_0^t F(\tau) T(t-\tau) d\tau \quad (4.8)$$

It is noted that in Equation 4.8, τ is a dummy variable of integration for the convolution integral.

Equations 4.6 to 4.8 are based on the Cowan + pulse correction model (100), which is the model used by the Proteus LFA Analysis software to calculate thermal diffusivity.

Equation 4.6 can be used to plot the temperature rise if the values for thermal diffusivity and Biot number are known, as shown on Figure 4.9 for L values of 0.01, 0.05, 0.1 and 0.2. The data analysis software follows the inverse procedure, by determining diffusivity based on the temperature vs. time curve, depending on the measurement conditions and the sample properties. The software includes different models that consider radial and axial heat losses due to convection and radiation. These models are evaluated at 2000 different points along the measurement curve, using non-linear regression methods.

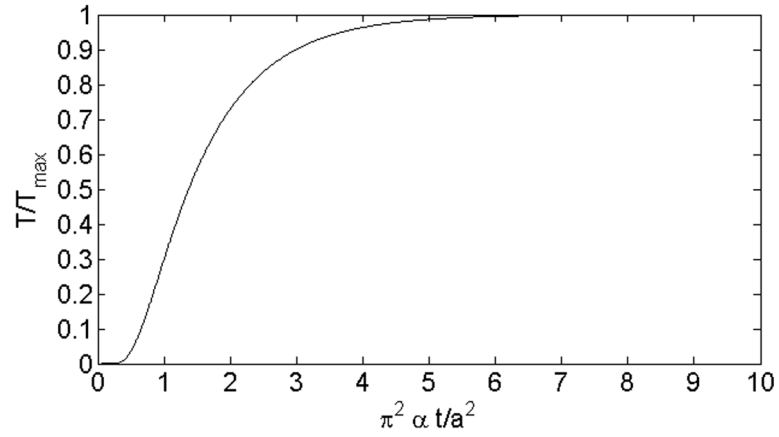


Figure 4.8 Temperature response of rear surface under adiabatic conditions

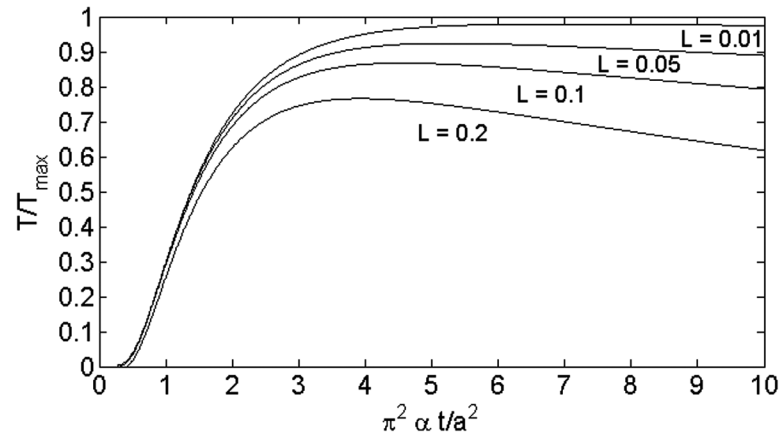


Figure 4.9 Temperature response under nonadiabatic conditions for varying values of the heat loss parameter L

4.5 Mechanical Properties Testing

4.5.1 Flexural Test Method

The flexural properties were determined with three-point loading under ambient conditions for all formulations, according to ASTM D 790 at a crosshead rate of 5.3 mm/min (49). Each rectangular sample was 3 mm thick, 127 mm long and 12.3 mm wide. The rectangular bar rests on two supports and the load was applied in the middle between the two supports, as shown in Figure 4.10. A span of 48 mm (corresponding to a 16:1 span/thickness ratio) was used in an Instru-Met (Union, NJ) Sintech screw-driven mechanical testing machine shown in Figure 4.11. The supports and the loading nose surfaces were cylindrical to prevent indentation on the sample or failure because of the stress concentration directly under the loading nose. Once the sample was loaded, deflection was measured with a linear variable displacement transducer. For each formulation, at least five samples were tested. A typical stress-strain curve for a typical polypropylene sample is shown in Figure 4.12.

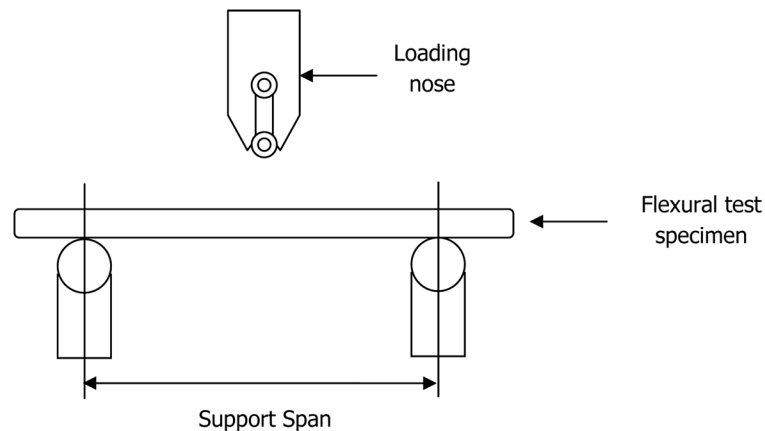


Figure 4.10 Three-Point Bend Test Method for Flexural Properties Measurement

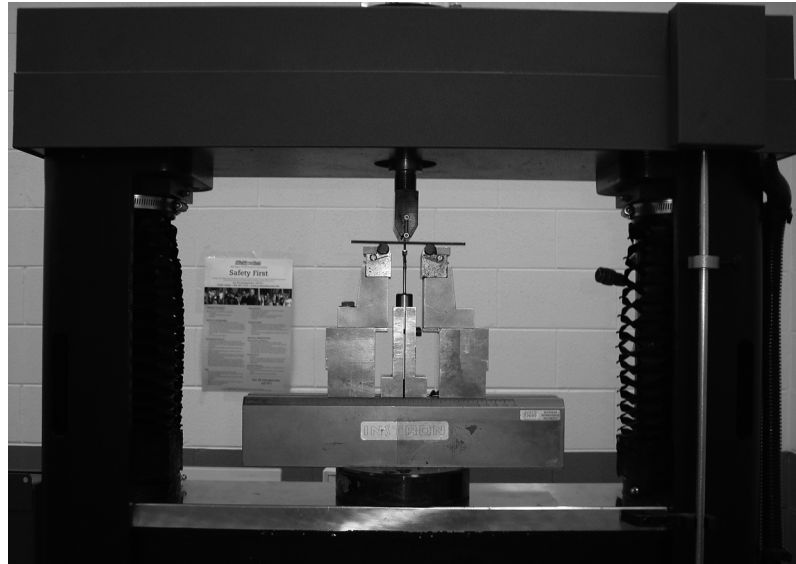


Figure 4.11 Instru-Met Sintech Screw Driven Mechanical Testing Machine set for 3-Point Bend Flexural Properties Testing

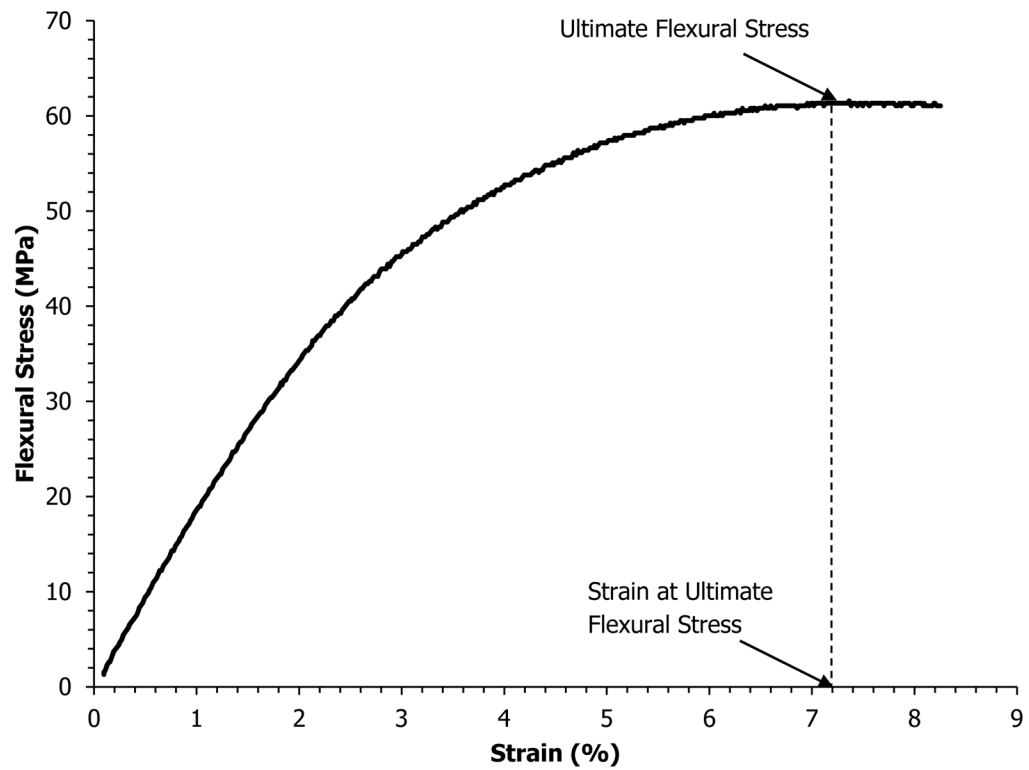


Figure 4.12 Typical Flexural Stress-Strain Curve for a Polypropylene Sample

4.5.2 Tensile Test Method

The tensile properties at ambient conditions from all formulations were determined with ASTM D 638 at a crosshead rate of 5 mm/min for reinforced plastics (48). The test specimens were ASTM Type I sample geometry, 165 mm long, 3.3 mm thick. An Instru-Met Sintech screw-driven mechanical testing machine was used and it is shown in Figure 4.13. Stress results were recorded by the testing machine. An extensometer was used to collect strain values. Using Microsoft Excel, the data recorded by the machine was used to create a stress-strain curve. A typical tensile stress-strain curve for a typical polypropylene sample is shown in Figure 4.14. For each formulation, at least five samples were tested. More tensile properties were obtained from the stress-strain curve, such as ultimate tensile stress and the strain (at ultimate tensile stress). The ultimate tensile stress or tensile strength is represented by the point where the stress-strain curve reaches its maximum value (see Figure 4.14). Since the pure polypropylene sample did not fracture, the point where the stress-strain curve shown in Figure 4.14 ends corresponds to a strain of 100%. In this example, the value for the ultimate tensile strength is 33 MPa and the strain at ultimate tensile strength is 8%.



Figure 4.13 Instru-Met Sintech Screw Driven Mechanical Testing Machine set for Tensile Properties Testing

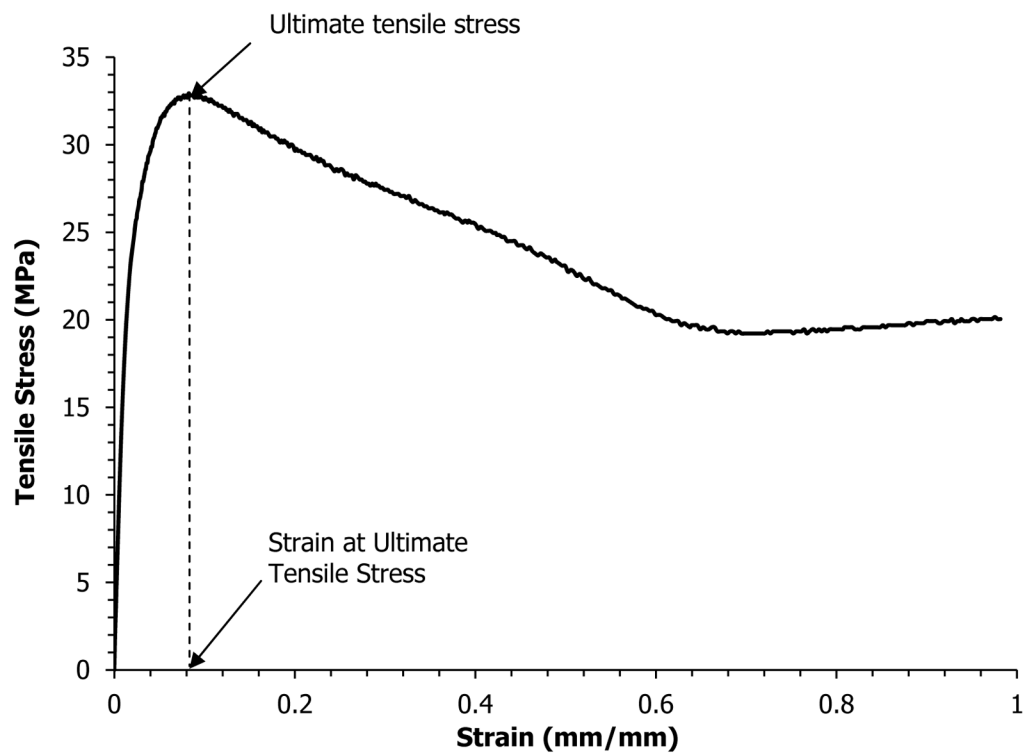


Figure 4.14 Typical Tensile Stress-Strain Curve for a Polypropylene Sample

4.5.3 Nanoscratch testing

To determine the adhesion of the filler particles to the polypropylene matrix, nanoscratch tests were performed on samples cut from the center of flexural specimens for the pure polypropylene and for the formulation containing 20 wt.% of Thermocarb TC-300 in polypropylene, as shown in Figure 4.15a. Then, the 3 mm-thick x 12.3 mm-long face was mounted in epoxy, as shown in Figure 4.15b.

Approximately 15 g of epoxy resin was added to the mold cup and allowed to cure overnight at room temperature. After curing, the sample in the epoxy resin was polished using a Buehler Ecomet 4 polishing wheel equipped with an Automet 2 Power Head and a 10-sample holder, shown in Figures 4.16 and 4.17, respectively. The sample holder was loaded with 8 additional neat epoxy samples to maintain an even load while polishing. The technical support department of Buehler provided a 5-step procedure used for polishing the samples, shown in Table 4.2. This procedure was followed for polishing both the polymer and the composite surfaces in epoxy.

Once the sample was mounted in epoxy and polished, it was tested with a MTS Nano Indenter XP shown in Figure 4.18. The typical test was run under a constant load of 40 mN. The scratch length was 500 μm at a speed of 10 $\mu\text{m/s}$. The data were collected at a rate of 5 Hz.

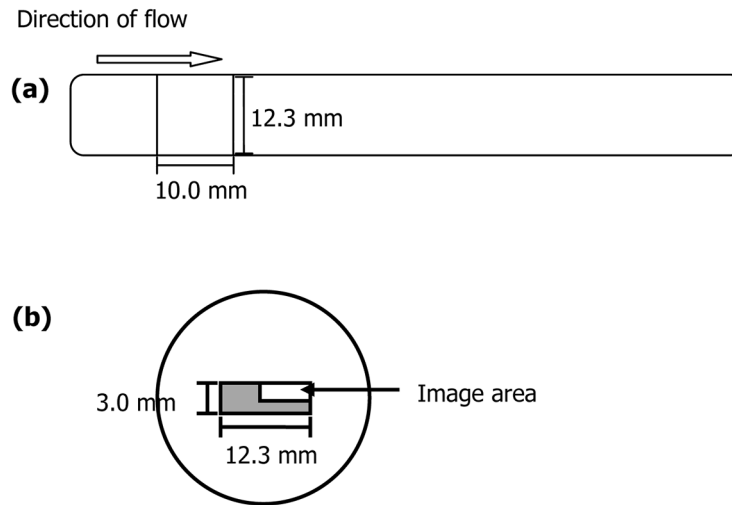


Figure 4.15 (a) Portion of Flexural Bar from where Nanoscratch Specimens were cut. (b) Sample Arrangement for Nanoscratch Testing

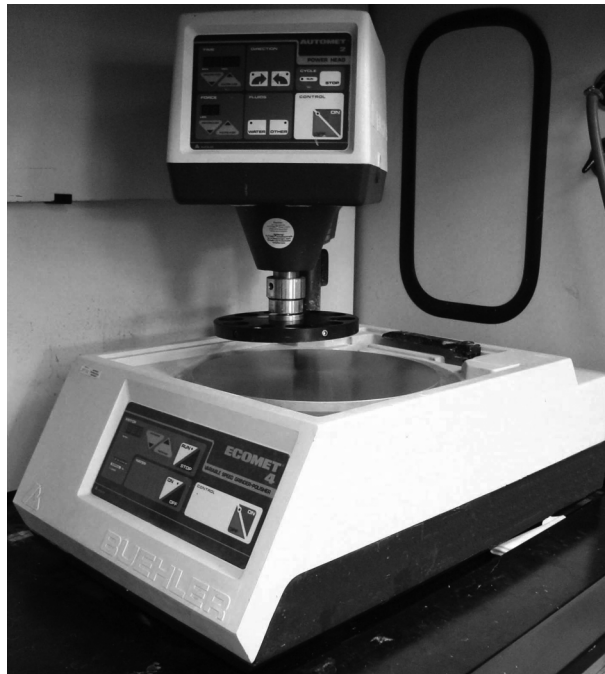


Figure 4.16 Polishing Apparatus for Nanoscratch Sample Preparation



Figure 4.17 10-Sample Holder Used in the Polishing Apparatus

For each sample, two sets of five scratches were made on each sample, and two samples of the composite containing 20 wt.% Thermocarb were tested. For the pure polypropylene, two sets of five scratches were made on one test specimen.

A Berkovich indenter was used for the tests with scratches made in the edge-forward direction, as shown in Figure 4.19. Data collected included the force on sample, penetration of the indenter

Table 4.2
Polishing procedure for preparing Nanoscratch test specimens

Polishing Surface	Lubricant	Abrasive	Time (min)	Force (lb)	RPM	Direction
CARBIMET ®	Water	SiC-320 grit	Until flat	5	230	Contrary to the sample holder rotation
CARBIMET ®	Water	SiC-600 grit	2	5	230	Contrary to the sample holder rotation
CARBIMET ®	Water	SiC-800 grit	2	5	230	Contrary to the sample holder rotation
TEXMET ® 1500	None	METADI ® Supreme-3µm	5	5	130	Contrary to the sample holder rotation
MICROCLOTH ®	None	MASTERPREP ®	3	5	130	Contrary to the sample holder rotation

relative to the surface of the sample, force along the scratch direction (friction force), and force normal to the scratch direction (lateral force). All the data were recorded with respect to distance along the scratch. The friction and lateral forces are also depicted in Figure 4.19.

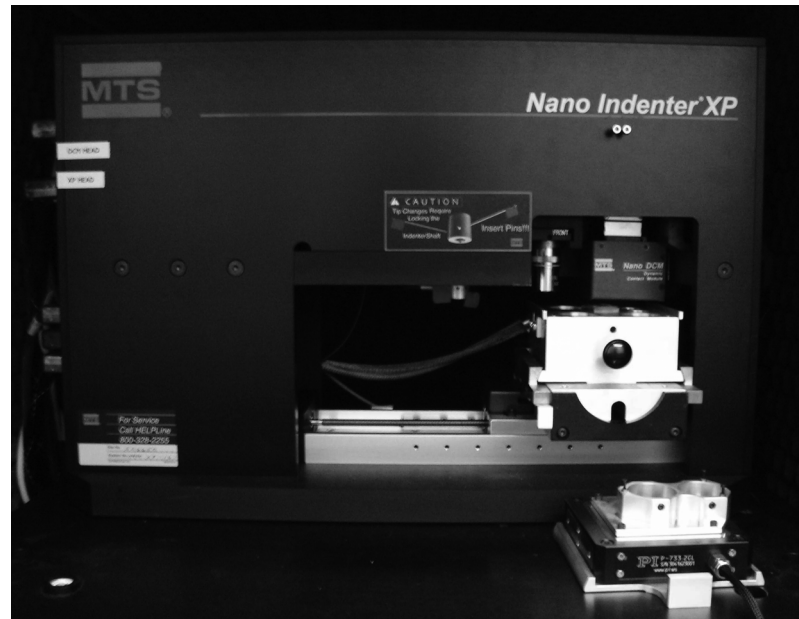


Figure 4.18 MTS Nano Indenter XP Used for Nanoscratch Testing

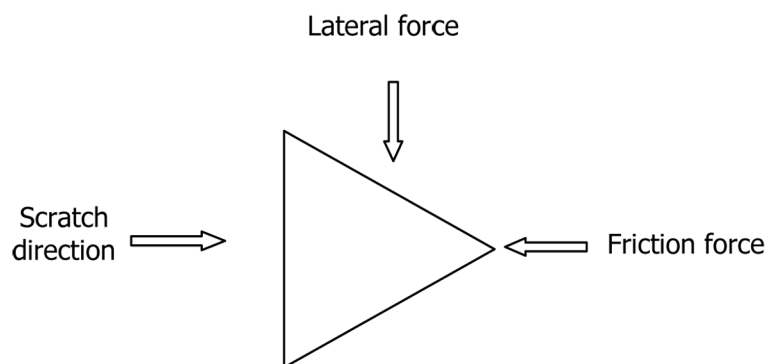


Figure 4.19 Scratch Direction Used in the Tests with the Berkovich Indenter

The nanoscratch test was performed in three steps:

- Original profile: A load of 20 μN was applied to the surface of the sample to determine the original morphology of the surface along the scratch path.
- Scratch segment: In this step, the depth measurements were corrected for roughness and initial slope of the sample by using information from the original profile.
- Residual profile: The corrections used in the scratch segment are also applied in this stage. In this project, the information of this stage was not used in the data analysis.

Equation 4.12 defines the crest factor, used to characterized the penetration during the scratch test (105). The measurement of the crest factor is used in analysis of waveforms as a measure of spikeness in the data, and is defined as the ratio of the peak amplitude to the root mean square of the penetration of the indenter in the composite surface:

$$\text{Crest factor} = \frac{|y_{\max} - y_{\min}|}{2\sqrt{\frac{1}{N} \sum_{j=0}^{N-1} y_j^2}} \quad (4.12)$$

where:

y_{\max} = maximum penetration along the scratch length

y_{\min} = minimum penetration along the scratch length

y = penetration (nm) along the scratch length

N = number of data points considered for a given scratch.

In this study, the data were collected over a scratch distance of 500 μm . The first and last 10 μm of the scratch length were not used in the data analysis for calculating the crest factor. This was done to neglect any end effects present at the beginning and end of the scratch length.

For the composite materials in this project, a shallow scratch depth indicates a high–stiffness, which corresponds to a filler–rich area, and a larger scratch depth indicates a lower stiffness, where the pure polymer matrix is present. Because the width of the groove generated by the scratch tip (ca. 30 μm) is large compared to the small size of the carbon black and carbon nanotubes, these composites could not be studied using the nanoscratch method. This method was only used in the composites containing synthetic graphite.

In order to compare the penetration to the scratch surface, photographs of the test specimens were taken using an Olympus BX 60 (Orangeburg, NY) optical microscope, equipped with an Olympus DP 10 video camera, both shown in Figure 4.20. The images were collected at a 200x magnification.

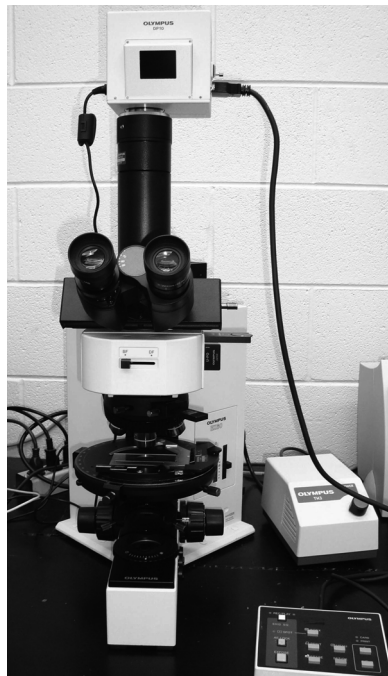


Figure 4.20 Olympus BX60 Reflected Light Microscope

Chapter 5: Experimental Results for Thermal Conductivity

Tests Using the Nanoflash Method

5.1 Introduction

It is known that polymers are characterized for being thermally and electrically insulating materials. However, these properties may be improved, thus allowing them to be used in other applications. One potential application for thermally conductive resins is for use as fuel cell bipolar plates. Bipolar plates serve the purpose of separating adjacent cells, while carrying hydrogen on one side, and oxygen from air on the other. Bipolar plates require high thermal and electrical conductivity to conduct the heat produced by the electrochemical reaction out of the fuel cell and to minimize ohmic losses.

The thermal conductivity of a polymer can be enhanced by addition of conductive filler materials, such as carbon or other metallic materials (44,59,75,106-116). Often a single type of carbon is used in thermosetting resins (often a vinyl ester) to produce a thermally and electrically conductive bipolar plate material (21,117-119). However, thermosetting resins cannot be remelted. Lately, the use of thermoplastic resins filled with carbon (i.e., polypropylene, liquid crystalline polymer, polyphenylene sulfide, polyethylene, etc.) has been considered for manufacturing fuel cell bipolar plates (72,120-123).

In this research work, carbon/polypropylene composites were developed and experiments were conducted to characterize their thermal properties. Polypropylene has been studied by several researchers for possible use for fuel cell bipolar plates (72,73). Polypropylene is a semi-crystalline thermoplastic with the possibility to be remelted and used again. The three different carbon fillers used in this project are carbon black, synthetic graphite and carbon nanotubes. The properties of these carbon fillers are explained more in detail in Chapter 3. In this chapter, we evaluate the effects and interactions of each filler on the thermal conductivity of the composite.

The results for the Nanoflash thermal conductivity tests described in Chapter 4 will be discussed in the following sections of this chapter. Appendix A summarizes the Nanoflash through-plane thermal conductivity results. The Nanoflash in-plane measurements for the thermal conductivity of the composites are shown in Appendix B.

5.2 Synthetic Graphite Length, Aspect Ratio and Orientation Results

The length and aspect ratio of the Thermocarb in the composites were typically 40 μm and 1.67, respectively. These results agree with the values corresponding to the raw Thermocarb and with prior work in nylon, polycarbonate and liquid crystal polymer matrices (23,33,34).

For the in-plane thermal conductivity samples, the synthetic graphite particles are primarily oriented in the in-plane measurement direction. In the composite samples used for through-plane thermal conductivity measurement, the fillers are primarily oriented transverse to the thermal conductivity measurement direction. These observations agree with prior work and photomicrographs can be seen elsewhere (22,23,29,33,34,124). Additional details in results for synthetic graphite length, aspect ratio and orientation can be found elsewhere (86).

5.3 Field Emission Scanning Electron Microscope (FESEM) Results

Figure 5.1 shows the carbon nanotubes (white fibers) and carbon black (spheres) in the sample containing all three filler types in polypropylene. The carbon nanotube network formed in the composite can be clearly observed in this figure.

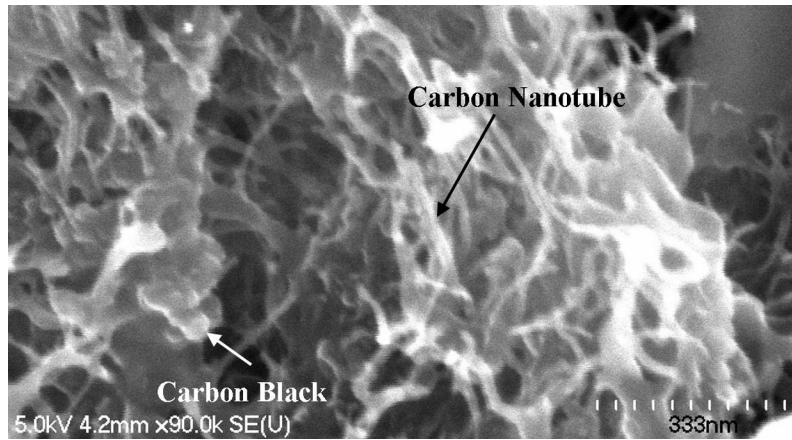


Figure 5.1 Field Emission Scanning Electron Microscope Photomicrograph of CB/SG/CNT in Polypropylene Composite

5.4 Nanoflash Through–Plane Thermal Conductivity Results

The thermal conductivity results on the through–plane direction are described in the following sections for single–filler formulations and for composites containing more than one filler in the polypropylene matrix. The results for each formulation are summarized in Appendix A, along with the composite density and specific heat values.

5.4.1 Through–Plane Thermal Conductivity Results for Single–Filler Formulations

Figures 5.2 and 5.3 show the mean through–plane thermal conductivity for the composites containing only varying amounts of single fillers as a function of filler volume fraction. These formulations correspond to those shown in Table 5.1 (shows mean, standard deviation and number of samples tested).

Figure 5.2 shows that carbon black (CB) does increase the through–plane thermal conductivity of the polymer from 0.21 W/m·K to 0.36 W/m·K for the composites containing 15 wt.% (8.1 vol.%) carbon black. Figure 5.2 also shows the through–plane thermal conductivity values for the CNT/PP composites. These composites have a higher conductivity as compared to the CB/PP

composites. Composites containing 15 wt.% (7.4 vol.%) carbon nanotubes have a thermal conductivity of 0.50 W/m·K.

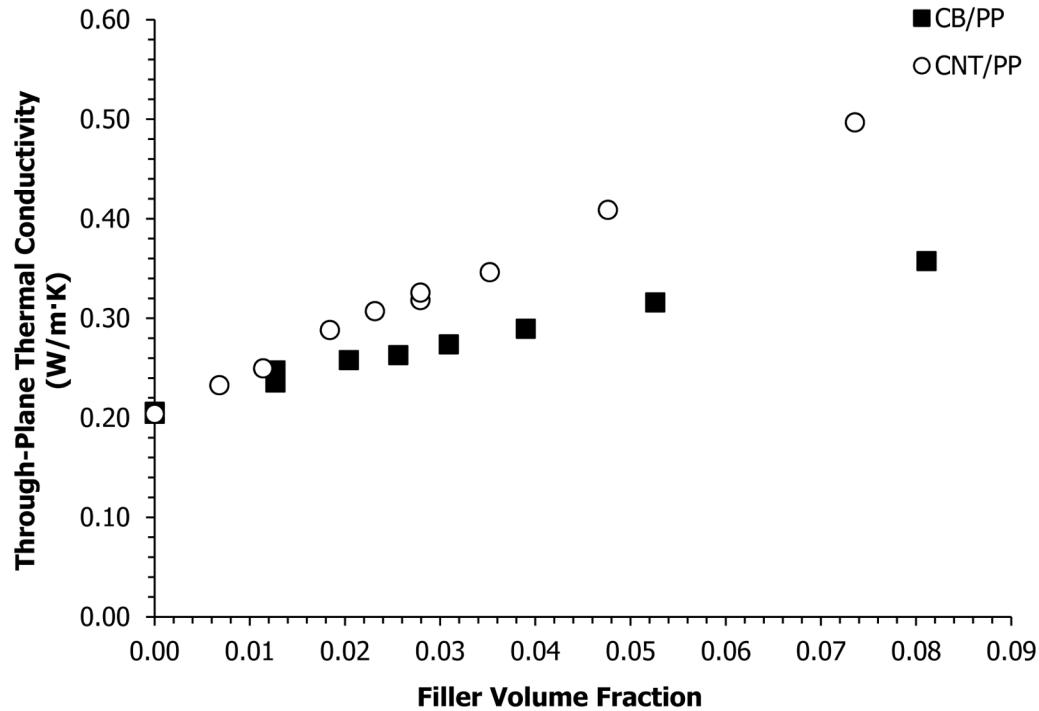


Figure 5.2 Single Filler Nanoflash Through-Plane Thermal Conductivity Results for CB/PP and CNT/PP Composites

Figure 5.3 shows the through-plane thermal conductivity for composites containing varying amounts of Thermocarb TC-300 synthetic graphite in polypropylene. Composites containing Thermocarb TC-300 synthetic graphite had the largest thermal conductivity values. The composite containing 80 wt.% (61.6 vol.%) synthetic graphite had a through-plane thermal conductivity of 9.47 W/m·K in polypropylene. Composites containing synthetic graphite likely had a higher thermal conductivity, compared to those containing carbon black and carbon nanotubes, due to the extremely high thermal conductivity of synthetic graphite (600 W/m·K in “a” crystallographic direction and approximately 60 W/m·K in “c” crystallographic direction). Again, recall that the highest single filler content that could be extruded and injection molded were 15 wt.% for carbon black, 80 wt.% for synthetic graphite, and 15 wt.% for carbon nanotubes.

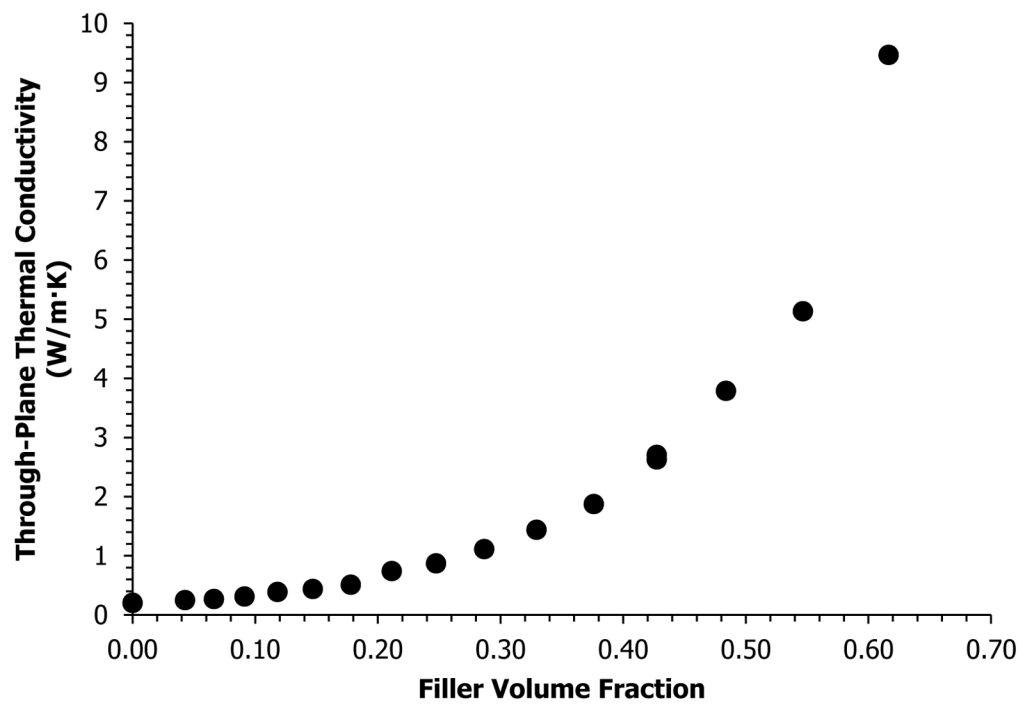


Figure 5.3 Single Filler Nanoflash Through-Plane Thermal Conductivity Results for SG/PP Composites

Table 5.1

Single Filler Loading Levels in Polypropylene and Nanoflash Thermal Conductivity Results

Formulation	Filler wt. %	Filler vol. %	Through-Plane Thermal Conductivity (W/m ² ·K)	In Plane Thermal Conductivity (W/m ² ·K)
PP	0.0	0.0	0.206 ± 0.002 n = 4	—
PP Replicate	0.0	0.0	0.204 ± 0.002 n = 4	—
2.5CB	2.5	1.27	0.248± 0.018 n = 4	0.287± 0.014 n = 3
2.5CB Replicate	2.5	1.27	0.236± 0.007 n = 4	0.301± 0.010 n = 3
4CB	4.0	2.04	0.258± 0.007 n = 4	0.325± 0.049 n = 3
5CB	5.0	2.56	0.263± 0.011 n = 4	0.345± 0.053 n = 3
6CB	6.0	3.09	0.274± 0.014 n = 4	0.355± 0.025 n = 3
7.5CB	7.5	3.90	0.290± 0.017 n = 4	0.369± 0.022 n = 3
10CB	10.0	5.26	0.316± 0.007 n = 4	0.411± 0.010 n = 3
15CB	15.0	8.11	0.358± 0.005 n = 4	0.457± 0.013 n = 3
10SG	10.0	4.27	0.252± 0.004 n = 4	0.567± 0.034 n = 3
15SG	15.0	6.62	0.269± 0.007 n = 4	0.664± 0.041 n = 3
20SG	20.0	9.13	0.312± 0.012 n = 4	0.928± 0.025 n = 3
25SG	25.0	11.81	0.390± 0.001 n = 4	1.236± 0.097 n = 3
30SG	30.0	14.69	0.439± 0.019 n = 4	1.507± 0.040 n = 3
35SG	35.0	17.79	0.512± 0.016 n = 4	2.068± 0.037 n = 3
40SG	40.0	21.13	0.743± 0.013 n = 4	3.108± 0.096 n = 3
45SG	45.0	24.74	0.872 ± 0.019 n = 4	4.167± 0.183 n = 3
50SG	50.0	28.66	1.114 ± 0.042 n = 4	5.434± 0.078 n = 3
55SG	55.0	32.93	1.441 ± 0.014 n = 4	7.172± 0.164 n = 3
60SG	60.0	37.60	1.875 ± 0.022 n = 4	9.428± 0.382 n = 3
65SG	65.0	42.70	2.707 ± 0.092 n = 4	12.999± 0.238 n = 3
65SG Replicate	65.0	42.70	2.631 ± 0.022 n = 4	12.528± 0.202 n = 3
70SG	70.0	48.40	3.788 ± 0.121 n = 4	17.947± 0.400 n = 3
75SG	75.0	54.66	5.134 ± 0.121 n = 4	24.420± 0.320 n = 3
80SG	80.0	61.64	9.468 ± 0.249 n = 4	33.565± 0.422 n = 3
1.5CNT	1.5	0.68	0.233± 0.007 n = 4	0.307± 0.014 n = 3
2.5CNT	2.5	1.14	0.250± 0.009 n = 4	0.340± 0.043 n = 3
4CNT	4.0	1.84	0.288± 0.006 n = 4	0.390± 0.023 n = 3
5CNT	5.0	2.31	0.307± 0.012 n = 4	0.395± 0.007 n = 3
6CNT	6.0	2.79	0.318± 0.008 n = 4	0.424± 0.021 n = 3
6CNT Replicate	6.0	2.79	0.326± 0.015 n = 4	0.451± 0.004 n = 3
7.5CNT	7.5	3.52	0.346± 0.006 n = 4	0.492± 0.011 n = 3
10CNT	10.0	4.76	0.409± 0.008 n = 4	0.619± 0.011 n = 3
15CNT	15.0	7.36	0.497± 0.023 n = 4	0.837± 0.068 n = 3

5.4.2 Factorial Design Analysis

Table 5.2 shows the factorial design formulations. For all fillers, the low loading level was zero wt.%. The high loading levels varied for each filler. The high loading levels were 2.5 wt.% for Ketjenblack EC-600 JD carbon black, 65 wt.% for Thermocarb TC-300 synthetic graphite, and 6 wt.% for FIBRIL™ carbon nanotubes. Because this project focuses on producing highly conductive composites, the loading levels were chosen so that the filler amounts would produce conductive composites, while still allowing the composite material to have a low enough viscosity to be extruded and injection molded into test specimens ($< 300 \text{ Pa}\cdot\text{s}$ at 230°C and shear rate of 500 s^{-1}). Table 5.3 shows the wt.% and the corresponding vol.% for all of the factorial design formulations (original and replicate).

Table 5.3 shows the mean, standard deviation, and number of specimens tested for the factorial design formulations (original and replicate). Table 5.3 shows that the composite containing all three fillers has a through-plane thermal conductivity of $8.5 \text{ W/m}\cdot\text{K}$. Using these results, an analysis of the factorial design was conducted using the mean through-plane thermal conductivity in units of $\text{W/m}\cdot\text{K}$ as the response. This analysis was performed using the Minitab version 13 Statistical Software package. For this analysis, the effects and P values for the thermal conductivity results were calculated. Small P values indicate that a factor (filler in this case) may have a significant effect on the composite thermal conductivity (125). For all statistical calculations, the 95% confidence level was used.

Factorial designs were used in the project since they are the most efficient type of experiment to determine the effect of each filler and any possible interactions between fillers. By using factorials, one can determine the effect that each factor (filler) has on the system by calculating a single value to quantify the change in thermal conductivity as the weight percent of filler is

Table 5.2
Filler Loadings in Factorial Design Formulations

Formulations	Ketjenblack wt. %	Thermocarb wt. %	FIBRIL™ wt. %
No filler	0	0	0
2.5CB	2.5	0	0
65SG	0	65	0
6CNT	0	0	6
2.5CB*65SG	2.5	65	0
2.5CB*6CNT	2.5	0	6
65SG*6CNT	0	65	6
2.5CB*65SG*6CNT	2.5	65	6

Table 5.3
Filler Loadings in Factorial Design Formulations and Thermal Conductivity Results

Formulations	Constituents			Through–Plane Thermal Conductivity (W/m·K)
No filler (PP) Original Replicate	PP	Wt. % 100	Vol. % 100	0.206 ± 0.002 n = 4 0.204 ± 0.002 n = 4
2.5CB Original Replicate	CB PP	Wt. % 2.5 97.5	Vol. % 1.3 98.7	0.248 ± 0.018 n = 4 0.236 ± 0.007 n = 4
65SG Original Replicate	SG PP	Wt. % 65 35	Vol. % 42.7 57.3	2.707 ± 0.092 n = 4 2.631 ± 0.022 n = 4
6CNT Original Replicate	CNT PP	Wt. % 6 94	Vol. % 2.8 97.2	0.318 ± 0.008 n = 4 0.326 ± 0.015 n = 4
2.5CB*65SG Original Replicate	CB SG PP	Wt. % 2.5 65 32.5	Vol. % 2.1 43.6 54.3	3.537 ± 0.037 n = 4 3.548 ± 0.074 n = 4
2.5CB*6CNT Original Replicate	CB CNT PP	Wt. % 2.5 6 91.5	Vol. % 1.3 2.8 95.9	0.362 ± 0.017 n = 4 0.357 ± 0.005 n = 4
65SG*6CNT Original Replicate	SG CNT PP	Wt. % 65 6 29	Vol. % 45.2 4.7 50.1	7.446 ± 0.220 n = 4 7.554 ± 0.160 n = 4
2.5CB*65SG*6CNT Original Replicate	CB SG CNT PP	Wt. % 2.5 65 6 26.5	Vol. % 2.2 46.2 4.8 46.8	8.503 ± 0.029 n = 4 8.469 ± 0.266 n = 4

increased. These calculated effects can then be ranked to determine which fillers and combinations of fillers produced a larger change (125).

The effects and P values are given in Table 5.4, showing the values for all of the filler combinations. Further investigation of Table 5.4 yields some important information regarding the effects that fillers have on composite thermal conductivity. First, for the composites containing only single fillers, a statistically significant increase (positive effect term) in composite through-plane thermal conductivity ($P < 0.05$) was observed for the three fillers. The largest effect in through-plane thermal conductivity of composite was produced by synthetic graphite, followed by carbon nanotubes and then carbon black. Synthetic graphite causes the largest increase (largest effect term) in composite thermal conductivity. Second, two of the combinations of two different fillers cause a statistically significant increase in composite thermal conductivity ($P < 0.05$). Multiple filler formulations containing carbon nanotubes and synthetic graphite caused the largest increase in through-plane thermal conductivity of the composite. The combination of these fillers increased the thermal conductivity, as the effect terms shown in Table 5.4 are positive. For example, since the combination of synthetic graphite and carbon nanotubes produced a statistically significant result, a positive synergistic effect was observed in the thermal conductivity of the composite. From this statistically significant result, we can expect the thermal conductivity to be higher than the additive effect of each single filler. This can be justified as conductive paths may be formed between carbon filler particles (125). In prior work, combinations of carbon black and synthetic graphite have also increased composite thermal conductivity in nylon 6,6, polycarbonate, and liquid crystal polymer based resins (23,29).

Table 5.4
Factorial Design Analysis for Through-plane Thermal Conductivity (W/m·K)

Term	Effect	P
Constant		0.000
2.5CB	0.484	0.000
65SG	5.267	0.000
6CNT	2.502	0.000
2.5CB*65SG	0.446	0.000
2.5CB*6CNT	0.028	0.139
65SG*6CNT	2.385	0.000
2.5CB*65SG*6CNT	0.028	0.142

5.5 In-Plane Thermal Conductivity Results

Table 5.1 shows the in-plane thermal conductivity (mean, standard deviation, and number of specimens tested) results for the formulations containing varying amounts of single fillers. Appendix B shows the in-plane thermal conductivities of the different composite formulations, as well as the density and specific heat values.

Figure 5.4 shows the mean in-plane thermal conductivity for the composites containing varying amounts of only carbon black or only carbon nanotubes in polypropylene. Figure 5.4 shows that carbon black does increase the thermal conductivity of the polymer from 0.21 W/m·K to 0.46 W/m·K for the composites containing 15 wt.% (8.1 vol.%) carbon black. Figure 5.4 also shows the thermal conductivity values for the CNT/PP composites. These composites have a higher conductivity as compared to the CB/PP composites. Composites containing 15 wt.% (7.4 vol.%) carbon nanotubes have a thermal conductivity of 0.84 W/m·K. In all cases, due to the orientation of the fillers in the composite sample, the in-plane thermal conductivity for the same formulation is slightly higher than the through-plane thermal conductivity (see Table 5.1).

Figure 5.5 shows the mean in-plane thermal conductivity for the composites containing varying amounts of only synthetic graphite in polypropylene. The in-plane thermal conductivity for the composite containing 75 wt.% (54.7 vol.%) and 80 wt.% (61.6 vol.%) synthetic graphite in

polypropylene are 24.4 and 33.6 W/m·K, respectively. These values are higher than the desired bipolar plate thermal conductivity of at least 20.0 W/m·K. Once again, due to the orientation of the fillers, the in-plane thermal conductivity for the same formulation is higher than the through-plane thermal conductivity (see Table 5.1).

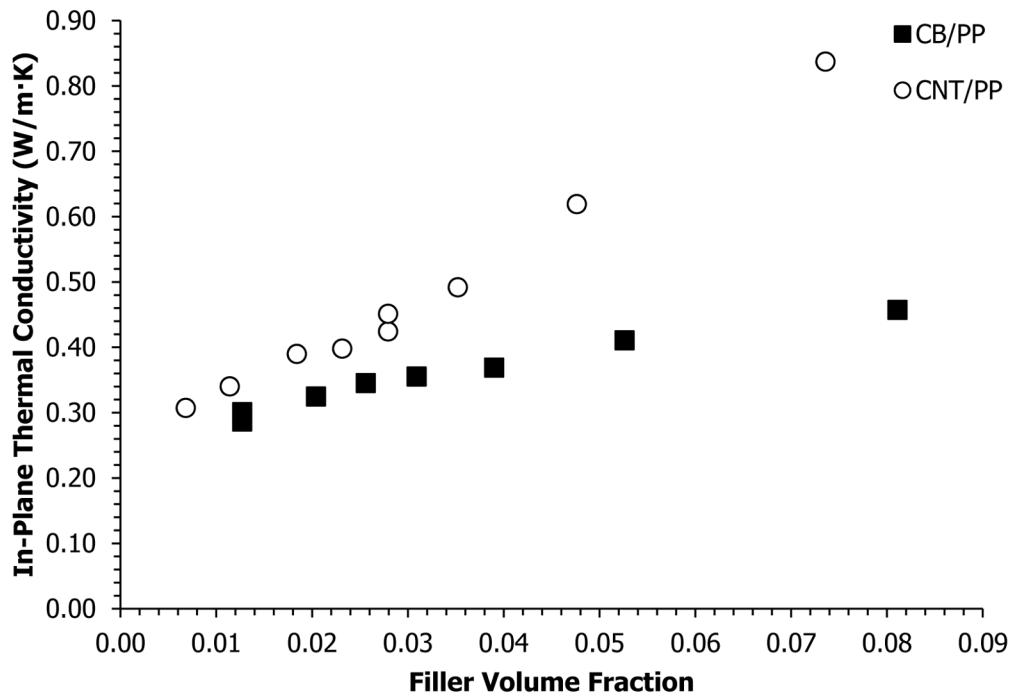


Figure 5.4 Single Filler Nanoflash In-Plane Thermal Conductivity Results for CB/PP and CNT/PP Composites

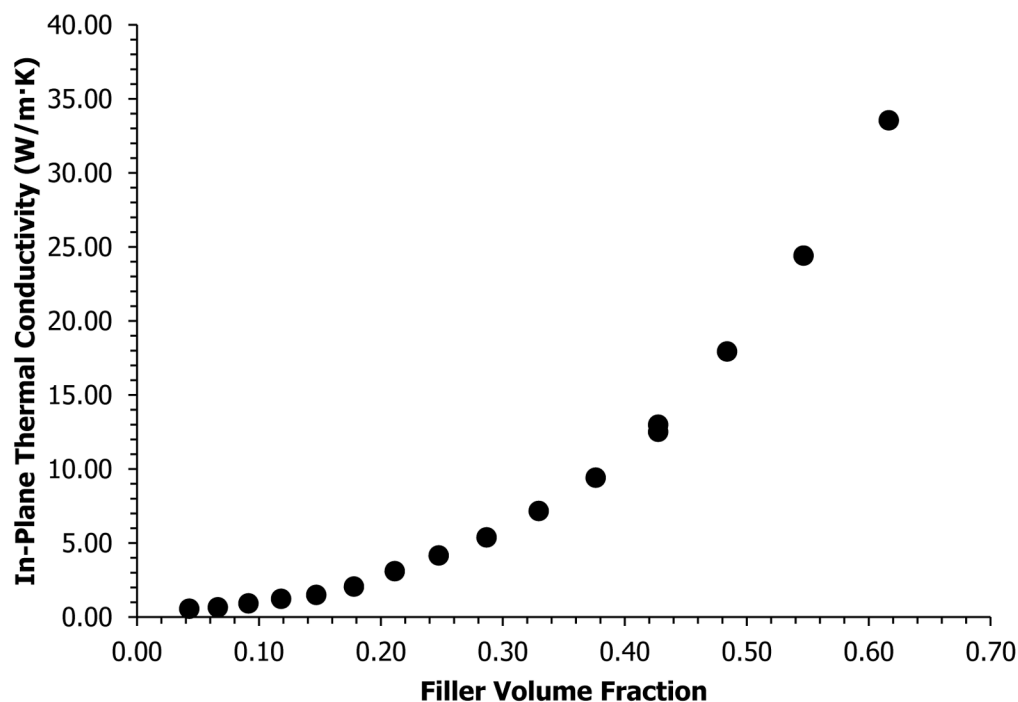


Figure 5.5 Single Filler Nanoflash In-Plane Thermal Conductivity Results for SG/PP Composites

The in-plane thermal conductivity for the formulation containing carbon black and carbon nanotubes (2.5CB*6CNT) was 0.477 ± 0.014 W/m·K, with $n = 3$ for the original and 0.481 ± 0.019 W/m·K, with $n = 3$ for the replicate. These values are slightly higher than the through-plane values (see Table 5.3) for these same formulations. The composites containing all the other combinations of different carbon fillers (see Table 5.2) could not be injection molded into flexural test bars (material was too viscous to fill the mold). Hence, the composite containing all three fillers in polypropylene (2.5CB*65SG*6CNT), which is most likely the most conductive formulation containing combination of fillers, was compression molded at 6.9 MPa at 230°C. The in-plane thermal conductivity is 37.0 W/m·K (standard deviation = 0.6 W/m·K for 3 samples tested) and the through-plane thermal conductivity is 8.54 W/m·K (standard deviation = 0.21 W/m·K for 4 samples tested) for this 3 filler compression molded sample. Once again, the in-plane thermal conductivity of the 3 filler compression molded sample is above the desired bipolar

plate thermal conductivity value of 20 W/m·K. The through-plane results are similar for the injection and compression molded 3 filler formulation.

5.6 Conclusions

The object of this research was to determine the effects and interactions of each filler on composite thermal conductivity. For the composites containing single carbon fillers, the largest increase in the thermal conductivity was observed for synthetic graphite, followed by carbon nanotubes, and then carbon black. For multiple filler formulations, the combination of synthetic graphite with carbon nanotubes, followed by the combination of synthetic graphite with carbon black, caused a statistically significant increase in composite through-plane thermal conductivity, e.g. when synthetic graphite and carbon nanotubes are combined into a composite, the composite thermal conductivity is higher than what would be expected from the additive effect of each single filler. This can be explained by the possible formation of thermally conductive pathways with these carbon fillers, resulting in an increased composite thermal conductivity. The in-plane thermal conductivity for the composite containing 75 wt.% (54.7 vol.%) and 80 wt.% (61.6 vol.%) synthetic graphite in polypropylene was 24.4 W/m·K and 33.6 W/m·K, respectively, which exceed the previous technical goal of 20.0 W/m·K, set by the Department of Energy for thermal conductivity of fuel cell bipolar plates. This thermal conductivity goal was also exceeded by the compression molded composite containing 2.5CB*65SG*6CNT, with an in plane thermal conductivity of 37 W/m·K.

Chapter 6: Thermal Conductivity Modeling

6.1 Introduction

In this chapter, we use models to estimate the composite thermal conductivity of carbon-filled polypropylene (PP) composites. The most versatile is Nielsen's model, used when dealing with conductive composites formed with short fiber/particulate fillers. This model has input parameters such as the thermal conductivities and concentrations of each component as well as filler properties such as orientation, packing, and aspect ratio (126-129). The modeling results will be compared with experimental results obtained using the Guarded Heat Flow Meter and the Flash test method methods, described in Chapter 4.

6.2 Thermal Conductivity Modeling Background

Nielsen's model (47,128) is based on the model for the viscosity of a fluid with dispersed spheres by Albert Einstein. However, it was applied for prediction of the elastic modulus of a two-phase composite. Lewis and Nielsen developed an improved model for the elastic modulus from the Halpin-Tsai equation (47). Nielsen added a parameter, Ψ , to the Halpin-Tsai equation, which considers the orientation and packing of the filler in the matrix material. Another modification introduced by Nielsen was the method for determining the model parameters using tables to introduce the effect of filler shape and orientation. While the first one only depended on the shape of the filler particles, the latter also included the orientation of the filler. This model was later adapted for thermal conductivity prediction.

6.2.1 Through-Plane Thermal Conductivity Modeling

In this work the next set of equations, known as Nielsen's Model, will be optimized to estimate the through-plane thermal conductivity k_{through} (W/m·K) of the conductive resins used in this project:

$$k_{\text{through}} = k_1 \frac{(1 + AB\phi_2)}{(1 - B\psi\phi_2)} \quad (6.1)$$

$$B = \frac{\left(\frac{k_2}{k_1} - 1 \right)}{\left(\frac{k_2}{k_1} + A \right)} \quad (6.2)$$

$$\psi \cong 1 + \frac{1 - \phi_m}{\phi_m^2} \phi_2 \quad (6.3)$$

where:

k_1 = Thermal conductivity of polypropylene, W/m·K

k_2 = Thermal conductivity of the carbon filler, W/m·K

ϕ_i = Volume fraction (i=1 for polypropylene, i=2 for carbon filler)

ϕ_m = Maximum packing fraction (See Table 6.2) (128)

A is a factor depending on shape and orientation of the filler, and B is a factor that considers the relative conductivity of both the polymer and the carbon filler. The A parameter has been determined for some filler types and orientation, which are shown in Table 6.1 (128).

McGee and McCullough (129) give the following expression for the ψ parameter, dependent on the volume fractions of both components and ϕ_m . In this project, the model using Equation 6.4 will be referred to as 'Modified Nielsen's Model'. Equation 6.4 was derived originally for prediction of tensile modulus by McGee and McCullough when performing experiments with natural silica in epoxy resin, and for glass spheres in epoxy and polyester resin (129).

Table 6.1

Typical A values for different filler shapes and orientation (128)

Filler Type	Aspect Ratio	A
Cubes	1	2
Spheres	1	1.5
Random Fibers	2	1.58
Random Fibers	4	2.08
Random Fibers	6	2.80
Random Fibers	10	4.93
Random Fibers	15	8.38
Uniaxially-oriented Fibers	–	$2L/D^a$
Uniaxially-oriented Fibers	–	0.5^b

^a Heat flow in direction of fibers^b Heat flow transverse to fiber direction

$$\psi \cong 1 + \frac{\phi_1}{\phi_m} \left[\phi_m (1 - \phi_1) + (1 - \phi_m) \phi_1 \right] \quad (6.4)$$

A standardized error, ε , was determined with Equation 6.5. The value obtained was used to compare experimental data with the values calculated using Nielsen's model.

$$\varepsilon = \frac{\sum_{i=1}^n (y_i - y_{\text{model}_i})^2}{\sum_{i=1}^n y_i^2} \quad (6.5)$$

where:

y_i = thermal conductivity result obtained experimentally (38,86)

y_{model} = thermal conductivity value determined by using Nielsen's model, W/m·K

and i indicates summation of the thermal conductivities for different concentrations of the same filler. If a value of $\varepsilon = 0$ is to be found, the experimental data will be identical to that obtained

Table 6.2Maximum Packing Fraction ϕ_m of common filler types (128)

Filler Shape	Packing order	ϕ_m
Spheres	Hexagonal Close	0.7405
Spheres	Face-centered Cubic	0.7405
Spheres	Body-centered Cubic	0.60
Spheres	Simple Cubic	0.524
Spheres	Random Loose	0.601
Spheres	Random Close	0.637
Irregular	Random Close	~0.637
Fibers	Three-dimensional Random	0.52
Fibers	Uniaxial Hexagonal Close	0.907
Fibers	Uniaxial Simple Cubic	0.785
Fibers	Uniaxial Random	0.82

applying the model. Nielsen's model requires the individual thermal conductivities of the matrix and fillers.

6.2.2 In-Plane Thermal Conductivity Modeling

It was also desired as part of this work to develop a simple model for the in-plane thermal conductivity, k_{in} . The work of Miller et al. (26) showed that at higher loading levels (up to 65 vol.%), Vectra liquid crystal polymer composites containing Thermocarb synthetic graphite exhibit an exponential dependence on the filler volume fraction. This model was only applied to model the data obtained through the Flash Method.

$$\sqrt{k_{in}k_{through}} = Ce^{D\phi_2} \quad (6.6)$$

where:

k_{in} =Calculated in-plane thermal conductivity of the composite

$k_{through}$ =Calculated through-plane thermal conductivity of the composite

ϕ_2 = Filler volume fraction

In this model, the parameters C and D were optimized to minimize the error between experimental and calculated results.

6.2.3 Multiple Filler Thermal Conductivity Modeling

For the experimental results obtained from the Flash method, we predicted the through-plane and in-plane thermal conductivities of formulations containing multiple fillers. In work performed by Weber (127), the original Nielsen's model for through-plane thermal conductivity was modified for use in prediction of through-plane thermal conductivity of composites with multiple fillers. The equations for multiple fillers are shown below:

$$k_{\text{through}} = k_1 \frac{(1 + \sum_{i=2}^n A_i B_i \phi_i)}{(1 - \sum_{i=2}^n B_i \psi_i \phi_i)} \quad (6.7)$$

$$B_i = \frac{\left(\frac{k_i}{k_1} - 1 \right)}{\left(\frac{k_i}{k_1} + A_i \right)} \quad (6.8)$$

$$\psi \cong 1 + \frac{\phi_1}{\phi_{m,i}} \left[\phi_{m,i} \phi_i + (1 - \phi_{m,i}) \phi_1 \right] \quad (6.9)$$

where:

k_1 = Thermal conductivity of polypropylene, W/m·K

k_i = Thermal conductivity of the i^{th} carbon filler, W/m·K

ϕ_1 = Volume fraction of polypropylene.

ϕ_i = Volume fraction of the i^{th} carbon filler.

$\phi_{m,i}$ = Maximum volume fraction of the i^{th} carbon filler.

The exponential function proposed for modeling in-plane thermal conductivity can also be extended for formulations containing multiple fillers, as shown in Equation 6.10. Since the test specimens for in-plane thermal conductivity were obtained from flexural bars (see Chapter 4 for further details), the only formulation that could be injection-molded was the one containing carbon black and carbon nanotubes. Therefore, Equation 6.10 only considers the volume fractions of these two fillers:

$$\sqrt{k_{\text{in}} k_{\text{through}}} = E e^{F\phi_{\text{CB}} + G\phi_{\text{CNT}}} \quad (6.10)$$

In this equation, the parameter E was averaged from the values of C used in Equation 6.6 for both carbon black and carbon nanotubes. F and G correspond to the values of D used for carbon black and carbon nanotubes, respectively in Equation 6.6.

6.3 Through-Plane Thermal Conductivity Modeling Results for Single-Filler Formulations

6.3.1 Guarded Heat Flow Meter Method

An experimental value of 0.205 W/m·K was obtained from the literature for the polypropylene matrix (47). For CB, the thermal conductivity is 2.1 W/m·K (130,131). For SG, the thermal conductivity is 600 W/m·K (80,81). For multiwalled CNT, the thermal conductivity reported in the literature ranges from 20 to 3000 W/m·K (132-136). For our modeling work, we used a conservative estimate of 20 W/m·K. When Nielsen's model is applied to predict the thermal conductivity of composite materials, fixed values are assigned for the parameters A and ϕ_m .

These values are obtained from the literature for dilute systems (low filler loading) (29,127,128) and typical values are 1.5 for spheres and less than 10 for most random fibers with an aspect ratio less than 15.4 (29).

In this project, using higher values of A is allowed since the composites produced have high filler concentrations. The A value used in the model is therefore an effective value for the composite (137,138). The values of ϕ_m are restricted to be above the maximum loading tested in our experiments and less than a larger value, which would represent an upper limit to the filler concentration that could be processed. Hence, the constraints on ϕ_m were set as follows:

$$\text{Carbon Black (CB)} : 0.0811 < \phi_m < 0.20$$

$$\text{Carbon Nanotubes (CNT)} : 0.0736 < \phi_m < 0.20$$

$$\text{Synthetic Graphite (SG)} : 0.616 < \phi_m < 0.850$$

The parameters A and ϕ_m used in Equations 6.1–6.3 were modified by using a two-parameter optimization to minimize the standardized error calculated from Equation 6.5. To calculate the parameter ψ for modeling the experimental results obtained through the guarded heat flow meter method, we used Equation 6.3, proposed by Nielsen. The results found were found to be (139):

$$\text{Carbon Black (CB)} : A = 70.5; \phi_m = 0.20; \varepsilon = 7.6 \times 10^{-4}$$

$$\text{Carbon Nanotubes (CNT)} : A = 15.7; \phi_m = 0.20; \varepsilon = 7.3 \times 10^{-4}$$

$$\text{Synthetic Graphite (SG)} : A = 8.4; \phi_m = 0.74; \varepsilon = 2.2 \times 10^{-3}$$

Figures 6.1 to 6.3 show a comparison between experimental data and the model results. We can see that for the three fillers, the results obtained by Nielsen's model show good agreement to the experimental data. In comparison to previous modeling research, the A value for CB/Vectra composites ($A = 1720$) (131) was significantly higher than that for the CB/PP composites ($A = 70$) but the ϕ_m values were similar. For SG/Vectra composites, the A and ϕ_m values were similar to those reported here ($A = 8.5$) and ($\phi_m = 0.8$) (130,140).

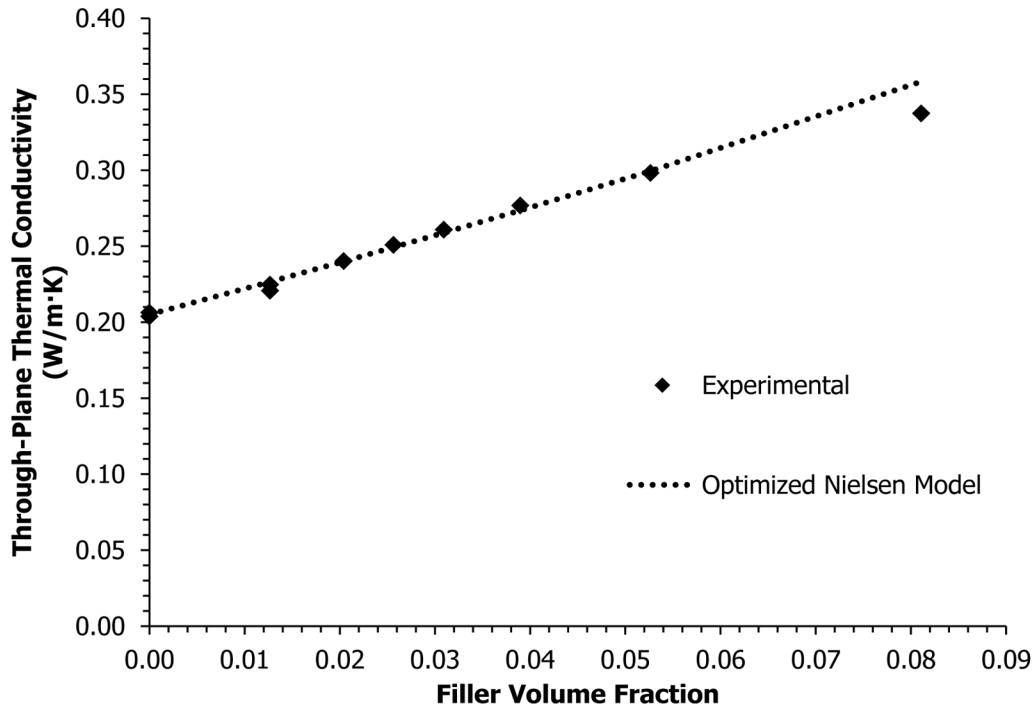


Figure 6.1 Experimental and theoretical through-plane thermal conductivities for CB/PP composites for the Guarded Heat Flow Meter

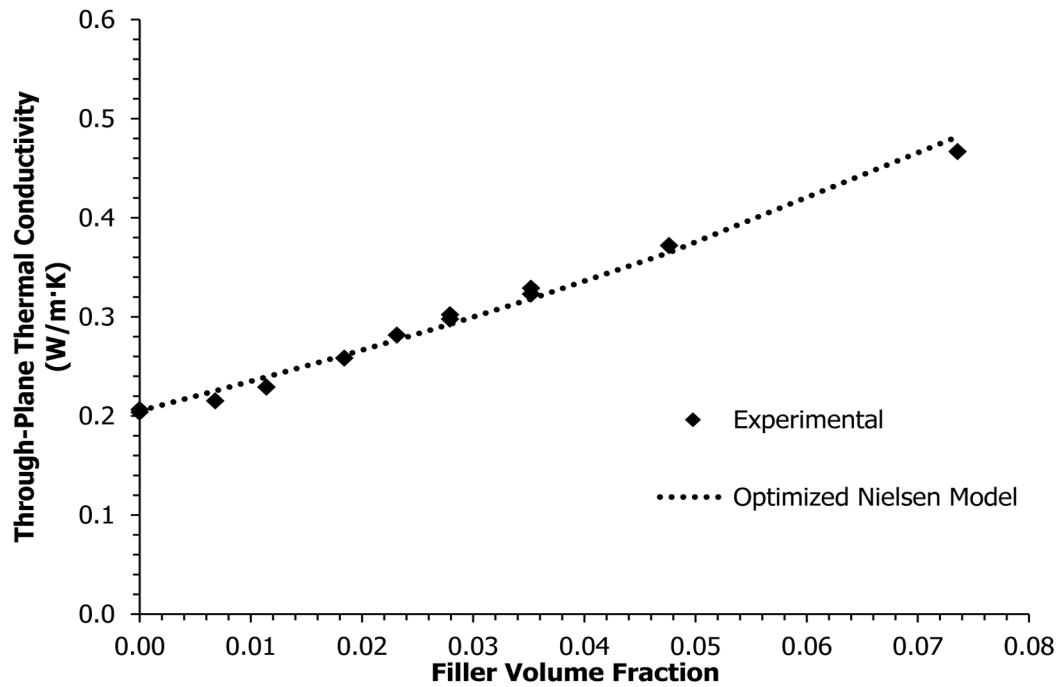


Figure 6.2 Experimental and theoretical through-plane thermal conductivities for CNT/PP composites for the Guarded Heat Flow Meter Method

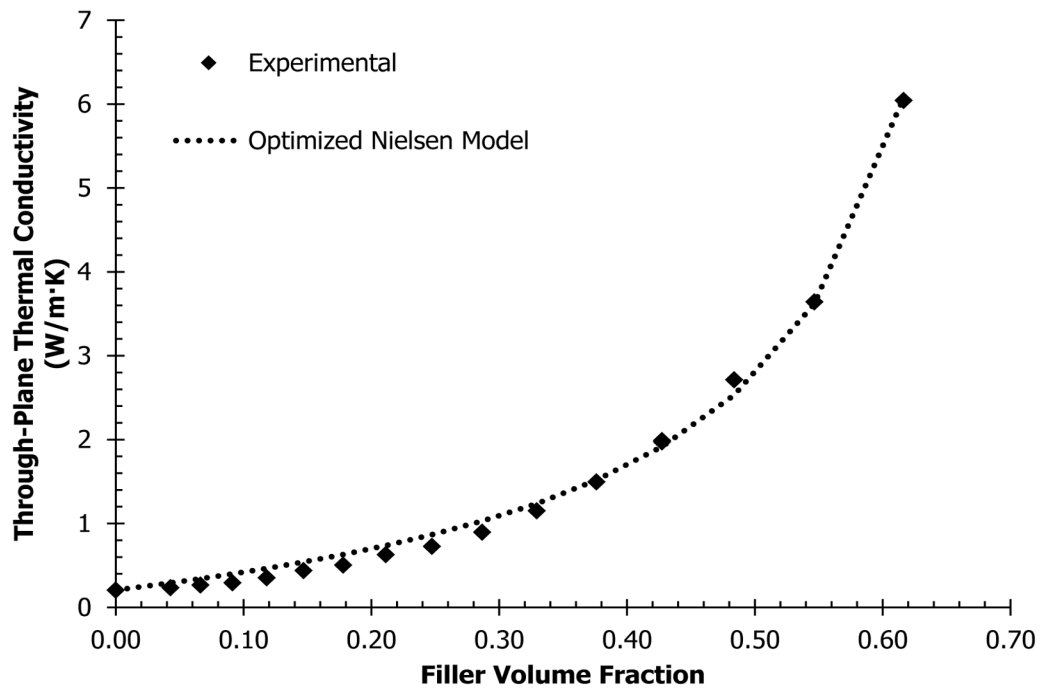


Figure 6.3 Experimental and theoretical through-plane thermal conductivities for SG/PP composites for the Guarded Heat Flow Meter

6.3.2 Flash Method

For the results obtained from the Flash method, we also used Nielsen's model. The same values for the thermal conductivities of the matrix and fillers from section 6.3.1 were used.

The use of values of A and ϕ_m from the literature yielded inaccurate results as they underpredict the thermal conductivity values, especially at high filler concentrations (126,127). (137,138) For the modeling of experimental results obtained using the Flash method, we used the equation for ψ proposed by McGee and McCullough (129). In order to fix this restriction of the model for high filler concentrations, the parameters A and ϕ_m used in Equations 6.1 and 6.4 were modified to minimize the standardized error calculated from Equation 6.5. The results found were (141):

Carbon Black (CB): $A = 122.8$; $\phi_m = 0.0811$; $\varepsilon = 1.26 \times 10^{-3}$

Carbon Nanotubes (CNT): $A = 13.1$; $\phi_m = 0.20$; $\varepsilon = 2.52 \times 10^{-3}$

Synthetic Graphite (SG): $A = 10.8$; $\phi_m = 0.617$; $\varepsilon = 1.55 \times 10^{-2}$

A comparison between experimental and model data are presented in Figures 6.4 to 6.6. We can see there is good agreement between these two sets of data. In these figures we can observe that the values for maximum packing fraction ϕ_m for carbon black and synthetic graphite, match the highest volume fraction used. Due to the high viscosity of the composites, we could not use higher volume fractions. The actual packing fraction is different than the values discussed in the literature, i.e. not random or uniaxial fibers (126,127). In addition, the large value of A for the carbon black proposes that for the filler volume fractions used in this study, the thermal conductivity follows the rule of mixtures. This can also be observed from the linear curve that represents the model results in Figure 6.4 (141).

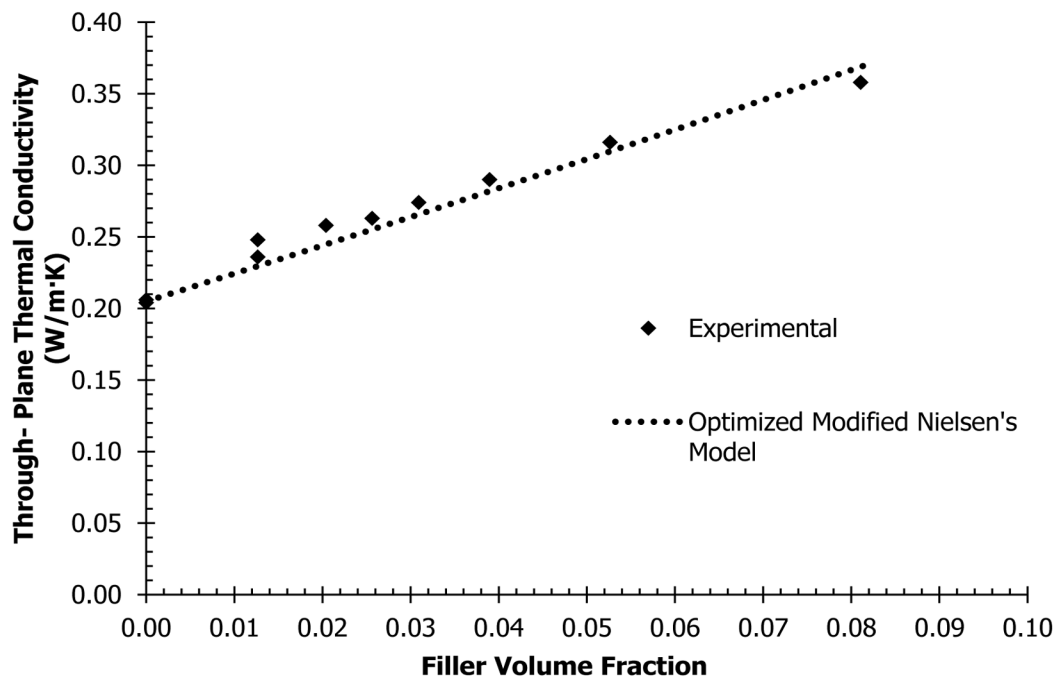


Figure 6.4 Experimental and theoretical through-plane thermal conductivities for CB/PP composites for the Flash Method

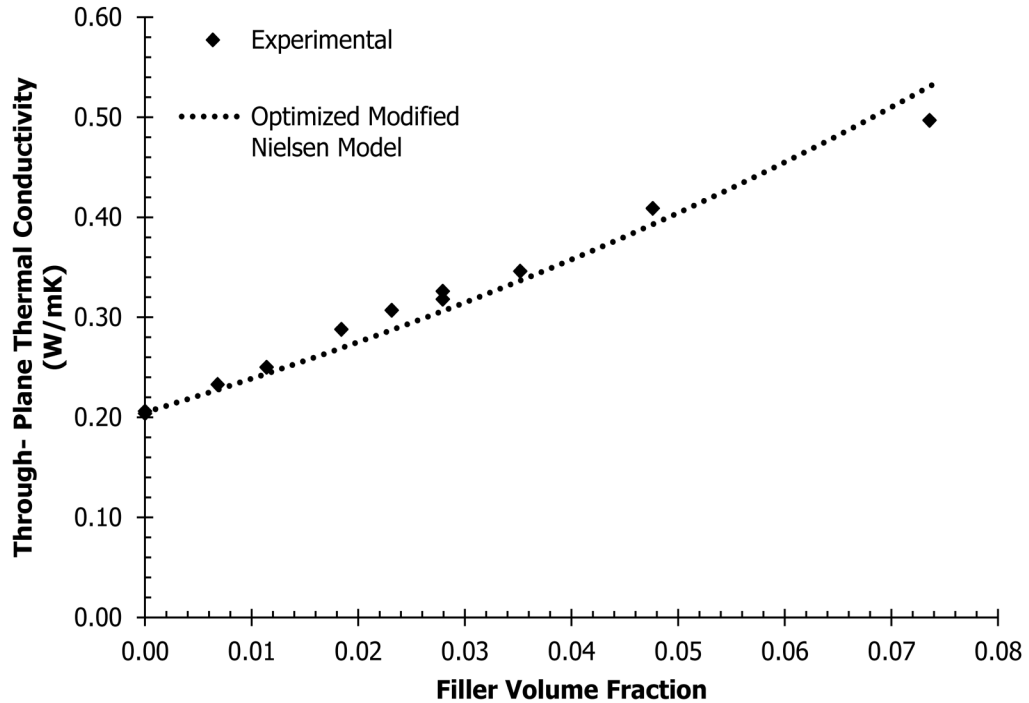


Figure 6.5 Experimental and theoretical through-plane thermal conductivities for CNT/PP composites for the Flash Method

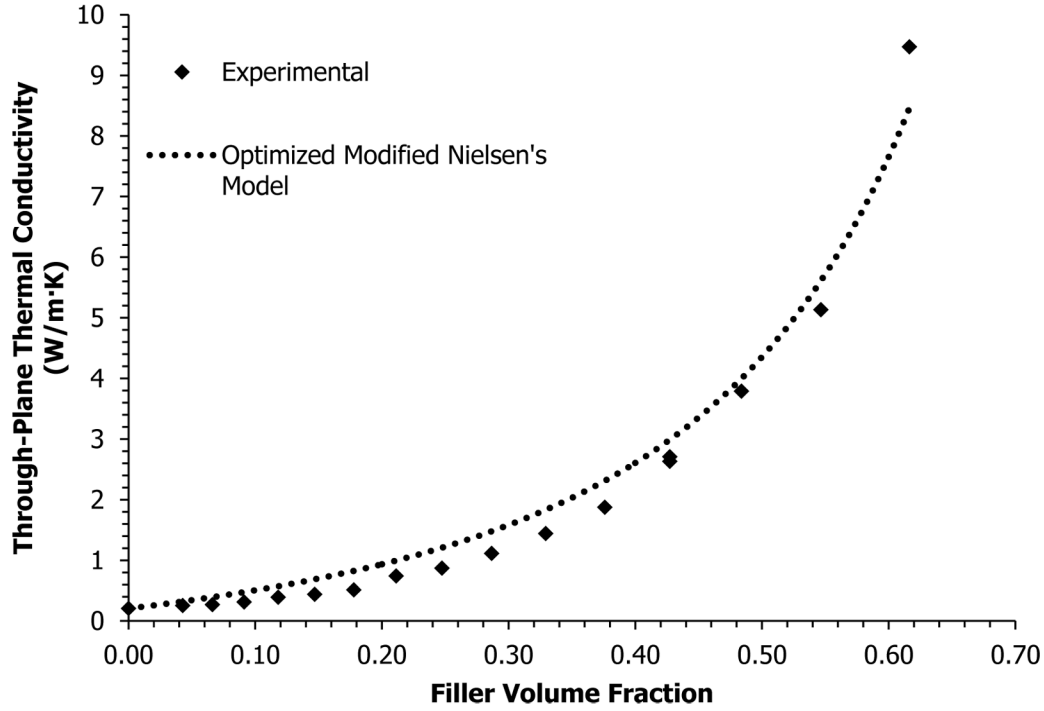


Figure 6.6 Experimental and theoretical through-plane thermal conductivities for SG/PP composites for the Flash Method

6.4 In-Plane Thermal Conductivity Modeling Results for Single-Filler Formulations

Recalling the model used for prediction of the in-plane thermal conductivity for formulations containing single fillers in polypropylene, we have that:

$$\sqrt{k_{in} k_{through}} = C e^{D\phi_2} \quad (6.6)$$

In these equations, we optimized the parameters C and D in order to minimize the error defined by Equation 6.5, obtaining the following results:

Carbon Black (CB): $C = 0.237$; $D = 7.238$; $\varepsilon = 1.19 \times 10^{-2}$

Carbon Nanotubes (CNT): $C = 0.247$; $D = 13.613$; $\varepsilon = 9.30 \times 10^{-3}$

Synthetic Graphite (SG): $C = 0.421$; $D = 6.071$; $\varepsilon = 1.61 \times 10^{-2}$

From these results, we can observe that even if the model is adjusted for C and D, the parameter C is close to the thermal conductivity of the pure polypropylene for composites with carbon black and carbon nanotubes, due to the low volume fractions used. For composites with synthetic graphite, the value was higher, because of the large variation in the volume fractions studied. In addition, we can also observe that the value of D is largest for carbon nanotubes, thus producing the largest effect on the thermal conductivity. The values of D for carbon black and synthetic graphite indicate that their effect on the thermal conductivity of the composites will be relatively similar. However, synthetic graphite allows production of highly-filled composites, causing an impact on the design of fuel cell bipolar plates. The modeling and experimental results for the in-plane thermal conductivity are shown in Figures 6.7 to 6.9 (141). We can see the model results are a good approximation to the experimental results.

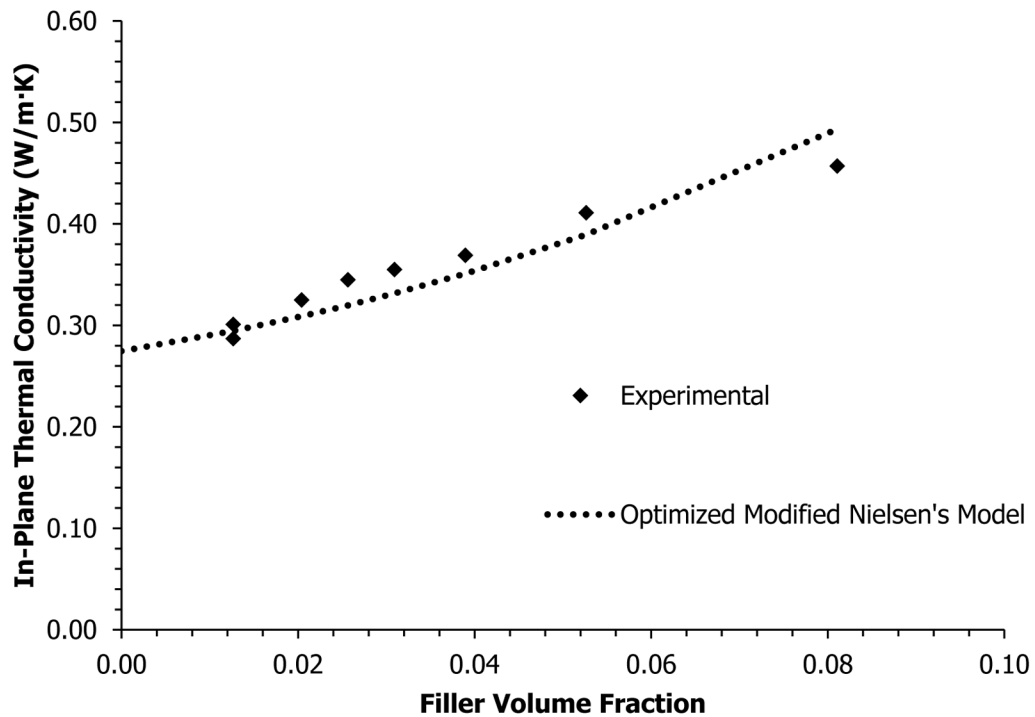


Figure 6.7 Experimental and theoretical through-plane thermal conductivities for CB/PP composites for the Flash Method

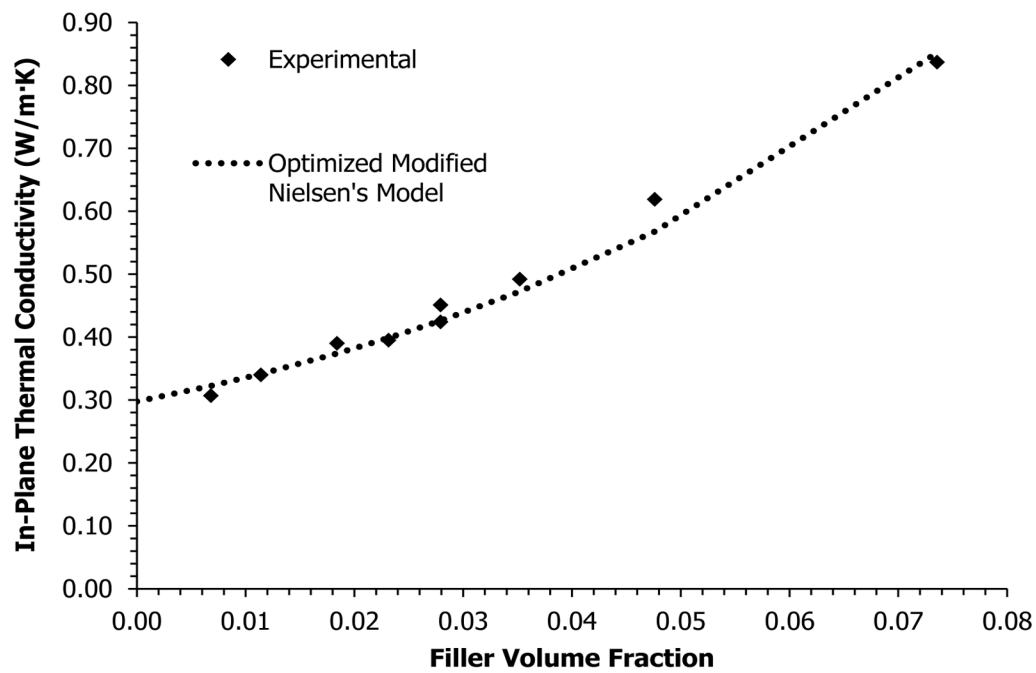


Figure 6.8 Experimental and theoretical through-plane thermal conductivities for CNT/PP composites for the Flash Method

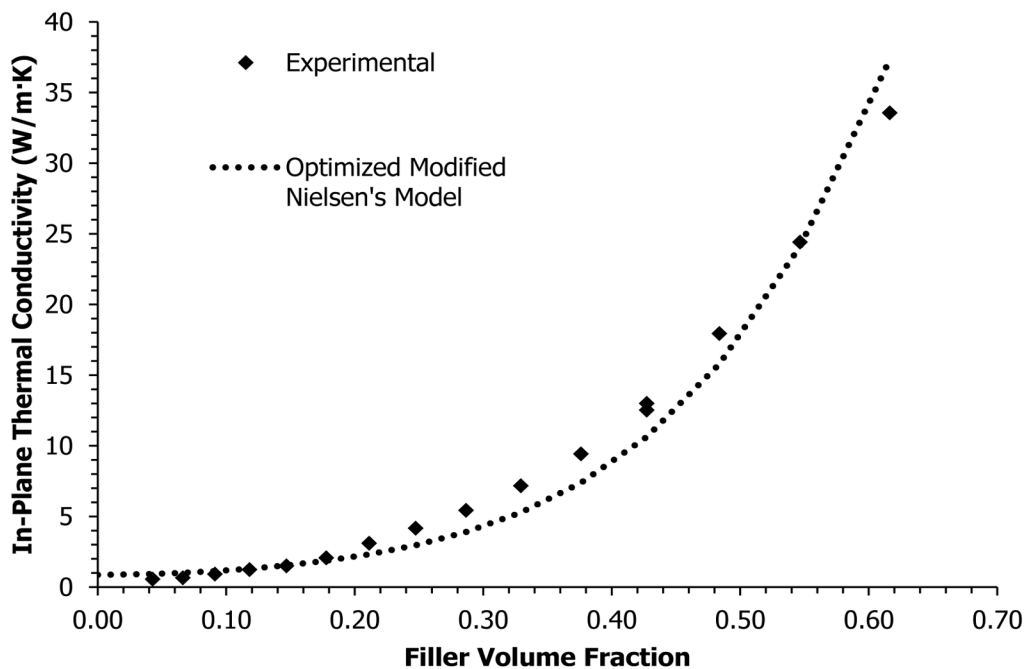


Figure 6.9 Experimental and theoretical through-plane thermal conductivities for SG/PP composites for the Flash Method

6.5 Modeling Results for Multiple-Filler Formulations

Table 6.3 shows the results for the through-plane thermal conductivity modeling (141). These results show good agreement with the experimental data for formulations containing two and three fillers in polypropylene. There are no additional adjustable parameters in the model. The model predicts an increase in the through-plane thermal conductivity of a composite with multiple fillers by two mechanisms: one of them consists of increasing the numerator by having more material with a high thermal conductivity, and the other mechanism by reducing the denominator, i.e., considering the 'ability' of each filler to occupy the volume within the matrix. This model can be applied for prediction of through-plane thermal conductivities of fuel cell bipolar plates with thermal conductivities different than those studied in our experiments.

In Equation 6.10 for prediction of in-plane thermal conductivity of composites containing both carbon black and carbon nanotubes, we found the following set of parameters:

$$E = 0.242$$

$$F = 7.238$$

$$G = 13.613$$

If we enter these values into Equation 6.10, they yield a predicted thermal conductivity of 0.514 W/m·K, which compares reasonably well with the experimental data of 0.477 W/m·K (original) and 0.481 W/m·K (replicate), producing an error of 5.3×10^{-3} (141). This model can be used to estimate, without additional parameters, the effect of multiple fillers on the in-plane thermal conductivity.

Table 6.3
Experimental and Modeling Results of Through-Plane
Thermal Conductivity using the Flash Method

Formulations	Constituents			Experimental Thermal Conductivity W/m·K	Predicted Thermal Conductivity W/m·K
		wt. %	vol. %		
No filler					0.205
Original	PP	100	100	$0.206 \pm 0.002 \ n = 4$	
Replicate				$0.204 \pm 0.002 \ n = 4$	
2.5 CB					0.230
Original	CB	2.5	1.3	$0.248 \pm 0.018 \ n = 4$	
Replicate	PP	97.5	98.7	$0.236 \pm 0.007 \ n = 4$	
65 SG					2.990
Original	SG	65	42.7	$2.707 \pm 0.092 \ n = 4$	
Replicate	PP	35	57.3	$2.631 \pm 0.022 \ n = 4$	
6 CNT					0.306
Original	CNT	6	2.8	$0.318 \pm 0.008 \ n = 4$	
Replicate	PP	94	97.2	$0.326 \pm 0.015 \ n = 4$	
2.5 CB, 65 SG					3.380
Original	CB	2.5	2.1	$3.537 \pm 0.037 \ n = 4$	
Replicate	SG	65	43.6	$3.548 \pm 0.074 \ n = 4$	
	PP	32.5	54.3		
2.5 CB, 6 CNT					0.337
Original	CB	2.5	1.3	$0.362 \pm 0.017 \ n = 4$	
Replicate	CNT	6	2.8	$0.357 \pm 0.005 \ n = 4$	
	PP	91.5	95.9		
65 SG, 6 CNT					8.075
Original	SG	65	45.2	$7.446 \pm 0.220 \ n = 4$	
Replicate	CNT	6	4.7	$7.554 \pm 0.160 \ n = 4$	
	PP	29	50.1		
2.5 CB, 65 SG, 6 CNT					10.662
Original	CB	2.5	2.2	$8.503 \pm 0.029 \ n = 4$	
Replicate	SG	65	46.2	$8.469 \pm 0.266 \ n = 4$	
	CNT	6	4.8		
	PP	26.5	46.8		

6.6 Conclusions

Theoretical values for the through-plane and in-plane thermal conductivities using the three different carbon fillers were determined by applying Nielsen's model for the experimental data obtained from the Guarded Heat Flow Meter method, and Modified Nielsen's model for the Flash method. For composites with varying amounts of single fillers, the models were optimized, so the values for parameters A and ϕ_m for through-plane conductivity, and C and D for in-plane conductivity, would minimize the difference between experimental and model results. For through-plane thermal conductivity of composites with multiple fillers, we used an adapted form of Nielsen's model so the terms in its equation could be written as a summation, allowing it to be applied for composites with more than one filler. The parameters used in the equation for estimation of in-plane thermal conductivity of single-filler formulations were used to obtain a new model which allowed to predict the in-plane thermal conductivity of composites containing carbon black and carbon nanotubes. In all cases, thermal conductivities calculated by using Nielsen's model were a good approximation to experimental data.

Comparing to previous modeling research, the A value for CB/Vectra ($A = 1720$) (131) composites was much higher than that for the CB/PP composites ($A = 70.5$), and the results for the ϕ_m are similar in both polymer matrices. For composites containing different amounts of synthetic graphite, the values of A and ϕ_m were similar for SG/PP (with $A = 8.5$ and $\phi_m = 0.8$) and SG/Vectra composites (130,140). These models may be useful in predicting composite through-plane and in-plane thermal conductivities for fuel cell bipolar plate applications.

Chapter 7: Experimental Results for Mechanical Properties Tests

7.1 Introduction

This chapter will describe the results of the tensile and flexural tests discussed in Chapter 4. Appendix C shows the flexural test results for each composite formulation. Results for tensile properties are summarized in Appendix D. Results from nanoscratch tests are discussed later in this chapter.

7.2 Synthetic Graphite Length, Aspect Ratio and Orientation Results

The injection molded polypropylene test specimens filled with Thermocarb TC-300 had a filler aspect ratio of 1.67 and a length of 40 μm . The tensile and flexural test specimens injection molded in this project are end-gated, therefore, the fillers are primarily aligned in the tensile and flexural measurement direction. These results show good agreement with values obtained from prior work for nylon, polycarbonate and liquid crystal polymer resins (23,33,34). Photomicrographs showing the orientation of the synthetic graphite are shown elsewhere (22,30,33,34,142). Additional details in results for synthetic graphite length, aspect ratio and orientation can be found elsewhere (86).

7.3 Flexural Test Results

The flexural results are presented in the following sub-sections, for single-filler formulations and for composites containing multiple fillers in polypropylene. The results for flexural modulus, flexural ultimate strength, yield flexural strength, flexural fracture stress and their corresponding strain values for each test specimen are shown in Appendix C.

7.3.1 Flexural Test Results for Single-Filler Formulations

Figures 7.1–7.3 show the flexural test results (mean and one standard deviation) for each formulation. The error bars are not displayed for formulations where the standard deviation for each formulation was less than the marker size in the graphs. For comparison with previous work, Figures 7.1 and 7.2 also show the results for carbon/Vectra composites, which will be described in Section 7.3.3. The flexural modulus results for composites with varying amounts of the single fillers in polypropylene are shown in Figure 7.1. An experimental flexural modulus of 1700 MPa was measured for the pure polypropylene. Adding each of the three single carbon fillers caused an increase in the flexural modulus. Addition of carbon black caused the modulus to increase from 1700 MPa to 2810 MPa, at a concentration of 8.11 vol.% (15 wt.%) carbon black. For synthetic graphite, the flexural modulus at 61.64 vol.% (80 wt.%) synthetic graphite was 15400 MPa. Adding carbon nanotubes increased the flexural module of the composites, reaching a value of 3110 MPa for a 7.36 vol.% (15 wt.%) carbon nanotubes.

The behavior of the flexural modulus graphs follows the same trend as the tensile modulus results. By comparing the results obtained for different carbon fillers in Figure 7.1, we can observe that the carbon nanotubes caused the largest increase in the tensile modulus, due to their high aspect ratio. The flexural modulus results for carbon black and synthetic graphite agree to the results published in the literature (143-147). The research work by Ansari found no improvement in flexural modulus for a composite containing 0.5 wt.% of multiwalled carbon nanotubes in polypropylene (148). Nevertheless, López Manchado et al. (149) and Ansari (148) found an increase in tensile modulus with increasing amounts of carbon nanotubes.

In Figure 7.2, it can be seen that the ultimate flexural strength of pure polypropylene was 60.8 MPa. The lowest ultimate flexural strength was obtained for the composite formulation containing 61.64 vol.% (80 wt.%) synthetic graphite, with a value of 43.1 MPa. The composites with 8.11 vol.% (15 wt.%) carbon black, which had a ultimate flexural strength of 59.5 MPa. This is

consistent with that seen in the literature (148-151). However, for formulations containing varying amounts of carbon nanotubes in polypropylene, we observed an increase in the ultimate flexural strength for higher filler concentrations, obtaining a value of 73.4 MPa for composites containing 7.36 vol.% (15 wt.%) of carbon nanotubes.

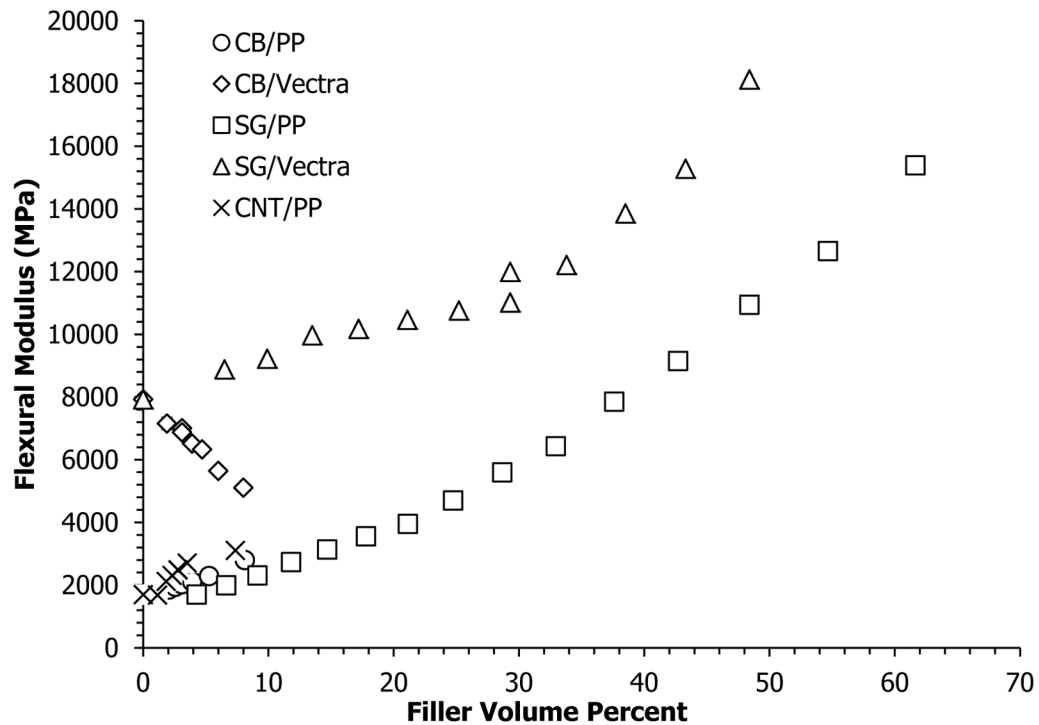


Figure 7.1 Single-Filler Flexural Modulus Results for CB/PP, SG/PP, CNT/PP, CB/Vectra and SG/Vectra Composites

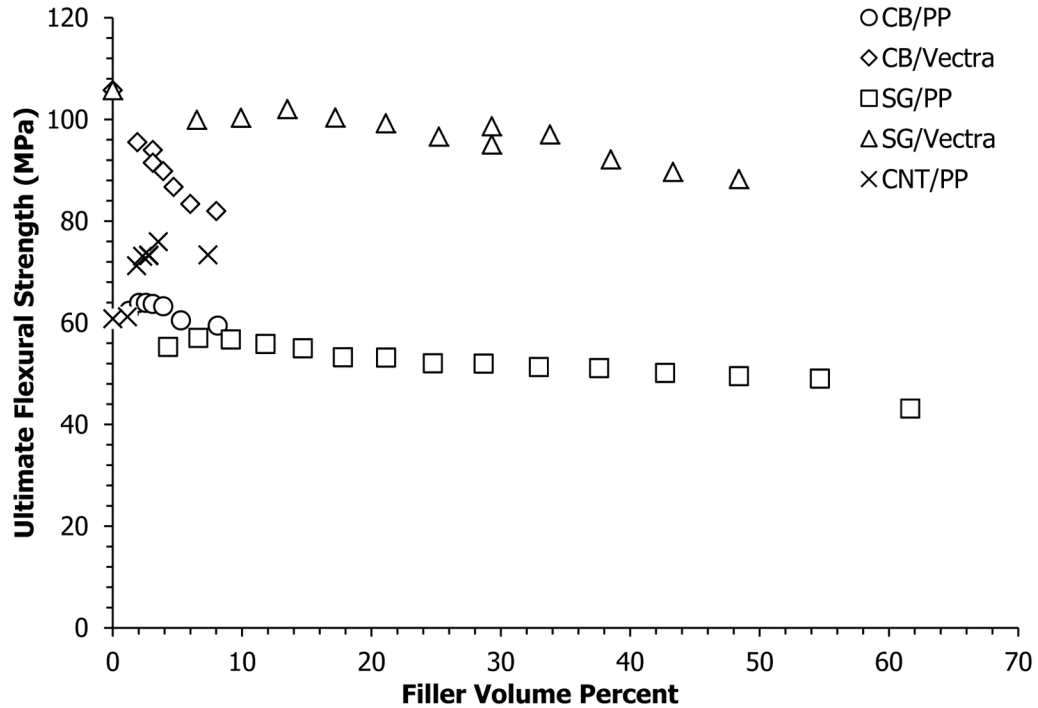


Figure 7.2 Single-Filler Ultimate Flexural Strength Results for CB/PP, SG/PP, CNT/PP, CB/Vectra and SG/Vectra Composites

Figure 7.3 illustrates the strain at ultimate flexural strength results for composites filled with carbon black, synthetic graphite and carbon nanotubes. The addition of any of these fillers caused the strain to decrease. The lowest value was observed in composites with synthetic graphite, decreasing from 7.78% for pure polypropylene to 0.44% for a filler concentration of 61.64 vol.% (80 wt.%) of synthetic graphite particles. At the highest concentration of carbon black (8.11 vol.%) and carbon nanotubes (7.36 vol.%), the strain at the ultimate flexural strength was measured to be 2.49% and 4.22% respectively.

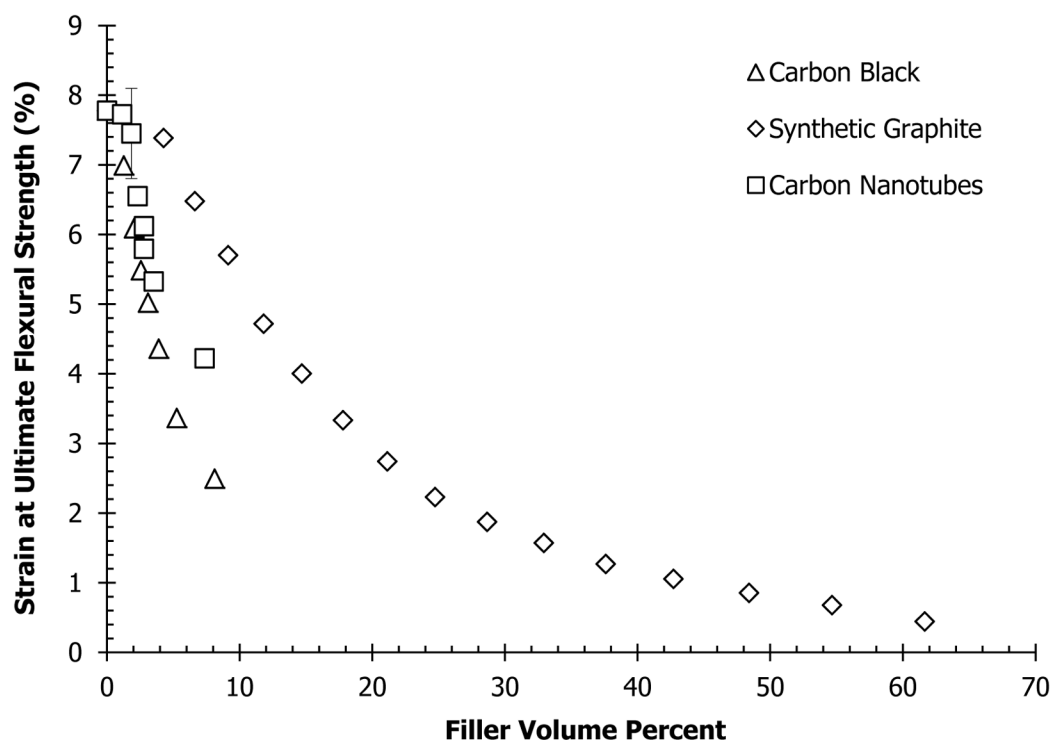


Figure 7.3 Strain at Ultimate Flexural Strength Results for Single-Filler Polypropylene-Based Formulations

7.3.2 Flexural Test Results for Multiple-Filler Formulations

For the multiple filler composites with 2.5 wt.% carbon black and 6 wt.% carbon nanotubes, the flexural modulus was 2370 MPa for the original polypropylene and 2330 MPa for the replicate. The results for the ultimate flexural strength for the original and replicate of the matrix are 66.7 MPa and 66.2 MPa, respectively. Third, the strain at the ultimate flexural strength was measured to be 4.54% for the original and 4.64% for the polypropylene replicate. The number of samples tested for polypropylene was $n=7$ and $n=10$ for the replicate. Addition of synthetic graphite particles (65 wt.%) caused a great increase in the composite viscosity, hence, flexural test specimens could not be injection molded for samples containing 65 wt.% synthetic graphite along with 2.5 wt.% carbon black and/or 6 wt.% carbon nanotubes.

7.3.3 Comparison of Flexural Results for Polypropylene and Liquid Crystal Polymer Composites

Because prior tensile and flexural strength tests were performed using carbon black and synthetic graphite in a Vectra liquid crystal polymer matrix (LCP) for use in fuel cell bipolar plate applications, a comparison is made in Figures 7.1 and 7.2 (152). Similar with the tensile results, synthetic graphite caused an increase in the flexural modulus in both matrices. In the polypropylene matrix, addition of carbon black caused an increase in the flexural modulus from 1700 MPa for the pure polypropylene to 2800 MPa for the highest carbon black concentration of 8.11 vol.% (15 wt.%). The neat Vectra has a flexural modulus of 7930 MPa and it decreased to 5100 MPa at 7.95 vol.% (10 wt.%) carbon black. For composites with synthetic graphite in both matrices, the flexural modulus of the polypropylene increased to 11000 MPa at 48.40 vol.% (70 wt.%) of filler and to 18100 MPa at 48.39 vol.% (60 wt.%) of synthetic graphite in Vectra.

A decrease in the ultimate flexural strength was observed in the composites with single amounts of carbon black and synthetic graphite in polypropylene and LCP as it can be seen in Figure 7.2. At a concentration of 8.11 vol.% (15 wt.%) of carbon black in polypropylene, the value measured for the ultimate flexural strength was 59.5 MPa and for the LCP composites with 7.95 vol.% (10 wt.%) carbon black, an ultimate flexural strength of 82.0 MPa was observed. The addition of synthetic graphite also caused a decrease in the ultimate flexural strength of the composites in the two different matrices. The ultimate flexural strength value measured for the composites containing 48.40 vol.% (70 wt.%) synthetic graphite in polypropylene was 49.5 MPa. The composites with 48.39 vol.% (60 wt.%) synthetic graphite in LCP, had an ultimate flexural strength of 88.3 MPa.

Overall, the tensile modulus and strength of the Vectra-based composites were higher. The rod-like shaped structure of the solid liquid crystal polymer contributes to the reinforcement of the composite (153,154).

7.4 Tensile Test Results

This section describes the tensile results for the composites containing different amounts of single fillers in polypropylene and for the formulations with multiple fillers. Appendix D summarizes the results for every sample tested for tensile properties.

7.4.1 Tensile Test Results for Single-Filler Formulations

Figure 7.4 shows typical stress-strain graphs for the composite materials used in this study. The tensile modulus, ultimate tensile strength and strain at ultimate tensile strength results are shown in Figures 7.5–7.7 for carbon/polypropylene composites, as the mean plus or minus one standard deviation, as a function of the filler volume fraction. The error bars are not shown for formulations where one standard deviation is less than the marker size. It is noted that results for Vectra composites are also included in Figures 7.5 and 7.6. These results will be discussed in the next section. For all the carbon/polypropylene samples tested, the ultimate tensile strength values were the same as the fracture tensile strength. The tensile modulus for the pure polypropylene was measured to be 1510 MPa.

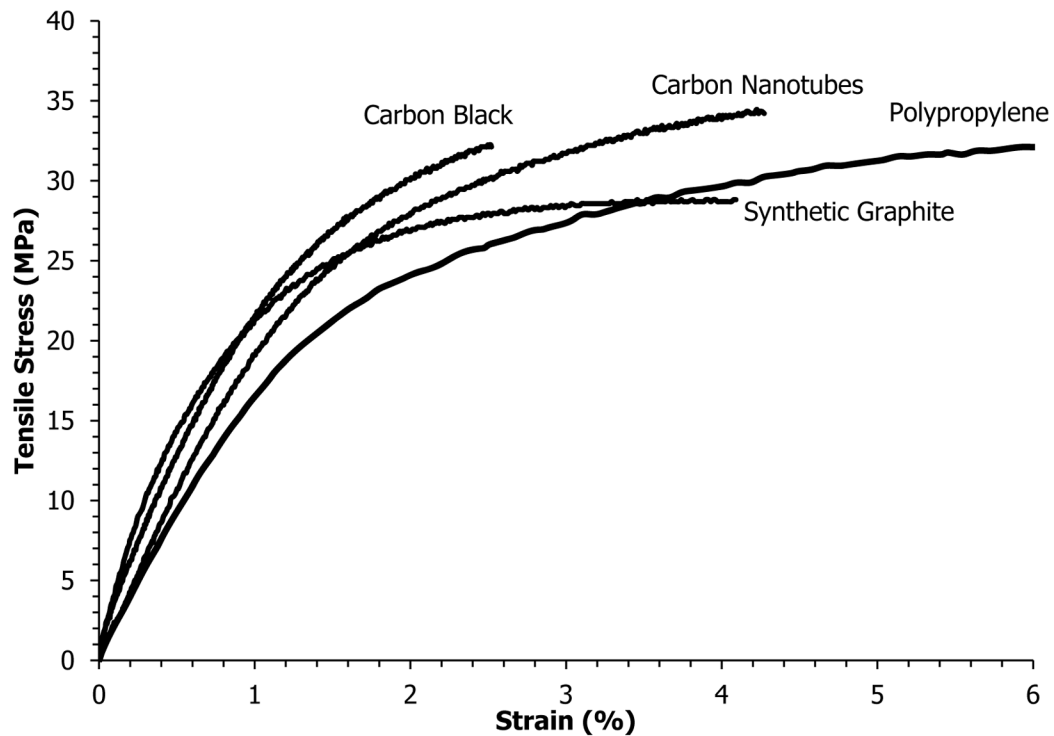


Figure 7.4 Typical Tensile Stress–Strain Plots for Pure Polypropylene (Initial Portion), Polypropylene with 6 wt.% Carbon Black, Polypropylene with 20 wt.% Synthetic Graphite, and Polypropylene with 6 wt.% Carbon Nanotubes

In Figure 7.5, it can be observed that the tensile modulus increases with filler concentrations for all three fillers. This is due to the fact that the tensile modulus of each filler is higher than that of the matrix (33). Another factor which may also contribute to this effect, is the adhesion between the filler particles and the matrix material. This effect will be described in Section 7.5. The carbon black was used in this project with the primary objective to increase electrical conductivity. The change in the modulus for composites with carbon black, was from 1510 MPa to 3240 MPa at 8.11 vol.% (15 wt.%). The highest value for tensile modulus was 16,200 MPa for a concentration of 61.64 vol.% (80 wt.%) of synthetic graphite particles in polypropylene. For the carbon nanotubes/polypropylene composites the value of the modulus increased from 1510 MPa to 3690 MPa at 7.36 vol.% (15 wt.%) carbon nanotubes. These results are consistent with those published in the literature, which also show an increase in tensile modulus with the addition of

carbon black, synthetic graphite and carbon nanotubes to polypropylene (90,145,146,148-150,155,156).

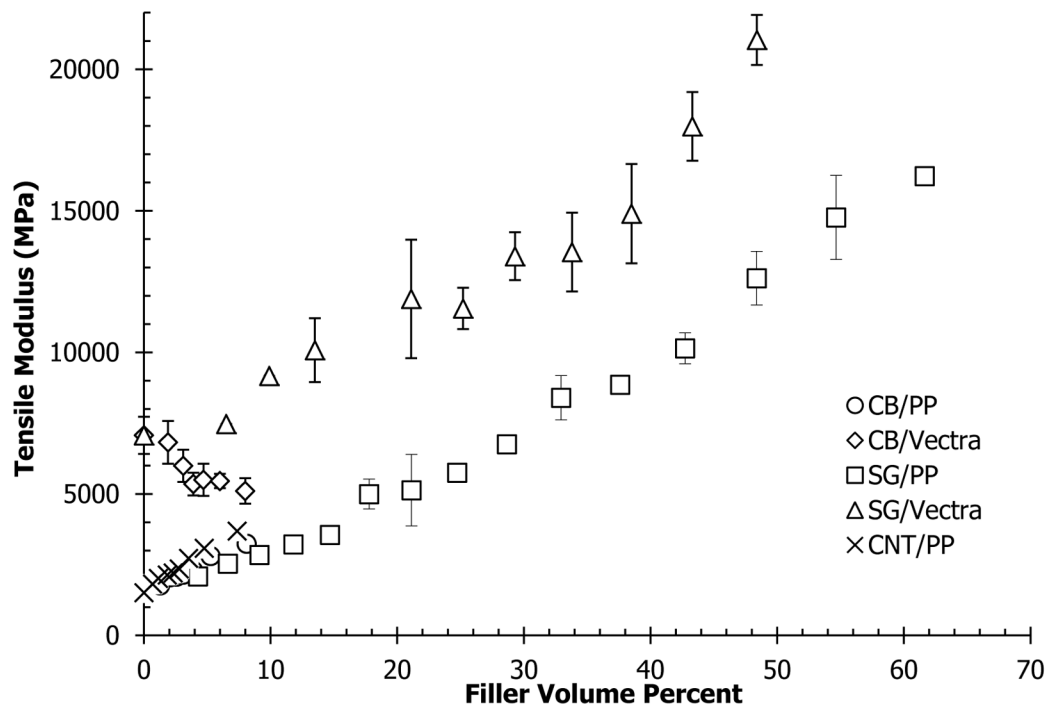


Figure 7.5 Single-Filler Tensile Modulus Results for CB/PP, SG/PP, CNT/PP, CB/Vectra and SG/Vectra Composites

Figure 7.6 shows the ultimate tensile strength for composites containing various amounts of single filler in polypropylene. It can be seen that carbon black causes a decrease in the ultimate tensile strength from 32.7 MPa to 30.2 MPa for the composites containing 8.11 vol.% (15 wt.%) carbon black. Composites containing synthetic graphite particles had the largest decrease in ultimate tensile strength values. The composite with 61.64 vol.% (80 wt.%) synthetic graphite had an ultimate tensile strength of 23.3 MPa. This behavior of the ultimate tensile strength agrees with prior work by Konell et al. (33).

The results of Chiu and Chiu (144) and Zhou et al. (157) show a very slight increase in ultimate tensile strength for carbon black in polypropylene. Composites containing synthetic graphite

particles had a similar decrease to carbon black in the values of the ultimate tensile strength. The behavior of the ultimate tensile strength using synthetic graphite agrees with prior work by Konell et al.(33) and with Akinci (156) for synthetic graphite in polypropylene. This result is likely because synthetic graphite (with an aspect ratio of 1.67) is not a reinforcing material.

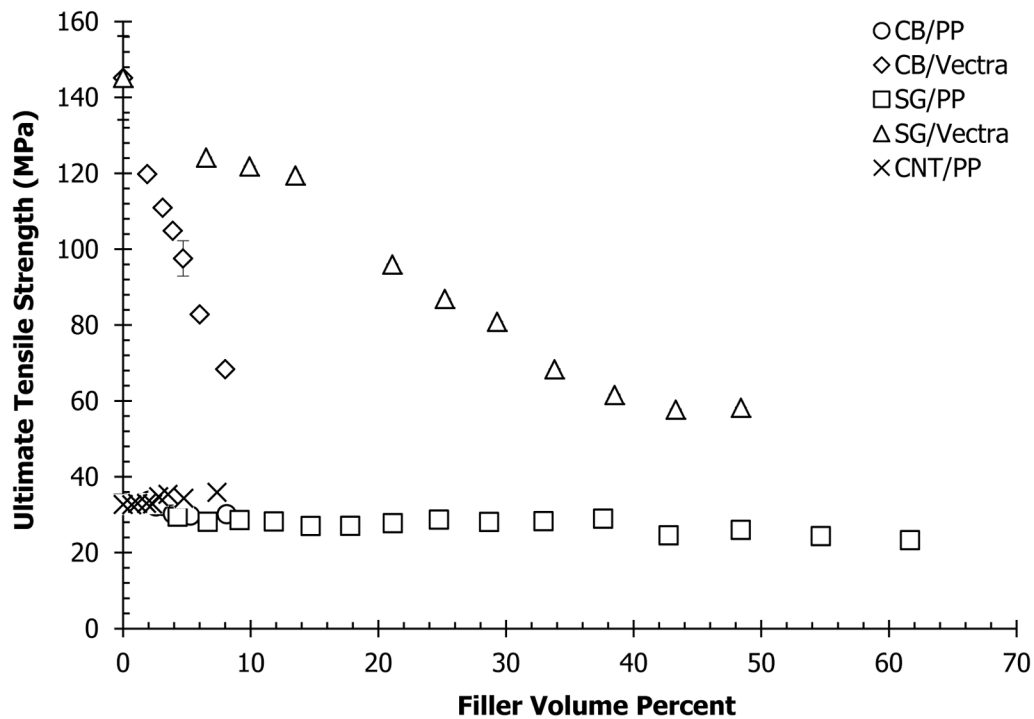


Figure 7.6 Single-Filler Ultimate Tensile Strength Results for CB/PP, SG/PP, CNT/PP, CB/Vectra and SG/Vectra Composites

Also in Figure 7.6, opposite to what occurred with carbon black and synthetic graphite, the addition of carbon nanotubes caused the ultimate tensile strength to increase slightly from 32.7 MPa (pure polypropylene) to 35.9 MPa at 7.36 vol.% (15 wt.%). This result was observed by others when low concentrations of carbon nanotubes are added to polypropylene (148-151) and can be explained by the high aspect ratio of this filler (85).

The strain at ultimate tensile stress results for the carbon black, synthetic graphite and carbon nanotubes in polypropylene are illustrated in Figure 7.7. It can be observed that strain values for

all three fillers decrease when filler is added. At the highest concentrations of carbon fillers, the strain at ultimate strength values were measured to be 1.26% for composites with 8.11 vol.% (15 wt.%) carbon black, 0.23% for formulations containing 61.64 vol.% (80 wt.%) synthetic graphite, and 2.19% for carbon nanotubes/polypropylene composites with a filler concentration of 7.36 vol.% (15 wt.%) carbon nanotubes. This decrease in the strain at ultimate tensile strength with the addition of carbon fillers, agrees with results observed by Huang (115) and Konell et al. (33).

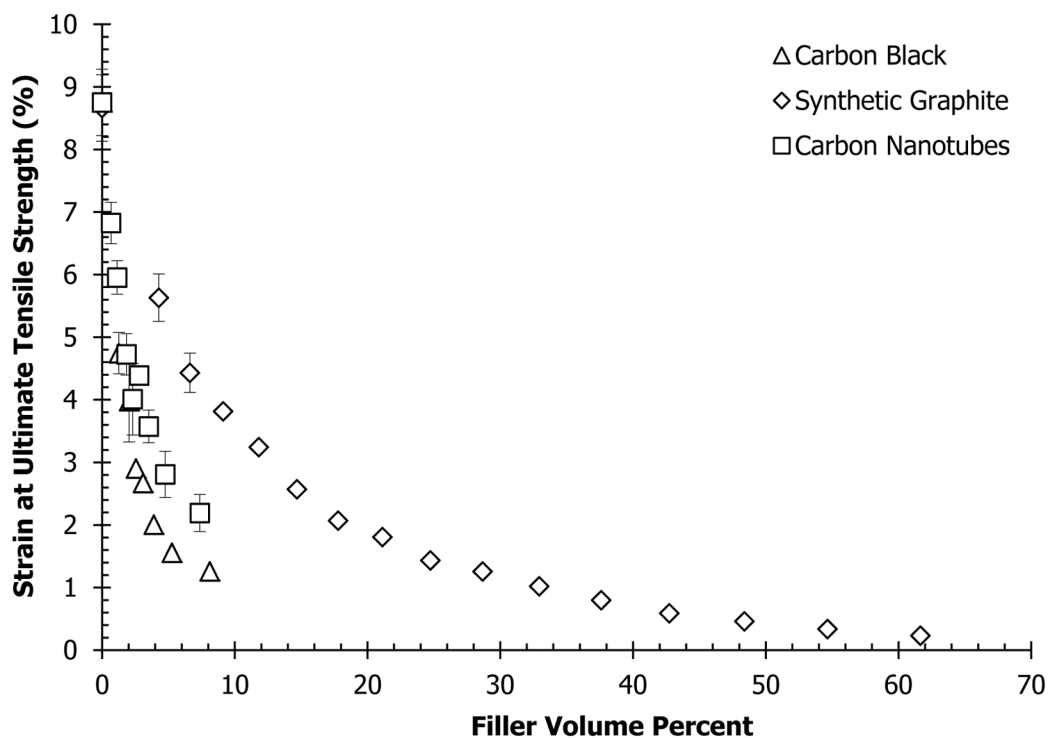


Figure 7.7 Strain at Ultimate Tensile Strength Results for Single-Filler Polypropylene-Based Formulations

7.4.2 Tensile Test Results for Multiple-Filler Formulations

The tensile modulus and ultimate tensile strength for the formulation containing 2.5 wt.% carbon black and 6 wt.% carbon nanotubes were 2890 MPa and 31.0 MPa, respectively. The strain at ultimate tensile strength was 2.05%. The number of samples tested was 7. A replicate with the

same wt.% of filler was also prepared. The results were similar, with a value for the tensile modulus of 2820 MPa. The ultimate tensile strength for this formulation was 33.2 MPa, with 6 samples tested. The strain at ultimate tensile strength was measured to be 2.32%. Once again, the composites containing combinations of different carbon fillers that included 65 wt.% synthetic graphite could not be injection molded into tensile bars, due to the high increase in the viscosity of the material.

7.4.3 Comparison of Tensile Results for Polypropylene and Liquid Crystal Polymer Composites

Figures 7.5 and 7.6 show the mean flexural modulus and ultimate flexural strength, respectively and one standard deviation for at least 5 specimens tested of composites with carbon black and synthetic graphite in polypropylene and in Vectra A950RX liquid crystal polymer matrices. The tensile modulus increased as a function of the filler volume percent with increasing filler concentration for both carbon black and synthetic graphite in the polypropylene, as indicated in Figure 7.5. This result is consistent for synthetic graphite in the liquid crystal polymer matrix. However, the addition of carbon black to LCP resulted in a reduction in tensile modulus. In the polypropylene matrix, addition of carbon black caused an increase in the tensile modulus from 1500 MPa for the pure polypropylene to 3240 MPa at a carbon black concentration of 8.11 vol.% (15 wt.%) carbon black. The neat Vectra has a tensile modulus of 7100 MPa and it decreased to 5100 MPa at 7.95 vol.% (10 wt.%) carbon black. For composites with synthetic graphite in both matrices, the tensile modulus of the polypropylene increased to 16200 MPa at 48.40 vol.% (70 wt.%) of filler and to 21000 MPa at 48.39 vol.% (60 wt.%) of synthetic graphite in Vectra. Results from previous research work has indicated that Vectra had poor adhesion to some carbon fillers, which justifies the poor tensile modulus results obtained for Vectra (62,158).

Figure 7.6 shows that both carbon black and synthetic graphite caused the ultimate tensile strength to decrease for LCP and polypropylene composites; however, the reduction is much

more significant in the LCP composites. Carbon black in polypropylene caused the smallest decrease in the ultimate tensile strength with values of 32.7 MPa for the neat polymer and 30.2 MPa for a concentration of 8.11 vol.% (15 wt.%) of carbon black. For comparison, the ultimate tensile strength for neat Vectra was 145.2 MPa and decreased to 68.4 MPa with a carbon black loading of 7.95 vol.% (10 wt.%). This result supports our assumption of poor adhesion of carbon black in Vectra.

The composites formed with synthetic graphite and polypropylene had an ultimate tensile strength of 26.0 MPa at a concentration of 48.40 vol.% (70 wt.%), which can be compared to the synthetic graphite/Vectra composite at 58.2 MPa at 48.39 vol.% (60 wt.%).

Again, the carbon/Vectra composites had better flexural properties than the carbon/polypropylene composites due to the liquid–crystalline structure of the Vectra.

7.5 Comparison of Nanoscratch Test Results for Polypropylene and Liquid Crystal Polymer Composites

Figure 7.8 is showing the displacement of the indenter of the MTS Nano Indenter XP as a function of the scratch distance for the composite containing 20 wt.% of synthetic graphite in polypropylene is shown in Figure 7.8. The degree of adhesion between the synthetic graphite particles and the polypropylene matrix affected the transition regions in the plot, between the filler rich area (lower penetration) and matrix–rich areas (higher penetration). A photomicrograph of the scratch surface is also shown in Figure 7.8.

Table 7.1 compares the crest factors penetration of the indenter in the composites with 20 wt.% synthetic graphite in both Vectra (31) and polypropylene. Results obtained in previous research work (32) has shown that the normalized crest factor (ratio of the composite crest factor to the polymer crest factor) can be used as a measure to compare the relative degree of adhesion between different composites having the same matrix but different types of fillers. A higher

normalized crest factor is indicative of a resistance of the composite to scratching, due to better filler/matrix adhesion.

In Table 7.1 we can observe that the crest factor for the matrix materials polypropylene and Vectra were close to zero. This is due to the absence of filler particles, which cause perturbations in the displacement. Table 7.1 also shows the normalized crest factor used to estimate the effect of filler/matrix adhesion. If we correlate the nanoscratch results to a relative increase in tensile modulus, we find for 48.40 vol.% (70 wt.%) of synthetic graphite in polypropylene, a modulus enhancement ratio (compared to the matrix) of 8.4 is found (12600 MPa/1510 MPa), while for 48.39 vol.% (60 wt.%) of synthetic graphite in Vectra, a modulus enhancement ratio was found to be 3.0 (21000 MPa/7070 MPa) which might be attributed to better filler/matrix adhesion for the polypropylene composites.

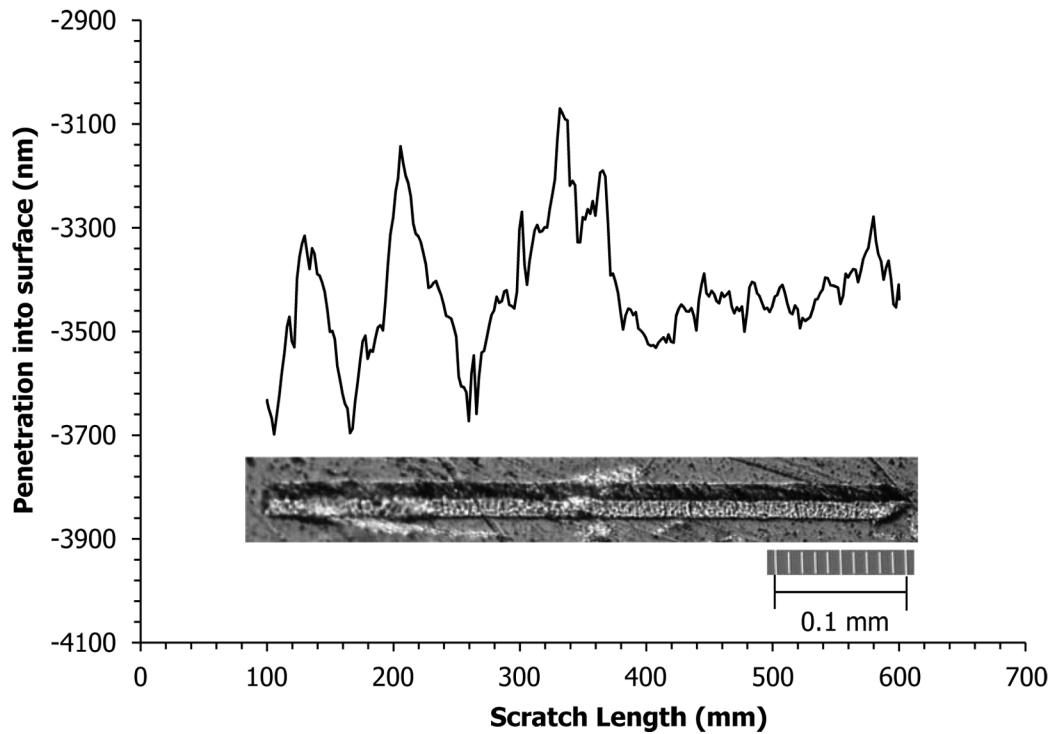


Figure 7.8 Displacement Normal to the Surface Under a Constant Force of 40 mN for Composites Containing 20 wt.% of Synthetic Graphite Particles in Polypropylene

Table 7.1
Crest Factors for Penetration in Polymer Composites (31)

Formulation	Number of scratch tests performed	Mean crest factor	Normalized crest factor (matrix = 1.00)
Thermocarb/Vectra	10	0.149	1.79
Thermocarb/Polypropylene	10	0.110	5.03
Pure Vectra	10	0.083	1.00
Pure Polypropylene	5	0.022	1.00

7.6 Conclusions

As described in this chapter, the tensile and flexural properties of carbon/polypropylene composites were measured in this project. The addition of different amounts of carbon fillers increases the tensile and flexural modulus of the composites. However, a decrease in the ultimate tensile and flexural strengths for single filler composites containing carbon black and synthetic graphite was observed. For carbon nanotubes/polypropylene composites, the ultimate tensile and flexural strengths were improved for higher filler concentrations. This result is expected due to the high aspect ratio (length/diameter=1000) of this material. The ultimate flexural strengths measured for all the composite formulations evaluated in this study exceeded the requirement of 25 MPa (9), set by the Department of Energy for use of these materials in fuel cell bipolar plates applications.

The experimental data obtained by performing Nanoscratch tests provide data that could be used to measure the degree of adhesion between fillers and the polymer matrix. The degree of adhesion can be represented by the normalized crest factor. When comparing crest factors of polypropylene composites with liquid crystal polymer composites, it can be seen that a better degree of adhesion exists for the carbon/polypropylene composites. Data analysis was done using the penetration into the composite surface as a function of the scratch distance and the results of this test agree with the results obtained for the tensile modulus of the composites.

Chapter 8: Tensile Modulus Modeling

8.1 Introduction

This chapter illustrates the use of different models to estimate the tensile modulus of carbon/polypropylene composites. There are multiple models available in the literature (146) used to predict the tensile modulus of a composite material containing two components, such as one matrix material and one filler. The following sections provide background and the results found using these models.

8.2 Tensile Modulus Modeling Background

8.2.1 Rule of Mixtures and Inverse Rule of Mixtures

The most basic models used in this project are the direct and inverse rule of mixtures. The rule of mixtures, or series model, typically overpredicts the modulus of short fiber/particulate composites, whereas the inverse rule of mixtures, or parallel model, typically underpredicts the modulus of short fiber/particulate composites (151). Equations 8.1 and 8.2 represent the rule of mixtures and inverse rule of mixtures, respectively.

$$E_C = \phi_1 E_1 + \phi_2 E_2 \quad (8.1)$$

$$\frac{1}{E_C} = \frac{\phi_1}{E_1} + \frac{\phi_2}{E_2} \quad (8.2)$$

where:

E_C = Tensile Modulus of the Composite

E_1 = Tensile Modulus of the Polypropylene Matrix

E_2 = Tensile Modulus of the Carbon Filler

ϕ_1 = Volume Fraction of the Polypropylene Matrix

ϕ_2 = Volume Fraction of the Carbon Filler

8.2.2 Halpin–Tsai Models

The Halpin–Tsai equations represent a more detailed model applicable for prediction of tensile modulus of composites filled with short fibers (146,159-161). The use of this model in previous studies has predicted experimental data accurately for low filler concentrations (less than 50 vol.%) (162).

The analysis of this model uses the longitudinal and transverse moduli of aligned unidirectional (oriented) short fiber composites, given in Equations 8.3 to 8.6, shown below.

$$\frac{E_L}{E_1} = \frac{1 + 2(L/d)\eta_L\phi_2}{1 - \eta_L\phi_2} \quad (8.3)$$

$$\frac{E_T}{E_1} = \frac{1 + 2\eta_T\phi_2}{1 - \eta_T\phi_2} \quad (8.4)$$

$$\eta_L = \frac{(E_2/E_1) - 1}{(E_2/E_1) + 2(L/d)} \quad (8.5)$$

$$\eta_T = \frac{(E_2/E_1) - 1}{(E_2/E_1) + 2} \quad (8.6)$$

where:

E_L = Longitudinal Tensile Modulus of the Composite

E_T = Transverse Tensile Modulus of the Composite

L = Filler length

d = Filler diameter

In this study, we will refer to Equation 8.3 as 'Halpin–Tsai Oriented Fiber Model'.

The longitudinal and transverse models can be combined for a two-dimensional random orientation of fibers, as shown in Equation 8.7 (146) and for a three-dimensional random orientation of fibers, as shown in Equation 8.8 (159).

$$E_C = \frac{3}{8}E_L + \frac{5}{8}E_T \quad \text{2D Randomly Oriented Fibers} \quad (8.7)$$

$$E_C = \frac{1}{5}E_L + \frac{4}{5}E_T \quad \text{3D Randomly Oriented Fibers} \quad (8.8)$$

8.2.3 Nielsen's Model

Nielsen (44,45,128,163) has developed a macroscopic model that is the most versatile for short fiber/particulate composites. Nielsen's model takes into account the concentrations and characteristics of the constituents of the composite material. In addition, it considers the properties of the filler materials, such as the aspect ratio, orientation and packing factors. The following equations define Nielsen's model and the parameters used in for estimation of the tensile modulus.

$$\frac{E_C}{E_1} = \frac{1 + AB\phi_2}{1 - B\psi\phi_2} \quad (8.9)$$

$$A = k_E - 1 \quad (8.10)$$

$$B = \frac{\frac{E_2}{E_1} - 1}{\frac{E_2}{E_1} + A} \quad (8.11)$$

$$\psi = 1 + \frac{1 - \phi_m}{\phi_m^2} \phi_2 \quad (8.12)$$

where:

ϕ_m = maximum packing fraction of the filler

In this project, Equations 8–9 to 8.12 will be referred to as 'Nielsen model'.

The constant, A , is related to the generalized Einstein coefficient, which is a function of the aspect ratio and orientation (random vs. unidirectional) of the filler. The maximum packing fraction ϕ_m is the actual volume of the filler particles divided by the apparent volume of the particles (164), and it depends on the particle shape (sphere, irregular particles, fibers) and packing order (random loose, random close, three-dimensional random, etc). The values of ϕ_m for different filler shapes were shown in Chapter 6. The parameter B in Equation 8.11 is related to the ratio of the tensile modulus of the matrix and filler. Equation 8.12 defines the factor ψ , which is related to the maximum packing fraction of the filler. We note that the value of $\psi\phi_2$, equivalent to a reduced volume fraction, approaches 1.0 when $\phi_2 = \phi_m$.

The values of the k_E and ϕ_m can be obtained theoretically. However, to obtain a better fit to experimental data, these parameters are assigned empirical values, which may differ from theoretical values.

An alternative to Equation 8.12 has been proposed by McGee and McCullough for calculating the parameter ψ (47,129,163). This equation is used when the tensile modulus of the filler is much greater than that of the polymer, and for values much higher than 1.0 for the generalized Einstein coefficient k_E (47). This equation is shown below:

$$\psi \cong 1 + \frac{\phi_1}{\phi_m} [\phi_m (1 - \phi_1) + (1 - \phi_m) \phi_1] \quad (8.13)$$

In this study, we will refer to Equations 8.9–8.11 and 8.13 as the ‘modified Nielsen model’.

8.3 Tensile Modulus Modeling Results

The mathematical models described in Section 8.2 use the tensile modulus of each constituent of the composite material. Based on the experimental results from Chapter 7, the tensile modulus of polypropylene was 1510 MPa. The tensile modulus of Ketjenblack EC–600 JD carbon black and Thermocarb TC–300 synthetic graphite used in previous modeling research for nylon 6,6 and polycarbonate–based composites was assumed to be 827 GPa (35). For the carbon nanotubes composites, the modulus of the filler was found in recent literature to range between 900 and 1060 GPa (165-168). For our modeling work, we selected an intermediate value of 1000 GPa.

The Halpin Tsai models also require the filler aspect ratio (length/diameter). For synthetic graphite, we used an aspect ratio of 1.67, whereas for carbon nanotubes, the aspect ratio assumed was 1000. This value can be calculated from the filler properties provided by the vendor (85). Finally, we assumed the carbon black particles to be spherical. Therefore, a value of 1.5 was used instead of the parameter $2(L/d)$ in the Halpin–Tsai model (44,128).

The values for the parameters A and ϕ_m are available in the literature for different types of filler particles, and they are listed in Section 6.2.1 of this dissertation (47,163). The selected values for this modeling work are listed below:

Ketjenblack EC–600 JD carbon black:

$$A = 1.5$$

$$\phi_m = 0.2$$

Thermocarb TC-300 synthetic graphite:

$$A = L/d \text{ (uniaxially oriented rods with aspect ratio } L/d = 1.68)$$

$$\phi_m = 0.637$$

Hyperion Catalysis International's Fibril™ carbon nanotubes:

$$A = 8.38 \text{ (random fibers with aspect ratio} = 15, \text{ largest published value)}$$

$$\phi_m = 0.2$$

It is noted that since the actual aspect ratio in our system is unknown, the A value of 8.38 for carbon nanotubes is only an estimate.

8.3.1 Basic and Halpin–Tsai Models Results

The tensile modulus values calculated using the inverse rule of mixtures, Halpin–Tsai and Nielsen models for single filler formulations are shown in Figures 8.1 to 8.3 for carbon black, synthetic graphite and carbon nanotubes in polypropylene, respectively. The rule of mixtures severely overpredicted the tensile modulus of the composites. As a result, this model is not included in these figures.

It can be observed from these figures that the lowest values obtained for all three fillers was obtained using the inverse rule of mixtures. Figures 13 and 14 show that the Halpin–Tsai models also underestimate the tensile modulus of composites with carbon black and synthetic graphite in the polypropylene matrix. On the contrary, the values obtained with the Halpin–Tsai models for the tensile modulus of carbon nanotubes composites were higher than the experimental data. This can be attributed to the highly aspect ratio of carbon nanotubes.

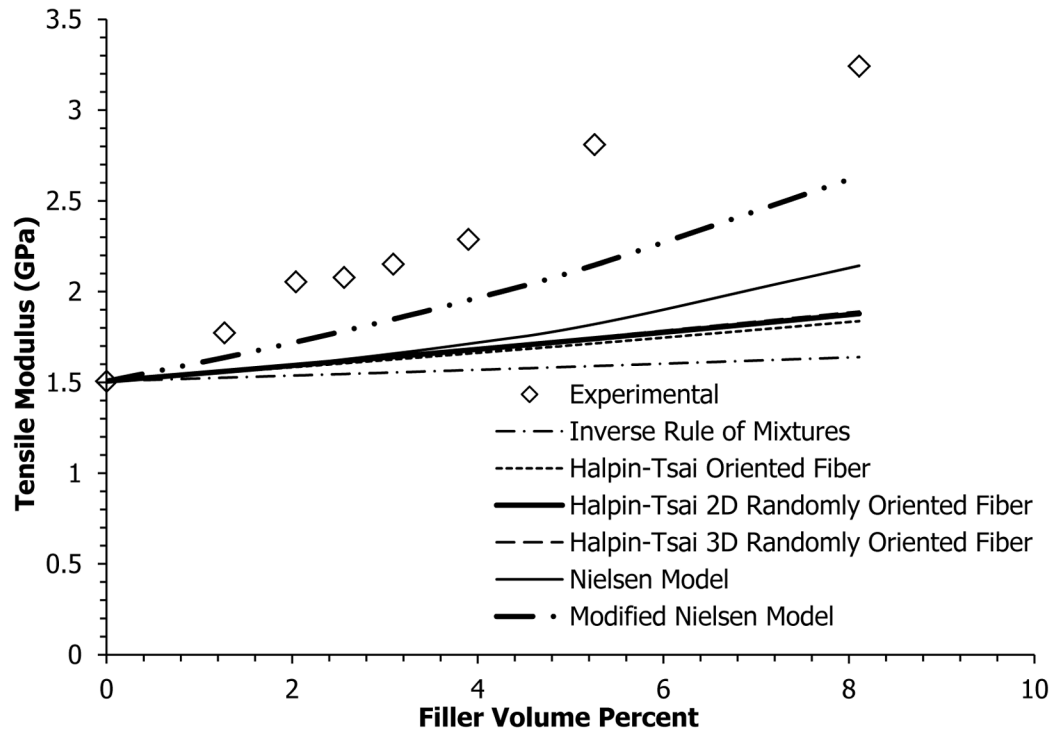


Figure 8.1 Tensile modulus modeling for carbon black in polypropylene. From lowest to highest, the models are Inverse Rule of Mixtures, Halpin–Tsai Oriented Fiber, 2D Halpin–Tsai, 3D Halpin–Tsai, Nielsen, and Modified Nielsen

8.3.2 Nielsen Model Results

Overall, the modified Nielsen’s model (Equations 8.9–8.11, and 8.13) yielded reasonable results for single filler polypropylene composites, for all the three fillers used in this study. This is consistent with the modeling results found by Konell et al. (35) for carbon black and synthetic graphite fillers in nylon 6,6 and polycarbonate resins. However, Keith et al. (31) found that for synthetic graphite in Vectra liquid crystal polymer composites, the Halpin–Tsai models showed better agreement to experimental data, and Nielsen’s model underpredicted the experimental tensile modulus values. This may be caused by poor adhesion of the synthetic graphite particles to the Vectra.

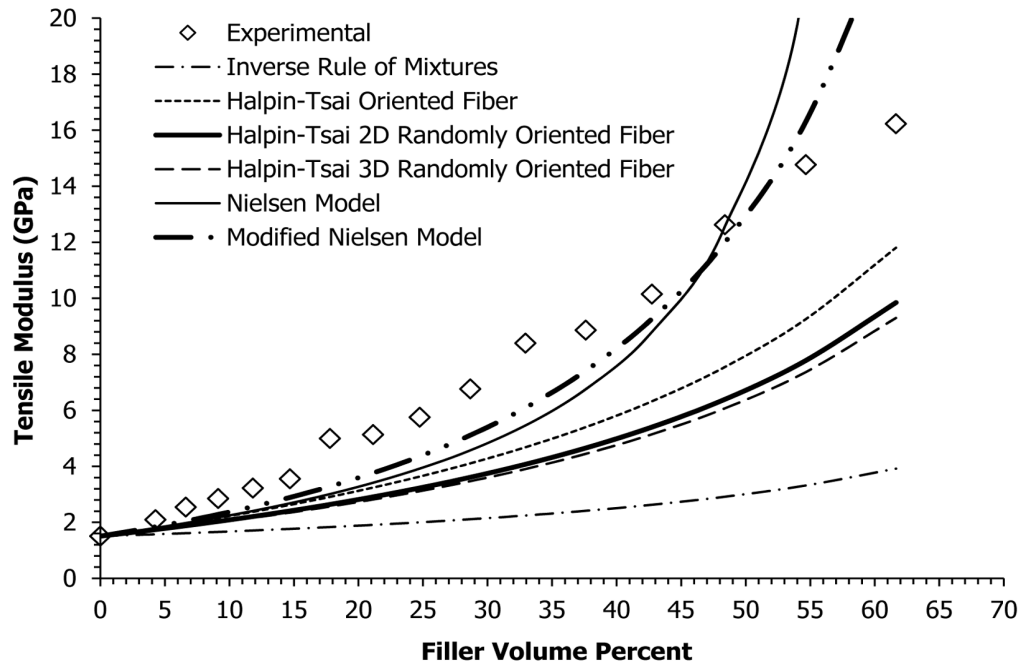


Figure 8.2 Tensile modulus modeling for synthetic graphite in polypropylene. From lowest to highest, the models at 55 vol.% are Inverse Rule of Mixtures, 3D Halpin–Tsai, 2D Halpin–Tsai, Halpin–Tsai Oriented Fiber, Modified Nielsen, and Nielsen

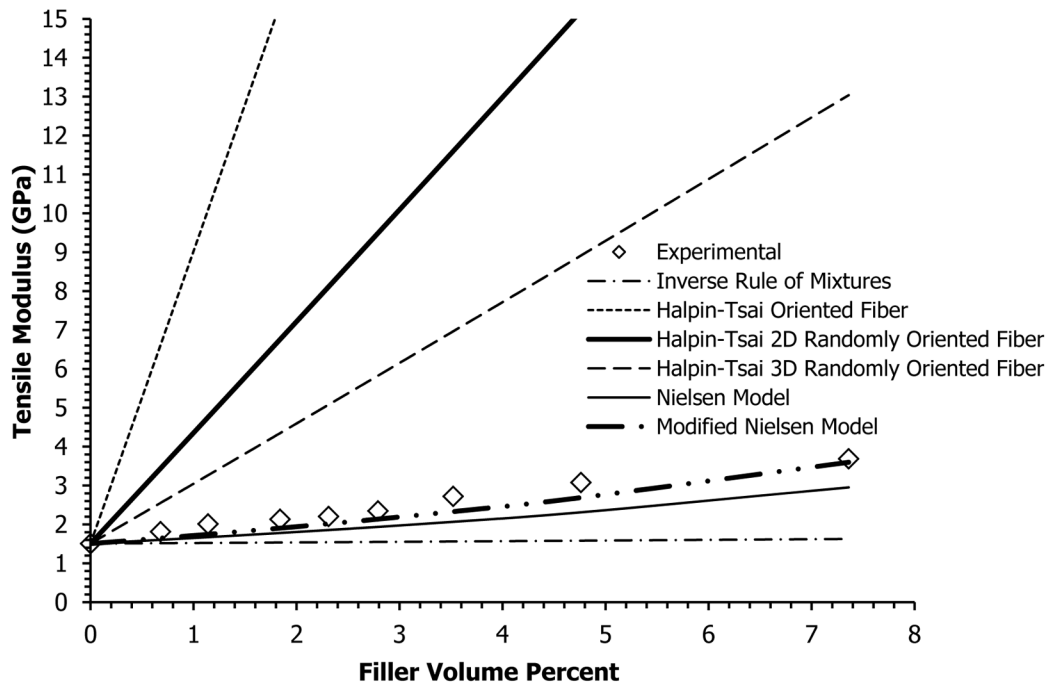


Figure 8.3 Tensile modulus modeling for carbon nanotubes in polypropylene. From lowest to highest, the models at are Inverse Rule of Mixtures, Nielsen, Modified Nielsen, 3D Halpin–Tsai, 2D Halpin–Tsai, and Halpin–Tsai Oriented Fiber

8.4 Conclusions

In this work, multiple mathematical models were applied to predict the tensile modulus of composites with varying amounts of carbon black, synthetic graphite and carbon nanotubes in a polypropylene matrix. Some of the models used include the rule of mixtures, inverse rule of mixtures, Halpin–Tsai oriented models and Nielsen’s models. The upper and lower limits of the predicted tensile modulus values are represented by the rule of mixtures and inverse rule of mixtures, respectively. For composites containing carbon black and synthetic graphite, the Halpin–Tsai and inverse rule of mixtures models yielded tensile modulus values lower than the experimental data. However, due to the high aspect ratio of carbon nanotubes, the Halpin–Tsai models overestimated the experimental results. In all cases, the modified Nielsen model was the most accurate model for prediction of the experimental tensile modulus, obtaining a higher deviation from experimental data for the carbon black and synthetic graphite composites.

Chapter 9: Development of Educational Tools in Hydrogen and Fuel Cell Technologies

9.1 Introduction

With the constant increase in student populations, universities have to face the challenge of maintaining effective education procedures to maintain their high standards. This is particularly true in the resource intensive engineering field. Technological advances in industry take place every day. Therefore, engineers and technicians must always keep learning to gain mastery in these new technologies, which can be done by the development of efficient and inexpensive methods to complement traditional education and training.

One of the areas most influenced by technological advances is the area of alternative energy sources. Therefore, it is a critical need to develop methodologies and tools to provide education and training to students from different engineering disciplines in these topics.

Research in engineering education in the field of alternative sources of energy has become a very important part of the Department of Energy programs in the United States. This is done through different agencies such as the Energy Efficiency and Renewable Energy (EERE). This agency works towards the investment in clean energy technologies, with the purpose of reducing dependence on foreign oil, protection of the environment and supporting the economy in the country (169).

The training necessary to progress towards the development of a clean energy career is provided by different academic institutions that offer degree programs or specializations in different clean energy fields or through other organizations that offer seminars in subjects related to energy efficiency and renewable energy (170).

This chapter explains more in detail, the different approaches to be used to make engineering students receive the appropriate background and skills in the area of alternative energy sources, particularly in hydrogen and fuel cell systems. In addition, the problem modules developed in this project for hydrogen and fuel cell technologies will be described.

9.2 Educational Approaches

9.2.1 Traditional Teaching Methodologies

In the past, education was transmitted through oral communication. The professor provided the lecture, and students were responsible for studying at home. At the conclusion of the unit, the evaluation was carried out by repeating a process called "assignment–study–recitation–test" (171). In addition the reliance on memorization of concepts instead of understanding the meaning or establishing a connection to assignments and real situations causes these practices to become inefficient in terms of the material learned by the student. This way, students tend to quickly forget what they memorized before a test (172).

Another problem with these practices of education is that professors usually try to cover all the material in the syllabus, thus forcing the pace of learning for some students. Traditional education approaches do not motivate students to work with others by promoting situations where they can collaborate with others in team work (172). When teachers do not provide proper background about how the material covered in class can be used to solve real life problems, the students tend to see the education process as a series of obstacles that need to be overcome to obtain a diploma or to obtain a satisfactory final grade, instead of learning the importance of the material in a specific course (172).

These traditional educational approaches were adopted in education in America until the late 19th century, when progressive education techniques were imported from Europe (171).

9.2.2 Problem–based Learning

Research in educational psychology has demonstrated that the traditional education practices discussed in section 9.2.1 of this work, lead to a low rate of knowledge retention (172).

A different approach to education is Problem–based learning (PBL). Dr. Howard Barrows and Ann Kelson of Southern Illinois University School of Medicine define PBL as both a curriculum and a process. The curriculum includes an adequate selection of problems that will require the student to obtain critical knowledge, proficiency in solving problems and teamwork skills. The educational process involved in PBL consists of the approaches used to solve problems or identification of challenges present in the students' life and career (173).

One of the common practices in PBL is that students work in groups towards the solution of real–world problems. PBL is a type of active learning which operates by an iterative method that allows students to recognize what information they know and the knowledge and skills they must acquire. The problems assigned to students provide them with the background and motivation for determining the solutions. PBL can be implemented as part of a class lecture and applied to courses in different majors (174).

Educational models based on PBL can help students enhance their problem–solving skills, research skills, and leadership and social skills as they learn to work in teams. In addition, PBL benefits students in the following ways (172,174):

- Increases motivation to learn concepts
- Enhances communication skills and critical thinking and writing
- Improves retention of concepts and information
- Stimulates the ability to work cooperatively in teams

- Allows the student to apply information learned previously and integrate the newly acquired skills to future challenges.

In the use of PBL, the instructor plays the role of providing tools for facilitating group learning, as well as a guide and evaluator of the students' efforts in solving problems. In addition to the students acquiring a more solid background in the topics included in the problems, the instructor learns jointly with students by observing the difficulties most of the students have when solving these problems. Therefore, instructors find interest and excitement in new teaching practices. However, PBL presents a challenge because the instructor must develop an adequate set of problems that will contribute to the students' profile after completing a course (174).

Studies indicate that students with experience in PBL techniques perform as well as other classmates on national exams (173).

9.2.3 Active Learning vs. Passive Learning

Every student who has attended school prefers certain courses, or considers some classes to be more interesting or exciting than others. These preferences frequently have an influence on the amount of material learned in a course. As students, we all have taken classes that offer learning methods based on activities or challenges used by professors, which produce a difference in the class outcomes. This difference can be caused by the use of active or passive learning.

In passive learning, the teacher's activities consist of delivering lectures by outlining the topics to be covered in a unit on the board and simply providing information to students by dictating, or writing answers to example problems on the board. Simply put, the instructor just tells the student how and what to think about a specific topic. The role of the student in passive learning consists of following the teacher's instructions and taking notes about aspects they consider important for a test. The evaluation methods in these courses are carried out by giving the

student tests including multiple choice questions that can be easily answered by memorizing the class notes.

On the other hand, there is active learning, in which the professor plans activities that stimulate students to self-guided learning by asking questions or assigning problems. The main difference between active and passive learning is that in active learning, the student relays information instead of just receiving it. Another difference is that even if the instructor plans an outline for the course, he does not require the class to follow it rigorously. Instead, the teacher will let the students participate actively by looking for answers and promoting discussions of the results found. As we see, students following active learning practices become more involved in the learning process. The use of active learning methodologies creates a fun learning process and the students modify their attitudes towards learning and develop answers for themselves. Therefore, active learning becomes a useful method to understanding real world situations and involvement of students in the acquisition of knowledge.

McCarthy and Anderson (175) obtained results suggesting that the use of active learning in the classroom contributes to the retention of information better than traditional education approaches. In their study, McCarthy and Anderson propose two activities applied to courses in social sciences and humanities. One of them is a role play where the students are required to be identified with one national or ethnic group during the colonization, thus making the student acquire a knowledge of multiculturalism during that period in history.

In engineering majors, the instructor can plan different activities which require the students to participate actively. As an example, Keith (176) proposes the Stanley Cup of Transport Phenomena, where a student is randomly selected and asked a question related to the lecture. If the student is present and answers the question correctly, he receives a prize and scores two points for his team. The 'playoffs' for the Transport Cup is an activity planned for the end of the semester, where the students review the concepts covered during the course in the form of

'Transport Jeopardy' in a similar way to the television show. This way, the team that earns the highest score from the individual questions during the semester and the Transport Jeopardy wins the Transport Cup. Another example of the use of active learning in engineering is the use of computer-based instruction, as proposed by Zheng and Keith (177,178). In this work they developed four JAVA applets for the chemical engineering courses of transport phenomena and chemical reactor design, which simulate four classic problems in these courses: one dimensional diffusion at unsteady state, one dimensional unsteady-state heat conduction and slabs, cylinders and spheres, Heisler charts for unsteady state heat transfer, and reaction and diffusion in porous catalytic substrates. These four JAVA applets allow students to better understand the dynamic behavior of heat and mass transfer processes, as they provide the student with animations showing how the temperature or concentration are changing with time.

These activities serve as examples of how active learning can be carried out in a classroom and the advantages it offers. The outcomes of these practices are that students become more active and interested in their learning processes, while at the same time they develop a sense of team work and competence.

9.3 Learning Styles

The process by which students learn information can take place in many different ways, e.g. seeing and hearing; reflecting and acting; reasoning logically and intuitively; memorizing and visualizing, and drawing analogies and building mathematical models. In a similar way, teaching methods are also different. Some instructors deliver lectures by providing demonstrations or discussions, while others focus on principles or real-world applications. The amount of information a student can learn during a lecture is determined by the abilities of the student and the compatibility of his learning style with the teaching methods adopted by the instructor (179).

The learning process can be described by a two-step mechanism: reception and processing of information. The reception occurs when external information perceived through the senses and internal information (originated by thoughts) is provided to students. In this step, the student decides what information they will retain or ignore. The processing of information is what yields different learning styles, as the information can be processed by memorization, inductive or deductive reasoning, reflection or action, and introspection or interaction with others. The result of these steps is that the material can be learned or not (179).

According to the way students receive and process information, they can be classified into learning-style models. Felder (180) notes that the Kolb Learning Style Model separates students as taking information in by either concrete experience or abstract conceptualization and internalizing information by active experimentation or reflective observation (181-184). These two preferences give way to four learning types:

- Type 1: concrete and reflective (answers the question "Why?")
- Type 2: abstract and reflective (answers the question, "What?")
- Type 3: abstract and active (answers the question, "How?")
- Type 4: concrete and active (answers the question, "What if?")

In order to meet the needs of all different kinds of learning styles, instructors work in the development of teaching strategies, thus inducing students to adopt a deep approach to learning. Felder and Brent (185) define three different categories of diversity that have an important effect in teaching methods and learning processes, which are:

- Students' learning styles
- Approaches to learning (surface, deep and strategic)
- Intellectual development levels (attitudes about the nature of knowledge and how it should be obtained and assessed)

Between these three categories, there are many common aspects which make the implementation of teaching techniques to address them more manageable (185). Felder and Silverman (179) provide different teaching techniques to address all learning styles, some of which are stated below:

- Provide learning motivation by relating the material being delivered to previous lessons or to what will be covered later in the same course, material from other courses or to particular students' experiences (Inductive/global)
- Find a balance when using materials emphasizing methods for solving practical problems (sensing/active) with materials focused on understanding fundamentals (intuitive/reflective)
- Make use of visual aids such as figures, schematics or videos to support verbal material (sensing/visual) and provide demonstrations and hands-on activities if possible (active)
- Use computer-aided instruction (sensing/active)
- Let the students take a break from writing notes to think about the concepts covered at that point of the lecture (reflective)

Although the diverse styles with which students learn are numerous, the inclusion of a relatively small number of techniques in an instructor's repertoire should be sufficient to meet the needs of most or all of the students in any class (179).

9.4 Hydrogen and Fuel Cell Education Curriculum

In an effort to create educational tools to better prepare engineering students in topics related to alternative energy sources, a series of problem modules have been developed in this project. These modules were created as part of the Department of Energy project with the objective of overcoming different educational barriers and misunderstandings in the use of hydrogen as an energy carrier and fuel cells. Hence, educating key audiences will help achieve the demonstration

of fuel cell fundamentals in the near terms to facilitate commercialization and market acceptance in the long term (186).

The Fuel Cell Technologies Program of the Department of Energy addresses the obstacles for development and deployment of hydrogen and fuel cells to decrease the dependence on fossil fuels and enable clean power generation. Some of the educational barriers identified by this program are (186):

- Little information for people outside the R&D community
- Conflicting public messages
- Disconnect between hydrogen information and dissemination networks

The Department of Energy is seeking to facilitate demonstrations and workshops in hydrogen and fuel cells. This is done through the Hydrogen Education subprogram, which has the objective of providing objective information to different types of audience involved in the use of hydrogen and fuel cells, such as government representatives, local communities and the public (186).

The educational tools developed in this work address the educational barriers mentioned earlier in this section by targeting efforts to educate undergraduate and graduate students of social sciences and engineering majors.

9.4.1 Educational Goals

In January 2003, President George W. Bush approved federal funding for research projects to develop passenger vehicles powered by fuel cells. As part of this initiative, it is paramount to develop educational programs related to hydrogen and fuel cells and creation of a hydrogen economy and infrastructure.

Through the proposed work for this Department of Energy Project, undergraduate and graduate university students will be introduced to key concepts, experiments and project assignments,

focusing on hydrogen technology. It is common that the curriculum in engineering programs at different universities delays in keeping up to date in emerging technologies. This project addresses this issue by the Enterprise program, which introduces research programs in hydrogen technology in the undergraduate engineering curriculum.

The hydrogen and fuel cells curriculum developed in this program has also the objective of coordinating effort with industry through contacts in the hydrogen, fuel cell systems and energy sectors, which provide input for the development of the educational modules described in the following sections of this work.

9.4.2 Description of Hydrogen and Fuel Cell Curriculum at Michigan Technological University

The proposed work for the educational section of this research work is organized into five different tasks, which are explained below in more detail. The following components of this hydrogen education project can be accessed through the Hydrogen Education website at Michigan Technological University (187).

➤ *Task 1: Develop and/or Refine Courses in Hydrogen Technology*

Before this project started, there were two courses in fuel cells developed at Michigan Technological University. The first one is Fuel Cell Fundamentals, which is an introductory course in fuel cell technologies and calculations applied to proton exchange membrane fuel cells offered for undergraduate students. The following are topics included in the material for this course:

- Introduction to fuel cells
- Fuel cell efficiency
- Effect of pressure and gas concentration on fuel cell performance
- Losses in fuel cell systems

- Mass balances in fuel cells
- Humidity and water management in proton exchange membrane fuel cells
- Thermal management of fuel cell systems
- Hydrogen economy

The other course is Fuel Cell Technology for advanced undergraduate and graduate students.

The material covered in this course is listed below:

- Introduction and basic information on fuel cell technology
- Efficiency and open circuit voltage
- Operational fuel cell voltages
- Proton exchange membrane fuel cells
- Alkaline fuel cells
- Direct methanol fuel cells
- Phosphoric acid fuel cells
- Molten carbonate fuel cells
- Solid oxide fuel cells
- Fuels and fuel reforming
- Balance of plant and delivering fuel cell power
- Fuel cell systems

Students at Michigan Technological University participating in the Alternative Fuels Group Enterprise requested the development of a formal course in the area of fuel cells, since it was not included in their standard curriculum. Therefore, the courses of Fuel Cell Fundamentals and Fuel Cell Technology were developed by Dr. Jason Keith and Dr. Abhijit Mukherjee, respectively.

In addition, two courses were also developed by Dr. Jason Keith. One of them introduces the student to different technologies for hydrogen production and hydrogen public and government policies. Some of the technologies included in this course for hydrogen production are steam–

methane reforming, coal and biomass gasification, and electrolysis of water powered by wind or solar energy. A full list of the topics covered in this course is shown below:

- History of energy production (Energy Consumption Analysis module)
- Energy sources and emissions (Energy Emissions Analysis module)
- Electric and hybrid vehicles (Battery Energy Analysis module)
- Fuel cells and fuel cell vehicles (Battery/Fuel Cell Vehicle Range module)
- Energy/Hydrogen from natural gas: steam reforming (Equilibrium Simulation of a Methane Steam Reformer module)
- Energy/Hydrogen from natural gas: separations (Hydrogen Purification module)
- Energy/Hydrogen from coal (Coal Gasification problem)
- Energy/Hydrogen from biomass (Biomass Gasification problem)
- Energy/Hydrogen from electrolysis/wind (Wind Energy problem)
- Energy/Hydrogen from solar (Solar Panel Design problem)
- Energy/Hydrogen from nuclear (no problem)
- Hydrogen public policy (no problem)

The last course developed as part of this education project was a laboratory course in hydrogen measurement. In this course, students work in groups of four to conduct the following sets of experiments organized in 4 parts:

- Dr. Fuel Cell: In these experiments, students determine the characteristic curve for a solar panel used to produce hydrogen when it is connected in parallel and in series.
- 50 W Fuel Cell Instructor: In this set of experiments, the students evaluate how different parameters such as current, voltage, hydrogen flow rate affect the efficiency of a 50 W fuel cell stack. In addition, students use the results obtained to scale this fuel cell to a large power level.

- Ballard Nexa 1.2 kW fuel cell: Here the students power a 1.2 kW fuel cell at different loads to obtain the stack voltage and current depending on the load, and the cell voltage, lower heating value (LHV) efficiency, hydrogen consumption rates and applied resistance.
- Fuel Cell Car: In this last experiment, the fuel economy of a fuel cell powered car is calculated.

These courses are part of the requirements for students in different engineering majors who are pursuing a minor in Hydrogen Technology, described in more detail in the following section.

➤ *Task 2: Develop Curriculum Programs in Hydrogen Technology*

The hydrogen education curriculum was implemented as a minor or concentration within the Enterprise Program at Michigan Technological University.

The enterprise program is offered to undergraduate students in engineering or business programs, either as a minor or as a concentration as part of their degree program, and consists of the integration of students from the second semester of freshman year, and sophomore, junior and senior years into a company-like project (188,189). Table 9.1 states the requirements for obtaining a minor in hydrogen technology.

Table 9.1
Components of Hydrogen Technology Minor (16 Credits Total)

Area	Number of Credits
Alternative Fuels Group Enterprise: Fuel cells or hydrogen design and implementation projects; 1 credit per course for Freshman, Sophomore and Junior level students and 2 credits per course for Senior-level students	4–6
Fuel Cells Course	1–3
Hydrogen Technology Course	1
Elective Courses: discipline specific with H ₂ or fuel cell applications (a partial listing is shown with chemical engineering as an example) CM3110 Transport/Unit Operations 1 CM3120 Transport/Unit Operations 2 CM 4000 Chemical Engineering Research CM 4310 Chemical Process Safety/Environ.	Remainder

In addition to the minor and concentration in Hydrogen Technology, a graduate certificate in Hybrid Electric Vehicle engineering was developed. This certificate provides a solid background on the design and operating characteristics of electric drive and hybrid vehicles. To earn this certificate, the student is required to complete 15 credits from the courses shown in Table 9.2.

The certificate in hybrid electric vehicle engineering can be obtained by students at undergraduate and graduate levels. This involves core courses related to this discipline and participation in laboratory courses will allow students to acquire hands-on experience in real-world situations occurring in electric and hybrid vehicles.

➤ *Task 3: Develop Modules for Core and Elective Engineering Courses*

In addition to the development of elective courses related to hydrogen technology and fuel cells, our research group developed supplemental material and projects for core courses in chemical engineering, electrical engineering and mechanical engineering. Through this we can foster an interest in engineering students from these majors in the hydrogen education curriculum.

The modules developed in this part of the project for the Chemical Engineering major are available online on the Fuel Cell Curriculum website (190,191). There are additional modules for other engineering disciplines also available online through the Hydrogen education website (187). Table 9.3 shows a list of some of the modules for different engineering programs.

Table 9.2
Required and Elective Courses for earning Graduate Certificate in
Hybrid Electric Vehicle Engineering

Required Courses	Number of Credits
EE/ MEEM 5295: Advanced Propulsion Systems for Electric Drive Vehicles	3 Credits
Any two of the following courses:	
EE/MEEM 4295: Introduction to Propulsion Systems for Electric Drive Vehicles	3 Credits
EE 4227: Power Electronics	3 Credits
MY/CM 5760: Vehicle Battery Cells and Systems	3 Credits
EE 5221: Advanced Electrical Machines	3 Credits
MEEM 5450: Vehicle Dynamics	3 Credits
Elective Courses	Number of Credits
EE/MEEM 4295: Introduction to Propulsion Systems for Electric Drive Vehicles	3 Credits
EE 4227: Power Electronics	3 Credits
MY/CM 5760: Vehicle Battery Cells and Systems	3 Credits
EE 5221: Advanced Electrical Machines	3 Credits
MEEM 5450: Vehicle Dynamics	3 Credits
EE/MEEM 4296: Introduction to Propulsion Systems for Electric Drive Vehicles Lab	1 Credit
EE/MEEM 5296: Advanced Propulsion Systems for Electric Drive Vehicles Lab	1 Credit
EE/MEEM 4750: Distributed Embedded Control Systems	3 Credits
EE/MEEM 5750: Distributed Embedded Control Systems	3 Credits
EE 5200: Advanced Methods in Power Systems	3 Credits
EE 3120: Electric Energy Systems	3 Credits
EE 4221: Power System Analysis 1	3 Credits
EE 4222: Power System Analysis 2	3 Credits
EE 5223: Power System Protection	3 Credits
EE 5230: Power System Operations	3 Credits
EE 5290: Selected Topics in Power Systems	3 Credits
MEEM 4220: IC Engines 1	3 Credits
MEEM 5200: Advanced Thermodynamics	3 Credits
MEEM 5250: IC Engines 2	3 Credits
MEEM 5670: Experimental Design in Engineering	3 Credits
MEEM 5680: Optimization	4 Credits
MEEM 5700: Dynamic Measurement and Signal Analysis	3 Credits
MEEM 5715: Linear Systems	3 Credits
MEEM 4260: Fuel Cell Technology	3 Credits
MEEM 5220: Fuel Cell Technology	3 Credits
MY 4165: Corrosion and Environmental Effects	3 Credits
MY 5100: Thermodynamics and Kinetics 1	3 Credits
MY 5110: Thermodynamics and Kinetics 2	3 Credits
MY 5410: Materials for Energy Applications	1 Credit
CM/ENT 3974: Fuel Cell Fundamentals	1 Credit
CM/ENT 3977: Fundamentals of Hydrogen as an Energy Carrier	1 Credit
CM/ENT 3978: Hydrogen Measurements Laboratory	1 Credit

Table 9.3

Problem modules developed as part of the Hydrogen and Fuel Cells education project for different engineering programs (187)

Department	Subject	Title of the Modules
Chemical Engineering (45 modules total)	Material and Energy Balances	<ul style="list-style-type: none">• Heat of Formation for Fuel Cell Applications• Material Balances in a Solid Oxide Fuel Cell• Energy Balance in a Solid Oxide Fuel Cell
	Thermodynamics	<ul style="list-style-type: none">• Vapor pressure and Humidity of Fuel Cell gases• Nernst Equation
Mechanical Engineering (27 modules total)	Combustion and Air Pollution	<ul style="list-style-type: none">• Hydrogen production costs• Hydrogen flammability• Theoretical fuel consumption and power
Electrical Engineering (11 modules total)	Circuits and Instrumentation	<ul style="list-style-type: none">• Fuel Cell series load analysis• Solid Oxide Fuel Cell stack performance: Single Load
Energy Modules (12 modules total)	Coal Energy	<ul style="list-style-type: none">• Material Balances on CO₂ Absorption/Stripping Process

All of these modules start by referencing the section of the textbook used for the corresponding course and stating the concepts covered by the problem module. Then the student is provided with the motivation and background required to solve the problem. In this section of the module, the importance of the calculations and applications to real-world problems is explained to the student, as well as the fundamentals and theories required to solve the module. After this, an example problem statement is presented to the student, with the solution explained in detail and a summary of the outcome and applications of the calculations presented in the module. Finally, the example problem is modified and assigned to the student as a homework problem or a project.

This type of problem modules have been implemented in the courses described in the section corresponding to Task 1 of this project and in graduate level courses of the Chemical Engineering program.

Additional to these modules, supplemental material for chemical engineering courses was developed, as it will be explained in the following section.

➤ *Task 4: Develop Modules to Supplement Commonly Used Chemical Engineering Texts*

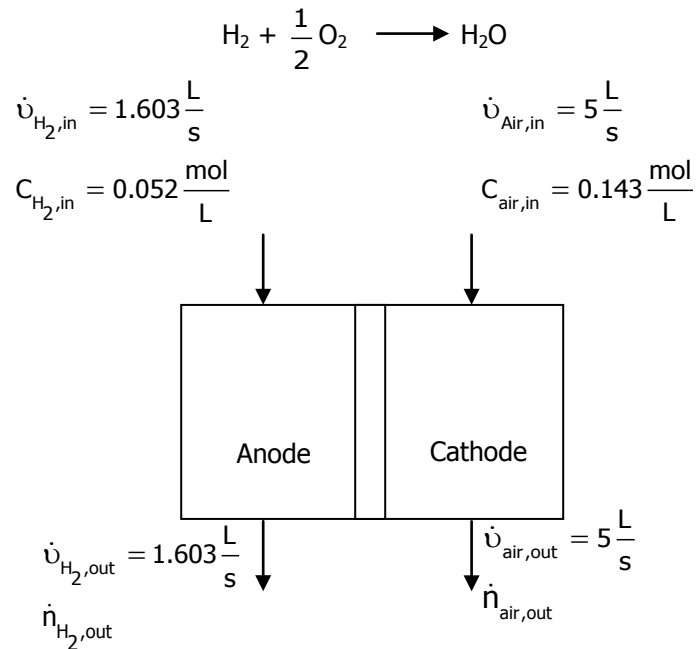
This task consists of the creation of new problem modules to supplement the chemical engineering textbooks “Elementary Principles of Chemical Processes”, third edition by R. M. Felder and R. W. Rousseau (1992) and “Transport Processes and Separation Process Principles (Includes Unit Operations)”, fourth edition by C.J. Geankoplis (1993).

The objective of this task is to emulate the successful Bioengineering Educational Materials Bank website (194) to facilitate the application of engineering principles to biology topics. In a similar way, the supplemental material developed in this project has the objective to introduce chemical engineering students to basic engineering principles, while providing background information and motivation in fuel cell and hydrogen technologies.

The supplementary material developed for the textbook by Felder and Rousseau includes 90 problem modules covering materials from Chapters 2 to 9, and Chapter 11. The following is an example of these modules.

Example 11.2-2 Transient Behavior of a Proton Exchange Membrane Fuel Cell

The following diagram is describing the reaction and process occurring inside a one-cell proton exchange membrane fuel cell:



The current produced by the fuel cell is a function of the amount of hydrogen reacted, and can be determined by the following equation:

$$\dot{n}_{\text{H}_2,\text{reacted}} = \frac{IN}{2F}$$

where:

I = Current produced by the fuel cell in amperes (A)

N = Number of fuel cells (here we have assumed 1 cell)

F = Faraday's constant = $96485 \frac{\text{C}}{\text{mol} \cdot \text{e}^-}$

Derive an equation for the current produced by the fuel cell as a function of time if 93% of the hydrogen is converted into products. Assume that the chemical reaction occurring in the fuel cell is a first order reaction.

Strategy

We can use material balances for hydrogen on the reactor and solve for the current I.

Solution

The general balance equation is given by:

$$\text{Accumulation} = \text{Input} - \text{Output} + \text{Generation} - \text{Consumption}$$

In this problem, each one of the terms in the material balance equation is described by the following equations:

$$\text{Accumulation} = \frac{dn_{H_2}}{dt}$$

$$\text{Input} = \dot{n}_{H_2, \text{in}} = \dot{V}_{H_2, \text{in}} C_{H_2, \text{in}}$$

$$\text{Output} = \dot{n}_{H_2, \text{out}} = \dot{n}_{H_2, \text{in}} - \dot{n}_{H_2, \text{reacted}}$$

$$\text{Generation} = 0$$

$$\text{Consumption} = \dot{n}_{H_2, \text{reacted}} = \frac{IN}{2F}$$

Substituting each equation in the material balance equation, we get:

$$\frac{dn_{H_2}}{dt} = \dot{n}_{H_2, \text{in}} - \dot{n}_{H_2, \text{out}} + 0 - \dot{n}_{H_2, \text{reacted}}$$

It is known that 93% of the hydrogen entering the reactor is converted into hydrogen. Thus,

$$\dot{n}_{H_2, \text{out}} = \dot{n}_{H_2, \text{in}} - \text{—————} = 0.07\dot{n}_{H_2, \text{in}}$$

This equation can be entered into the material balance equation to yield:

$$\frac{dn_{H_2}}{dt} = \text{_____} - 0.07\dot{n}_{H_2, in} - \dot{n}_{H_2, reacted}$$

Writing the amount of hydrogen reacted in terms of the current, gives:

$$\frac{dn_{H_2}}{dt} = \text{_____} - \frac{IN}{2F}$$

The reaction rate indicates the consumption rate of hydrogen. For a first order reaction, the rate will be given by:

$$r = kn_{H_2}$$

where:

$$k = \text{reaction rate constant in s}^{-1}$$

The amount of hydrogen reacted can be obtained also by using the rate equation:

$$kn_{H_2} = \dot{n}_{H_2, reacted}$$

Writing the consumption rate of hydrogen in terms of the current, we get:

$$kn_{H_2} = \text{_____}$$

This equation can be differentiated to obtain the change of moles of hydrogen with time, as a function of the change in the current with respect to time:

$$k \frac{dn_{H_2}}{dt} = \text{_____} \frac{dI}{dt}$$

Solving for $\frac{dn_{H_2}}{dt}$, we have:

$$\frac{dn_{H_2}}{dt} = \text{_____} \frac{dI}{dt}$$

Substituting this equation into the mass balance equation yields:

$$\text{_____} \frac{dI}{dt} = \text{_____} - \frac{IN}{2F}$$

Solving for the change in the current with time, we have:

$$\frac{dI}{dt} = \text{_____} - kI$$

Entering all the known quantities into this equation gives the following result:

$$\frac{dI}{dt} = \frac{2 \left(\frac{\text{C}}{\text{mol} \cdot e^-} \right) k}{1} 0.93 \left[\left(\frac{\text{L}}{\text{s}} \right) \left(0.052 \frac{\text{mol}}{\text{L}} \right) \right] - kI$$

$$\frac{dI}{dt} = \text{_____} k - kI$$

Initially, there is no hydrogen reacting in the fuel cell. Thus, the current generated is equal to zero:

$$@t=0, I = 0$$

Separating and integrating the equation for the rate of change for the current, we get:

$$\frac{dI}{\text{_____} k - kI} = dt$$

$$\int_0^I \frac{dI}{\text{_____} k - kI} = \int_0^t dt$$

$$-\frac{1}{k} [\ln(\text{_____} k - kI) - \text{_____}] = t$$

Using logarithmic equation properties, this equation can be rewritten as follows:

$$\ln \frac{(\text{_____} k - kI)}{(14959k)} = -kt$$

Taking the exponential of both left and right hand sides of this equation, eliminates the natural logarithm on the left side and allows us to solve for the current I as shown in the following steps.

$$\text{_____} k - kI = 14959ke^{-kt}$$

$$\text{_____} - I = \frac{14959ke^{-kt}}{\text{_____}}$$

$$I = \boxed{\text{_____}}$$

In a real fuel cell, the reaction rate is more complicated, but this example has shown how there is a delay in the response to load changes in a fuel cell.

As we can see in this example, the student is provided with a problem in the form of a workbook, where some of the values must be entered in the blanks. The module starts by giving the necessary parameters and explanation of the problem, followed by a strategy or starting point for determining the solution to the problem. This workbook format guides the student by explaining the procedure to determine the required values to obtain the final solution. The list of supplementary modules for the textbook by R. M. Felder and R. W. Rousseau is shown in Appendix E of this dissertation.

For the textbook by C. J. Geankoplis, a set of 75 problems similar to the example shown previously were developed. The same workbook format was used for these modules. This list of modules is shown in Appendix F.

The educational tools developed as part of Task 4 of this project are proposed to supplement the textbooks used for the courses of Fundamentals of Chemical Engineering and Transport/Unit Operations 1 and 2 of the Chemical Engineering program at Michigan Technological University, and can also be used by faculty at other institutions as they are available online at the hydrogen education website (187).

➤ *Task 5: Project Management and Reporting*

The progress made in the development of the educational tools in this project has been presented in quarterly reports to the Department of Energy and disseminated through the Annual Conferences of the American Institute for Chemical Engineers and American Society of Engineering Education in years from 2009 to 2011. Through these seminars, we introduced the different modules to students, faculty at other universities and people working in industry, thus targeting the Department of Energy barriers of disconnection between information in hydrogen and fuel cells and dissemination networks.

9.5 Preliminary Module Assessment

In this section, I show the results obtained from students feedback after using the modules described in Task 3 in Section 9.4.2 of this work. This information is also reported by Keith et al. (195). During Fall 2010, fifteen students registered for the course of Fundamentals of Hydrogen as an Energy Carrier at Michigan Technological University. In this semester, there were ten homework assignments. In six of these assignments, students were assigned the modules described in Section 9.4.2, with the exception of the solution to the home problem.

This project received approval from the Institutional Review Board (MTU Protocol # M0277, Hydrogen Education at Michigan Technological University) to use human subjects in the classroom. The following survey was created and distributed students during the final lecture of the semester. From the fifteen students registered in this course, twelve participated in this survey, and the results are summarized below (195):

1. I felt that the instructional material helped facilitate my learning.

Strongly Agree	<i>7 responses</i>
Agree	<i>5 Responses</i>
Ambivalent	<i>0 Responses</i>
Disagree	<i>0 Responses</i>
Strongly Disagree	<i>0 Responses</i>

2. I felt that the lecture showed me how to apply engineering principles to alternative energy/hydrogen technology systems.

Strongly Agree	<i>7 responses</i>
Agree	<i>5 Responses</i>

Ambivalent *0 Responses*

Disagree *0 Responses*

Strongly Disagree *0 Responses*

3. I felt that the homework problems allowed me to apply my engineering principles to alternative energy/hydrogen technology systems.

Strongly Agree *7 responses*

Agree *5 Responses*

Ambivalent *0 Responses*

Disagree *0 Responses*

Strongly Disagree *0 Responses*

4. Please provide any additional comments you may have on this course and/or the instructional modules:

Sample responses:

"The modules allowed us to understand the problems being asked. They provided examples for how to complete the problem without giving away the answers."

"I liked how the h.w. assignments were set up as real-world problems so we could see how this would/is actually applied."

"Although interesting, they were easy and failed to engage me."

The feedback provided by students who took this course show very good acceptance of the modules. This indicates the students seem to enjoy the material covered in the course, as well as the teaching approaches and homework assignments.

An additional survey was approved by the Institutional Review Board (MTU Protocol # M0639, Energy Knowledge Survey) for use of human subjects in the classroom. This survey was applied at the first class meeting as a pre-test survey and again at the last class meeting as a post-test survey. From the fifteen students registered in this course, fourteen participated in the pre-test and ten participated in the post-test. The first five questions were taken from the tenth national report card survey on energy knowledge (196). The following results were obtained from these surveys (195):

1. How is most electricity in the United States generated? Is it...

- | | |
|-----------------------------------|--|
| a. By burning oil, coal, and wood | <u>Correct Answer;</u> <i>Pre-test 71%, Post-test 100%</i> |
| b. With nuclear power | <i>Pre-test 14%, Post-test 0%</i> |
| c. Through solar energy, or | <i>Pre-test 0%, Post-test 0%</i> |
| d. At hydroelectric power plants? | <i>Pre-test 14%, Post-test 0%</i> |
| e. Don't know | <i>Pre-test 0%, Post-test 0%</i> |

2. Which of the following uses the most energy in the average home? Is it...

- | | |
|----------------------------------|---|
| a. Lighting rooms | <i>Pre-test 0%, Post-test 10%</i> |
| b. Heating water | <i>Pre-test 21%, Post-test 0%</i> |
| c. Heating and cooling rooms, or | <u>Correct Answer;</u> <i>Pre-test 64%, Post-test 90%</i> |
| d. Refrigerating food? | <i>Pre-test 7%, Post-test 0%</i> |
| e. Don't know | <i>Pre-test 7%, Post-test 0%</i> |

3. Which fuel is used to generate the most energy in the U.S. each year? Is it...

- | | |
|--------------|---|
| a. Petroleum | <u>Correct Answer;</u> <i>Pre-test 21%, Post-test 50%</i> |
|--------------|---|

b. Coal *Pre-test 43%, Post-test 40%*

c. Natural gas, or *Pre-test 7%, Post-test 10%*

d. Nuclear? *Pre-test 14%, Post-test 0%*

e. Don't know *Pre-test 14%, Post-test 0%*

4. Though the U.S. has only 4% of the world's population, what percentage of the world's energy does it consume? Is it...

a. 5% *Pre-test 0%, Post-test 0%*

b. 15% *Pre-test 21%, Post-test 10%*

c. 20%, or *Pre-test 43%, Post-test 30%*

d. 25%? Correct Answer; *Pre-test 14%, Post-test 60%*

e. Don't know *Pre-test 21%, Post-test 0%*

5. In the past ten years, has the average miles per gallon of gasoline used by vehicles in the U.S.

...

a. Increased *Pre-test 71%, Post-test 90%*

b. Remained the same *Pre-test 7%, Post-test 0%*

c. Gone down, or Correct Answer; *Pre-test 14%, Post-test 0%*

d. Not been tracked? *Pre-test 0%, Post-test 0%*

e. Don't know *Pre-test 7%, Post-test 10%*

Please also show any work for the following questions:

1. Estimate the pounds of carbon dioxide emissions per gallon of gasoline.

- a. 2 *Pre-test 21%, Post-test 10%*
- b. 3 *Pre-test 7%, Post-test 40%*
- c. 20 Correct Answer; *Pre-test 14%, Post-test 10%*
- d. 200 *Pre-test 14%, Post-test 20%*
- e. Don't know *Pre-test 57%, Post-test 20%*

2. How many kg of hydrogen are needed to provide the same amount of energy as one gallon of gasoline?

- a. 0.5 *Pre-test 14%, Post-test 10%*
- b. 1 Correct Answer; *Pre-test 21%, Post-test 30%*
- c. 2 *Pre-test 7%, Post-test 10%*
- d. 5 *Pre-test 14%, Post-test 30%*
- e. Don't know *Pretest 43%, Posttest 20%*

3. During a 10 hour period (8am–6pm) what is the incident solar energy over a 50 m² collection area in kW·hr in the US Southwest?

- a. 50 *Pre-test 7%, Post-test 10%*
- b. 100 *Pre-test 7%, Post-test 0%*
- c. 200 *Pre-test 7%, Post-test 20%*
- d. 300 Correct Answer; *Pre-test 14%, Post-test 30%*

e. Don't know *Pre-test 64%, Post-test 40%*

4. Power from the wind is proportional to the wind speed raised to what exponent?

a. $1/2$ *Pre-test 36%, Post-test 20%*

b. 1 *Pre-test 0%, Post-test 0%*

c. 2 *Pre-test 14%, Post-test 50%*

d. 3 Correct Answer; *Pre-test 0%, Post-test 20%*

e. Don't know *Pre-test 50%, Post-test 10%*

The national averages for correct answers on the first five questions of this survey are 36%, 66%, 36%, 50%, and 17%, respectively, as indicated by the energy report from the National Environmental Education & Training Foundation (196). Therefore, the students enrolled in this course that took the pretest did better than the national average on one question, average on two questions, and below average on two questions. For the post-test results, the students that participated in the survey scored above average on four of the five questions. The only one that was below average was for the fifth question on fuel economy. This may be due to the class discussions on the improvement of internal combustion engine operation.

The last four questions in this survey were based on the course material. It was expected students would have no knowledge prior to the pre-test and some knowledge for the post-test. One observation that can be made based on the students' answers is that there was not a big improvement in obtaining the correct answer from taking the course. Another observation is that at the beginning of the course, some of the students selected "Don't know" as answer for some questions. By taking the course, the students felt more confident in providing an answer. However, it is noted that the students did not show any work for any of the problems, which indicates that students just guessed their answers. Therefore, this survey will be modified so

students will have to provide for a numerical answer instead of having to answer multiple-choice questions.

9.6 Conclusions

This chapter has described some of the educational approaches commonly used in higher education, as well as a comparison of the traditional and active learning methodologies for educating students. These methodologies need to be adapted to address different learning styles adopted by students.

This chapter also describes the work performed to create educational tools to better prepare engineering students in topics related to alternative energy sources. These tools consist of the creation of new courses particularly in the area of hydrogen and fuel cells, with the objective of introducing these energy technologies to students in different engineering disciplines. A series of problem modules were developed as part of the material covered in these courses. These modules include different real-world energy problems which provide the student with motivation, fundamental concepts and examples of the calculations for designing fuel cell systems and determining important variables in fuel cell systems, such as gas flow rates or heat transfer.

In addition, supplementary materials were developed for the textbooks by Felder and Rousseau, and Geankoplis, used in core chemical engineering courses, such as Transport Unit/Operations and Material and Energy Balances.

Students' feedback indicates a good acceptance of the modules as positive comments were received. A second survey about knowledge in the areas of energy technology showed an improvement in the students after taking the Fundamentals of Hydrogen as an Energy Carrier, although some modifications have been proposed to better evaluate the improvement in the future.

Chapter 10: Summary and Future Work Recommendations

10.1 Introduction

Because of the increases in foreign oil demand, fuel cells have been considered a feasible alternative to the current technologies in the transportation sector. There are different research institutions and industries investing resources to develop fuel cell technologies. However, there are also technical limitations which have delayed the introduction of this technology in the market.

One important component of fuel cells is the bipolar plate. This component has multiple functions in a fuel cell:

- Provides mechanical support to the fuel cell stack
- Separates the anode of a fuel cell from the cathode of the adjacent cell
- Conducts the heat produced by the electrochemical reaction out of the system
- Circulates hydrogen on the anode side and oxygen from air on the cathode side of the adjacent fuel cell
- Facilitates the flow of electrons out of the fuel cell system to power the external load

In this study we developed carbon-filled polypropylene composites for application as fuel cell bipolar plates. The objectives of this work are the development and characterization of thermal and mechanical properties of the test specimens produced, as well as to understand what factors produce a change in the properties of the polypropylene matrix.

To fulfill these objectives, three different carbon fillers were added to a polypropylene matrix to produce the composite materials. The carbon fillers used in this project were Ketjenblack EC-600 JD carbon black, Thermocarb TC-300 synthetic graphite and Hyperion Catalysis International's

FibrilTM multi-walled carbon nanotubes. The concentrations of fillers used in the composite materials range from 2.5 wt.% to 15 wt.% for carbon black, 10 wt.% to 80 wt.% for synthetic graphite, and 2.5 wt.% to 15 wt.% of carbon nanotubes. The multiple filler formulations were produced by 3 combinations of two fillers (2.5CB*65SG, 2.5CB*6CNT, and 65SG*6CNT) and three fillers (2.5CB*65SG*6CNT). After determining the experimental properties of the materials produced in this research work, we applied mathematical models to predict the thermal conductivity and tensile modulus of the composites.

In addition to the technical requirements for fuel cells to emerge in the market, there exist educational barriers and misunderstanding in the use of hydrogen as an energy carrier and fuel cells that need to be overcome. Therefore, it is paramount to educate key audiences, such as engineering students, government officials and local communities. Several educational tools were developed in this work to educate undergraduate and graduate students of different engineering majors and were tested in university courses.

10.2 Thermal Conductivity Testing

The thermal characterization experiments conducted in this study indicate the thermal conductivity of the carbon/polypropylene composites are a function of the carbon fillers. By comparing the thermal conductivity values obtained for the different composite formulations, we observe the largest increase corresponds to synthetic graphite, followed by carbon nanotubes, and then carbon black. For multiple filler formulations, a statistically significant increase in through-plane thermal conductivity was observed in composites with a combination of synthetic graphite and carbon nanotubes, followed by composites containing synthetic graphite and carbon black. This behavior can be attributed to the possible formation of thermally conductive pathways with these carbon fillers, resulting in an increased composite thermal conductivity. The previous technical goal established by the Department of Energy for thermal conductivity of bipolar plates of 20.0 W/m·K was exceeded by injection molded formulations containing 75 wt.% (54.7 vol.%)

and 80 wt.% (61.6 vol.%) synthetic graphite in polypropylene, with thermal conductivities of 24.4 W/m·K and 33.6 W/m·K, respectively. This value was also reached by the test specimens produced by compression molding, containing 2.5 wt.% carbon black (2.2 vol.%), 65 wt.% synthetic graphite (46.2 vol.%) and 6 wt.% carbon nanotubes (4.8 vol.%), yielding the highest overall value of 37.0 W/m·K.

10.3 Thermal Conductivity Modeling

After determining experimental values for the different composite formulations produced in this project, Nielsen's model was used for predicting thermal conductivity values for the experimental results obtained from the Guarded Heat Flow Meter method and also for the Flash method. The optimization of the parameters A and ϕ_m for through-plane conductivity, and C and D for in-plane conductivity in these models minimized the difference between experimental and model results.

Nielsen's model was adapted for the prediction of through-plane thermal conductivity of composites containing multiple fillers. In a similar way, the parameters used in the equation for the prediction of in-plane thermal conductivity of single-filler formulations were used to obtain a new model which allowed to estimate the in-plane thermal conductivity of composites containing carbon black and carbon nanotubes. The thermal conductivity values obtained using Nielsen's model yielded values similar to the experimental results obtained through both the Guarded Heat Flow Meter and the Flash methods. For carbon nanotubes and synthetic graphite, the parameters of A and ϕ_m obtained for both experimental methods were similar. However, a larger value for the parameter A was obtained for the data from the flash method. The large value of A and the linear behavior of Nielsen's model for carbon black indicate that at the volume fractions studied in this project, the thermal conductivity follows the rule of mixtures.

10.4 Testing of Mechanical Properties

Another part of this project consisted of the characterization of tensile and flexural properties of carbon/polypropylene composites fabricated in this project. For all single filler formulations the tensile and flexural modulus increased with higher filler concentrations. Opposite to what occurred with the tensile and flexural modulus, a decrease in tensile and flexural strengths of composites with carbon black in polypropylene, and synthetic graphite in polypropylene was observed. However, the tensile and flexural strengths of carbon nanotube formulations were increased. This can be justified by the high aspect ratio of this filler (length/diameter = 1000). The technical specification for flexural strength of bipolar plates set by the Department of Energy is 25 MPa, which is exceeded by all the composite formulations developed in this work.

As part of the mechanical tests performed in this project, Nanoscratch tests were conducted to evaluate the degree of adhesion between the filler particles and the polymer matrix. This adhesion force can be estimated by the crest factor obtained from the penetration of the indenter into the composite surface as a function of the scratch distance. The experimental data obtained by performing Nanoscratch tests provide data that could be used to measure the degree of adhesion between fillers and the polymer matrix. The degree of adhesion can be represented by the normalized crest factor. When comparing crest factors of polypropylene composites with liquid crystal polymer composites, it can be seen that a better degree of adhesion exists for the carbon/polypropylene composites. Data analysis was done using the penetration into the composite surface as a function of the scratch distance and the results of this test agree with the results obtained for the tensile modulus of the composites. The normalized crest factor (ratio of the composite crest factor to the polymer crest factor) for composites containing 20 wt.% synthetic graphite in polypropylene (9.1 vol.%) was compared to previous results obtained for formulations containing 20 wt.% synthetic graphite (13.5 vol.%) in Vectra liquid crystal polymer (31). The higher value found for the polypropylene composites suggests there is a better

adhesion between the synthetic graphite particles in the polypropylene matrix, due to the resistance of the composite to scratching.

10.5 Tensile Modulus Modeling

As was done for the thermal conductivity of the polypropylene-based composites, after obtaining experimental results for tensile modulus, we proceeded to apply different mathematical models to predict the tensile modulus of the composites. The models used in this section were the rule of mixtures, inverse rule of mixtures, Halpin–Tsai oriented models and Nielsen’s models. To predict the tensile modulus values, we used values for the tensile modulus of the filler from the literature (35,165-168) and for the matrix material, we used the experimental value measured in this project. In all composite formulations, the modified Nielsen’s model yielded the lowest standardized error between the experimental and modeling data.

10.6 Development of Hydrogen and Fuel Cell Technology Curriculum

As mentioned in Section 10.1 of this chapter, in this work we developed a series of educational tools to better prepare students in fuel cell technology and the use hydrogen as an energy carrier. To address the educational challenges that create misunderstandings in the use of hydrogen for fuel cells, we divided our work into five different tasks:

- Develop and/or Refine Courses in Hydrogen Technology
- Develop Curriculum Programs in Hydrogen Technology
- Develop Modules for Core and Elective Engineering Courses
- Develop Modules to Supplement Commonly Used Chemical Engineering Texts
- Project Management and Reporting

Some of the work done as part of these five tasks consist of the creation of problem modules to include in the new courses in the area of hydrogen and fuel cells, as well as core courses in the

chemical engineering curriculum, such as material and energy balances, and transport phenomena. In addition, the creation of a graduate certificate in hybrid electric vehicles and an enterprise program allows students from engineering and business majors to participate in the solution of real-world problems and work in company-like projects. These programs will provide students with hands-on experience in processes occurring in electric and hybrid vehicles and alternative energy.

One section of this Hydrogen and Fuel Cell Curriculum project consisted of the development of 165 problem modules for the commonly used textbooks 'Elementary Principles of Chemical Processes' by Felder and Rousseau, and 'Transport Processes and Separation Process Principles (Includes Unit Operations)' by C. J. Geankoplis. This set of modules includes problems that illustrate real situations occurring within fuel cell systems, such as material and energy balances, flow of reactant gases on the bipolar plate channels, humidity of inlet air, among others. These were developed as an educational component of this doctoral dissertation. These modules are presented in a workbook format, and guide the students by explaining the steps to obtain the solution of the problem.

The modules developed in this project were evaluated by applying a survey to students participating in these courses. Results from these evaluations indicate a positive acceptance of the problem modules developed in this study, as all students strongly agree or agree on the effectiveness of the modules, using a 5-point Likert scale. An additional survey was applied to students to assess the student's knowledge in the area of energy technology. This survey showed an improvement in the students after taking a course in Hydrogen as an Energy Carrier.

10.7 Future Work Recommendations

In this study we evaluated the effect of carbon black, synthetic graphite and carbon nanotubes in the thermal and mechanical properties of a polypropylene matrix. The materials produced in this

project surpassed the technical goals in these two areas set by the Department of Energy. However, there are other parameters important for bipolar plates in fuel cells, such as hydrogen permeability and corrosion. The hydrogen permeability could be determined by measuring the transmitted through the bipolar plate using a gas chromatograph equipped with a hydrogen detector. This represents an important area for future characterization of these materials, as the corrosion may affect the electrical properties of the bipolar plate. The material used to fabricate bipolar plates must be hydrogen impermeable, to avoid the diffusion of hydrogen to the cathode side of the bipolar plate, causing a decrease in the efficiency of the fuel cell system.

Of all the materials produced in this project, the highest thermal conductivity value was obtained for the in-plane thermal conductivity of compression molded test specimens. One possibility is to measure the properties of compression-molded materials containing lower amounts of carbon fillers.

In the part of this research that corresponds to engineering education, there are some of the modules which have not been formally evaluated, such as the supplementary material for textbooks used in the core chemical engineering courses. In addition, it would be useful to develop additional modules, especially in the areas of wind energy, solar energy, and water energy, which are similar in design to the fuel cell modules developed to date. As these are renewable sources of energy, it would be valuable to develop new real-world examples to illustrate how these natural resources can be used to generate power for different applications.

References

1. Energy and Transportation: Challenges for the Chemical Sciences in the 21st Century. Washington, DC: National Academic Press; 2003.
2. EIA - 2010 International Energy Outlook - World Energy Demand and Economic Outlook [Internet]. ; [updated July 27, 2010, cited June 3, 2011]. Available from: <http://www.eia.doe.gov/oiaf/ieo/world.html>
3. Hydrogen Posture Plan - Integrated Research, Development and Demonstration Plan [Internet]. 2004; ; [updated February, 2004, cited June 3, 2011]. Available from: http://www.netl.doe.gov/technologies/hydrogen_clean_fuels/refshelf/pubs/HydrogenPosturePlan04.pdf
4. Hydrogen [Internet]. ; [updated 2010, cited June 3, 2011]. Available from: <http://www.energy.gov/energysources/hydrogen.htm>
5. Annual Energy Review 2009 [Internet]. ; [updated August, 2010, cited June 3, 2011]. Available from: <http://www.eia.doe.gov/emeu/aer/pdf/aer.pdf>
6. Barbir F. PEM Fuel Cells - Theory and Practice. Burlington, MA: Elsevier Academic Press; 2005.
7. Li X. Principles of Fuel Cells. New York, NY: Taylor Francis Group; 2006.
8. Larminie J, Dicks A. Fuel Cell Systems Explained. West Sussex, England: John Wiley & Sons Ltd.; 2003.
9. Fuel Cells Technical Plan [Internet]. ; [updated 2007, cited June 3, 2011]. Available from: http://www1.eere.energy.gov/hydrogenandfuelcells/mypp/pdfs/fuel_cells.pdf
10. Zhao TS, Kreuwe K-D., Van Nguyen T. Advances in Fuel Cells. Oxford, UK: Elsevier Ltd.; 2008.
11. Grove WR. On Voltaic Series and the Combination of Gases by Platinum. Philosophical Magazine and Journal of Science 1839;3(14):127 - 130.
12. Grove WR. On a Gaseous Voltaic Battery. Philosophical Magazine and Journal of Science 1842;3(21):417 - 420.
13. Fuel Cells Compendium. Brandon N, Thompsett D, editors. Oxford, UK: Elsevier Ltd.; 2005.
14. Fuel Cell Technology Showcase - History of Fuel Cells [Internet]. SAE International; [updated 2011, cited June 3, 2011]. Available from: <http://www.sae.org/fuelcells/fuelcells-history.htm>
15. Fuel Cell Basics - Historical Perspective [Internet]. ; [updated 2011, cited June 3, 2011]. Available from: http://www.fctec.com/fctec_history.asp
16. Srinivasan S. Fuel Cells: From Fundamentals to Applications. New York, NY: Springer; 2006.

17. Blomen LJM. Fuel Cell Systems. Mugerwa MN, editors. New York, NY: Plenum Press; 1993.
18. O'Hayre RP, Cha S-W, Colella WG, Prinz FB. Fuel Cell Fundamentals. New York, NY: John Wiley & Sons Inc.; 2009.
19. Economical High Performance Thermoplastic Composite Bipolar Plates (Small Business Technology Transfer Project) [Internet]. ; [updated 2006, cited June 3, 2011]. Available from: http://www.hydrogen.energy.gov/pdfs/progress06/v_d_5_bortner.pdf
20. Gas Diffusion Layer [Internet]. ; [updated 2006, cited June 3, 2011]. Available from: <http://fuelcell.com/gasdiffusionlayer.aspx>
21. Wilson MS, Busick DN; Composite Bipolar Plate for Electrochemical Cells 2001.
22. King JA, Miller MG, Barton RL, Keith JM, Hauser RA, Peterson KR, Sutter LL. Journal of Applied Polymer Science 2006;99(4):1552 - 1558.
23. King JA, Barton RL, Hauser RA, Keith JM. Polymer Composites 2008;29(4):421 - 428.
24. Hauser RA, King JA, Pagel RM, Keith JM. Journal of Applied Polymer Science 2008;109(4):2145 - 2155.
25. Keith JM, Hingst CD, Miller MG, King JA. Polymer Composites 2006;27(1):1 - 7.
26. Miller MG, Keith JM, King JA, Edwards BJ, Klinkenberg N. Polymer Composites 2006;27(4):388 - 394.
27. Keith JM, King JA, Miller MG, Tomson AM. Journal of Applied Polymer Science 2006;102(6):5456 - 5462.
28. Heiser JA, King JA. Polymer Composites 2004;25(2):186 - 193.
29. Weber EH, Clingerman ML, King JA. Journal of Applied Polymer Science 2003;88(1):112 - 122.
30. Keith JM, King JA, Grant PW, Cole AJ, Klett BM, Miskioglu I. Polymer Composites 2008;29(1):15 - 21.
31. Keith JM, King JA, Miskioglu I, Roache SC. Polymer Composites 2009;30(8):1166 - 1174.
32. King JA, Miskioglu I, Wright-Charlesworth DD, Van Karsen CD. Journal of Applied Polymer Science 2007;103(1):328 - 335.
33. Konell JP, King JA, Miskioglu I. Polymer Composites 2004;25(2):172 - 185.
34. Heiser JA, King JA, Konell JP, Miskioglu I, Sutter LL. Journal of Applied Polymer Science 2004;91(5):2881 - 2893.
35. Konell JP, King JA, Miskioglu I. Journal of Applied Polymer Science 2003;90(6):1716 - 1728.

36. Mepsted GO, Moore JM. Handbook of Fuel Cells-Fundamentals, Technology, and Applications. Vielstich W, Gasteiger, H.A., Lamm, A., editors: John Wiley & Sons; 2003.
37. Middelmann E, Kout W, Vogelaar B, Lenssen J, de Waal E. Journal of Power Sources 2003;118(1, 2):44 - 46.
38. King JA, López Gaxiola D, Johnson BA, Keith JM. Journal of Composite Materials 2010;44(7):839 - 855.
39. Incropera FP, DeWitt DP. Fundamentals of Heat and Mass Transfer. New York, NY: John Wiley & Sons Inc.; 1996.
40. Parrott JE, Stuckes AD. Thermal Conductivity of Solids. London, UK: Pion Limited; 1975.
41. Berman R. Thermal Conduction in Solids. Oxford, UK: Oxford University Press; 1976.
42. Bird RB, Stewart WE, Lightfoot EN. Transport Phenomena. New York, NY: John Wiley & Sons Inc.; 2002.
43. Tong P, Li B, Hu B. Physical Review B 1999;59(13):8639 - 8645.
44. Bigg DM. Polymer Composites 1986;7(3):125 - 140.
45. Issi JP. Improved Materials for Thermal Management. 1992 July 27, 1992; Wilmington, DE.
46. Tang L-G, Kardos JL. Polymer Composites 1997;18(1):100 - 113.
47. Nielsen LE. Mechanical Properties of Polymers and Composites. New York, NY: Marcel Dekker Inc.; 1994.
48. American Society for Testing and Materials. ASTM Standard D-638 - Standard Test Method for Tensile Properties of Plastics. Philadelphia, PA 1998.
49. American Society for Testing and Materials. ASTM Standard D-790 - Standard Test Methods for Flexural Properties of Unreinforced and Reinforced Plastics and Electrical Insulating Materials. Philadelphia, PA 2004.
50. Chow TS. Journal of Materials Science 1980;15(8):1873 - 1888.
51. López Gaxiola D, Jubinski MM, Keith JM, King JA, Miskioglu I. Journal of Applied Polymer Science 2010;118(3):1620 - 1633.
52. Schwartz MM. Composite Materials Handbook. New York, NY: McGraw - Hill; 1984.
53. Jing X, Zhao W, Lan L. Journal of Material Science Letters 2000;19(5):377 - 379.
54. Gokturk HS, Fiske T, Kalyon DM. Journal of Applied Polymer Science 1993;50(11):1891 - 1901.
55. Fiske T, Gokturk HS, Kalyon DM. Journal of Materials Science 1997;32(20):5551 - 5560.

56. Yi J-Y, Choi G-M. Journal of Electroceramics 1999;3(4):361 - 369.
57. Ludwig H-C, Fischer G, Becker H. Composites Science and Technology 1995;53(2):235 - 239.
58. Sanou M, Chung B, Cohen C. Polymer Engineering and Science 1985;25(16):1008 - 1016.
59. Bigg DM. Polymer Composites 1985;6(1):20 - 28.
60. Weber ME, Kamal MR. Polymer Composites 1997;18(6):711 - 725.
61. Kardos JL, Cheng FS, Tolbert TL. Polymer Engineering and Science 1973;13(6):455 - 461.
62. King JA, Buttry DA, Adams DF. Polymer Composites 1993;14(4):292 - 300.
63. Drzal LT, Madhukar M. Journal of Materials Science 1993;23(1):569 - 610.
64. Kardos JL. Chemtech 1984;14:430.
65. Kenyon AS, Duffey HJ. Polymer Engineering and Science 1967;7(3):189 - 193.
66. Active and Cooperative Learning [Internet]. ; [cited June 3, 2011]. Available from: <http://www.calstatela.edu/dept/chem/chem2/Active/index.htm#define>
67. Bonwell CC, Eison JA. Active Learning: Creating Excitement in the Classroom. Washington, DC: American Society of Higher Education; 1991. Report nr 1.
68. Prince M. Journal of Engineering Education 2004;93(3):223 - 231.
69. Vernon D, Blake R. Academic Medicine 1993;68(7):550 - 563.
70. Albanese M, Mitchell S. Academic Medicine 1993;68(1):52 - 81.
71. Dow Chemical Company. Technical Information - Dow H7012-35RN Polypropylene Resin. Midland, MI 2005.
72. Mighri F, Huneault MA, Champagne MF. Polymer Engineering and Science 2004;44(9):1755 - 1765.
73. Wang Y. Conductive Thermoplastic Composite Blends for Flow Field Plates for Use in Polymer Electrolyte Membrane Cells (PEMFC). Waterloo, Ontario, Canada: University of Waterloo; 2006.
74. Accorsi J, Romero E. Plastics Engineering 1995;51:29 - 35.
75. Donnet J-B, Bansal RC, Wang M-J. Carbon Black. New York, NY: Marcel Dekker Inc.; 1993.
76. Burgess KA, Lyon F. Encyclopedia of Polymer Science and Technology. Mark HF, Bikales, N. M., Overberger, C. G., Menges, G. , editors. New York, NY: John Wiley & Sons Inc.; 1985.

77. Spinelli F. *Plastics, Additives and Modifiers Handbook*. Edenbaum J, editors. New York, NY: Chapman & Hall; 1996.
78. Akzo Nobel. *Akzo Nobel Electrically Conductive Ketjenblack Product Literature*. Chicago, IL 1999.
79. Graphite [Internet]. ; [cited June 3, 2011]. Available from: <http://www.asbury.com/Graphite.html#synthetic>
80. Asbury Carbons. *Asbury Carbons Product Information*. Asbury, NJ 2004.
81. Conoco Inc. *Conoco Carbons Products Literature*. 1999.
82. Paradise M, Goswami T. *Materials and Design* 2007;28(5):1477 - 1489.
83. Ramirez A. *Bell Labs Technical Journal* 2005;10(3):171 - 185.
84. Bierdel M, Buchholz S, Michele V, Mleczko L, Rudolf R, Voetz M, Wolf A. *Physica Status Solidi B* 2007;244(11):3939 - 3943.
85. Hyperion Catalysis International. *Hyperion Catalysis International Fibril Product Literature*. Cambridge, MA 2008.
86. Johnson BA. *Thermally and Electrically Conductive Polypropylene Based Resins for Fuel Cell Bipolar Plates*. Houghton, MI: Michigan Technological University; 2009.
87. Niigata Engineering Co. Ltd. *Niigata Model NE85UA4 Plastic Injection Mold Machine* Niigata, Japan.
88. Master Precision Molds Inc. *Four Cavity Mold*. Greenville, MI.
89. Fuel Cells Jolt Plastics Innovation [Internet]. ; [updated 2001, cited June 3, 2011]. Available from: <http://www.ptonline.com/articles/fuel-cells-jolt-plastics-innovation>
90. Chodák I, Omastová M, Pionteck J. *Journal of Applied Polymer Science* 2001;82(8):1903 - 1906.
91. American Society for Testing and Materials. *ASTM Standard D-433 - Evaluating Thermal Conductivity of Gasket Materials*. Philadelphia, PA 1996.
92. Heiser JA, King JA, Konell JP, Miskioglu I., Sutter LL. *Advances in Polymer Technology* 2004;23(2):135 - 146.
93. LFA 447 Nanoflash ® Product Brochure [Internet]. ; [cited June 4, 2011]. Available from: <http://www.netzsch-thermal-analysis.com/en/literatur/download/180/>
94. American Society for Testing and Materials. *ASTM Standard E-1461 - Standard Test Method for Thermal Diffusivity by the Flash Method*. Philadelphia, PA 2007.
95. Blumm J. *The New LFA Nanoflash*. Selb, Germany: NETZSCH - Gerätebau.

96. Manuelian M, Campbell R. Thermal Diffusivity, Specific Heat and Thermal Conductivity of Composites. NETZSCH Instruments; 2008.
97. Assael MJ, Gialou K. International Journal of Thermophysics 2003;24(3):667 - 674.
98. Yang G, Midone AD, Johnson KW. Physical Review B 1992;45(1):157 - 160.
99. Typical Properties of Vespel® SP-1, SP-21, SP-22, SP-211, SP-3 [Internet]. ; [cited June 4, 2011]. Available from:
http://www2.dupont.com/Vespel/en_US/assets/downloads/vespel_s/sp1.pdf.
100. Cowan RD. Journal of Applied Physics 1963;34(4):926 - 927.
101. Clark LM, Taylor RE. Journal of Applied Physics 1975;46(2):714 - 719.
102. Koski JA. Improved data reduction methods for laser pulse diffusivity determination with the use of minicomputers. In: Sengers JV, editor. Eighth Symposium of Thermophysical Properties. Volume 2. New York, NY: American Society of Mechanical Engineers; 1981.
103. Parker WJ, Jenkins RJ, Butler CP, Abbott GL. Journal of Applied Physics 1963;32(9):1679 - 1684.
104. Carslaw HS, Jaeger JC. Conduction of Heat in Solids. Oxford, UK: Clarendon Press; 1959.
105. Broch JT. Mechanical Vibrations and Shock Measurements. Naerum, Denmark: Bruel & Kjaer; 1972.
106. Finan JM. Thermally Conductive Thermoplastic Materials. Society of Plastics Engineers Annual Technical Conference 1999. p 1547 - 1550.
107. Agari Y, Uno T. Journal of Applied Polymer Science 1985;30(5):2225 - 2235.
108. Bigg DM. Polymer Engineering and Science 1977;17(12):842 - 847.
109. Nagata W, Iwabuki H, Nigo H. Composite Interfaces 1999;6(5):483 - 495.
110. Demain A. Thermal conductivity of polymer-chopped carbon fiber composites. Louvain la Neuve, Belgium: Universite Catholique de Louvain; 1994.
111. King JA, Tucker KW, Meyers JD, Weber EH, Clingerman ML, Ambrosius KR. Polymer Composites 2001;22(1):142 - 154.
112. Murthy MV. Permanent EMI Shielding of Plastics using Copper Fibers. Society of Plastics Engineers Annual Technical Conference 1994. p 1396 - 1400.
113. Simon R. Polymer News 1985;11:102 - 108.
114. Mapleston P. Moden Plastics 1992;69:80 - 83.
115. Huang J-C. Advances in Polymer Technology 2002;21(4):299 - 313.
116. Bigg DM. Polymer Engineering and Science 1979;19(16):1188 - 1192.

117. Braun JC, Zabriskie JE Jr., Neutzler JK, Fuchs M, Gustafson RC; Fuel Cell Collector Plate and Method of Fabrication 2001.
118. Loutfy RO, Hecht M; Low - cost Molded Plastic Fuel Cell Separator Plate with Conductive Elements 2003.
119. Mehta V, Cooper JS. Journal of Power Sources 2003;114(1):32 - 53.
120. Huang J, Baird DG, McGrath JE. Journal of Power Sources 2005;150:110 - 119.
121. Wolf H, Willert Porada M. Journal of Power Sources 2006;153:41 - 46.
122. Robberg K, Trapp V. Graphite based bipolar plates. In: Vielstick WG, H. A., Lamm, A., editor. Handbook of Fuel Cells-Fundamentals, Technology and Applications. Volume 3. New York, NY: John Wiley & Sons Ltd.; 2003.
123. Hermann A, Chaudhur T, Spagnol P. International Journal of Hydrogen Energy 2005;30(12):1297 - 1302.
124. King JA, Johnson BA, Via MD, Ciarkowski CJ. Journal of Applied Polymer Science 2009;112(1):425 - 433.
125. Montgomery DC. Design and Analysis of Experiments. New York, NY: John Wiley & Sons Inc.; 2001.
126. Weber EH, Clingerman ML, King JA. Journal of Applied Polymer Science 2003;88(1):123 - 130.
127. Weber EH. Development and Modeling of Thermally Conductive Polymer/Carbon Composites. Houghton, MI: Michigan Technological University; 2001.
128. Nielsen LE. Industrial and Engineering Chemistry Fundamentals 1974;13(1):17 - 20.
129. McGee S, McCullough RL. Polymer Composites 1981;2(4):149 - 161.
130. Hauser RA. Synergistic Effects and Modeling of Thermally Conductive Resins for Fuel Cell Bipolar Plate Applications. Houghton, MI: Michigan Technological University; 2008.
131. Keith JM, King JA, Lenhart KM, Zimny B. Journal of Applied Polymer Science 2007;105(6):3309 - 3316.
132. Hone J, Whitney M, Piskoti C, Zettl A. Physical Review B 1999;59(4):R2514 - R2516.
133. Yi W, Lu L, Dian-Lin Z, Pan ZW, Xie SS. Physical Review B 1999;59(14):R9015 - R9018.
134. Hone J, Llaguno MC, Nemes NM, Johnson AT, Fischer JE, Walters DA, Cassavant MJ, Schmidt J, Smalley RE. Applied Physics Letters 2000;77(5):666 - 668.
135. Kim P, Shi L, Majumdar A, McEuen PL. Physical Review Letters 2001;87(21):215502-1 - 215502-4.

136. Yang DJ, Zhang Q, Chen G, Yoon SF, Ahn J, Wang SG, Zhou Q, Wang Q, Li JQ. *Physical Review B* 2002;66:165440-1 - 165440-6.
137. King JA, Tucker KW, Vogt BD, Weber EH, Quan C. *Polymer Composites* 1999;20(5):643 - 654.
138. Miller MG. *Development and Modeling of Thermally Conductive Resins for Fuel Cell Bipolar Plate Applications*. Houghton, MI: Michigan Technological University; 2006.
139. López Gaxiola D, Keith JM, King JA, Johnson BA. *Journal of Applied Polymer Science* 2009;114(5):3261 - 3267.
140. Hauser RA, Keith JM, King JA, Holdren JL. *Journal of Applied Polymer Science* 2008;110(5):2914 - 2923.
141. López Gaxiola D, Keith JM, Na M, King JA, Johnson BA. *Journal of Composite Materials* 2010;45(12):1271 - 1284.
142. King JA, Morrison FA, Keith JM, Miller MG, Smith RC, Cruz M, Neuhalfen AM, Barton RL. *Journal of Applied Polymer Science* 2006;101(4):2680 - 2688.
143. Petrovic ZS, Martinovic B, Divjakovic V. *Journal of Applied Polymer Science* 1993;49(9):1659 - 1669.
144. Chiu H-T, Chiu W-M. *Journal of Applied Polymer Science* 1996;61(4):607 - 612.
145. Mali TJ. *Thermoplastic Composites for Polymer Electrolyte Membrane Fuel Cell Bipolar Plates*. Waterloo, Ontario, Canada: University of Waterloo; 2006.
146. Kalaitzidou K, Fukushima H, Miyagawa H, Drzal L. *Polymer Engineering and Science* 2007;47(11):1796 - 1803.
147. Arai T, Tominaga Y, Asai S, Sumita M. *Journal of Polymer Science, Part B: Polymer Physics* 2005;43(18):2568 - 2577.
148. Ansari MNM, Ismail H, Zein SHS. *Journal of Reinforced Plastic and Composites* 2009;28(20):2473 - 2485.
149. López Manchado MA, Valentini L, Biagiotti J, Kenny JM. *Carbon* 2005;43(7):1499 - 1505.
150. Bao SP, Tjong SC. *Materials Science and Engineering A* 2008;485(1-2):508 - 516.
151. Blake R, Guńko YK, Coleman J, Cadek M, Fonseca A, Nagy JB, Blau WJ. *Journal of the American Chemical Society* 2004;126(33):10226 - 10227.
152. King JA, Keith JM, Glenn OL, Miskioglu I, Cole AJ, McLaughlin SR, Pagel RM. *Journal of Applied Polymer Science* 2008;108(3):1657 - 1666.
153. Vectra Liquid Crystal Polymer (LCP) [Internet]. ; [updated October 2007, cited June 4, 2011]. Available from: www.ticona.com/markets/vectrabr_e.pdf

154. Vallejo FJ, Iribarren I, Eguiazábal JI, Nazábal J. Journal of Polymer Engineering Science 2002;42(8):1686 - 1693.
155. Kaynak A, Polat A, Yilmazer U. Materials Research Bulletin 1996;31(10):1195 - 1206.
156. Akinci A. Archives of Materials Science and Engineering 2009;35(2):91 - 94.
157. Zhou Z, Wang S, Zhang Y. Journal of Applied Polymer Science 2006;102(5):4823 - 4830.
158. King JA, Buttry DA, Adams DF. Polymer Composites 1993;14(4):301 - 307.
159. Mallick PK. Composites Engineering Handbook. New York, NY: Marcel Dekker Inc.; 1997.
160. Halpin JC, Kardos JL. Polymer Engineering and Science 1976;16(5):344 - 352.
161. Halpin JC. Journal of Composite Materials 1969;3(4):732 - 734.
162. Hewitt RL, de Malherbe MC. Journal of Composite Materials 1970;4(2):280 - 282.
163. Nielsen LE. Journal of Applied Physics 1970;41(11):4626 - 4627.
164. Nielsen LE. Polymer Rheology. New York, NY: Marcel Dekker Inc.; 1977.
165. Coleman JN, Khan U, Gun'ko YK. Advanced Materials 2006;18(6):689 - 706.
166. Brcic M, Canadija M, Brnic J, Lanc D, Krscanski S, Vukelic G. Estonian Journal of Engineering 2009;15(2):77 - 86.
167. Li C, Chou T-W. Composites Science and Technology 2003;63(11):1517 - 1524.
168. Kashyap KT, Patil RG. Bulletin of Material Science 2008;31(2):185 - 187.
169. Clean Energy for America 's Future [Internet]. ; [updated 2010, cited June 4, 2011]. Available from:
http://www1.eere.energy.gov/office_eere/pdfs/eere_programs_overview.pdf
170. Energy Education and Workforce Development [Internet]. ; [updated 2010, cited June 4, 2011]. Available from:
http://www1.eere.energy.gov/education/educational_professional.html
171. Beck RH. The Three R's Plus: What Today's Schools are Trying to Do and Why. University of Minnesota Press; 2009.
172. Problem - Based Learning [Internet]. ; [cited June 4, 2011]. Available from:
<http://userwww.sfsu.edu/~rpurser/revised/pages/problem.htm>
173. Problem - Based Learning [Internet]. ; [updated 2001, cited June 4, 2011]. Available from: <http://www.mcli.dist.maricopa.edu/pbl/info.html>
174. Problem - Based Learning at University of Delaware [Internet]. ; [cited June 4, 2011]. Available from: <http://www.udel.edu/inst/>

175. McCarthy JP, Anderson L. Innovative Higher Education 2000;24(4):279 - 294.
176. Keith JM. The Stanley Cup of Transport Phenomena. American Society for Engineering Education Annual Conference & Exposition. Portland, OR: American Society for Engineering Education; 2005.
177. Zheng H, Keith JM. Web – Based Instructional Tools for Heat and Mass Transfer. 2003; Nashville, TN. American Society for Engineering Education.
178. Zheng H, Keith JM. Chemical Engineering Education 2004;38:282 - 285.
179. Felder RM, Silverman LK. Journal of Engineering Education 1988;78(7):674 - 681.
180. Felder RM. ASEE Prism 1996;6(4):18 - 23.
181. Kolb DA. Experiential Learning: Experience as the Source of Learning and Development. New Jersey: Prentice Hall; 1984.
182. McCarthy B. The 4MAT System: Teaching to Learning Styles with Right/Left Mode Techniques. Excel Inc.; 1987.
183. Stice JE. Journal of Engineering Education 1987;77(5):291 - 296.
184. Harb JN, Durrant SO, Terry RE. Journal of Engineering Education 1993;82(2):70 - 77.
185. Felder RM, Brent R. Journal of Engineering Education 2005;94(1):57 - 72.
186. Fuel Cells Technical Plan - Education [Internet]. ; [updated 2009, cited June 4, 2011]. Available from: <http://www1.eere.energy.gov/hydrogenandfuelcells/mypp/pdfs/education.pdf>
187. Hydrogen Education at Michigan Technological University [Internet]. ; [updated 2008, cited June 4, 2011]. Available from: <http://www.chem.mtu.edu/~jmkeith/h2ed/>
188. Keith JM. A Student – Driven Enterprise in Fuel Cells and Alternative Fuels. American Society for Engineering Education Annual Conference. Salt Lake City, UT: American Society for Engineering Education; 2004.
189. Keith JM, Opella KC, Miller MG, King JA, Gwaltney GD, Green CA, Meldrum JS, Bradley SA. Engineering Education in Alternative Energy. American Society for Engineering Education Annual Conference. Chicago, IL: American Society for Engineering Education; 2006.
190. The Fuel Cell Curriculum Project Website [Internet]. ; [updated 2008, cited June 4, 2011]. Available from: http://www.chem.mtu.edu/~jmkeith/fuel_cell_curriculum/
191. Keith JM, Chmielewski D, Fogler HS, Thomas V. CACHE Module Development for Introducing Energy into the Chemical Engineering Curriculum: Fuel Cells. American Society for Engineering Education Annual Conference. Pittsburgh, PA: American Society for Engineering Education; 2008.

192. Felder RM, Rousseau RW. Elementary Principles of Chemical Processes. New York, NY: John Wiley & Sons Inc.; 2005.
193. Geankoplis CJ. Transport Processes and Separation Process Principles (Includes Unit Operations). New Jersey: Pearson Education Inc.; 2003.
194. BioENGR Educational Materials Bank [Internet]. ; [updated April 2006, cited June 4, 2011]. Available from: <http://www.engr.sjsu.edu/~bioemb/>
195. Keith JM, López Gaxiola D, Crowl D, Caspary D, Mukherjee A, Meng D, Naber J, Allen J, Lukowski J, Solomon B, Meldrum J, Edgar T. Development and Assessment of Energy Modules in the Chemical Engineering Curriculum. American Society for Engineering Education Annual Conference. Vancouver, BC, Canada: American Society for Engineering Education; 2011.
196. The National Environmental Education & Training Foundation. American's Low "Energy IQ": A Risk to Our Energy Future. 2002.

Appendix A: Through-plane thermal conductivity results using the Flash Method

Test settings:

- Temperature: 80°C
- 5 shots per sample
- Voltage: 304V
- Light filter: 100%
- Pulse width: Medium

Table A.1

2.5 wt.% Ketjenblack EC-600 JD in Dow Polypropylene Semi Crystalline
Homopolymer Resin H7012-35RN

Test Date	Disk number	Specific Heat (J/g·K)	Thermal conductivity (W/m·K)	Diffusivity (mm ² /s)
3-2-2009	EA2.5P-TC-26-1	2.315	0.249	0.118
3-2-2009	EA2.5P-TC-29-1	2.334	0.269	0.127
3-2-2009	EA2.5P-TC-23-1	2.175	0.249	0.126
3-24-2009	EA2.5P-TC-23-2	2.126	0.224	0.116
	Average	2.2375	0.2478	0.1218
	Standard Deviation	0.1027	0.0184	0.0056
	Number of samples	4	4	4

Calibration sample used: 2mm thick, 25.4 mm diameter Vespel SP1 disk.

Density used for thermal conductivity calculation: 0.9114 g/cm³.

Table A.2
2.5 wt.% Ketjenblack EC-600 JD in Dow Polypropylene Semi Crystalline
Homopolymer Resin H7012-35RN Replicate

Test Date	Disk number	Specific Heat (J/g·K)	Thermal conductivity (W/m·K)	Diffusivity (mm ² /s)
3-26-2009	EA2.5PR-TC-17-1	2.255	0.242	0.118
3-26-2009	EA2.5PR-TC-17-2	2.174	0.226	0.114
3-26-2009	EA2.5PR-TC-28-2	2.214	0.239	0.119
3-26-2009	EA2.5PR-TC-31-2	2.215	0.235	0.116
Average		2.2145	0.2355	0.1168
Standard Deviation		0.0331	0.0070	0.0022
Number of samples		4	4	4

Calibration sample used: 2mm thick, 25.4 mm diameter Vespel SP1 disk.

Density used for thermal conductivity calculation: 0.9114 g/cm³.

Table A.3
4 wt.% Ketjenblack EC-600 JD in Dow Polypropylene Semi Crystalline
Homopolymer Resin H7012-35RN

Test Date	Disk number	Specific Heat (J/g·K)	Thermal conductivity (W/m·K)	Diffusivity (mm ² /s)
3-6-2009	EA4P-TC-22-1	2.067	0.253	0.133
3-6-2009	EA4P-TC-7-2	2.066	0.255	0.135
3-6-2009	EA4P-TC-11-1	1.992	0.255	0.140
3-25-2009	EA4P-TC-8-2	2.187	0.269	0.134
Average		2.0780	0.258	0.1355
Standard Deviation		0.0807	0.0074	0.0031
Number of samples		4	4	4

Calibration sample used: 2mm thick, 25.4 mm diameter Vespel SP1 disk.

Density used for thermal conductivity calculation: 0.9184 g/cm³.

Table A.4
5 wt.% Ketjenblack EC-600 JD in Dow Polypropylene Semi Crystalline
Homopolymer Resin H7012-35RN

Test Date	Disk number	Specific Heat (J/g·K)	Thermal conductivity (W/m·K)	Diffusivity (mm ² /s)
3-5-2009	EA5P-TC-27-1	2.147	0.272	0.137
3-5-2009	EA5P-TC-27-2	2.063	0.247	0.130
3-5-2009	EA5P-TC-28-2	2.110	0.266	0.137
3-24-2009	EA5P-TC-14-2	2.089	0.267	0.138
Average		2.1023	0.2630	0.1355
Standard Deviation		0.0355	0.0110	0.0037
Number of samples		4	4	4

Calibration sample used: 2mm thick, 25.4 mm diameter Vespel SP1 disk.

Density used for thermal conductivity calculation: 0.9231 g/cm³.

Table A.5
6 wt.% Ketjenblack EC-600 JD in Dow Polypropylene Semi Crystalline
Homopolymer Resin H7012-35RN

Test Date	Disk number	Specific Heat (J/g·K)	Thermal conductivity (W/m·K)	Diffusivity (mm ² /s)
3-6-2009	EA6P-TC-15-1	1.953	0.268	0.148
3-6-2009	EA6P-TC-20-2	1.981	0.259	0.141
3-6-2009	EA6P-TC-10-1	2.060	0.276	0.145
3-24-2009	EA6P-TC-10-2	2.192	0.292	0.143
Average		2.0465	0.2738	0.1443
Standard Deviation		0.1071	0.0140	0.0030
Number of samples		4	4	4

Calibration sample used: 2mm thick, 25.4 mm diameter Vespel SP1 disk

Density used for thermal conductivity calculation: 0.9278 g/cm³.

Table A.6
7.5 wt.% Ketjenblack EC-600 JD in Dow Polypropylene Semi Crystalline
Homopolymer Resin H7012-35RN

Test Date	Disk number	Specific Heat (J/g·K)	Thermal conductivity (W/m·K)	Diffusivity (mm ² /s)
2-26-2009	EA7.5P-TC-21-1	2.046	0.309	0.162
2-26-2009	EA7.5P-TC-29-1	2.127	0.285	0.143
2-26-2009	EA7.5P-TC-22-1	1.978	0.296	0.160
3-24-2009	EA7.5P-TC-29-2	2.037	0.268	0.141
Average		2.047	0.2895	0.1515
Standard Deviation		0.0613	0.0174	0.0110
Number of samples		4	4	4

Calibration sample used: 2mm thick, 25.4 mm diameter Vespel SP1 disk.

Density used for thermal conductivity calculation: 0.9351 g/cm³.

Table A.7
10 wt.% Ketjenblack EC-600 JD in Dow Polypropylene Semi Crystalline
Homopolymer Resin H7012-35RN

Test Date	Disk number	Specific Heat (J/g·K)	Thermal conductivity (W/m·K)	Diffusivity (mm ² /s)
3-5-2009	EA10P-TC-33-2	1.930	0.307	0.168
3-5-2009	EA10P-TC-23-1	1.969	0.316	0.169
3-5-2009	EA10P-TC-28-2	1.973	0.317	0.170
3-24-2009	EA10P-TC-21-1	1.999	0.324	0.171
Average		1.9678	0.3160	0.1695
Standard Deviation		0.0285	0.0070	0.0013
Number of samples		4	4	4

Calibration sample used: 2mm thick, 25.4 mm diameter Vespel SP1 disk

Density used for thermal conductivity calculation: 0.9474 g/cm³.

Table A.8
15 wt.% Ketjenblack EC-600 JD in Dow Polypropylene Semi Crystalline
Homopolymer Resin H7012-35RN

Test Date	Disk number	Specific Heat (J/g·K)	Thermal conductivity (W/m·K)	Diffusivity (mm ² /s)
2-25-2009	EA15P-TC-23-1	2.077	0.365	0.181
2-25-2009	EA15P-TC-24-1	2.048	0.358	0.180
2-25-2009	EA15P-TC-28-1	2.050	0.353	0.177
3-24-2009	EA15P-TC-23-2	2.044	0.354	0.178
Average		2.0548	0.3575	0.1790
Standard Deviation		0.0150	0.0054	0.0018
Number of samples		4	4	4

Calibration sample used: 2mm thick, 25.4 mm diameter Vespel SP1 disk.

Density used for thermal conductivity calculation: 0.9730 g/cm³.

Table A.9
10 wt.% Thermocarb TC-300 in Dow Polypropylene Semi Crystalline
Homopolymer Resin H7012-35RN

Test Date	Disk number	Specific Heat (J/g·K)	Thermal conductivity (W/m·K)	Diffusivity (mm ² /s)
2-12-2009	EB10P-TC-22-2	2.133	0.253	0.124
2-12-2009	EB10P-TC-8-1	2.004	0.250	0.123
2-12-2009	EB10P-TC-14-2	2.188	0.257	0.126
3-25-2009	EB10P-TC-22-1	2.069	0.247	0.125
Average		2.099	0.258	0.125
Standard Deviation		0.080	0.004	0.001
Number of samples		4	4	4

Calibration sample used: 2mm thick, 25.4 mm diameter Vespel SP1 disk.

Density used for thermal conductivity calculation: 0.9573 g/cm³.

Table A.10

15 wt.% Thermocarb TC-300 in Dow Polypropylene Semi Crystalline
Homopolymer Resin H7012-35RN

Test Date	Disk number	Specific Heat (J/g·K)	Thermal conductivity (W/m·K)	Diffusivity (mm ² /s)
2-11-2009	EB15P-TC-16-2	1.943	0.268	0.140
2-11-2009	EB15P-TC-11-1	1.943	0.260	0.136
2-11-2009	EB15P-TC-19-2	1.931	0.275	0.143
2-11-2009	EB15P-TC-33-1	1.938	0.274	0.143
Average		1.939	0.269	0.141
Standard Deviation		0.006	0.007	0.003
Number of samples		4	4	4

Calibration sample used: 2mm thick, 25.4 mm diameter Vespel SP1 disk.

Density used for thermal conductivity calculation: 0.9887 g/cm³.

Table A.11

20 wt.% Thermocarb TC-300 in Dow Polypropylene Semi Crystalline
Homopolymer Resin H7012-35RN

Test Date	Disk number	Specific Heat (J/g·K)	Thermal conductivity (W/m·K)	Diffusivity (mm ² /s)
2-11-2009	EB20P-TC-16-1	1.923	0.302	0.154
2-11-2009	EB20P-TC-16-2	1.856	0.309	0.157
2-11-2009	EB20P-TC-18-1	1.826	0.330	0.168
2-11-2009	EB20P-TC-33-1	1.930	0.307	0.156
Average		1.884	0.312	0.159
Standard Deviation		0.051	0.012	0.006
Number of samples		4	4	4

Calibration sample used: 2mm thick, 25.4 mm diameter Vespel SP1 disk.

Density used for thermal conductivity calculation: 1.0223 g/cm³.

Table A.12

25 wt.% Thermocarb TC-300 in Dow Polypropylene Semi Crystalline
Homopolymer Resin H7012-35RN

Test Date	Disk number	Specific Heat (J/g·K)	Thermal conductivity (W/m·K)	Diffusivity (mm ² /s)
2-9-2009	EB25P-TC-35-2	1.805	0.390	0.191
2-9-2009	EB25P-TC-32-1	1.884	0.391	0.191
2-9-2009	EB25P-TC-29-2	1.927	0.389	0.190
2-9-2009	EB25P-TC-16-1	1.935	0.391	0.191
Average		1.888	0.390	0.191
Standard Deviation		0.059	0.001	0.005
Number of samples		4	4	4

Calibration sample used: 2mm thick, 25.4 mm diameter Vespel SP1 disk.

Density used for thermal conductivity calculation: 1.0583 g/cm³.

Table A.13

30 wt.% Thermocarb TC-300 in Dow Polypropylene Semi Crystalline
Homopolymer Resin H7012-35RN

Test Date	Disk number	Specific Heat (J/g·K)	Thermal conductivity (W/m·K)	Diffusivity (mm ² /s)
2-6-2009	EB30P-TC-9-1	1.708	0.440	0.235
2-9-2009	EB30P-TC-13-2	1.855	0.440	0.235
2-6-2009	EB30P-TC-24-2	1.684	0.436	0.233
2-9-2009	EB30P-TC-34-1	1.869	0.439	0.234
Average		1.779	0.439	0.234
Standard Deviation		0.096	0.002	0.001
Number of samples		4	4	4

Calibration sample used: 2mm thick, 25.4 mm diameter Vespel SP1 disk.

Density used for thermal conductivity calculation: 1.0968 g/cm³.

Table A.14

35 wt.% Thermocarb TC-300 in Dow Polypropylene Semi Crystalline
Homopolymer Resin H7012-35RN

Test Date	Disk number	Specific Heat (J/g·K)	Thermal conductivity (W/m·K)	Diffusivity (mm ² /s)
2-6-2009	EB35P-TC-19-1	1.661	0.508	0.269
2-6-2009	EB35P-TC-14-1	1.765	0.536	0.284
2-6-2009	EB35P-TC-29-2	1.642	0.502	0.266
2-6-2009	EB35P-TC-30-2	1.701	0.502	0.265
Average		1.692	0.512	0.271
Standard Deviation		0.054	0.016	0.009
Number of samples		4	4	4

Calibration sample used: 2mm thick, 25.4 mm diameter Vespel SP1 disk.

Density used for thermal conductivity calculation: 1.1383 g/cm³.

Table A.15

40 wt.% Thermocarb TC-300 in Dow Polypropylene Semi Crystalline
Homopolymer Resin H7012-35RN

Test Date	Disk number	Specific Heat (J/g·K)	Thermal conductivity (W/m·K)	Diffusivity (mm ² /s)
2-5-2009	EB40P-TC-12-2	1.833	0.735	0.339
2-6-2009	EB40P-TC-23-1	1.884	0.765	0.348
2-5-2009	EB40P-TC-18-1	1.849	0.728	0.333
2-6-2009	EB40P-TC-18-2	1.858	0.744	0.339
Average		1.856	0.743	0.340
Standard Deviation		0.021	0.014	0.006
Number of samples		4	4	4

Calibration sample used: 3 mm thick, 25.4 mm diameter Pyrex 7740 disk.

Density used for thermal conductivity calculation: 1.1831 g/cm³.

Table A.16

45 wt.% Thermocarb TC-300 in Dow Polypropylene Semi Crystalline
Homopolymer Resin H7012-35RN

Test Date	Disk number	Specific Heat (J/g·K)	Thermal conductivity (W/m·K)	Diffusivity (mm ² /s)
2-5-2009	EB45P-TC-14-2	1.799	0.938	0.424
2-5-2009	EB45P-TC-28-1	1.679	0.853	0.412
2-5-2009	EB45P-TC-9-2	1.682	0.840	0.406
2-5-2009	EB45P-TC-23-2	1.709	0.855	0.406
Average		1.717	0.872	0.412
Standard Deviation		0.060	0.019	0.008
Number of samples		4	4	4

Calibration sample used: 3 mm thick, 25.4 mm diameter Pyrex 7740 disk.

Density used for thermal conductivity calculation: 1.2315 g/cm³.

Table A.17

50 wt.% Thermocarb TC-300 in Dow Polypropylene Semi Crystalline
Homopolymer Resin H7012-35RN

Test Date	Disk number	Specific Heat (J/g·K)	Thermal conductivity (W/m·K)	Diffusivity (mm ² /s)
2-5-2009	EB50P-TC-14-2	1.636	1.086	0.517
2-5-2009	EB50P-TC-16-1	1.683	1.174	0.544
2-5-2009	EB50P-TC-33-2	1.535	1.110	0.563
3-26-2009	EB50P-TC-16-2	1.646	1.085	0.514
Average		1.625	1.114	0.535
Standard Deviation		0.063	0.042	0.023
Number of samples		4	4	4

Calibration sample used: 3 mm thick, 25.4 mm diameter Pyrex 7740 disk.

Density used for thermal conductivity calculation: 1.2841 g/cm³.

Table A.18

55 wt.% Thermocarb TC-300 in Dow Polypropylene Semi Crystalline
Homopolymer Resin H7012-35RN

Test Date	Disk number	Specific Heat (J/g·K)	Thermal conductivity (W/m·K)	Diffusivity (mm ² /s)
2-2-2009	EB55P-TC-30-2	1.620	1.420	0.654
2-2-2009	EB55P-TC-20-2	1.586	1.443	0.664
2-2-2009	EB55P-TC-16-2	1.568	1.440	0.663
2-2-2009	EB55P-TC-8-2	1.652	1.459	0.672
Average		1.607	1.441	0.663
Standard Deviation		0.033	0.014	0.007
Number of samples		4	4	4

Calibration sample used: 3 mm thick, 25.4 mm diameter Pyroceram 9606 disk.

Density used for thermal conductivity calculation: 1.3413 g/cm³.

Table A.19

60 wt.% Thermocarb TC-300 in Dow Polypropylene Semi Crystalline
Homopolymer Resin H7012-35RN

Test Date	Disk number	Specific Heat (J/g·K)	Thermal conductivity (W/m·K)	Diffusivity (mm ² /s)
1-30-2009	EB60P-TC-26-1	1.587	1.871	0.891
1-30-2009	EB60P-TC-25-1	1.509	1.899	0.904
2-2-2009	EB60P-TC-25-2	1.496	1.843	0.878
2-2-2009	EB60P-TC-14-1	1.523	1.887	0.899
Average		1.529	1.875	0.893
Standard Deviation		0.026	0.022	0.011
Number of samples		4	4	4

Calibration sample used: 3 mm thick, 25.4 mm diameter Pyroceram 9606 disk.

Density used for thermal conductivity calculation: 1.4039 g/cm³.

Table A.20

65 wt.% Thermocarb TC-300 in Dow Polypropylene Semi Crystalline
Homopolymer Resin H7012-35RN

Test Date	Disk number	Specific Heat (J/g·K)	Thermal conductivity (W/m·K)	Diffusivity (mm ² /s)
1-29-2009	EB65P-TC-16-1	1.528	2.583	1.194
1-29-2009	EB65P-TC-15-1	1.517	2.689	1.242
1-29-2009	EB65P-TC-16-2	1.469	2.789	1.289
1-29-2009	EB65P-TC-17-1	1.531	2.765	1.278
Average		1.511	2.707	1.251
Standard Deviation		0.029	0.093	0.043
Number of samples		4	4	4

Calibration sample used: 3 mm thick, 25.4 mm diameter Pyroceram 9606 disk.

Density used for thermal conductivity calculation: 1.4726 g/cm³.

Table A.21

65 wt.% Thermocarb TC-300 in Dow Polypropylene Semi Crystalline
Homopolymer Resin H7012-35RN Replicate

Test Date	Disk number	Specific Heat (J/g·K)	Thermal conductivity (W/m·K)	Diffusivity (mm ² /s)
1-29-2009	EB65PR-TC-6-1	1.529	2.620	1.168
1-29-2009	EB65PR-TC-14-2	1.542	2.608	1.163
1-30-2009	EB65PR-TC-14-1	1.523	2.661	1.186
1-29-2009	EB65PR-TC-31-2	1.564	2.633	1.174
Average		1.539	2.631	1.173
Standard Deviation		0.018	0.023	0.010
Number of samples		4	4	4

Calibration sample used: 3 mm thick, 25.4 mm diameter Pyroceram 9606 disk.

Density used for thermal conductivity calculation: 1.4726 g/cm³.

Table A.22

70 wt.% Thermocarb TC-300 in Dow Polypropylene Semi Crystalline
Homopolymer Resin H7012-35RN

Test Date	Disk number	Specific Heat (J/g·K)	Thermal conductivity (W/m·K)	Diffusivity (mm ² /s)
1-21-2009	EB70P-TC-17-1	1.486	3.709	1.613
2-3-2009	EB70P-TC-20-1	1.556	3.962	1.645
1-26-2009	EB70P-TC-20-2	1.445	3.704	1.605
1-26-2009	EB70P-TC-13-2	1.491	3.778	1.637
Average		1.497	3.788	1.625
Standard Deviation		0.042	0.121	0.019
Number of samples		4	4	4

Calibration sample used: 3 mm thick, 25.4 mm diameter Pyroceram 9606 disk.

Density used for thermal conductivity calculation: 1.5484 g/cm³.

Table A.23

75 wt.% Thermocarb TC-300 in Dow Polypropylene Semi Crystalline
Homopolymer Resin H7012-35RN

Test Date	Disk number	Specific Heat (J/g·K)	Thermal conductivity (W/m·K)	Diffusivity (mm ² /s)
1-21-2009	EB75P-TC-6-1	1.425	5.293	2.276
1-21-2009	EB75P-TC-16-1	1.386	5.095	2.191
1-21-2009	EB75P-TC-16-2	1.405	5.146	2.213
1-21-2009	EB75P-TC-22-2	1.438	5.003	2.152
Average		1.414	5.134	2.208
Standard Deviation		0.023	0.121	0.052
Number of samples		4	4	4

Calibration sample used: 3 mm thick, 25.4 mm diameter Pyroceram 9606 disk.

Density used for thermal conductivity calculation: 1.6324 g/cm³.

Table A.24

80 wt.% Thermocarb TC-300 in Dow Polypropylene Semi Crystalline
Homopolymer Resin H7012-35RN

Test Date	Disk number	Specific Heat (J/g·K)	Thermal conductivity (W/m·K)	Diffusivity (mm ² /s)
1-21-2009	EB80P-TC-26-1	1.282	9.457	4.263
1-20-2009	EB80P-TC-14-1	1.286	9.121	4.112
1-21-2009	EB80P-TC-27-1	1.269	9.620	4.337
1-21-2009	EB80P-TC-26-2	1.288	9.673	4.361
Average		1.281	9.468	4.268
Standard Deviation		0.008	0.249	0.112
Number of samples		4	4	4

Calibration sample used: 3 mm thick, 25.4 mm diameter Pyroceram 9606 disk.

Density used for thermal conductivity calculation: 1.7260 g/cm³.

Table A.25

1.5 wt.% Hyperion FIBRIL™ nanotubes in Dow Polypropylene
Semi Crystalline Homopolymer Resin H7012-35RN

Test Date	Disk number	Specific Heat (J/g·K)	Thermal conductivity (W/m·K)	Diffusivity (mm ² /s)
2-24-2009	EQ1.5P-TC-26-1	2.170	0.225	0.114
2-24-2009	EQ1.5P-TC-29-1	2.266	0.241	0.117
2-24-2009	EQ1.5P-TC-29-2	2.219	0.230	0.115
3-24-2009	EQ1.5P-TC-23-1	2.095	0.235	0.124
Average		2.1875	0.2328	0.1175
Standard Deviation		0.0731	0.0068	0.0045
Number of samples		4	4	4

Calibration sample used: 2mm thick, 25.4 mm diameter Vespel SP1 disk.

Density used for thermal conductivity calculation: 0.9075 g/cm³.

Table A.26
2.5 wt.% Hyperion FIBRIL™ nanotubes in Dow Polypropylene
Semi Crystalline Homopolymer Resin H7012-35RN

Test Date	Disk number	Specific Heat (J/g·K)	Thermal conductivity (W/m·K)	Diffusivity (mm ² /s)
2-24-2009	EQ2.5P-TC-24-1	2.139	0.240	0.123
2-24-2009	EQ2.5P-TC-28-1	2.226	0.251	0.124
2-24-2009	EQ2.5P-TC-32-1	2.231	0.261	0.128
3-20-2009	EQ2.5P-TC-28-2	2.236	0.247	0.121
Average		2.2080	0.2498	0.1240
Standard Deviation		0.0462	0.0088	0.0029
Number of samples		4	4	4

Calibration sample used: 2mm thick, 25.4 mm diameter Vespel SP1 disk.

Density used for thermal conductivity calculation: 0.9125 g/cm³.

Table A.27
4 wt.% Hyperion FIBRIL™ nanotubes in Dow Polypropylene
Semi Crystalline Homopolymer Resin H7012-35RN

Test Date	Disk number	Specific Heat (J/g·K)	Thermal conductivity (W/m·K)	Diffusivity (mm ² /s)
2-24-2009	EQ4P-TC-23-1	2.210	0.293	0.144
2-24-2009	EQ4P-TC-25-1	2.203	0.289	0.143
2-24-2009	EQ4P-TC-29-1	2.174	0.280	0.140
3-20-2009	EQ4P-TC-29-2	2.175	0.291	0.145
Average		2.1905	0.2883	0.1430
Standard Deviation		0.0187	0.0057	0.0022
Number of samples		4	4	4

Calibration sample used: 2mm thick, 25.4 mm diameter Vespel SP1 disk.

Density used for thermal conductivity calculation: 0.9202 g/cm³.

Table A.28

5 wt.% Hyperion FIBRIL™ nanotubes in Dow Polypropylene
Semi Crystalline Homopolymer Resin H7012-35RN

Test Date	Disk number	Specific Heat (J/g·K)	Thermal conductivity (W/m·K)	Diffusivity (mm ² /s)
2-24-2009	EQ5P-TC-30-1	1.989	0.294	0.160
2-24-2009	EQ5P-TC-32-1	2.122	0.313	0.160
2-24-2009	EQ5P-TC-28-1	2.115	0.322	0.165
3-20-2009	EQ5P-TC-32-2	2.167	0.300	0.150
Average		2.0983	0.3073	0.1588
Standard Deviation		0.0764	0.0126	0.0063
Number of samples		4	4	4

Calibration sample used: 2mm thick, 25.4 mm diameter Vespel SP1 disk.

Density used for thermal conductivity calculation: 0.9254 g/cm³.

Table A.29

6 wt.% Hyperion FIBRIL™ nanotubes in Dow Polypropylene
Semi Crystalline Homopolymer Resin H7012-35RN

Test Date	Disk number	Specific Heat (J/g·K)	Thermal conductivity (W/m·K)	Diffusivity (mm ² /s)
2-20-2009	EQ6P-TC-31-1	2.026	0.314	0.166
2-20-2009	EQ6P-TC-28-1	2.110	0.329	0.168
2-20-2009	EQ6P-TC-26-1	2.066	0.312	0.162
3-20-2009	EQ6P-TC-28-2	2.090	0.318	0.164
Average		2.0730	0.3183	0.1650
Standard Deviation		0.0361	0.0076	0.0026
Number of samples		4	4	4

Calibration sample used: 2mm thick, 25.4 mm diameter Vespel SP1 disk.

Density used for thermal conductivity calculation: 0.9307 g/cm³.

Table A.30

6 wt.% Hyperion FIBRIL™ nanotubes in Dow Polypropylene
Semi Crystalline Homopolymer Resin H7012-35RN Replicate

Test Date	Disk number	Specific Heat (J/g·K)	Thermal conductivity (W/m·K)	Diffusivity (mm ² /s)
2-20-2009	EQ6PR-TC-7-2	2.063	0.313	0.163
2-20-2009	EQ6PR-TC-25-1	2.108	0.322	0.164
2-20-2009	EQ6PR-TC-14-2	2.202	0.347	0.169
3-20-2009	EQ6PR-TC-25-2	2.116	0.321	0.163
Average		2.1222	0.3258	0.1648
Standard Deviation		0.0581	0.0147	0.0029
Number of samples		4	4	4

Calibration sample used: 2mm thick, 25.4 mm diameter Vespel SP1 disk.

Density used for thermal conductivity calculation: 0.9307 g/cm³.

Table A.31

7.5 wt.% Hyperion FIBRIL™ nanotubes in Dow Polypropylene
Semi Crystalline Homopolymer Resin H7012-35RN

Test Date	Disk number	Specific Heat (J/g·K)	Thermal conductivity (W/m·K)	Diffusivity (mm ² /s)
2-19-2009	EQ7.5P-TC-29-1	2.107	0.373	0.189
4-13-2009	EQ7.5P-TC-29-2	2.016	0.342	0.181
4-13-2009	EQ7.5P-TC-30-2	2.005	0.338	0.180
4-13-2009	EQ7.5P-TC-32-2	1.989	0.385	0.206
Average		2.0293	0.3595	0.1995
Standard Deviation		0.0530	0.0231	0.0171
Number of samples		4	4	4

Calibration sample used: 2mm thick, 25.4 mm diameter Vespel SP1 disk.

Density used for thermal conductivity calculation: 0.9387 g/cm³.

Table A.32

7.5 wt.% Hyperion FIBRIL™ nanotubes in Dow Polypropylene
Semi Crystalline Homopolymer Resin H7012-35RN Replicate

Test Date	Disk number	Specific Heat (J/g·K)	Thermal conductivity (W/m·K)	Diffusivity (mm ² /s)
2-26-2009	EQ7.5PR-TC-32-2	2.127	0.352	0.176
2-26-2009	EQ7.5PR-TC-10-1	2.089	0.350	0.179
2-26-2009	EQ7.5PR-TC-21-1	2.059	0.345	0.178
3-20-2009	EQ7.5PR-TC-10-2	2.006	0.338	0.179
Average		2.0703	0.3463	0.178
Standard Deviation		0.0511	0.0062	0.0014
Number of samples		4	4	4

Calibration sample used: 2mm thick, 25.4 mm diameter Vespel SP1 disk.

Density used for thermal conductivity calculation: 0.9387 g/cm³.

Table A.33

10 wt.% Hyperion FIBRIL™ nanotubes in Dow Polypropylene
Semi Crystalline Homopolymer Resin H7012-35RN

Test Date	Disk number	Specific Heat (J/g·K)	Thermal conductivity (W/m·K)	Diffusivity (mm ² /s)
2-19-2009	EQ10P-TC-21-1	2.051	0.410	0.210
3-17-2009	EQ10P-TC-10-2	1.997	0.398	0.209
3-17-2009	EQ10P-TC-21-2	2.069	0.414	0.210
3-17-2009	EQ10P-TC-14-2	2.109	0.414	0.206
Average		2.0565	0.4090	0.2088
Standard Deviation		0.0465	0.0076	0.0019
Number of samples		4	4	4

Calibration sample used: 2mm thick, 25.4 mm diameter Vespel SP1 disk.

Density used for thermal conductivity calculation: 0.9524 g/cm³.

Table A.34
15 wt.% Hyperion FIBRIL™ nanotubes in Dow Polypropylene
Semi Crystalline Homopolymer Resin H7012-35RN

Test Date	Disk number	Specific Heat (J/g·K)	Thermal conductivity (W/m·K)	Diffusivity (mm ² /s)
2-19-2009	EQ15P-TC-36-1	1.847	0.466	0.257
3-17-2009	EQ15P-TC-27-1	1.956	0.496	0.258
3-17-2009	EQ15P-TC-20-1	1.959	0.522	0.271
3-17-2009	EQ15P-TC-20-2	1.985	0.503	0.258
Average		1.9368	0.4968	0.2610
Standard Deviation		0.0612	0.0233	0.0067
Number of samples		4	4	4

Calibration sample used: 2mm thick, 25.4 mm diameter Vespel SP1 disk.

Density used for thermal conductivity calculation: 0.9809 g/cm³.

Table A.35
2.5 wt.% Ketjenblack EC-600 JD and 65 wt.% Thermocarb TC-300 in Dow Polypropylene Semi
Crystalline Homopolymer Resin H7012-35RN

Test Date	Disk number	Specific Heat (J/g·K)	Thermal conductivity (W/m·K)	Diffusivity (mm ² /s)
2-13-2009	EA2.5B65P-TC-35-2	1.382	3.545	1.707
2-13-2009	EA2.5B65P-TC-34-1	1.337	3.499	1.686
2-13-2009	EA2.5B65P-TC-34-2	1.414	3.585	1.687
2-13-2009	EA2.5B65P-TC-28-1	1.381	3.520	1.696
Average		1.379	3.537	1.694
Standard Deviation		0.032	0.037	0.010
Number of samples		4	4	4

Calibration sample used: 3 mm thick, 25.4mm diameter Pyroceram 9606 disk.

Density used for thermal conductivity calculation: 1.5034 g/cm³.

Table A.36

2.5 wt.% Ketjenblack EC-600 JD and 65 wt.% Thermocarb TC-300 in Dow Polypropylene Semi Crystalline Homopolymer Resin H7012-35RN Replicate

Test Date	Disk number	Specific Heat (J/g·K)	Thermal conductivity (W/m·K)	Diffusivity (mm ² /s)
1-27-2009	EA2.5B65PR-TC-18-2	1.375	3.534	1.710
1-27-2009	EA2.5B65PR-TC-12-2	1.380	3.467	1.672
1-27-2009	EA2.5B65PR-TC-20-2	1.402	3.647	1.731
1-27-2009	EA2.5B65PR-TC-20-1	1.401	3.542	1.683
Average		1.390	3.548	1.699
Standard Deviation		0.014	0.074	0.027
Number of samples		4	4	4

Calibration sample used: 3 mm thick, 25.4mm diameter Pyroceram 9606 disk.

Density used for thermal conductivity calculation: 1.5034 g/cm³.

Table A.37

2.5 wt.% Ketjenblack EC-600 JD and 6 wt.% Hyperion FIBRIL™ nanotubes in Dow Polypropylene Semi Crystalline Homopolymer Resin H7012-35RN

Test Date	Disk number	Specific Heat (J/g·K)	Thermal conductivity (W/m·K)	Diffusivity (mm ² /s)
2-13-2009	EA2.5Q6P-TC-41-1	1.940	0.340	0.186
2-13-2009	EA2.5Q6P-TC-25-1	2.074	0.370	0.189
3-24-2009	EA2.5Q6P-TC-9-1	2.049	0.359	0.186
2-13-2009	EA2.5Q6P-TC-14-1	1.997	0.380	0.202
Average		2.015	0.362	0.191
Standard Deviation		0.059	0.017	0.008
Number of samples		4	4	4

Calibration sample used: 2 mm thick, 25.4mm diameter Vespel SP1 disk.

Density used for thermal conductivity calculation: 0.9429 g/cm³.

Table A.38

2.5 wt.% Ketjenblack EC-600 JD and 6 wt.% Hyperion FIBRIL™ nanotubes in Dow Polypropylene
Semi Crystalline Homopolymer Resin H7012-35RN Replicate

Test Date	Disk number	Specific Heat (J/g·K)	Thermal conductivity (W/m·K)	Diffusivity (mm ² /s)
2-17-2009	EA2.5Q6PR-TC-21-1	2.023	0.360	0.189
2-17-2009	EA2.5Q6PR-TC-34-1	2.049	0.359	0.186
2-17-2009	EA2.5Q6PR-TC-7-2	2.059	0.349	0.180
3-24-2009	EA2.5Q6PR-TC-34-2	2.084	0.360	0.183
Average		2.054	0.357	0.185
Standard Deviation		0.025	0.005	0.004
Number of samples		4	4	4

Calibration sample used: 2 mm thick, 25.4mm diameter Vespel SP1 disk.

Density used for thermal conductivity calculation: 0.9429 g/cm³.

Table A.39

65 wt.% Thermocarb TC-300 and 6 wt.% Hyperion FIBRIL™ nanotubes in Dow Polypropylene
Semi Crystalline Homopolymer Resin H7012-35RN

Test Date	Disk number	Specific Heat (J/g·K)	Thermal conductivity (W/m·K)	Diffusivity (mm ² /s)
3-17-2009	EB65Q6P-TC-37-1	1.365	7.678	3.614
3-17-2009	EB65Q6P-TC-1-1	1.319	7.289	3.549
3-17-2009	EB65Q6P-TC-38-1	1.313	7.230	3.537
4-3-2009	EB65Q6P-TC-37-2	1.374	7.587	3.546
Average		1.343	7.446	3.562
Standard Deviation		0.156	0.220	0.035
Number of samples		4	4	4

Calibration sample used: 3 mm thick, 25.4mm diameter Pyroceram 9606 disk.

Density used for thermal conductivity calculation: 1.5567 g/cm³.

Table A.40

6 wt.% Hyperion FIBRIL™ nanotubes and 65 wt.% Thermocarb TC-300 in Dow Polypropylene Semi Crystalline Homopolymer Resin H7012-35RN Replicate

Test Date	Disk number	Specific Heat (J/g·K)	Thermal conductivity (W/m·K)	Diffusivity (mm ² /s)
3-17-2009	EB65Q6PR-TC-1-2	1.359	7.496	3.544
1-20-2009	EB65Q6PR-TC-16-1	1.304	7.421	3.595
1-20-2009	EB65Q6PR-TC-21-1	1.326	7.511	3.638
4-8-2009	EB65Q6PR-TC-18-1	1.345	7.787	3.718
Average		1.334	7.554	3.624
Standard Deviation		0.024	0.160	0.074
Number of samples		4	4	4

Calibration sample used: 3 mm thick, 25.4mm diameter Pyroceram 9606 disk.

Density used for thermal conductivity calculation: 1.5567 g/cm³.

Table A.41

2.5 wt.% Ketjenblack EC-600 JD, 65 wt.% Thermocarb TC-300 and 6 wt.% Hyperion FIBRIL™ nanotubes in Dow Polypropylene Semi Crystalline Homopolymer Resin H7012-35RN Injection Molded

Test Date	Disk number	Specific Heat (J/g·K)	Thermal conductivity (W/m·K)	Diffusivity (mm ² /s)
1-26-2009	EA2.5B65Q6P-TC-33-2	1.290	8.543	4.182
1-27-2009	EA2.5B65Q6P-TC-13-2	1.319	8.501	4.161
1-26-2009	EA2.5B65Q6P-TC-56-1	1.324	8.475	4.149
1-26-2009	EA2.5B65Q6P-TC-33-1	1.227	8.494	4.353
Average		1.290	8.503	4.211
Standard Deviation		0.044	0.029	0.095
Number of samples		4	4	4

Calibration sample used: 3 mm thick, 25.4mm diameter Pyroceram 9606 disk.

Density used for thermal conductivity calculation: 1.5911 g/cm³.

Table A.42

2.5 wt.% Ketjenblack EC-600 JD, 65 wt.% Thermocarb TC-300 and 6 wt.% Hyperion FIBRIL™
nanotubes in Dow Polypropylene Semi Crystalline Homopolymer Resin
H7012-35RN Injection Molded Replicate

Test Date	Disk number	Specific Heat (J/g·K)	Thermal conductivity (W/m·K)	Diffusivity (mm ² /s)
1-20-2009	EA2.5B65Q6PR-TC-53-2	1.321	8.662	4.130
4-7-2009	EA2.5B65Q6PR-TC-23-1	1.305	8.534	4.111
4-7-2009	EA2.5B65Q6PR-TC-37-2	1.307	8.007	3.883
4-7-2009	EA2.5B65Q6PR-TC-53-1	1.334	8.643	4.072
Average		1.319	8.469	4.049
Standard Deviation		0.008	0.266	0.113
Number of samples		4	4	4

Calibration sample used: 3 mm thick, 25.4mm diameter Pyroceram 9606 disk.

Density used for thermal conductivity calculation: 1.5911 g/cm³.

Table A.43

2.5 wt.% Ketjenblack EC-600 JD, 65 wt.% Thermocarb TC-300 and 6 wt.% Hyperion FIBRIL™
nanotubes in Dow Polypropylene Semi Crystalline Homopolymer Resin
H7012-35RN Compression Molded

Test Date	Disk number	Specific Heat (J/g·K)	Thermal conductivity (W/m·K)	Diffusivity (mm ² /s)
2-25-2009	EA2.5B65Q6P- TC-1C-1	1.401	8.309	3.727
3-25-2009	EA2.5B65Q6P- TC-4C-1	1.409	8.413	3.752
3-25-2009	EA2.5B65Q6P- TC-4C-2	1.470	8.751	3.741
4-6-2009	EA2.5B65Q6P-TC-8C-1	1.425	8.693	3.835
Average		1.426	8.542	3.763
Standard Deviation		0.031	0.214	0.049
Number of samples		4	4	4

Calibration sample used: 3 mm thick, 25.4mm diameter Pyroceram 9606 disk.

Density used for thermal conductivity calculation: 1.5911 g/cm³.

Appendix B: In-plane thermal conductivity results using the Flash Method

Test settings:

- Temperature: 80°C
- 5 shots per sample
- Voltage: 304V
- Light filter: 100%
- Pulse width: Medium

Table B.1

2.5 wt.% Ketjenblack EC-600 JD in Dow Polypropylene Semi Crystalline
Homopolymer Resin H7012-35RN

Test Date	Sample number	Thermal conductivity (W/m·K)	Diffusivity (mm ² /s)
3-26-2009	EA2.5P-F-27-1	0.294	0.148
3-26-2009	EA2.5P-F-29-1	0.296	0.149
3-31-2009	EA2.5P-F-27-2	0.270	0.136
Average		0.2867	0.1443
Standard Deviation		0.0145	0.0072
Number of samples		3	3

Calibration sample used: 2 mm thick, 25.4mm diameter Vespel SP1 disk.

Used specific heat of 2.175 J/ g·K

Density used for thermal conductivity calculation: 0.9114 g/cm³.

Table B.2

2.5 wt.% Ketjenblack EC-600 JD in Dow Polypropylene Semi Crystalline
Homopolymer Resin H7012-35RN Replicate

Test Date	Sample number	Thermal conductivity (W/m·K)	Diffusivity (mm ² /s)
3-26-2009	EA2.5PR-F-31-1	0.298	0.148
3-26-2009	EA2.5PR-F-15-1	0.293	0.145
3-31-2009	EA2.5PR-F-15-2	0.312	0.155
Average		0.301	0.1493
Standard Deviation		0.0098	0.0051
Number of samples		3	3

Calibration sample used: 2 mm thick, 25.4mm diameter Vespel SP1 disk.

Used specific heat of 2.214 J/ g·K

Density used for thermal conductivity calculation: 0.9114 g/cm³.

Table B.3

4 wt.% Ketjenblack EC-600 JD in Dow Polypropylene Semi Crystalline
Homopolymer Resin H7012-35RN

Test Date	Sample number	Thermal conductivity (W/m·K)	Diffusivity (mm ² /s)
3-25-2009	EA4P-F-26-1	0.306	0.154
3-24-2009	EA4P-F-32-1	0.287	0.144
3-31-2009	EA4P-F-26-2	0.381	0.192
Average		0.3247	0.1633
Standard Deviation		0.0497	0.0253
Number of samples		3	3

Calibration sample used: 2 mm thick, 25.4mm diameter Vespel SP1 disk.

Used specific heat of 2.165 J/ g·K

Density used for thermal conductivity calculation: 0.9184 g/cm³.

Table B.4

5 wt.% Ketjenblack EC-600 JD in Dow Polypropylene Semi Crystalline
Homopolymer Resin H7012-35RN

Test Date	Sample number	Thermal conductivity (W/m·K)	Diffusivity (mm ² /s)
3-25-2009	EA5P-F-17-1	0.311	0.152
3-24-2009	EA5P-F-31-1	0.319	0.156
3-31-2009	EA5P-F-31-2	0.406	0.198
Average		0.3453	0.1687
Standard Deviation		0.0527	0.0255
Number of samples		3	3

Calibration sample used: 2 mm thick, 25.4mm diameter Vespel SP1 disk.

Used specific heat of 2.221 J/ g·K

Density used for thermal conductivity calculation: 0.9231 g/cm³.

Table B.5

6 wt.% Ketjenblack EC-600 JD in Dow Polypropylene Semi Crystalline
Homopolymer Resin H7012-35RN

Test Date	Sample number	Thermal conductivity (W/m·K)	Diffusivity (mm ² /s)
3-24-2009	EA6P-F-28-1	0.327	0.163
3-31-2009	EA6P-F-28-2	0.374	0.186
4-7-2009	EA6P-F-20-2	0.365	0.181
Average		0.3554	0.1677
Standard Deviation		0.0248	0.0165
Number of samples		3	3

Calibration sample used: 2 mm thick, 25.4mm diameter Vespel SP1 disk.

Used specific heat of 2.169 J/ g·K

Density used for thermal conductivity calculation: 0.9278 g/cm³.

Table B.6

7.5 wt.% Ketjenblack EC-600 JD in Dow Polypropylene Semi Crystalline
Homopolymer Resin H7012-35RN

Test Date	Sample number	Thermal conductivity (W/m·K)	Diffusivity (mm ² /s)
4-7-2009	EA7.5P-F-22-2	0.348	0.188
4-8-2009	EA7.5P-F-15-3	0.368	0.199
4-13-2009	EA7.5P-F-20-2	0.391	0.211
Average		0.369	0.1717
Standard Deviation		0.0215	0.0057
Number of samples		3	3

Calibration sample used: 2 mm thick, 25.4mm diameter Vespel SP1 disk.

Used specific heat of 1.978 J/ g·K

Density used for thermal conductivity calculation: 0.9351 g/cm³.

Table B.7

10 wt.% Ketjenblack EC-600 JD in Dow Polypropylene Semi Crystalline
Homopolymer Resin H7012-35RN

Test Date	Sample number	Thermal conductivity (W/m·K)	Diffusivity (mm ² /s)
3-24-2009	EA10P-F-26-1	0.421	0.217
3-24-2009	EA10P-F-33-1	0.409	0.211
4-7-2009	EA10P-F-26-2	0.402	0.207
Average		0.4107	0.2083
Standard Deviation		0.0096	0.0103
Number of samples		3	3

Calibration sample used: 2 mm thick, 25.4mm diameter Vespel SP1 disk.

Used specific heat of 2.051 J/ g·K

Density used for thermal conductivity calculation: 0.9474 g/cm³.

Table B.8

15 wt.% Ketjenblack EC-600 JD in Dow Polypropylene Semi Crystalline
Homopolymer Resin H7012-35RN

Test Date	Sample number	Thermal conductivity (W/m·K)	Diffusivity (mm ² /s)
3-23-2009	EA15P-F-31-1	0.442	0.219
3-30-2009	EA15P-F-23-2	0.465	0.230
4-8-2009	EA15P-F-23-3	0.465	0.230
Average		0.4573	0.2263
Standard Deviation		0.0133	0.0064
Number of samples		3	3

Calibration sample used: 2 mm thick, 25.4mm diameter Vespel SP1 disk.

Used specific heat of 2.077 J/ g·K

Density used for thermal conductivity calculation: 0.9730 g/cm³.

Table B.9

10 wt.% Thermocarb TC-300 in Dow Polypropylene Semi Crystalline
Homopolymer Resin H7012-35RN

Test Date	Sample number	Thermal conductivity (W/m·K)	Diffusivity (mm ² /s)
3-16-2009	EB10P-F-29-1	0.607	0.290
3-16-2009	EB10P-F-32-1	0.542	0.259
4-6-2009	EB10P-F-32-2	0.553	0.264
Average		0.567	0.271
Standard Deviation		0.035	0.017
Number of samples		3	3

Calibration sample used: 2 mm thick, 25.4mm diameter Vespel SP1 disk.

Used specific heat of 2.188 J/ g·K

Density used for thermal conductivity calculation: 0.9573 g/cm³.

Table B.10

15 wt.% Thermocarb TC-300 in Dow Polypropylene Semi Crystalline
Homopolymer Resin H7012-35RN

Test Date	Sample number	Thermal conductivity (W/m·K)	Diffusivity (mm ² /s)
3-6-2009	EB15P-F-18-1	0.705	0.368
3-6-2009	EB15P-F-34-1	0.664	0.346
4-3-2009	EB15P-F-34-2	0.623	0.325
Average		0.664	0.346
Standard Deviation		0.041	0.022
Number of samples		3	3

Calibration sample used: 2 mm thick, 25.4mm diameter Vespel SP1 disk.

Used specific heat of 1.938 J/ g·K

Density used for thermal conductivity calculation: 0.9887 g/cm³.

Table B.11

20 wt.% Thermocarb TC-300 in Dow Polypropylene Semi Crystalline
Homopolymer Resin H7012-35RN

Test Date	Sample number	Thermal conductivity (W/m·K)	Diffusivity (mm ² /s)
3-6-2009	EB20P-F-31-1	0.904	0.460
3-6-2009	EB20P-F-25-1	0.926	0.471
4-3-2009	EB20P-F-31-2	0.953	0.485
Average		0.928	0.472
Standard Deviation		0.025	0.013
Number of samples		3	3

Calibration sample used: 2 mm thick, 25.4mm diameter Vespel SP1 disk.

Used specific heat of 1.922 J/ g·K

Density used for thermal conductivity calculation: 1.0223 g/cm³.

Table B.12

25 wt.% Thermocarb TC-300 in Dow Polypropylene Semi Crystalline
Homopolymer Resin H7012-35RN

Test Date	Sample number	Thermal conductivity (W/m·K)	Diffusivity (mm ² /s)
3-6-2009	EB25P-F-27-1	1.341	0.655
3-6-2009	EB25P-F-24-1	1.218	0.595
4-3-2009	EB25P-F-27-2	1.149	0.562
Average		1.236	0.604
Standard Deviation		0.097	0.047
Number of samples		3	3

Calibration sample used: 2 mm thick, 25.4mm diameter Vespel SP1 disk.

Used specific heat of 1.934 J/ g·K

Density used for thermal conductivity calculation: 1.0583 g/cm³.

Table B.13

30 wt.% Thermocarb TC-300 in Dow Polypropylene Semi Crystalline
Homopolymer Resin H7012-35RN

Test Date	Sample number	Thermal conductivity (W/m·K)	Diffusivity (mm ² /s)
4-3-2009	EB30P-F-33-1	1.462	0.780
3-5-2009	EB30P-F-23-1	1.521	0.812
3-5-2009	EB30P-F-23-2	1.539	0.821
Average		1.507	0.804
Standard Deviation		0.040	0.022
Number of samples		3	3

Calibration sample used: 2 mm thick, 25.4mm diameter Vespel SP1 disk.

Used specific heat of 1.708 J/ g·K

Density used for thermal conductivity calculation: 1.0968 g/cm³.

Table B.14

35 wt.% Thermocarb TC-300 in Dow Polypropylene Semi Crystalline
Homopolymer Resin H7012-35RN

Test Date	Sample number	Thermal conductivity (W/m·K)	Diffusivity (mm ² /s)
3-5-2009	EB35P-F-28-1	2.067	1.094
3-5-2009	EB35P-F-16-1	2.105	1.113
4-3-2009	EB35P-F-16-2	2.032	1.075
Average		2.068	1.094
Standard Deviation		0.037	0.019
Number of samples		3	3

Calibration sample used: 2 mm thick, 25.4mm diameter Vespel SP1 disk.

Used specific heat of 1.661 J/ g·K

Density used for thermal conductivity calculation: 1.1383 g/cm³.

Table B.15

40 wt.% Thermocarb TC-300 in Dow Polypropylene Semi Crystalline
Homopolymer Resin H7012-35RN

Test Date	Sample number	Thermal conductivity (W/m·K)	Diffusivity (mm ² /s)
3-4-2009	EB40P-F-16-1	3.165	1.461
3-4-2009	EB40P-F-21-1	3.162	1.459
4-3-2009	EB40P-F-16-2	2.998	1.383
Average		3.108	1.434
Standard Deviation		0.096	0.044
Number of samples		3	3

Calibration sample used: 3 mm thick, 25.4mm diameter Pyrex 7740 disk.

Used specific heat of 1.832 J/ g·K

Density used for thermal conductivity calculation: 1.1831 g/cm³.

Table B.16

45 wt.% Thermocarb TC-300 in Dow Polypropylene Semi Crystalline
Homopolymer Resin H7012-35RN

Test Date	Sample number	Thermal conductivity (W/m·K)	Diffusivity (mm ² /s)
3-4-2009	EB45P-F-17-1	3.966	1.884
3-4-2009	EB45P-F-32-1	4.325	2.055
4-1-2009	EB45P-F-32-2	4.210	2.000
Average		4.167	1.979
Standard Deviation		0.183	0.087
Number of samples		3	3

Calibration sample used: 3 mm thick, 25.4mm diameter Pyrex 7740 disk.

Used specific heat of 1.709 J/ g·K

Density used for thermal conductivity calculation: 1.2315 g/cm³.

Table B.17

50 wt.% Thermocarb TC-300 in Dow Polypropylene Semi Crystalline
Homopolymer Resin H7012-35RN

Test Date	Sample number	Thermal conductivity (W/m·K)	Diffusivity (mm ² /s)
3-4-2009	EB50P-F-20-1	5.430	2.513
3-4-2009	EB50P-F-31-1	5.536	2.563
4-1-2009	EB50P-F-31-2	5.358	2.480
Average		5.434	2.519
Standard Deviation		0.078	0.042
Number of samples		3	3

Calibration sample used: 3 mm thick, 25.4mm diameter Pyrex 7740 disk.

Used specific heat of 1.683 J/ g·K

Density used for thermal conductivity calculation: 1.2841 g/cm³.

Table B.18

55 wt.% Thermocarb TC-300 in Dow Polypropylene Semi Crystalline
Homopolymer Resin H7012-35RN

Test Date	Sample number	Thermal conductivity (W/m·K)	Diffusivity (mm ² /s)
2-20-2009	EB55P-F-27-1	7.139	3.286
2-20-2009	EB55P-F-19-1	7.350	3.382
4-1-2009	EB55P-F-27-2	7.027	3.235
Average		7.172	3.301
Standard Deviation		0.164	0.075
Number of samples		3	3

Calibration sample used: 3 mm thick, 25.4mm diameter Pyroceram 9606 disk.

Used specific heat of 1.620 J/ g·K

Density used for thermal conductivity calculation: 1.3413 g/cm³.

Table B.19

60 wt.% Thermocarb TC-300 in Dow Polypropylene Semi Crystalline
Homopolymer Resin H7012-35RN

Test Date	Sample number	Thermal conductivity (W/m·K)	Diffusivity (mm ² /s)
2-19-2009	EB60P-F-19-1	9.511	4.489
2-19-2009	EB60P-F-32-1	9.762	4.607
4-1-2009	EB60P-F-19-2	9.011	4.253
Average		9.428	4.450
Standard Deviation		0.382	0.180
Number of samples		3	3

Calibration sample used: 3 mm thick, 25.4mm diameter Pyroceram 9606 disk.

Used specific heat of 1.509 J/ g·K

Density used for thermal conductivity calculation: 1.4039 g/cm³.

Table B.20

65 wt.% Thermocarb TC-300 in Dow Polypropylene Semi Crystalline
Homopolymer Resin H7012-35RN

Test Date	Sample number	Thermal conductivity (W/m·K)	Diffusivity (mm ² /s)
2-17-2009	EB65P-F-22-1	12.987	5.757
2-17-2009	EB65P-F-27-1	13.248	5.876
4-1-2009	EB65P-F-22-2	12.773	5.666
Average		12.999	5.766
Standard Deviation		0.238	0.105
Number of samples		3	3

Calibration sample used: 3 mm thick, 25.4mm diameter Pyroceram 9606 disk.

Used specific heat of 1.530 J/ g·K

Density used for thermal conductivity calculation: 1.4726 g/cm³.

Table B.21

65 wt.% Thermocarb TC-300 in Dow Polypropylene Semi Crystalline
Homopolymer Resin H7012-35RN Replicate

Test Date	Sample number	Thermal conductivity (W/m·K)	Diffusivity (mm ² /s)
2-18-2009	EB65PR-F-27-1	12.725	5.672
2-18-2009	EB65PR-F-20-1	12.538	5.589
4-1-2009	EB65PR-F-27-2	12.321	5.492
Average		12.528	5.584
Standard Deviation		0.202	0.090
Number of samples		3	3

Calibration sample used: 3 mm thick, 25.4mm diameter Pyroceram 9606 disk.

Used specific heat of 1.523 J/ g·K

Density used for thermal conductivity calculation: 1.4726 g/cm³.

Table B.22

70 wt.% Thermocarb TC-300 in Dow Polypropylene Semi Crystalline
Homopolymer Resin H7012-35RN

Test Date	Sample number	Thermal conductivity (W/m·K)	Diffusivity (mm ² /s)
2-13-2009	EB70P-F-20-1	17.778	7.708
2-13-2009	EB70P-F-30-1	18.404	7.981
4-1-2009	EB70P-F-20-2	17.659	7.659
Average		17.947	7.783
Standard Deviation		0.400	0.174
Number of samples		3	3

Calibration sample used: 3 mm thick, 25.4mm diameter Pyroceram 9606 disk.

Used specific heat of 1.489 J/ g·K

Density used for thermal conductivity calculation: 1.5484 g/cm³.

Table B.23

75 wt.% Thermocarb TC-300 in Dow Polypropylene Semi Crystalline
Homopolymer Resin H7012-35RN

Test Date	Sample number	Thermal conductivity (W/m·K)	Diffusivity (mm ² /s)
2-13-2009	EB75P-F-23-1	24.262	10.435
2-12-2009	EB75P-F-26-1	24.789	10.662
4-1-2009	EB75P-F-23-2	24.210	10.413
Average		24.420	10.503
Standard Deviation		0.320	0.138
Number of samples		3	3

Calibration sample used: 3 mm thick, 25.4mm diameter Pyroceram 9606 disk.

Used specific heat of 1.425 J/ g·K

Density used for thermal conductivity calculation: 1.6324 g/cm³.

Table B.24

80 wt.% Thermocarb TC-300 in Dow Polypropylene Semi Crystalline
Homopolymer Resin H7012-35RN

Test Date	Sample number	Thermal conductivity (W/m·K)	Diffusivity (mm ² /s)
3-31-2009	EB80P-F-22-3	33.789	15.232
3-26-2009	EB80P-F-22-2	33.078	14.912
3-26-2009	EB80P-F-18-2	33.828	15.250
	Average	33.565	15.131
	Standard Deviation	0.422	0.190
	Number of samples	3	3

Calibration sample used: 3 mm thick, 25.4mm diameter Pyrocera 9606 disk.

Used specific heat of 1.285 J/ g·K

Density used for thermal conductivity calculation: 1.7260 g/cm³.

Table B.25

1.5 wt.% Hyperion FIBRIL™ nanotubes in Dow Polypropylene
Semi Crystalline Homopolymer Resin H7012-35RN

Test Date	Sample number	Thermal conductivity (W/m·K)	Diffusivity (mm ² /s)
3-23-2009	EQ1.5P-F-16-1	0.316	0.154
3-23-2009	EQ1.5P-F-25-1	0.291	0.142
3-30-2009	EQ1.5P-F-16-2	0.315	0.153
	Average	0.3073	0.1497
	Standard Deviation	0.0142	0.0067
	Number of samples	3	3

Calibration sample used: 2 mm thick, 25.4mm diameter Vespel SP1 disk.

Used specific heat of 2.266 J/ g·K

Density used for thermal conductivity calculation: 0.9075 g/cm³.

Table B.26
2.5 wt.% Hyperion FIBRIL™ nanotubes in Dow Polypropylene
Semi Crystalline Homopolymer Resin H7012-35RN

Test Date	Sample number	Thermal conductivity (W/m·K)	Diffusivity (mm ² /s)
3-23-2009	EQ2.5P-F-22-1	0.353	0.174
3-23-2009	EQ2.5P-F-28-1	0.292	0.144
3-31-2009	EQ2.5P-F-28-2	0.376	0.185
	Average	0.3403	0.1677
	Standard Deviation	0.0434	0.0212
	Number of samples	3	3

Calibration sample used: 2 mm thick, 25.4mm diameter Vespel SP1 disk.

Used specific heat of 2.226 J/ g·K

Density used for thermal conductivity calculation: 0.9125 g/cm³.

Table B.27
4 wt.% Hyperion FIBRIL™ nanotubes in Dow Polypropylene
Semi Crystalline Homopolymer Resin H7012-35RN

Test Date	Sample number	Thermal conductivity (W/m·K)	Diffusivity (mm ² /s)
3-23-2009	EQ4P-F-22-1	0.364	0.179
3-23-2009	EQ4P-F-24-1	0.399	0.196
3-31-2009	EQ4P-F-22-2	0.407	0.200
	Average	0.3900	0.1917
	Standard Deviation	0.0229	0.0111
	Number of samples	3	3

Calibration sample used: 2 mm thick, 25.4mm diameter Vespel SP1 disk.

Used specific heat of 2.210 J/ g·K

Density used for thermal conductivity calculation: 0.9202 g/cm³.

Table B.28
5 wt.% Hyperion FIBRIL™ nanotubes in Dow Polypropylene
Semi Crystalline Homopolymer Resin H7012-35RN

Test Date	Sample number	Thermal conductivity (W/m·K)	Diffusivity (mm ² /s)
3-20-2009	EQ5P-F-33-1	0.401	0.205
4-6-2009	EQ5P-F-33-3	0.395	0.202
4-6-2009	EQ5P-F-22-2	0.388	0.198
	Average	0.3947	0.191
	Standard Deviation	0.0065	0.0145
	Number of samples	3	3

Calibration sample used: 2 mm thick, 25.4mm diameter Vespel SP1 disk.

Used specific heat of 2.115 J/ g·K

Density used for thermal conductivity calculation: 0.9254 g/cm³.

Table B.29
6 wt.% Hyperion FIBRIL™ nanotubes in Dow Polypropylene
Semi Crystalline Homopolymer Resin H7012-35RN

Test Date	Sample number	Thermal conductivity (W/m·K)	Diffusivity (mm ² /s)
3-20-2009	EQ6P-F-18-1	0.400	0.208
4-6-2009	EQ6P-F-18-3	0.435	0.226
4-6-2009	EQ6P-F-25-2	0.438	0.228
	Average	0.4243	0.2053
	Standard Deviation	0.0211	0.0025
	Number of samples	3	3

Calibration sample used: 2 mm thick, 25.4mm diameter Vespel SP1 disk.

Used specific heat of 2.066 J/ g·K

Density used for thermal conductivity calculation: 0.9307 g/cm³.

Table B.30
6 wt.% Hyperion FIBRIL™ nanotubes in Dow Polypropylene
Semi Crystalline Homopolymer Resin H7012-35RN Replicate

Test Date	Sample number	Thermal conductivity (W/m·K)	Diffusivity (mm ² /s)
3-18-2009	EQ6PR-F-23-1	0.455	0.222
4-13-2009	EQ6PR-F-23-2	0.452	0.221
4-13-2009	EQ6PR-F-23-3	0.447	0.218
	Average	0.4513	0.2250
	Standard Deviation	0.0040	0.0061
	Number of samples	3	3

Calibration sample used: 2 mm thick, 25.4mm diameter Vespel SP1 disk.

Used specific heat of 2.202 J/ g·K

Density used for thermal conductivity calculation: 0.9307 g/cm³.

Table B.31
7.5 wt.% Hyperion FIBRIL™ nanotubes in Dow Polypropylene
Semi Crystalline Homopolymer Resin H7012-35RN

Test Date	Sample number	Thermal conductivity (W/m·K)	Diffusivity (mm ² /s)
3-18-2009	EQ7.5P-F-21-1	0.500	0.260
3-18-2009	EQ7.5P-F-27-1	0.497	0.258
3-30-2009	EQ7.5P-F-27-2	0.479	0.249
	Average	0.4920	0.2557
	Standard Deviation	0.0114	0.0059
	Number of samples	3	3

Calibration sample used: 2 mm thick, 25.4mm diameter Vespel SP1 disk.

Used specific heat of 2.049 J/ g·K

Density used for thermal conductivity calculation: 0.9387 g/cm³.

Table B.32
7.5 wt.% Hyperion FIBRIL™ nanotubes in Dow Polypropylene
Semi Crystalline Homopolymer Resin H7012-35RN Replicate

Test Date	Sample number	Thermal conductivity (W/m·K)	Diffusivity (mm ² /s)
3-18-2009	EQ7.5PR-F-18-1	0.449	0.225
3-18-2009	EQ7.5PR-F-28-1	0.463	0.232
3-30-2009	EQ7.5PR-F-18-2	0.514	0.258
	Average	0.4753	0.2383
	Standard Deviation	0.0342	0.0174
	Number of samples	3	3

Calibration sample used: 2 mm thick, 25.4mm diameter Vespel SP1 disk.

Used specific heat of 2.127 J/ g·K

Density used for thermal conductivity calculation: 0.9387 g/cm³.

Table B.33
10 wt.% Hyperion FIBRIL™ nanotubes in Dow Polypropylene
Semi Crystalline Homopolymer Resin H7012-35RN

Test Date	Sample number	Thermal conductivity (W/m·K)	Diffusivity (mm ² /s)
3-17-2009	EQ10P-F-20-1	0.617	0.321
3-17-2009	EQ10P-F-28-1	0.610	0.318
3-30-2009	EQ10P-F-20-2	0.631	0.329
	Average	0.6193	0.3227
	Standard Deviation	0.0107	0.0057
	Number of samples	3	3

Calibration sample used: 2 mm thick, 25.4mm diameter, Vespel SP1 disk.

Used specific heat of 2.017 J/ g·K

Density used for thermal conductivity calculation: 0.9387 g/cm³.

Table B.34
15 wt.% Hyperion FIBRIL™ nanotubes in Dow Polypropylene
Semi Crystalline Homopolymer Resin H7012-35RN

Test Date	Sample number	Thermal conductivity (W/m·K)	Diffusivity (mm ² /s)
3-17-2009	EQ15P-F-18-1	0.915	0.476
3-17-2009	EQ15P-F-26-1	0.813	0.423
3-30-2009	EQ15P-F-26-2	0.784	0.408
	Average	0.8373	0.4357
	Standard Deviation	0.0688	0.0357
	Number of samples	3	3

Calibration sample used: 2 mm thick, 25.4mm diameter Vespel SP1 disk.

Used specific heat of 1.959 J/ g·K

Density used for thermal conductivity calculation: 0.9809 g/cm³.

Table B.35
2.5 wt.% Ketjenblack EC-600 JD, 6 wt.% Hyperion FIBRIL™ nanotubes in Dow Polypropylene
Semi Crystalline Homopolymer Resin H7012-35RN.

Test Date	Sample number	Thermal conductivity (W/m·K)	Diffusivity (mm ² /s)
3-4-2009	EA2.5Q6P-F-20-1	0.470	0.250
3-4-2009	EA2.5Q6P-F-17-1	0.469	0.249
4-13-2009	EA2.5Q6P-F-17-2	0.493	0.262
	Average	0.4773	0.2537
	Standard Deviation	0.0136	0.0072
	Number of samples	3	3

Calibration sample used: 2 mm thick, 25.4mm diameter Vespel SP1 disk.

Used specific heat of 1.997 J/ g·K

Density used for thermal conductivity calculation: 0.9429 g/cm³.

Table B.36

2.5 wt.% Ketjenblack EC-600 JD, 6 wt.% Hyperion FIBRIL™ nanotubes in Dow Polypropylene Semi Crystalline Homopolymer Resin H7012-35RN Replicate.

Test Date	Sample number	Thermal conductivity (W/m·K)	Diffusivity (mm ² /s)
3-3-2009	EA2.5Q6PR-F-28-1	0.459	0.236
4-10-2009	EA2.5Q6PR-F-33-2	0.495	0.255
4-14-2009	EA2.5Q6PR-F-28-3	0.489	0.252
	Average	0.4810	0.2477
	Standard Deviation	0.0193	0.0102
	Number of samples	3	3

Calibration sample used: 2 mm thick, 25.4mm diameter Vespel SP1 disk.

Used specific heat of 2.059 J/ g·K

Density used for thermal conductivity calculation: 0.9429 g/cm³.

Table B.37

2.5 wt.% Ketjenblack EC-600 JD, 65 wt.% Thermocarb TC-300 and 6 wt.% Hyperion FIBRIL™ nanotubes in Dow Polypropylene Semi Crystalline Homopolymer Resin H7012-35RN Compression molded.

Test Date	Sample number	Thermal conductivity (W/m·K)	Diffusivity (mm ² /s)
4-10-2009	EA2.5B65Q6P-F-1C-3	36.308	15.934
4-14-2009	EA2.5B65Q6P-F-1C-4	37.472	16.445
4-14-2009	EA2.5B65Q6P-F-1C-5	37.268	16.355
	Average	37.0160	16.2447
	Standard Deviation	0.6216	0.2728
	Number of samples	3	3

Calibration sample used: 3 mm thick, 25.4mm diameter Pyroceram 9606 disk.

Used specific heat of 1.432 J/ g·K

Density used for thermal conductivity calculation: 1.5911 g/cm³.

Appendix C: Flexural strength test results

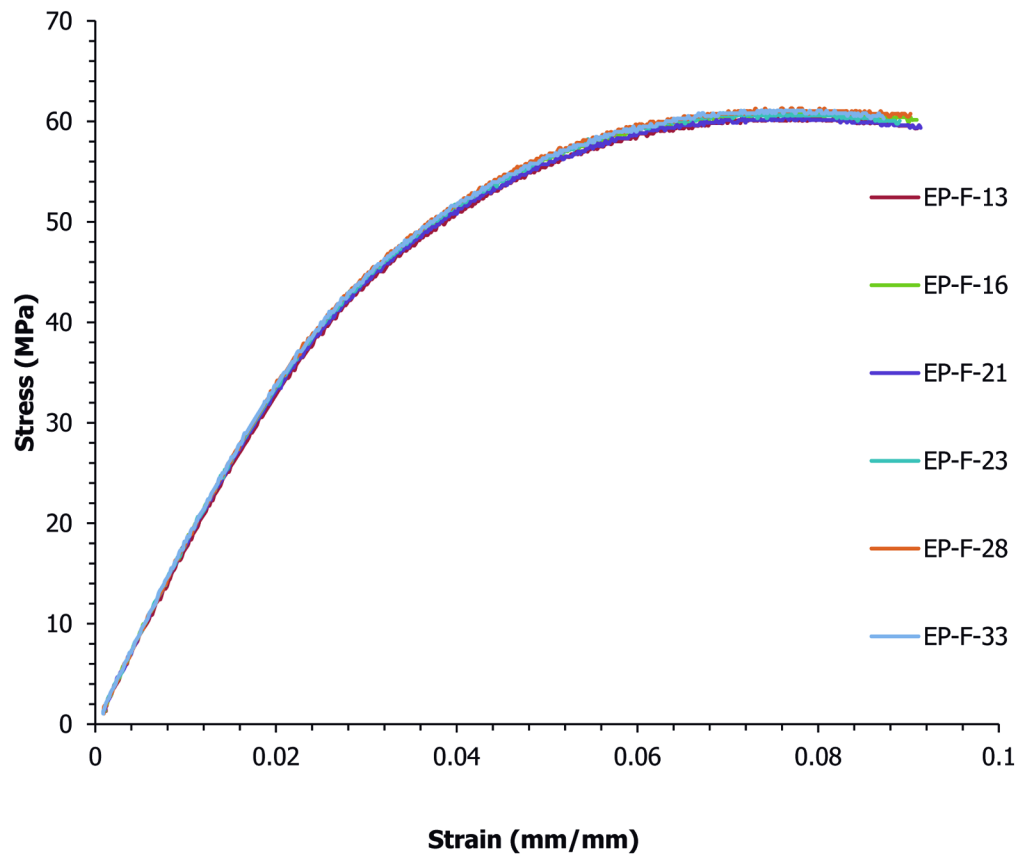


Figure C.1 Flexural results for EP

Table C.1

Flexural test results for Dow Polypropylene Semi Crystalline Homopolymer Resin H7012-35RN Injection Molded

Test Date	Sample Number	Flexural maximum Stress (MPa)	Flexural Strain at Maximum Stress (%)	0.1% Offset Yield Flexural Stress (MPa)	Strain at 0.1% Offset Yield Flexural Stress (%)	Flexural Fracture Stress (MPa)	Flexural Strain at Fracture Stress (%)	Flexural Modulus (MPa)
4/27/2009	EP-F-13	60.3	8.03	35.2	2.20	-	>100%	1697
4/27/2009	EP-F-16	60.9	7.91	35.0	2.11	-	>100%	1748
4/27/2009	EP-F-21	60.4	7.89	39.4	2.52	-	>100%	1639
4/27/2009	EP-F-23	60.8	7.31	37.9	2.35	-	>100%	1688
4/27/2009	EP-F-28	61.3	7.80	36.8	2.26	-	>100%	1714
4/27/2009	EP-F-33	61.1	7.73	37.1	2.28	-	>100%	1714
Average		60.8	7.78	36.9	2.29	-	N/A	1700
Standard deviation		0.4	0.25	1.6	0.14	-	N/A	36
Number of samples		6	6	6	6	-	6	6

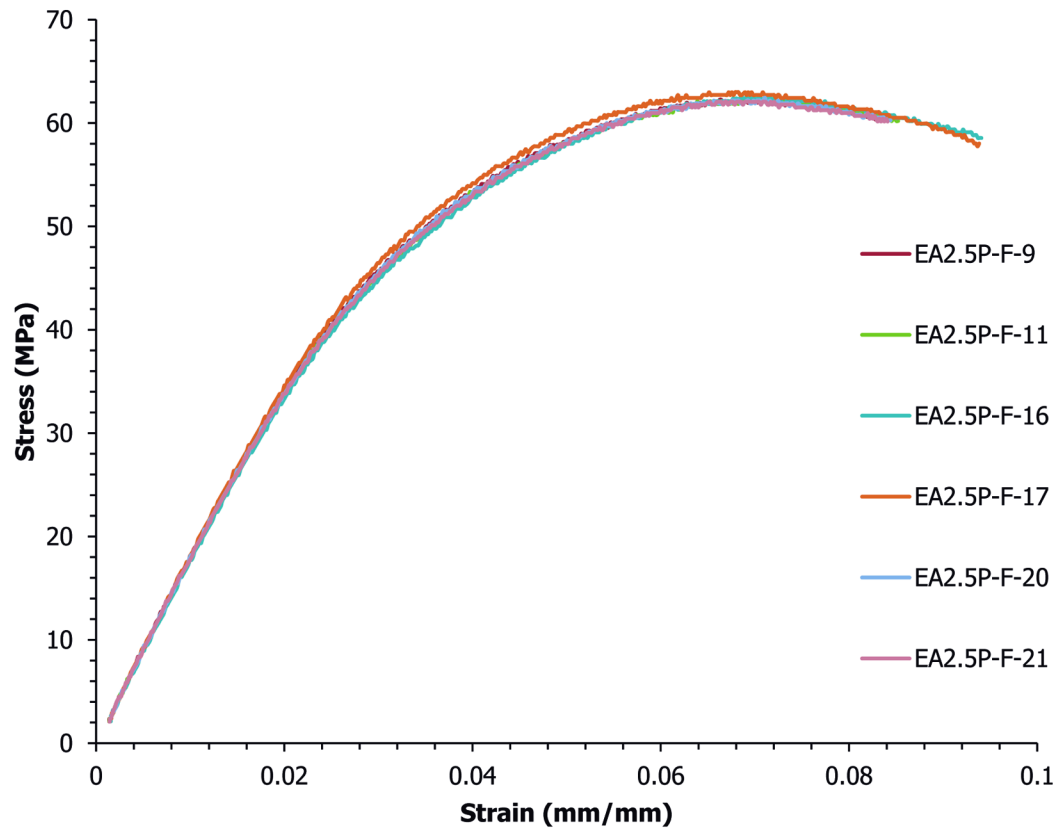


Figure C.2 Flexural results for EA2.5P

Table C.2

Flexural test results for 2.5 wt.% Ketjenblack EC-600 JD in Dow Polypropylene Semi Crystalline
Homopolymer Resin H7012-35RN Injection Molded

Test Date	Sample Number	Flexural maximum Stress (MPa)	Flexural Strain at Maximum Stress (%)	0.1% Offset Yield Flexural Stress (MPa)	Strain at 0.1% Offset Yield Flexural Stress (%)	Flexural Fracture Stress (MPa)	Flexural Strain at Fracture Stress (%)	Flexural Modulus (MPa)
4/27/2009	EA2.5P-F-9	62.3	7.01	36.9	2.22	59.8	8.42	1748
4/27/2009	EA2.5P-F-11	62.1	7.15	35.5	2.14	59.1	8.95	1750
4/27/2009	EA2.5P-F-16	62.4	6.93	39.4	2.48	-	-	1666
4/27/2009	EA2.5P-F-17	63.0	6.89	39.6	2.39	-	-	1736
4/27/2009	EA2.5P-F-20	62.5	7.11	39.0	2.39	59.2	8.85	1702
4/27/2009	EA2.5P-F-21	62.1	6.86	38.2	2.35	59.6	8.83	1711
Average		62.4	6.99	38.1	2.33	59.4	8.76	1719
Standard deviation		0.3	0.12	1.6	0.12	0.3	0.24	32
Number of samples		6	6	6	6	4	4	6

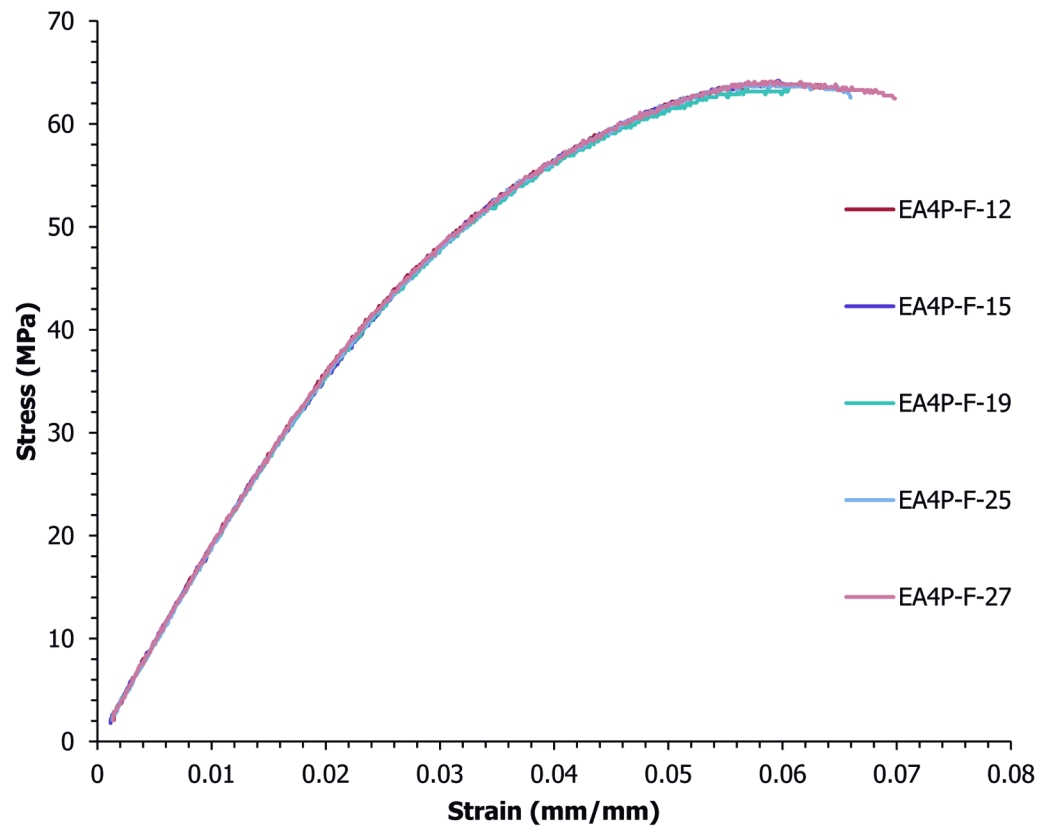


Figure C.3 Flexural results for EA4P

Table C.3

Flexural test results for 4 wt.% Ketjenblack EC-600 JD in Dow Polypropylene Semi Crystalline
Homopolymer Resin H7012-35RN Injection Molded

Test Date	Sample Number	Flexural maximum Stress (MPa)	Flexural Strain at Maximum Stress (%)	0.1% Offset Yield Flexural Stress (MPa)	Strain at 0.1% Offset Yield Flexural Stress (%)	Flexural Fracture Stress (MPa)	Flexural Strain at Fracture Stress (%)	Flexural Modulus (MPa)
4/27/2009	EA4P-F-12	64.1	6.53	35.5	1.99	64.1	6.53	1891
4/27/2009	EA4P-F-15	64.2	6.08	36.4	2.08	64.2	6.08	1848
4/27/2009	EA4P-F-19	63.4	6.10	35.6	2.01	63.4	6.10	1860
4/27/2009	EA4P-F-25	63.9	5.84	35.8	2.03	63.9	5.84	1858
4/27/2009	EA4P-F-27	64.1	5.89	38.0	2.16	63.6	6.55	1859
Average		63.9	6.09	36.3	2.05	63.8	6.22	1863
Standard deviation		0.3	0.27	1.0	0.07	0.3	0.31	16
Number of samples		5	5	5	5	5	5	5

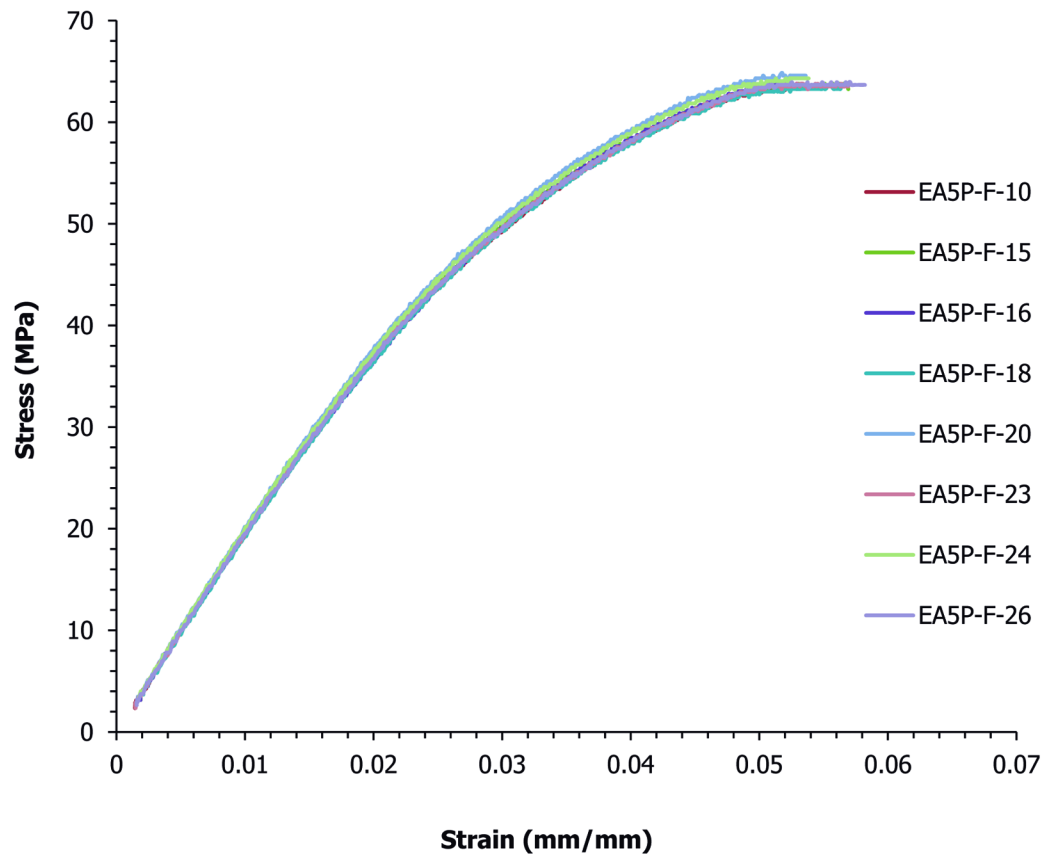


Figure C.4 Flexural results for EA5P

Table C.4

Flexural test results for 5 wt.% Ketjenblack EC-600 JD in Dow Polypropylene Semi Crystalline
Homopolymer Resin H7012-35RN Injection Molded

Test Date	Sample Number	Flexural maximum Stress (MPa)	Flexural Strain at Maximum Stress (%)	0.1% Offset Yield Flexural Stress (MPa)	Strain at 0.1% Offset Yield Flexural Stress (%)	Flexural Fracture Stress (MPa)	Flexural Strain at Fracture Stress (%)	Flexural Modulus (MPa)
4/27/2009	EA5P-F-10	63.4	5.30	34.4	1.85	63.4	5.30	1964
4/27/2009	EA5P-F-15	63.8	5.62	35.8	1.93	63.8	5.62	1967
4/27/2009	EA5P-F-16	63.9	5.07	36.1	1.98	63.9	5.07	1926
4/27/2009	EA5P-F-18	63.5	5.56	37.5	2.08	63.5	5.56	1914
4/27/2009	EA5P-F-20	64.9	5.36	38.0	2.02	64.9	5.36	1984
4/27/2009	EA5P-F-23	63.8	5.75	36.6	1.99	63.8	5.75	1949
4/27/2009	EA5P-F-24	64.3	5.38	36.9	1.98	64.3	5.38	1974
4/27/2009	EA5P-F-26	63.9	5.85	36.2	1.96	63.9	5.85	1947
Average		63.9	5.49	36.4	1.97	63.9	5.49	1953
Standard deviation		0.5	0.26	1.1	0.06	0.5	0.26	24
Number of samples		8	8	8	8	8	8	8

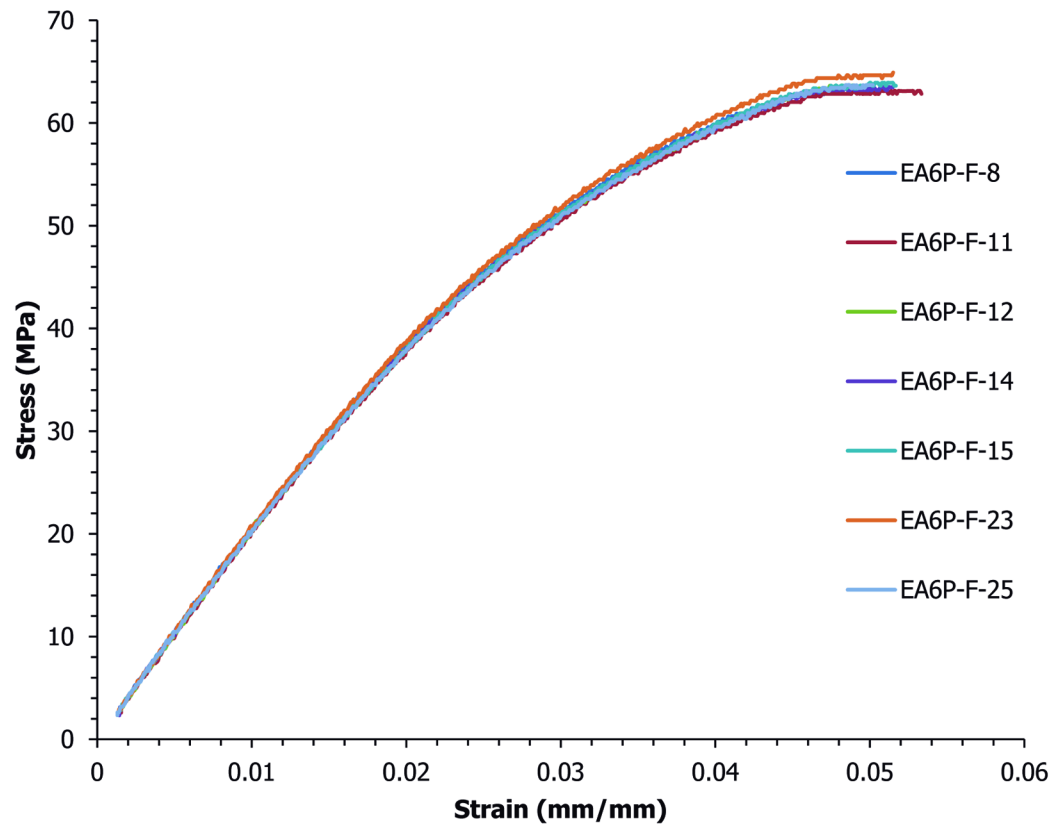


Figure C.5 Flexural results for EA6P

Table C.5

Flexural test results for 6 wt.% Ketjenblack EC-600 JD in Dow Polypropylene Semi Crystalline
Homopolymer Resin H7012-35RN Injection Molded

Test Date	Sample Number	Flexural maximum Stress (MPa)	Flexural Strain at Maximum Stress (%)	0.1% Offset Yield Flexural Stress (MPa)	Strain at 0.1% Offset Yield Flexural Stress (%)	Flexural Fracture Stress (MPa)	Flexural Strain at Fracture Stress (%)	Flexural Modulus (MPa)
4/27/2009	EA6P-F-8	63.3	4.85	35.2	1.81	63.3	4.85	2067
4/27/2009	EA6P-F-11	63.1	5.01	35.5	1.86	63.1	5.01	2017
4/27/2009	EA6P-F-12	63.6	4.98	34.5	1.79	63.6	4.98	2050
4/27/2009	EA6P-F-14	63.5	4.89	37.6	1.98	63.5	4.89	2004
4/27/2009	EA6P-F-15	63.9	5.15	35.8	1.88	63.9	5.15	2019
4/27/2009	EA6P-F-23	64.9	5.21	36.9	1.89	64.9	5.21	2060
4/27/2009	EA6P-F-25	63.7	5.05	37.2	1.96	63.7	5.05	2009
Average		63.7	5.02	36.1	1.88	63.7	5.02	2032
Standard deviation		0.6	0.13	1.2	0.07	0.6	0.13	26
Number of samples		7	7	7	7	7	7	7

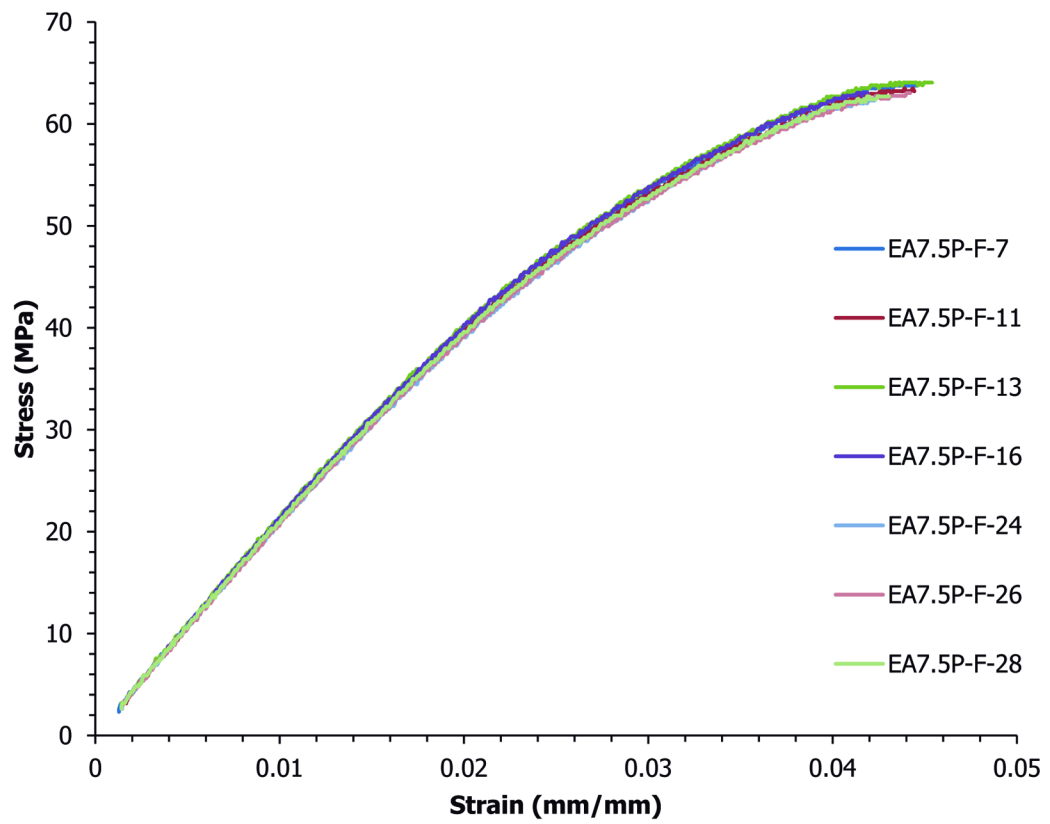


Figure C.6 Flexural results for EA7.5P

Table C.6

Flexural test results for 7.5 wt.% Ketjenblack EC-600 JD in Dow Polypropylene Semi Crystalline
Homopolymer Resin H7012-35RN Injection Molded

Test Date	Sample Number	Flexural maximum Stress (MPa)	Flexural Strain at Maximum Stress (%)	0.1% Offset Yield Flexural Stress (MPa)	Strain at 0.1% Offset Yield Flexural Stress (%)	Flexural Fracture Stress (MPa)	Flexural Strain at Fracture Stress (%)	Flexural Modulus (MPa)
4/27/2009	EA7.5P-F-7	63.8	4.46	37.5	1.86	63.8	4.46	2135
4/27/2009	EA7.5P-F-11	63.5	4.39	37.1	1.86	63.5	4.39	2130
4/27/2009	EA7.5P-F-13	64.3	4.58	35.9	1.77	64.3	4.58	2164
4/27/2009	EA7.5P-F-16	63.3	4.22	38.9	1.93	63.3	4.22	2131
4/27/2009	EA7.5P-F-24	62.3	4.27	37.4	1.90	62.3	4.27	2082
4/27/2009	EA7.5P-F-26	63.0	4.42	38.3	1.95	63.0	4.42	2079
4/27/2009	EA7.5P-F-28	62.7	4.19	38.0	1.91	62.7	4.19	2105
Average		63.3	4.36	37.6	1.88	63.3	4.36	2118
Standard deviation		0.7	0.14	0.9	0.06	0.7	0.14	31
Number of samples		7	7	7	7	7	7	7

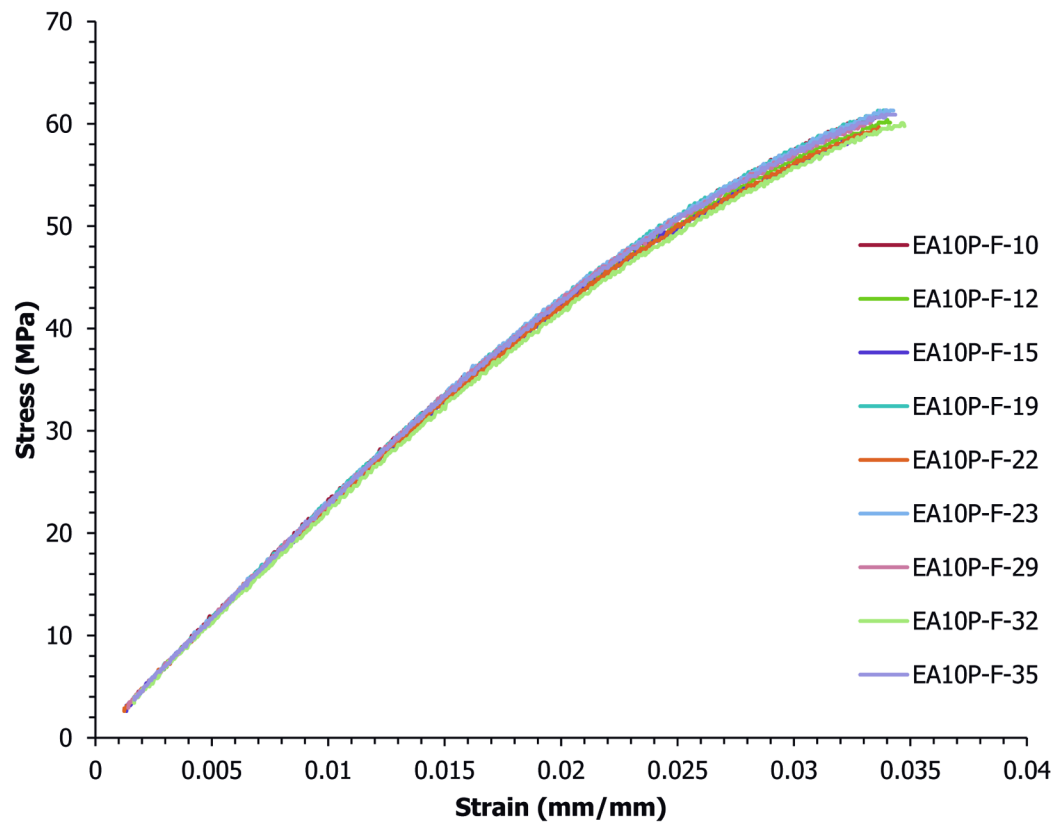


Figure C.7 Flexural results for EA10P

Table C.7

Flexural test results for 10 wt.% Ketjenblack EC-600 JD in Dow Polypropylene Semi Crystalline
Homopolymer Resin H7012-35RN Injection Molded

Test Date	Sample Number	Flexural maximum Stress (MPa)	Flexural Strain at Maximum Stress (%)	0.1% Offset Yield Flexural Stress (MPa)	Strain at 0.1% Offset Yield Flexural Stress (%)	Flexural Fracture Stress (MPa)	Flexural Strain at Fracture Stress (%)	Flexural Modulus (MPa)
4/27/2009	EA10P-F-10	60.8	3.01	37.7	1.74	60.8	3.01	2315
4/27/2009	EA10P-F-12	60.4	3.43	37.4	1.74	60.4	3.43	2293
4/27/2009	EA10P-F-15	59.4	3.36	39.4	1.85	59.4	3.36	2257
4/27/2009	EA10P-F-19	61.3	3.39	37.7	1.72	61.3	3.39	2337
4/27/2009	EA10P-F-22	59.7	3.40	35.6	1.65	59.7	3.40	2308
4/27/2009	EA10P-F-23	61.6	3.46	40.2	1.85	61.6	3.46	2302
4/27/2009	EA10P-F-29	60.4	3.34	38.1	1.75	60.4	3.34	2312
4/27/2009	EA10P-F-32	60.0	3.47	38.6	1.83	60.0	3.47	2231
4/27/2009	EA10P-F-35	60.9	3.44	38.8	1.80	60.9	3.44	2307
Average		60.5	3.36	38.2	1.77	60.5	3.36	2296
Standard deviation		0.7	0.14	1.3	0.07	0.7	0.14	32
Number of samples		9	9	9	9	9	9	9

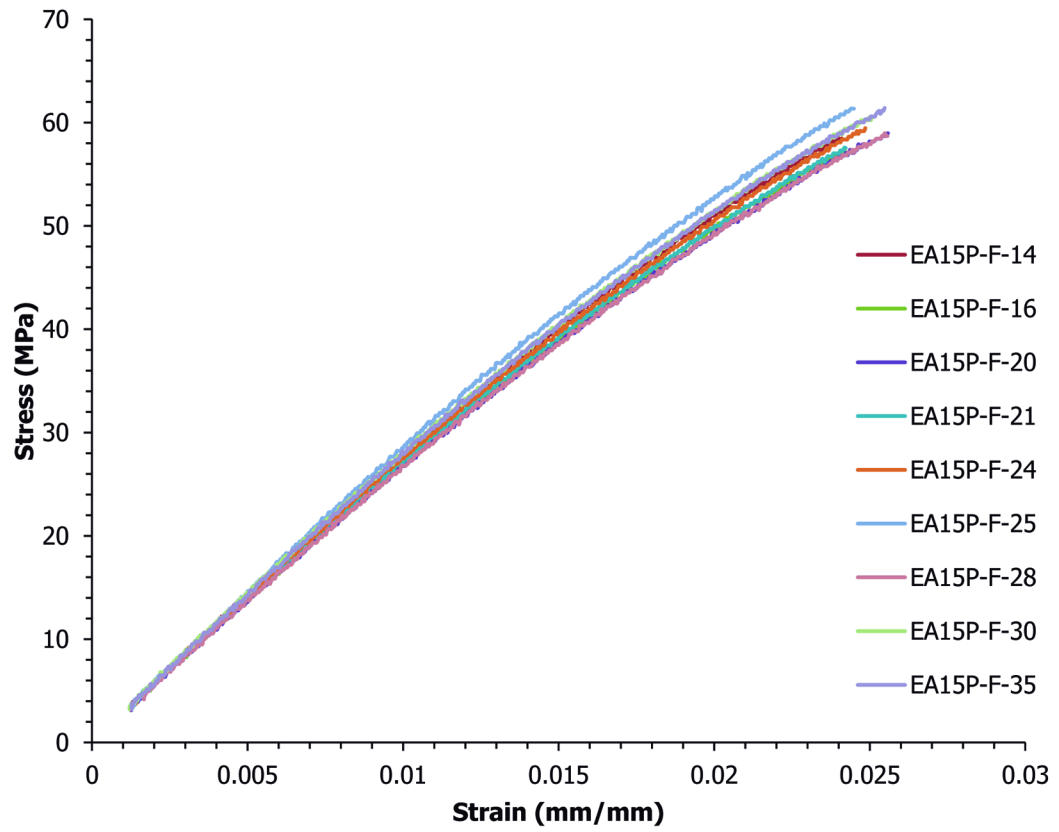


Figure C.8 Flexural results for EA15P

Table C.8

Flexural test results for 15 wt.% Ketjenblack EC-600 JD in Dow Polypropylene Semi Crystalline
Homopolymer Resin H7012-35RN Injection Molded

Test Date	Sample Number	Flexural maximum Stress (MPa)	Flexural Strain at Maximum Stress (%)	0.1% Offset Yield Flexural Stress (MPa)	Strain at 0.1% Offset Yield Flexural Stress (%)	Flexural Fracture Stress (MPa)	Flexural Strain at Fracture Stress (%)	Flexural Modulus (MPa)
4/27/2009	EA15P-F-14	58.5	2.43	40.8	1.53	58.5	2.43	2861
4/27/2009	EA15P-F-16	57.5	2.44	40.6	1.57	57.5	2.44	2767
4/27/2009	EA15P-F-20	59.2	2.58	41.3	1.63	59.2	2.58	2718
4/27/2009	EA15P-F-21	57.6	2.42	41.4	1.60	57.6	2.42	2769
4/27/2009	EA15P-F-24	59.5	2.50	41.2	1.57	59.5	2.50	2813
4/27/2009	EA15P-F-25	61.9	2.47	44.9	1.65	61.9	2.47	2901
4/27/2009	EA15P-F-28	59.0	2.55	41.4	1.63	59.0	2.55	2711
4/27/2009	EA15P-F-30	60.5	2.50	42.1	1.57	60.5	2.50	2868
4/27/2009	EA15P-F-35	61.4	2.57	42.7	1.61	61.4	2.57	2842
Average		59.5	2.49	41.8	1.60	59.5	2.49	2805
Standard deviation		1.6	0.06	1.3	0.04	1.6	0.06	68
Number of samples		9	9	9	9	9	9	9

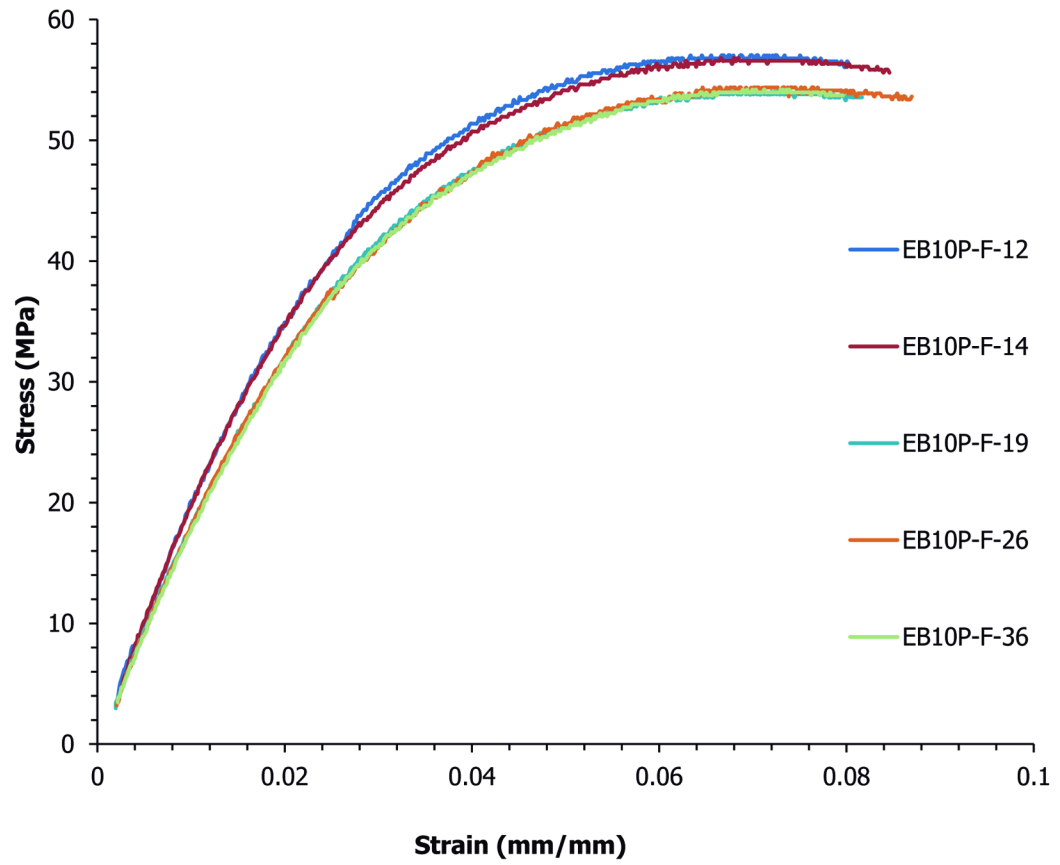


Figure C.9 Flexural results for EB10P

Table C.9

Flexural test results for 10 wt.% Thermocarb TC-300 in Dow Polypropylene Semi Crystalline
Homopolymer Resin H7012-35RN Injection Molded

Test Date	Sample Number	Flexural maximum Stress (MPa)	Flexural Strain at Maximum Stress (%)	0.1% Offset Yield Flexural Stress (MPa)	Strain at 0.1% Offset Yield Flexural Stress (%)	Flexural Fracture Stress (MPa)	Flexural Strain at Fracture Stress (%)	Flexural Modulus (MPa)
4/30/2009	EB10P-F-12	57.0	7.50	33.7	1.91	-	-	1876
4/30/2009	EB10P-F-14	56.8	6.66	36.1	2.11	-	-	1803
4/30/2009	EB10P-F-19	54.1	7.13	36.0	2.35	-	-	1601
4/30/2009	EB10P-F-26	54.4	7.65	35.2	2.28	-	-	1617
4/30/2009	EB10P-F-36	54.2	7.98	34.0	2.22	-	-	1610
Average		55.3	7.39	35.0	2.17	-	-	1701
Standard deviation		1.5	0.51	1.1	0.17	-	-	129
Number of samples		5	5	5	5	-	-	5

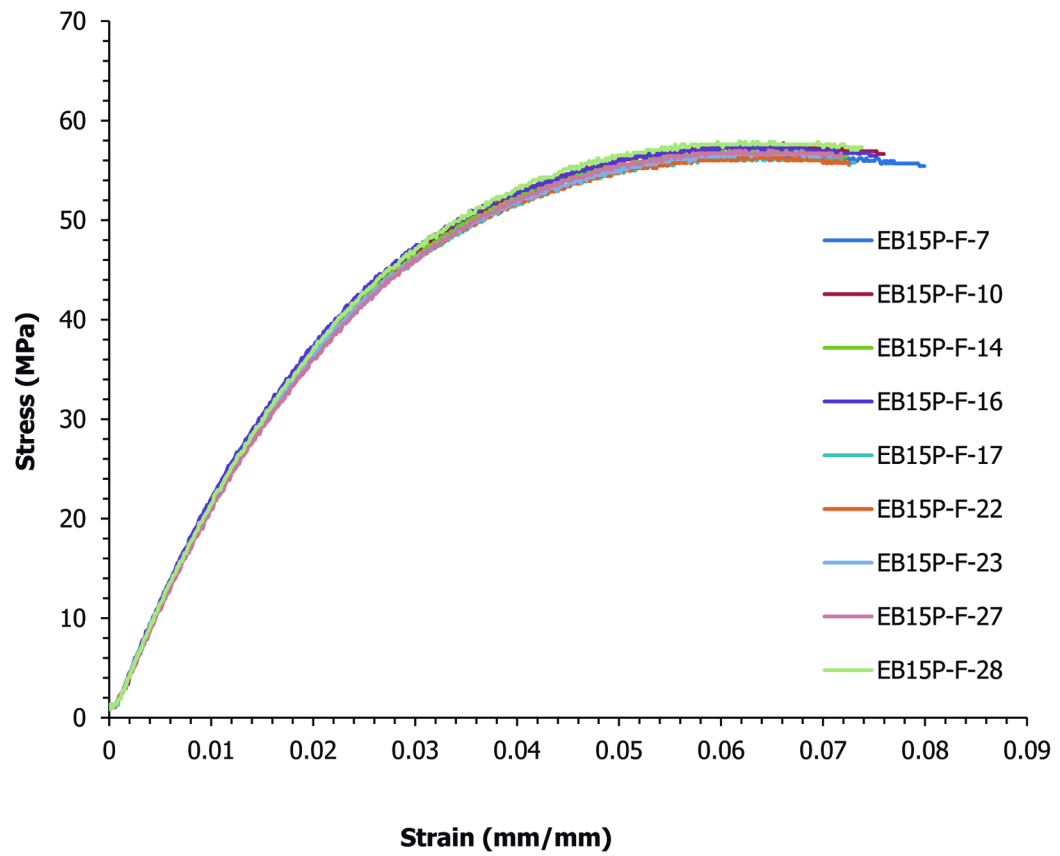


Figure C.10 Flexural results for EB15P

Table C.10

Flexural test results for 15 wt.% Thermocarb TC-300 in Dow Polypropylene Semi Crystalline
Homopolymer Resin H7012-35RN Injection Molded

Test Date	Sample Number	Flexural maximum Stress (MPa)	Flexural Strain at Maximum Stress (%)	0.1% Offset Yield Flexural Stress (MPa)	Strain at 0.1% Offset Yield Flexural Stress (%)	Flexural Fracture Stress (MPa)	Flexural Strain at Fracture Stress (%)	Flexural Modulus (MPa)
4/30/2009	EB15P-F-7	56.7	6.50	34.1	1.78	-	-	2036
4/30/2009	EB15P-F-10	57.7	6.61	34.3	1.83	-	-	1984
4/30/2009	EB15P-F-14	57.2	6.27	32.7	1.72	-	-	2034
4/30/2009	EB15P-F-16	57.5	6.20	39.3	2.17	-	-	1908
4/30/2009	EB15P-F-17	56.3	6.53	35.8	1.97	-	-	1926
4/30/2009	EB15P-F-22	56.3	6.46	32.8	1.73	-	-	2015
4/30/2009	EB15P-F-23	56.9	6.74	34.3	1.84	-	-	1984
4/30/2009	EB15P-F-27	57.0	6.51	31.2	1.64	-	-	2030
4/30/2009	EB15P-F-28	57.9	6.49	33.4	1.73	-	-	2052
Average		57.1	6.48	34.2	1.82	-	-	1997
Standard deviation		0.6	0.16	2.3	0.16	-	-	51
Number of samples		9	9	9	9	-	-	9

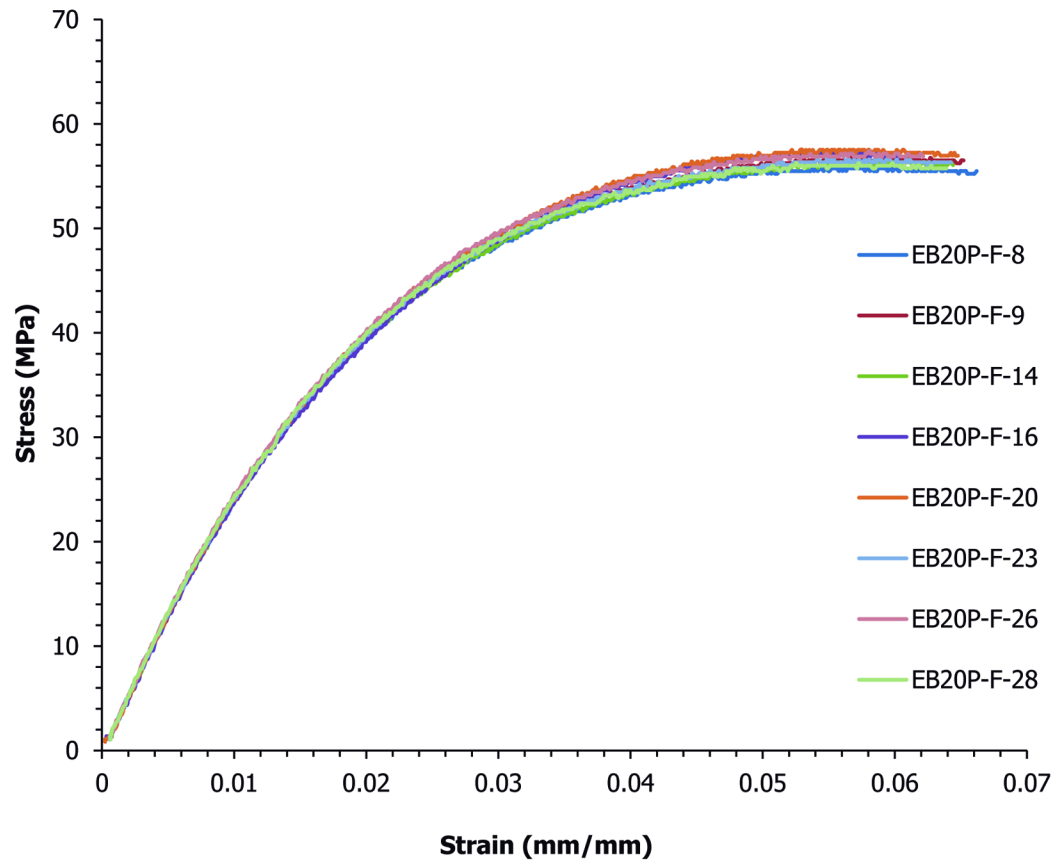


Figure C.11 Flexural results for EB20P

Table C.11

Flexural test results for 20 wt.% Thermocarb TC-300 in Dow Polypropylene Semi Crystalline
Homopolymer Resin H7012-35RN Injection Molded

Test Date	Sample Number	Flexural maximum Stress (MPa)	Flexural Strain at Maximum Stress (%)	0.1% Offset Yield Flexural Stress (MPa)	Strain at 0.1% Offset Yield Flexural Stress (%)	Flexural Fracture Stress (MPa)	Flexural Strain at Fracture Stress (%)	Flexural Modulus (MPa)
4/30/2009	EB20P-F-8	55.7	5.70	32.1	1.48	-	-	2344
4/30/2009	EB20P-F-9	56.8	5.70	32.9	1.52	-	-	2347
4/30/2009	EB20P-F-14	56.3	5.70	32.0	1.47	-	-	2362
4/30/2009	EB20P-F-16	57.5	5.61	34.5	1.65	-	-	2242
4/30/2009	EB20P-F-20	57.5	5.69	33.0	1.52	-	-	2326
4/30/2009	EB20P-F-23	56.6	5.69	35.4	1.68	-	-	2262
4/30/2009	EB20P-F-26	57.4	5.81	33.8	1.55	-	-	2346
4/30/2009	EB20P-F-28	56.3	5.73	34.9	1.64	-	-	2284
Average		56.8	5.70	33.6	1.56	-	-	2314
Standard deviation		0.7	0.05	1.3	0.08	-	-	45
Number of samples		8	8	8	8	-	-	8

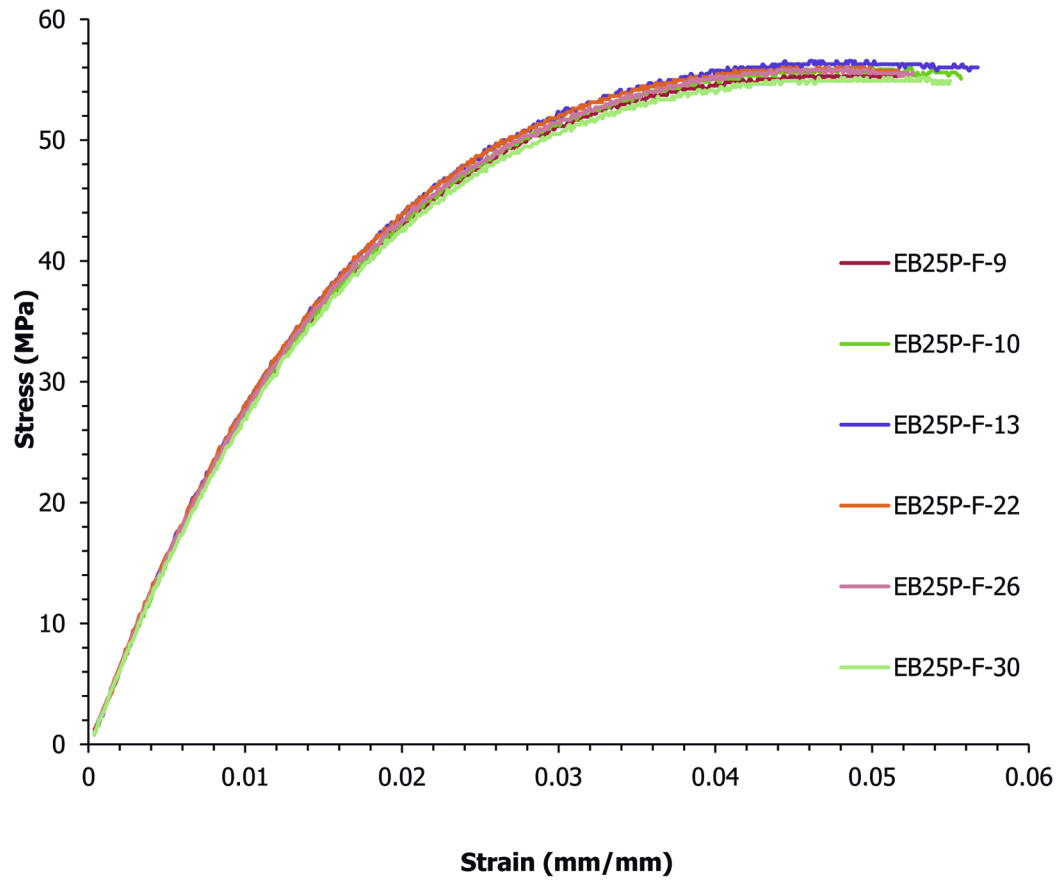


Figure C.12 Flexural results for EB25P

Table C.12

Flexural test results for 25 wt.% Thermocarb TC-300 in Dow Polypropylene Semi Crystalline
Homopolymer Resin H7012-35RN Injection Molded

Test Date	Sample Number	Flexural maximum Stress (MPa)	Flexural Strain at Maximum Stress (%)	0.1% Offset Yield Flexural Stress (MPa)	Strain at 0.1% Offset Yield Flexural Stress (%)	Flexural Fracture Stress (MPa)	Flexural Strain at Fracture Stress (%)	Flexural Modulus (MPa)
4/30/2009	EB25P-F-9	55.3	4.63	31.5	1.22	-	-	2821
4/30/2009	EB25P-F-10	56.1	4.94	32.3	1.25	-	-	2815
4/30/2009	EB25P-F-13	56.5	4.68	38.0	1.56	-	-	2600
4/30/2009	EB25P-F-22	56.0	4.54	34.6	1.34	-	-	2781
4/30/2009	EB25P-F-26	56.1	4.73	34.1	1.34	-	-	2749
4/30/2009	EB25P-F-30	55.2	4.80	33.9	1.38	-	-	2659
Average		55.9	4.72	34.1	1.35	-	-	2738
Standard deviation		0.5	0.14	2.2	0.12	-	-	90
Number of samples		6	6	6	6	-	-	6

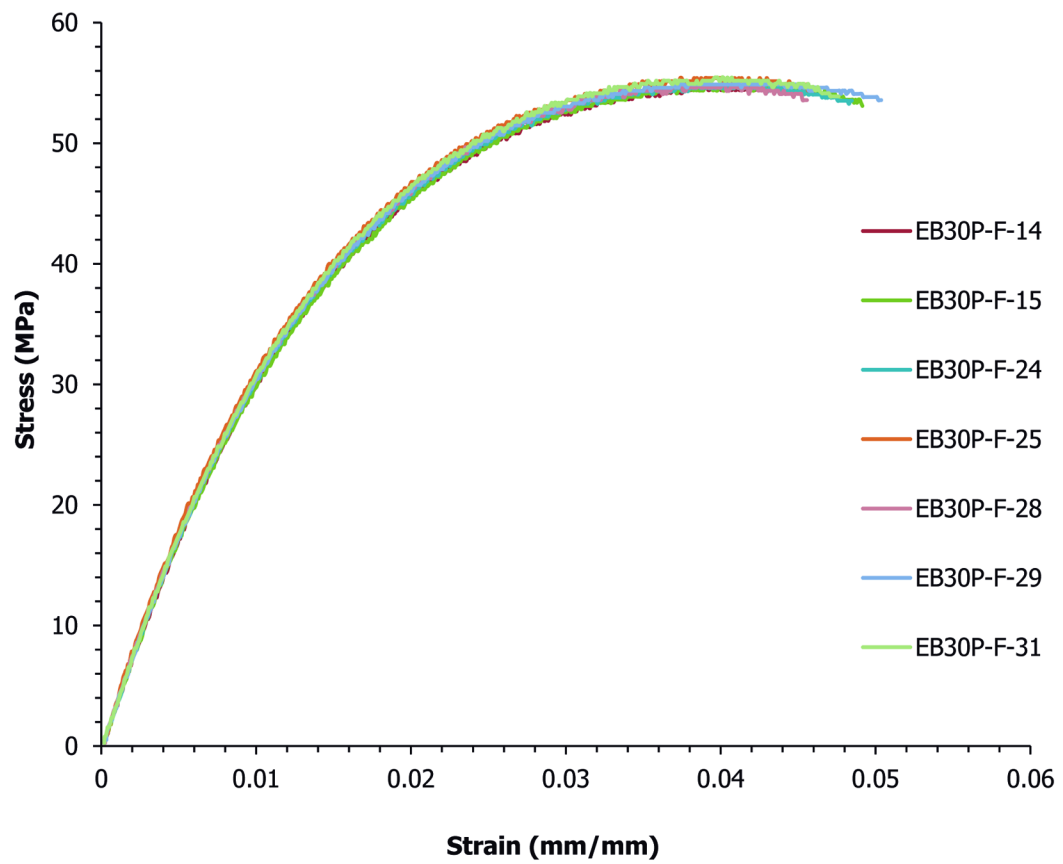


Figure C.13 Flexural results for EB30P

Table C.13

Flexural test results for 30 wt.% Thermocarb TC-300 in Dow Polypropylene Semi Crystalline
Homopolymer Resin H7012-35RN Injection Molded

Test Date	Sample Number	Flexural maximum Stress (MPa)	Flexural Strain at Maximum Stress (%)	0.1% Offset Yield Flexural Stress (MPa)	Strain at 0.1% Offset Yield Flexural Stress (%)	Flexural Fracture Stress (MPa)	Flexural Strain at Fracture Stress (%)	Flexural Modulus (MPa)
4/30/2009	EB30P-F-14	54.7	3.91	32.1	1.10	-	-	3214
4/30/2009	EB30P-F-15	54.9	4.08	32.1	1.11	-	-	3182
4/30/2009	EB30P-F-24	54.8	3.91	36.2	1.31	-	-	3008
4/30/2009	EB30P-F-25	55.4	3.95	34.8	1.19	-	-	3191
4/30/2009	EB30P-F-28	54.9	3.95	34.1	1.17	-	-	3198
4/30/2009	EB30P-F-29	55.1	4.27	36.1	1.30	-	-	3024
4/30/2009	EB30P-F-31	55.4	3.96	34.3	1.19	-	-	3159
Average		55.0	4.00	34.2	1.19	-	-	3140
Standard deviation		0.3	0.13	1.7	0.08	-	-	86
Number of samples		7	7	7	7	-	-	7

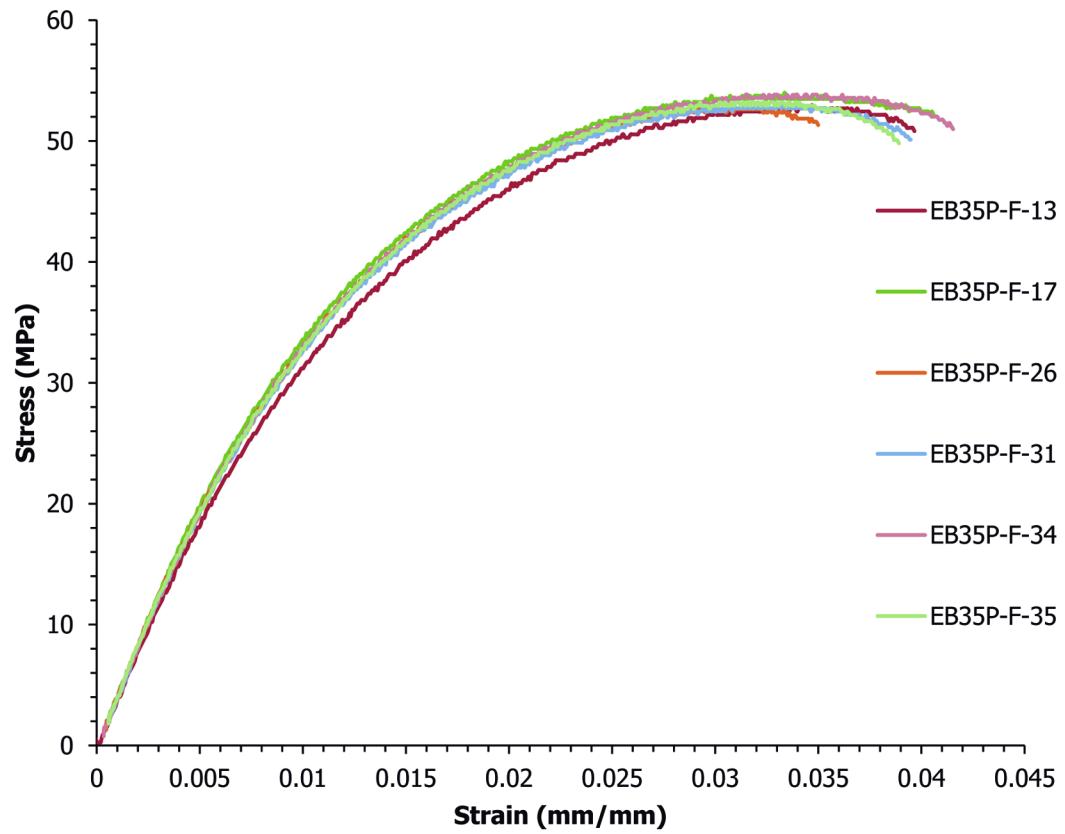


Figure C.14 Flexural results for EB35P

Table C.14

Flexural test results for 35 wt.% Thermocarb TC-300 in Dow Polypropylene Semi Crystalline
Homopolymer Resin H7012-35RN Injection Molded

Test Date	Sample Number	Flexural maximum Stress (MPa)	Flexural Strain at Maximum Stress (%)	0.1% Offset Yield Flexural Stress (MPa)	Strain at 0.1% Offset Yield Flexural Stress (%)	Flexural Fracture Stress (MPa)	Flexural Strain at Fracture Stress (%)	Flexural Modulus (MPa)
4/30/2009	EB35P-F-13	53.0	3.47	29.8	0.94	-	-	3588
4/30/2009	EB35P-F-17	54.0	3.34	33.3	0.99	-	-	3750
4/30/2009	EB35P-F-26	52.6	3.26	33.8	1.05	-	-	3582
4/30/2009	EB35P-F-31	53.0	3.30	35.4	1.14	-	-	3410
4/30/2009	EB35P-F-34	53.8	3.30	34.8	1.09	-	-	3520
4/30/2009	EB35P-F-35	53.2	3.32	34.6	1.09	-	-	3507
Average		53.3	3.33	33.6	1.05	-	-	3559
Standard deviation		0.5	0.07	2.0	0.07	-	-	113
Number of samples		6	6	6	6	-	-	6

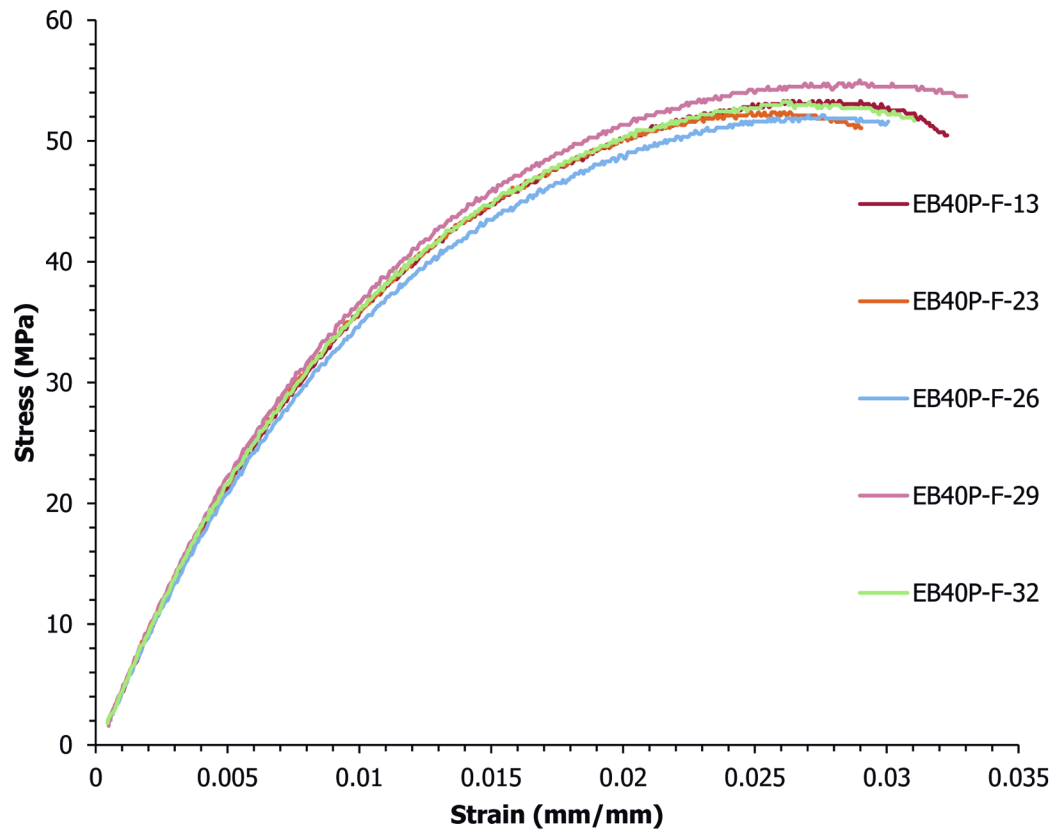


Figure C.15 Flexural results for EB40P

Table C.15

Flexural test results for 40 wt.% Thermocarb TC-300 in Dow Polypropylene Semi Crystalline
Homopolymer Resin H7012-35RN Injection Molded

Test Date	Sample Number	Flexural maximum Stress (MPa)	Flexural Strain at Maximum Stress (%)	0.1% Offset Yield Flexural Stress (MPa)	Strain at 0.1% Offset Yield Flexural Stress (%)	Flexural Fracture Stress (MPa)	Flexural Strain at Fracture Stress (%)	Flexural Modulus (MPa)
4/30/2009	EB40P-F-13	53.3	2.82	35.5	0.99	-	-	4034
4/30/2009	EB40P-F-23	52.4	2.61	35.5	0.99	50.0	3.01	4008
4/30/2009	EB40P-F-26	52.1	2.76	35.6	1.05	51.1	3.10	3782
4/30/2009	EB40P-F-29	55.0	2.90	37.1	1.03	54.2	3.12	4032
4/30/2009	EB40P-F-32	53.2	2.62	36.9	1.04	51.9	3.07	3938
Average		53.2	2.74	36.1	1.02	51.8	3.08	3959
Standard deviation		1.1	0.12	0.8	0.03	1.8	0.05	106
Number of samples		5	5	5	5	4	4	5

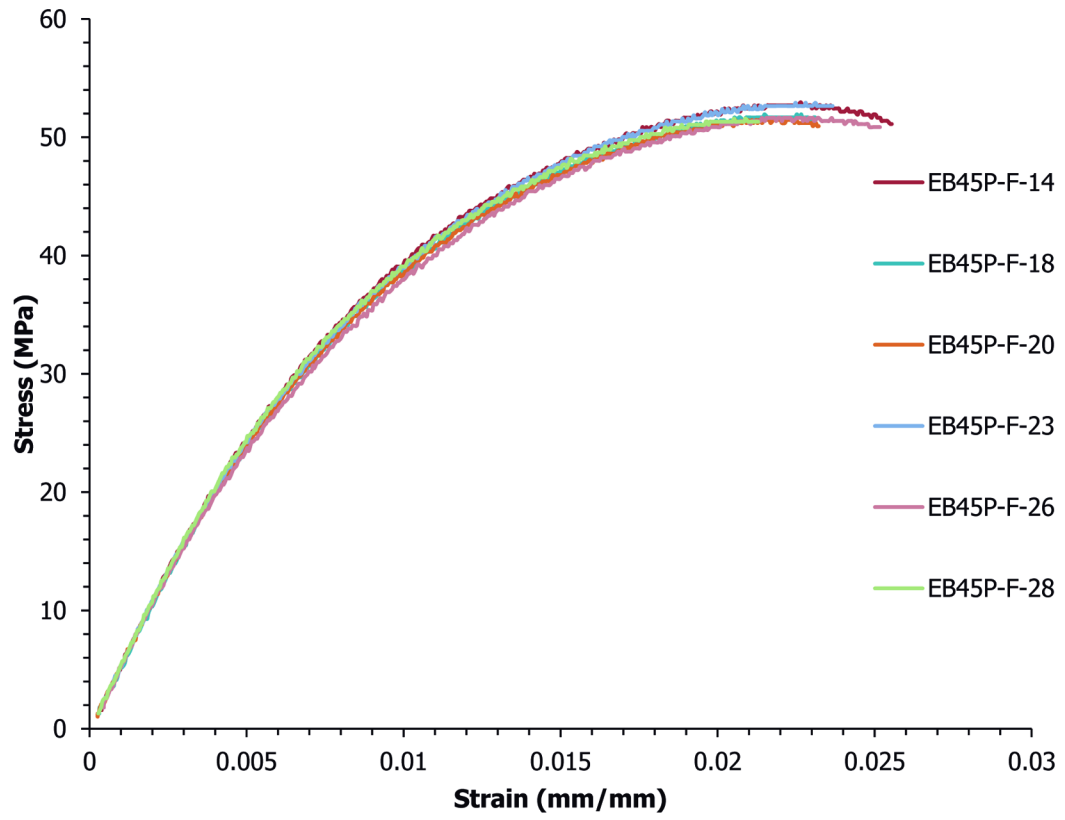


Figure C.16 Flexural results for EB45P

Table C.16

Flexural test results for 45 wt.% Thermocarb TC-300 in Dow Polypropylene Semi Crystalline
Homopolymer Resin H7012-35RN Injection Molded

Test Date	Sample Number	Flexural maximum Stress (MPa)	Flexural Strain at Maximum Stress (%)	0.1% Offset Yield Flexural Stress (MPa)	Strain at 0.1% Offset Yield Flexural Stress (%)	Flexural Fracture Stress (MPa)	Flexural Strain at Fracture Stress (%)	Flexural Modulus (MPa)
4/30/2009	EB45P-F-14	53.0	2.26	35.1	0.83	50.6	2.61	4833
4/30/2009	EB45P-F-18	51.9	2.27	35.1	0.86	47.8	2.60	4650
4/30/2009	EB45P-F-20	51.5	2.19	34.9	0.85	48.6	2.50	4712
4/30/2009	EB45P-F-23	52.9	2.25	36.3	0.88	49.8	2.65	4650
4/30/2009	EB45P-F-26	51.6	2.36	35.4	0.90	48.3	2.73	4492
4/30/2009	EB45P-F-28	51.6	2.05	34.4	0.81	47.4	2.40	4880
Average		52.1	2.23	35.2	0.85	48.7	2.58	4703
Standard deviation		0.7	0.10	0.6	0.03	1.2	0.12	140
Number of samples		6	6	6	6	6	6	6

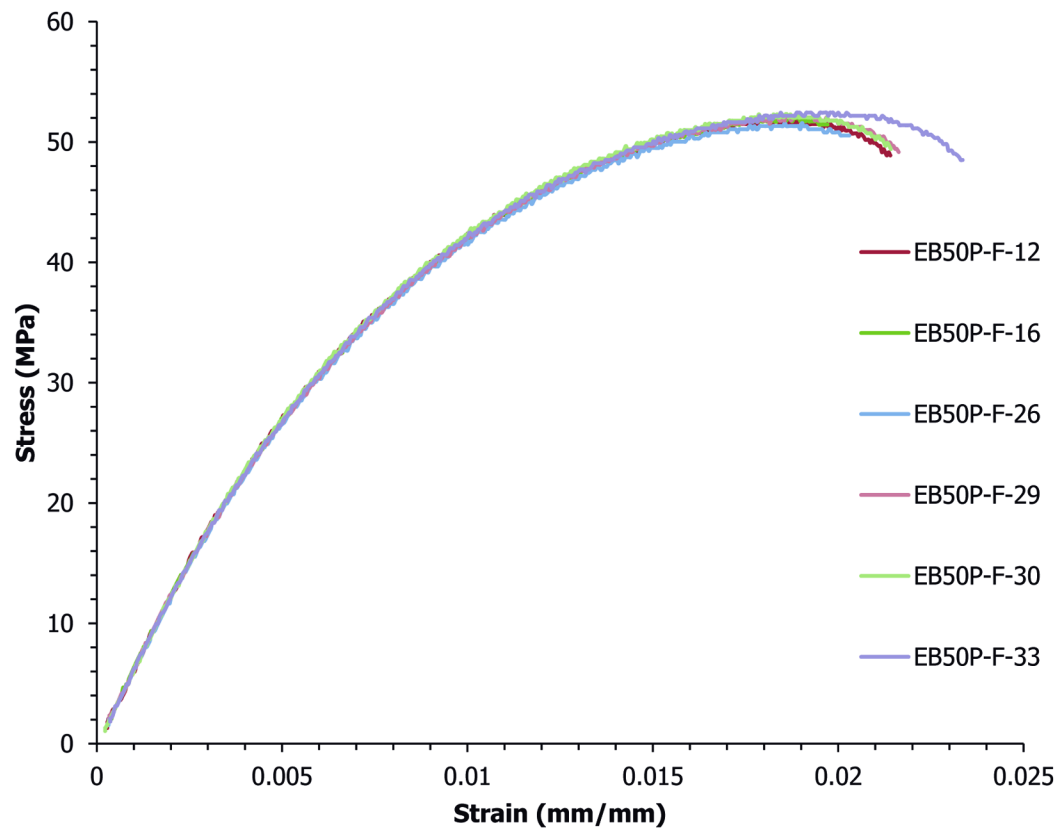


Figure C.17 Flexural results for EB50P

Table C.17

Flexural test results for 50 wt.% Thermocarb TC-300 in Dow Polypropylene Semi Crystalline
Homopolymer Resin H7012-35RN Injection Molded

Test Date	Sample Number	Flexural maximum Stress (MPa)	Flexural Strain at Maximum Stress (%)	0.1% Offset Yield Flexural Stress (MPa)	Strain at 0.1% Offset Yield Flexural Stress (%)	Flexural Fracture Stress (MPa)	Flexural Strain at Fracture Stress (%)	Flexural Modulus (MPa)
4/30/2009	EB50P-F-12	51.8	1.82	34.1	0.70	46.3	2.20	5707
4/30/2009	EB50P-F-16	52.0	1.89	33.5	0.68	49.1	2.10	5741
4/30/2009	EB50P-F-26	51.6	1.86	35.3	0.75	44.8	2.21	5439
4/30/2009	EB50P-F-29	52.0	1.84	34.3	0.71	49.4	2.15	5608
4/30/2009	EB50P-F-30	52.3	1.89	35.2	0.73	50.5	2.10	5581
4/30/2009	EB50P-F-33	52.4	1.96	35.4	0.74	49.3	2.30	5529
Average		52.0	1.87	34.6	0.72	48.2	2.18	5601
Standard deviation		0.3	0.05	0.8	0.03	2.2	0.08	112
Number of samples		6	6	6	6	6	6	6

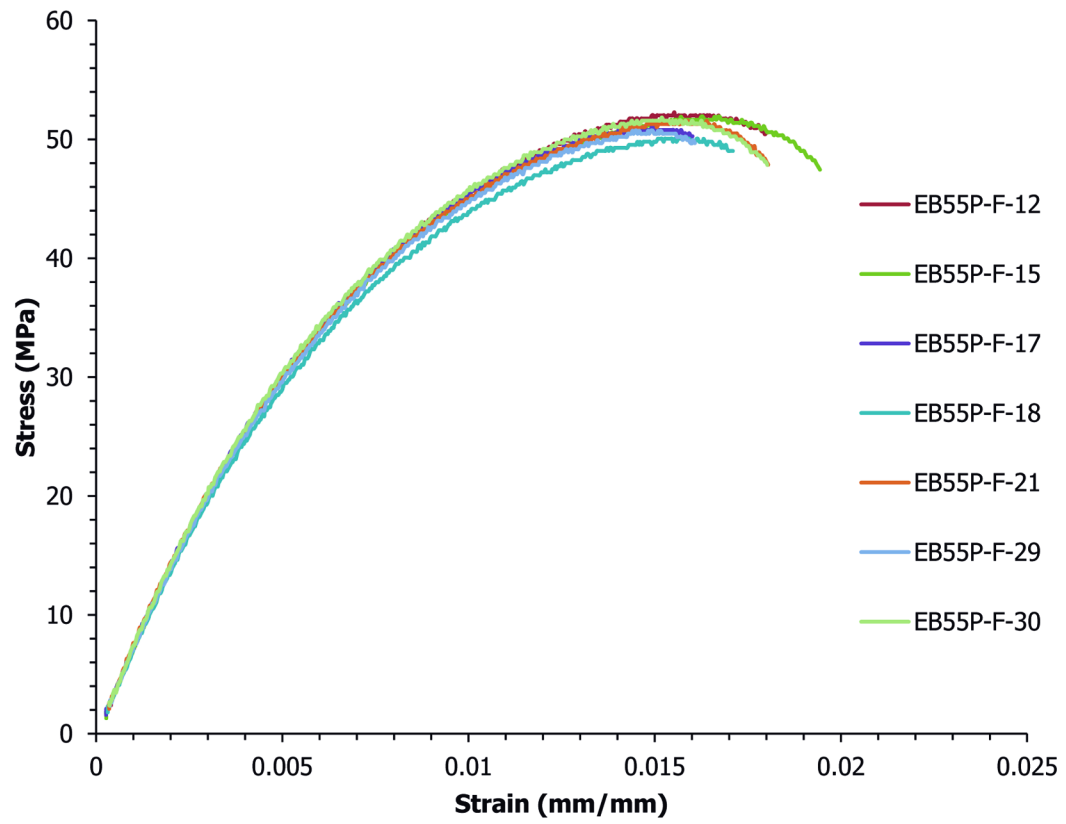


Figure C.18 Flexural results for EB55P

Table C.18

Flexural test results for 55 wt.% Thermocarb TC-300 in Dow Polypropylene Semi Crystalline
Homopolymer Resin H7012-35RN Injection Molded

Test Date	Sample Number	Flexural maximum Stress (MPa)	Flexural Strain at Maximum Stress (%)	0.1% Offset Yield Flexural Stress (MPa)	Strain at 0.1% Offset Yield Flexural Stress (%)	Flexural Fracture Stress (MPa)	Flexural Strain at Fracture Stress (%)	Flexural Modulus (MPa)
4/30/2009	EB55P-F-12	52.3	1.55	35.6	0.65	49.4	1.85	6543
4/30/2009	EB55P-F-15	51.9	1.67	34.6	0.62	47.5	1.95	6638
4/30/2009	EB55P-F-17	51.1	1.50	36.8	0.68	46.8	1.70	6367
4/30/2009	EB55P-F-18	50.1	1.62	35.2	0.67	47.8	1.75	6224
4/30/2009	EB55P-F-21	51.6	1.64	35.8	0.66	45.8	1.85	6439
4/30/2009	EB55P-F-29	50.7	1.52	35.8	0.66	47.3	1.70	6376
4/30/2009	EB55P-F-30	51.9	1.52	37.0	0.68	47.9	1.80	6460
Average		51.4	1.57	35.8	0.66	47.5	1.80	6435
Standard deviation		0.8	0.07	0.8	0.02	1.1	0.09	133
Number of samples		7	7	7	7	7	7	7

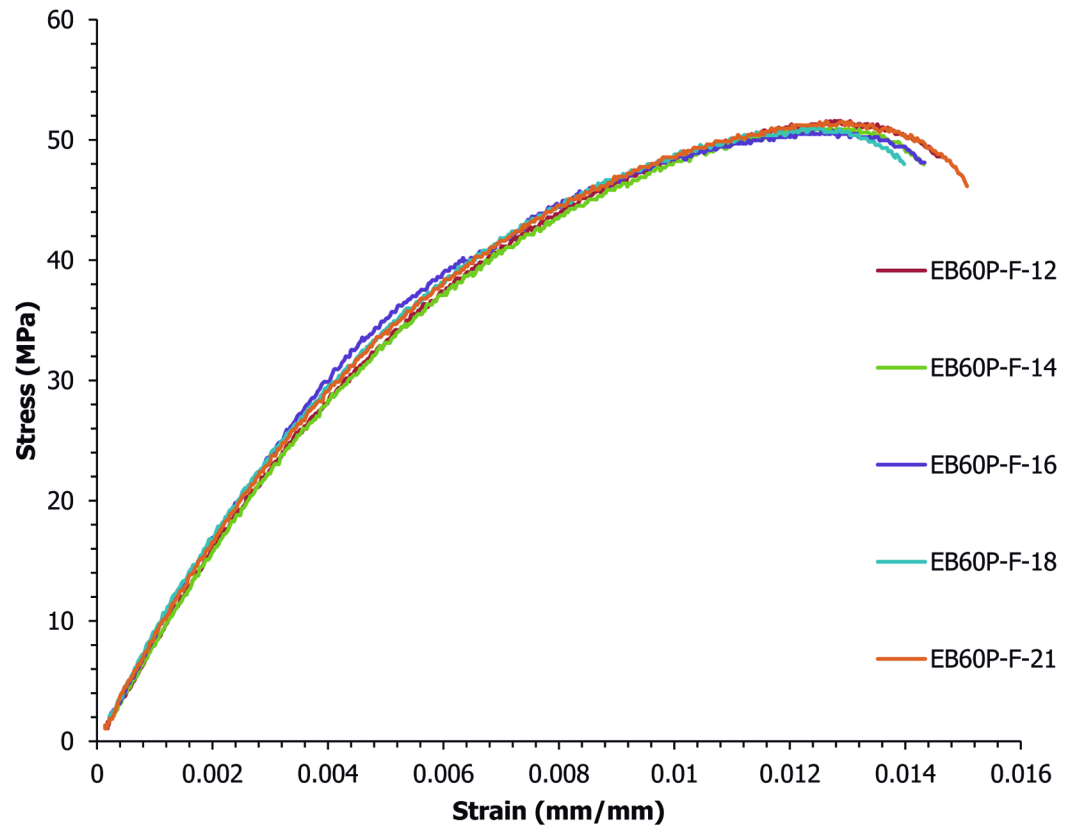


Figure C.19 Flexural results for EB60P

Table C.19

Flexural test results for 60 wt.% Thermocarb TC-300 in Dow Polypropylene Semi Crystalline
Homopolymer Resin H7012-35RN Injection Molded

Test Date	Sample Number	Flexural maximum Stress (MPa)	Flexural Strain at Maximum Stress (%)	0.1% Offset Yield Flexural Stress (MPa)	Strain at 0.1% Offset Yield Flexural Stress (%)	Flexural Fracture Stress (MPa)	Flexural Strain at Fracture Stress (%)	Flexural Modulus (MPa)
4/30/2009	EB60P-F-12	51.6	1.29	35.3	0.55	48.9	1.45	7870
4/30/2009	EB60P-F-14	50.9	1.30	34.7	0.54	49.0	1.40	7878
4/30/2009	EB60P-F-16	50.8	1.24	39.1	0.60	47.3	1.45	7772
4/30/2009	EB60P-F-18	50.9	1.25	37.1	0.58	48.0	1.40	7852
4/30/2009	EB60P-F-21	51.5	1.27	36.8	0.57	46.7	1.50	7907
Average		51.1	1.27	36.6	0.57	47.98	1.44	7856
Standard deviation		0.4	0.03	1.7	0.02	1.01	0.04	51
Number of samples		5	5	5	5	5	5	5

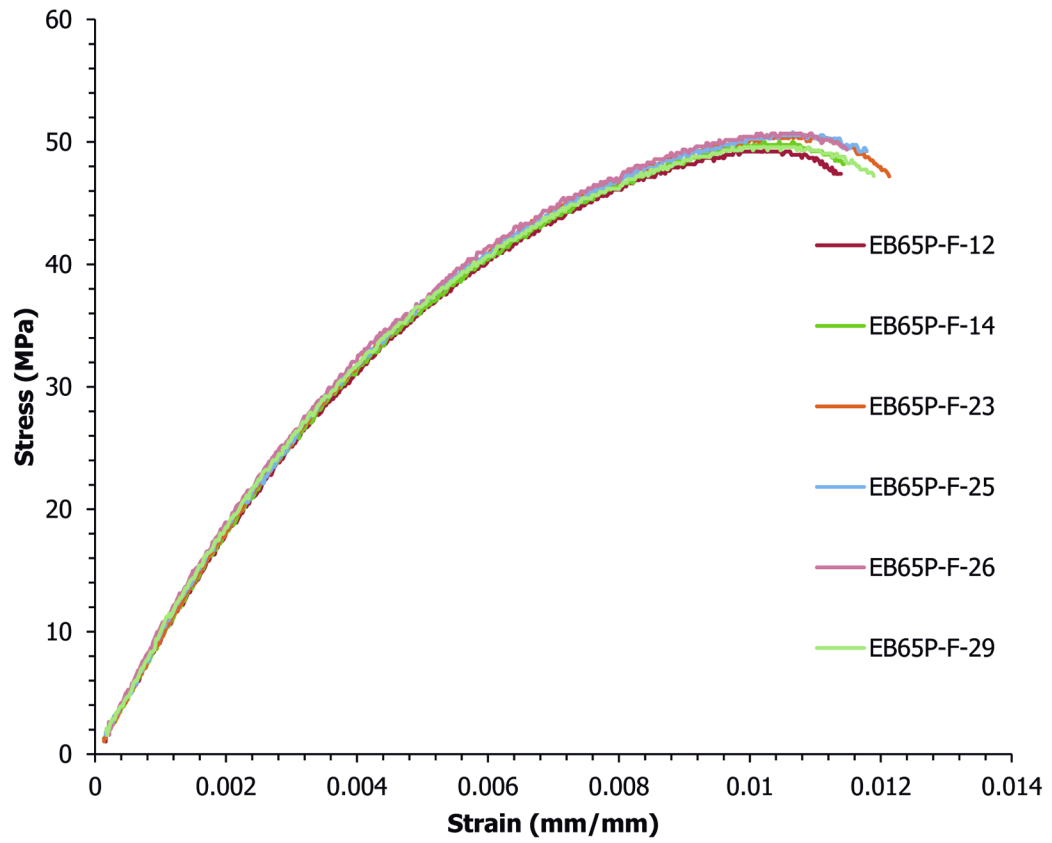


Figure C.20 Flexural results for EB65P

Table C.20

Flexural test results for 65 wt.% Thermocarb TC-300 in Dow Polypropylene Semi Crystalline
Homopolymer Resin H7012-35RN Injection Molded

Test Date	Sample Number	Flexural maximum Stress (MPa)	Flexural Strain at Maximum Stress (%)	0.1% Offset Yield Flexural Stress (MPa)	Strain at 0.1% Offset Yield Flexural Stress (%)	Flexural Fracture Stress (MPa)	Flexural Strain at Fracture Stress (%)	Flexural Modulus (MPa)
4/30/2009	EB65P-F-12	49.5	1.02	36.0	0.50	46.6	1.15	9137
4/30/2009	EB65P-F-14	50.0	1.05	35.4	0.48	46.6	1.17	9294
4/30/2009	EB65P-F-23	50.6	1.08	37.3	0.51	47.7	1.20	9086
4/30/2009	EB65P-F-25	50.8	1.07	37.3	0.51	47.9	1.20	9062
4/30/2009	EB65P-F-26	50.7	1.09	37.0	0.50	48.3	1.18	9217
4/30/2009	EB65P-F-29	49.6	1.02	36.8	0.50	44.4	1.23	9145
Average		50.2	1.06	36.6	0.50	46.9	1.19	9157
Standard deviation		0.6	0.03	0.8	0.01	1.4	0.03	86
Number of samples		6	6	6	6	6	6	6

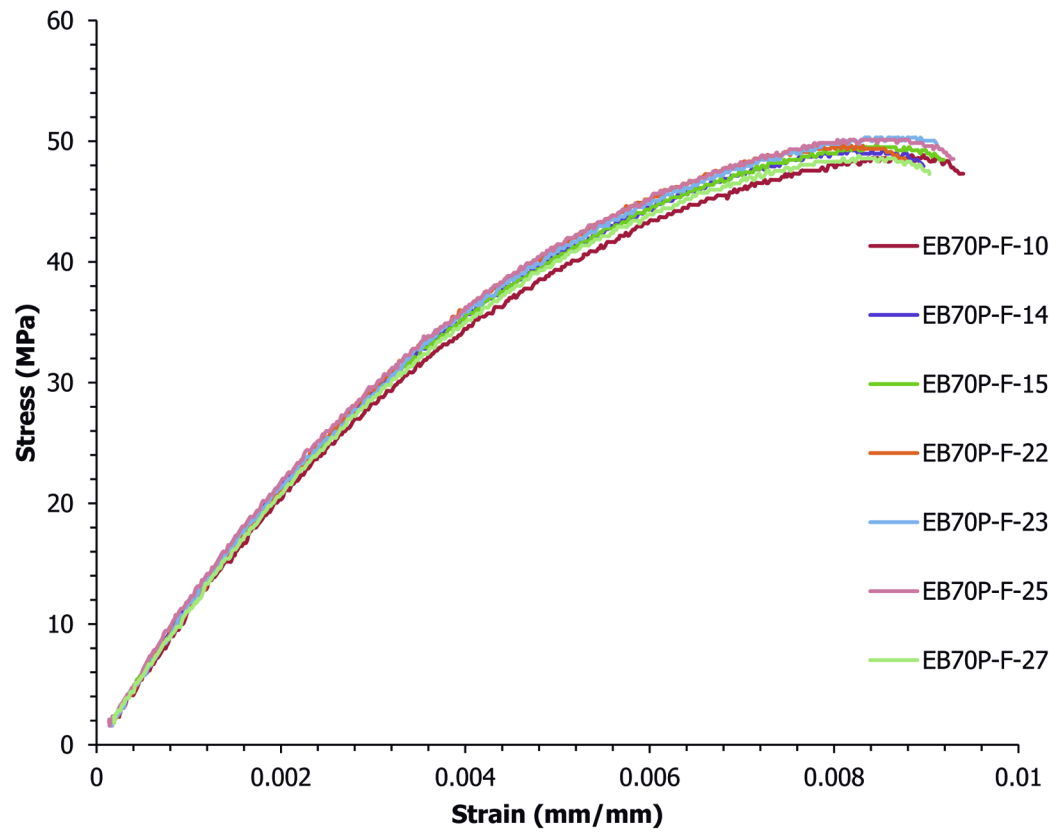


Figure C.21 Flexural results for EB70P

Table C.21

Flexural test results for 70 wt.% Thermocarb TC-300 in Dow Polypropylene Semi Crystalline
Homopolymer Resin H7012-35RN Injection Molded

Test Date	Sample Number	Flexural maximum Stress (MPa)	Flexural Strain at Maximum Stress (%)	0.1% Offset Yield Flexural Stress (MPa)	Strain at 0.1% Offset Yield Flexural Stress (%)	Flexural Fracture Stress (MPa)	Flexural Strain at Fracture Stress (%)	Flexural Modulus (MPa)
4/30/2009	EB70P-F-10	48.9	0.88	36.3	0.44	46.5	0.96	10771
4/30/2009	EB70P-F-14	49.2	0.85	38.6	0.46	46.4	0.92	10767
4/30/2009	EB70P-F-15	49.8	0.85	37.3	0.44	47.2	0.94	11041
4/30/2009	EB70P-F-22	49.6	0.82	39.4	0.46	46.7	0.90	10922
4/30/2009	EB70P-F-23	50.3	0.88	38.5	0.45	48.7	0.94	10974
4/30/2009	EB70P-F-25	50.1	0.87	38.1	0.43	48.5	0.93	11461
4/30/2009	EB70P-F-27	48.8	0.83	38.0	0.46	47.5	0.90	10710
Average		49.5	0.85	38.0	0.45	47.4	0.93	10949
Standard deviation		0.6	0.03	1.0	0.01	0.9	0.02	256
Number of samples		7	7	7	7	7	7	7

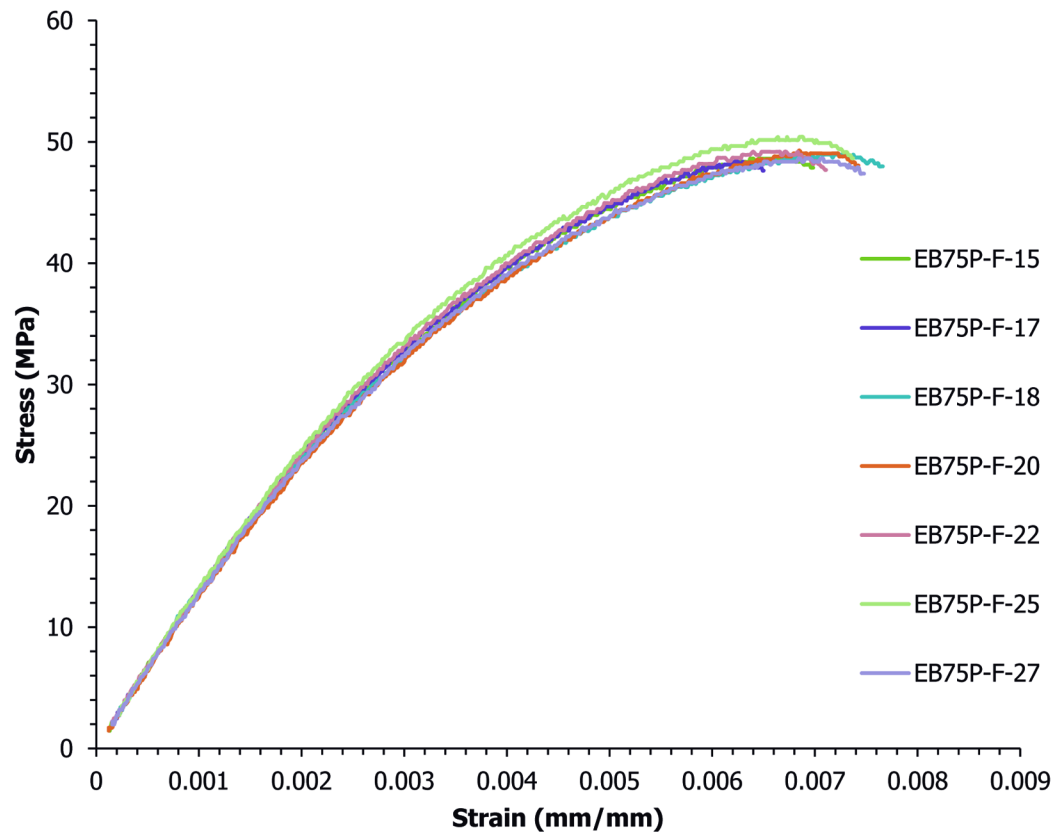


Figure C.22 Flexural results for EB75P

Table C.22

Flexural test results for 75 wt.% Thermocarb TC-300 in Dow Polypropylene Semi Crystalline
Homopolymer Resin H7012-35RN Injection Molded

Test Date	Sample Number	Flexural maximum Stress (MPa)	Flexural Strain at Maximum Stress (%)	0.1% Offset Yield Flexural Stress (MPa)	Strain at 0.1% Offset Yield Flexural Stress (%)	Flexural Fracture Stress (MPa)	Flexural Strain at Fracture Stress (%)	Flexural Modulus (MPa)
4/30/2009	EB75P-F-15	48.6	0.67	40.8	0.42	48.6	0.67	12714
4/30/2009	EB75P-F-17	48.4	0.62	40.7	0.42	48.4	0.62	12727
4/30/2009	EB75P-F-18	49.0	0.72	39.7	0.42	49.0	0.72	12542
4/30/2009	EB75P-F-20	49.3	0.68	40.2	0.43	49.3	0.68	12241
4/30/2009	EB75P-F-22	49.2	0.67	41.0	0.42	49.2	0.67	12827
4/30/2009	EB75P-F-25	50.4	0.67	42.1	0.43	50.4	0.67	13006
4/30/2009	EB75P-F-27	48.6	0.71	40.5	0.42	48.6	0.71	12554
Average		49.1	0.68	40.7	0.42	49.1	0.68	12659
Standard deviation		0.7	0.03	0.7	0.00	0.7	0.03	244
Number of samples		7	7	7	7	7	7	7

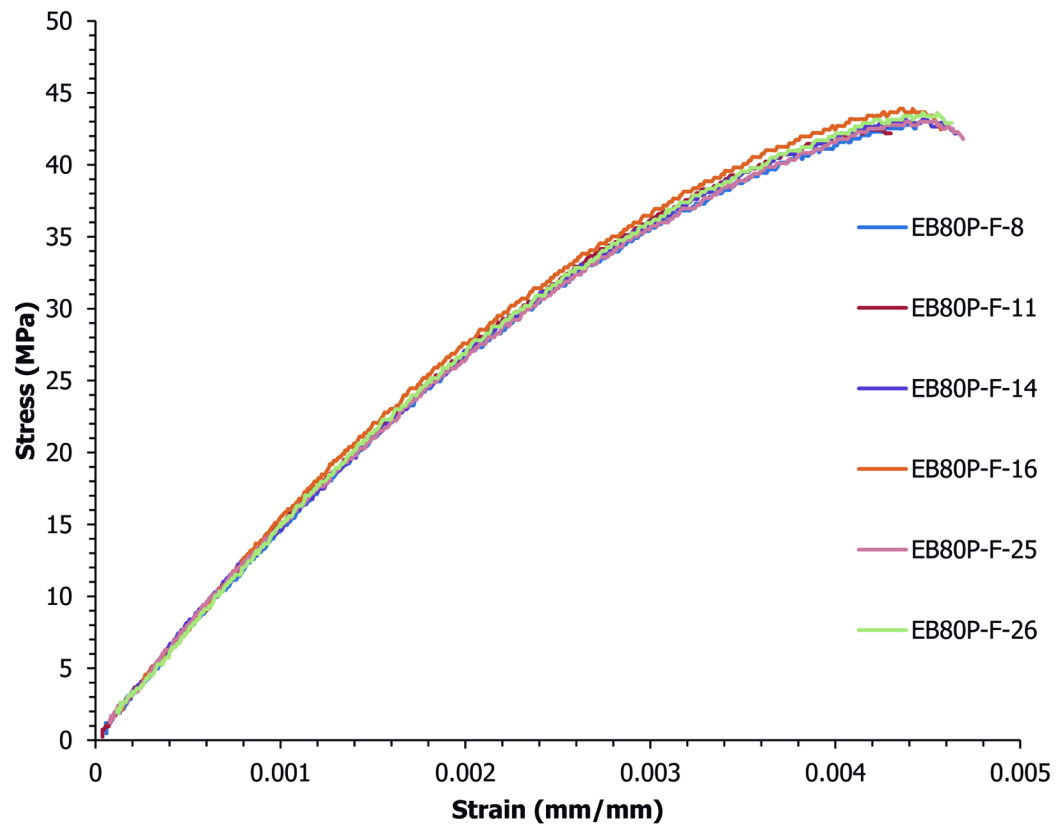


Figure C.23 Flexural results for EB80P

Table C.23

Flexural test results for 80 wt.% Thermocarb TC-300 in Dow Polypropylene Semi Crystalline
Homopolymer Resin H7012-35RN Injection Molded

Test Date	Sample Number	Flexural maximum Stress (MPa)	Flexural Strain at Maximum Stress (%)	0.1% Offset Yield Flexural Stress (MPa)	Strain at 0.1% Offset Yield Flexural Stress (%)	Flexural Fracture Stress (MPa)	Flexural Strain at Fracture Stress (%)	Flexural Modulus (MPa)
4/30/2009	EB80P-F-8	42.8	0.45	39.2	0.36	42.8	0.45	15390
4/30/2009	EB80P-F-11	42.4	0.43	39.5	0.35	42.4	0.43	15722
4/30/2009	EB80P-F-14	43.1	0.45	39.8	0.36	43.1	0.45	15617
4/30/2009	EB80P-F-16	43.9	0.44	41.3	0.37	43.9	0.44	15277
4/30/2009	EB80P-F-25	43.0	0.45	38.7	0.35	43.0	0.45	15705
4/30/2009	EB80P-F-26	43.6	0.45	41.0	0.38	43.6	0.45	14649
Average		43.1	0.44	39.9	0.36	43.1	0.44	15393
Standard deviation		0.5	0.01	1.0	0.01	0.5	0.01	406
Number of samples		6	6	6	6	6	6	6

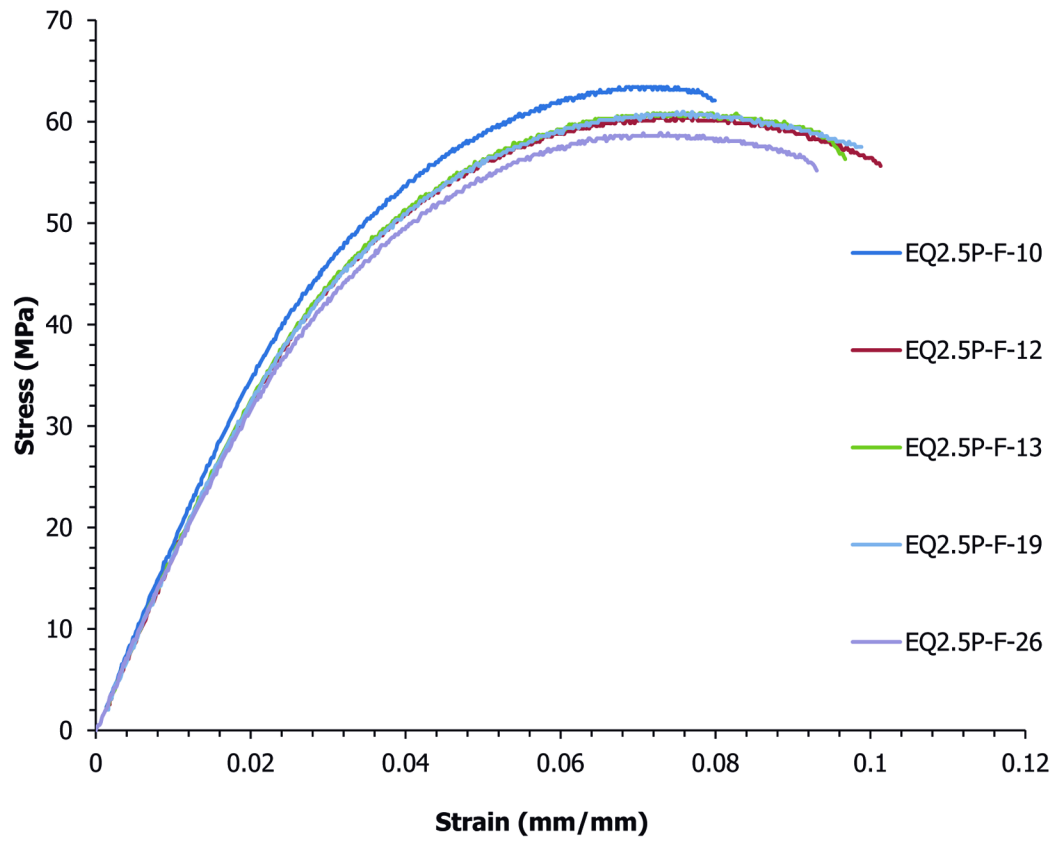


Figure C.24 Flexural results for EQ2.5P

Table C.24

Flexural test results for 2.5 wt.% Hyperion FIBRIL™ nanotubes in Dow Polypropylene Semi Crystalline
Homopolymer Resin H7012-35RN Injection Molded

Test Date	Sample Number	Flexural maximum Stress (MPa)	Flexural Strain at Maximum Stress (%)	0.1% Offset Yield Flexural Stress (MPa)	Strain at 0.1% Offset Yield Flexural Stress (%)	Flexural Fracture Stress (MPa)	Flexural Strain at Fracture Stress (%)	Flexural Modulus (MPa)
4/27/2009	EQ2.5P-F-10	63.4	7.23	35.1	2.06			1803
4/27/2009	EQ2.5P-F-12	60.4	7.68	36.5	2.35	-	-	1634
4/27/2009	EQ2.5P-F-13	60.8	7.49	34.9	2.20			1669
4/27/2009	EQ2.5P-F-19	61.0	7.70	38.7	2.52	-	-	1602
4/30/2009	EQ2.5P-F-26	60.4	8.53	33.7	2.09			1709
Average		61.2	7.73	35.8	2.24			1683
Standard deviation		1.3	0.49	1.9	0.19			78
Number of samples		5	5	5	5			5

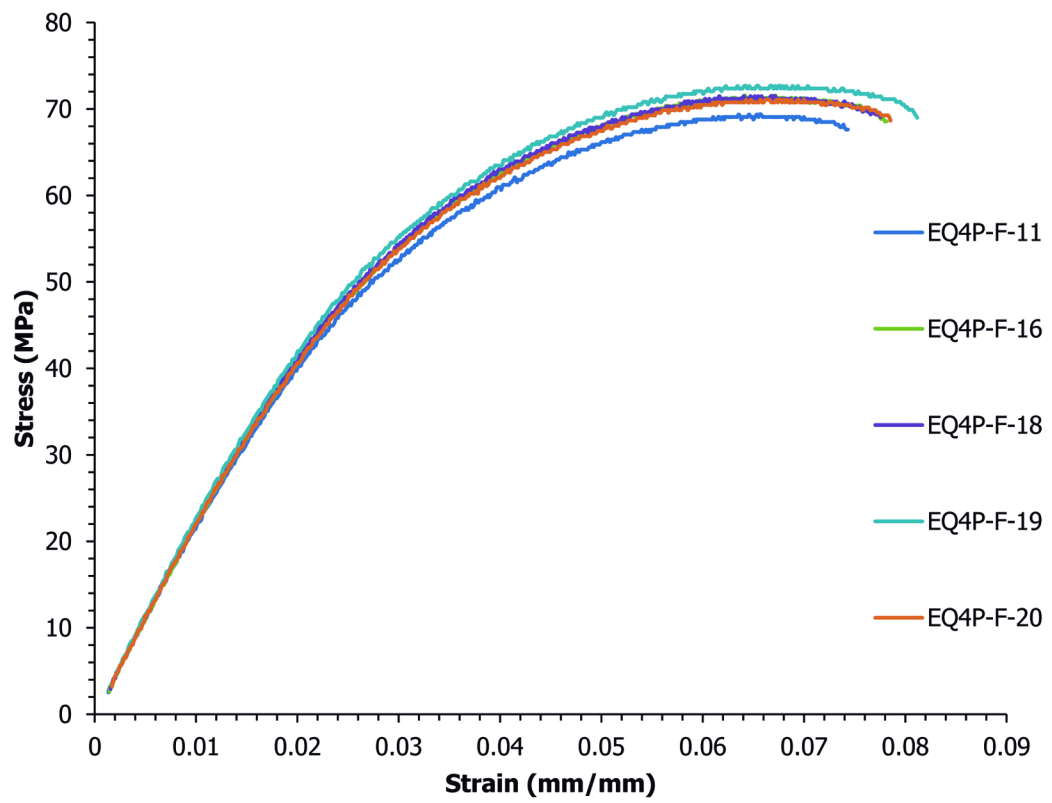


Figure C.25 Flexural results for EQ4P

Table C.25

Flexural test results for 4 wt.% Hyperion FIBRIL™ nanotubes in Dow Polypropylene Semi Crystalline Homopolymer Resin H7012-35RN Injection Molded

Test Date	Sample Number	Flexural maximum Stress (MPa)	Flexural Strain at Maximum Stress (%)	0.1% Offset Yield Flexural Stress (MPa)	Strain at 0.1% Offset Yield Flexural Stress (%)	Flexural Fracture Stress (MPa)	Flexural Strain at Fracture Stress (%)	Flexural Modulus (MPa)
4/27/2009	EQ4P-F-11	69.4	6.58	38.3	1.90	69.4	6.58	2135
4/27/2009	EQ4P-F-16	71.6	7.97	39.4	1.93	71.6	7.97	2162
4/27/2009	EQ4P-F-18	71.5	7.84	45.8	2.30	68.8	7.77	2085
4/27/2009	EQ4P-F-19	72.7	6.94	46.6	2.30	69.9	8.07	2118
4/27/2009	EQ4P-F-20	71.1	7.93	43.3	2.18	69.0	7.85	2101
Average		71.2	7.45	42.7	2.12	69.7	7.65	2120
Standard deviation		1.2	0.65	3.7	0.20	1.1	0.61	30
Number of samples		5	5	5	5	5	5	5

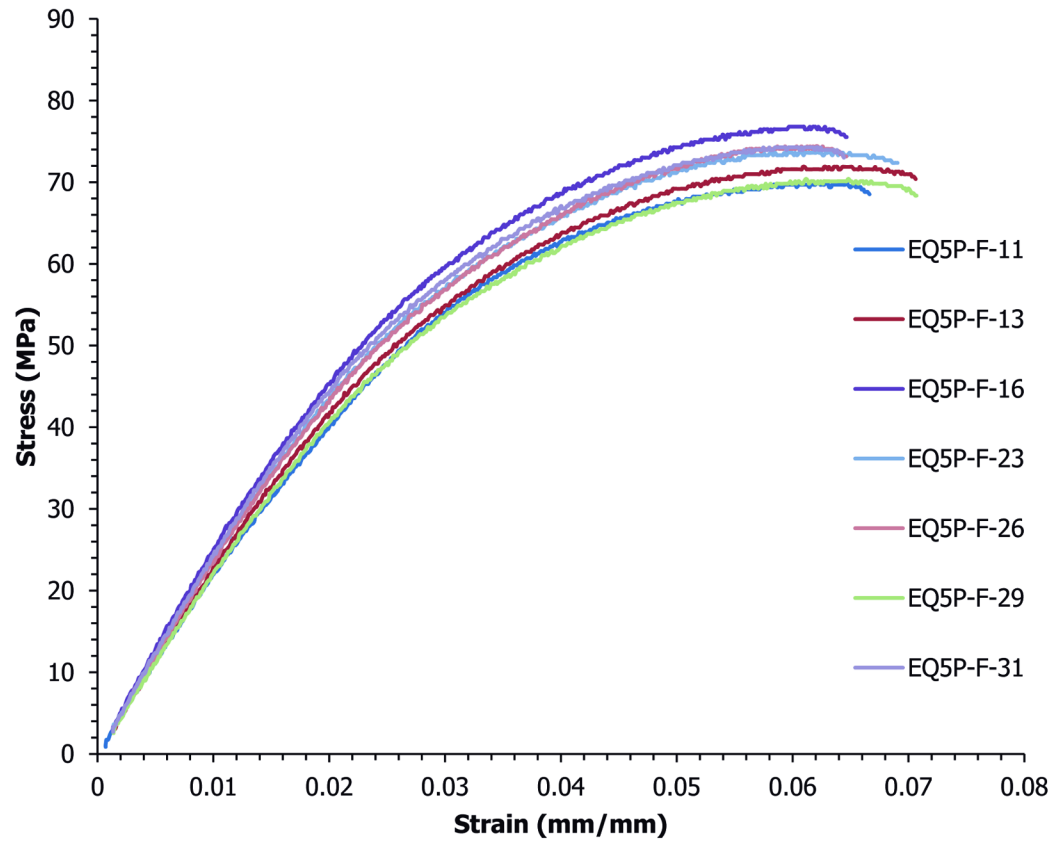


Figure C.26 Flexural results for EQ5P

Table C.26

Flexural test results for 5 wt.% Hyperion FIBRIL™ nanotubes in Dow Polypropylene Semi Crystalline Homopolymer Resin H7012-35RN Injection Molded

Test Date	Sample Number	Flexural maximum Stress (MPa)	Flexural Strain at Maximum Stress (%)	0.1% Offset Yield Flexural Stress (MPa)	Strain at 0.1% Offset Yield Flexural Stress (%)	Flexural Fracture Stress (MPa)	Flexural Strain at Fracture Stress (%)	Flexural Modulus (MPa)
4/27/2009	EQ5P-F-11	70.0	6.71	25.6	1.19	70.0	6.71	2346
4/27/2009	EQ5P-F-13	71.9	6.29	30.8	1.41	71.9	6.29	2369
4/27/2009	EQ5P-F-16	76.8	6.20	49.1	2.23	76.8	6.20	2325
4/27/2009	EQ5P-F-23	73.9	6.98	42.0	1.92	72.7	6.81	2315
4/27/2009	EQ5P-F-26	74.4	6.13	40.8	1.87	74.4	6.13	2322
4/27/2009	EQ5P-F-29	70.4	7.11	41.5	2.07	70.4	7.11	2121
4/27/2009	EQ5P-F-31	74.3	6.44	43.1	1.93	74.3	6.44	2376
Average		73.1	6.55	39.0	1.80	72.9	6.53	2311
Standard deviation		2.4	0.39	8.0	0.37	2.4	0.36	87
Number of samples		7	7	7	7	7	7	7

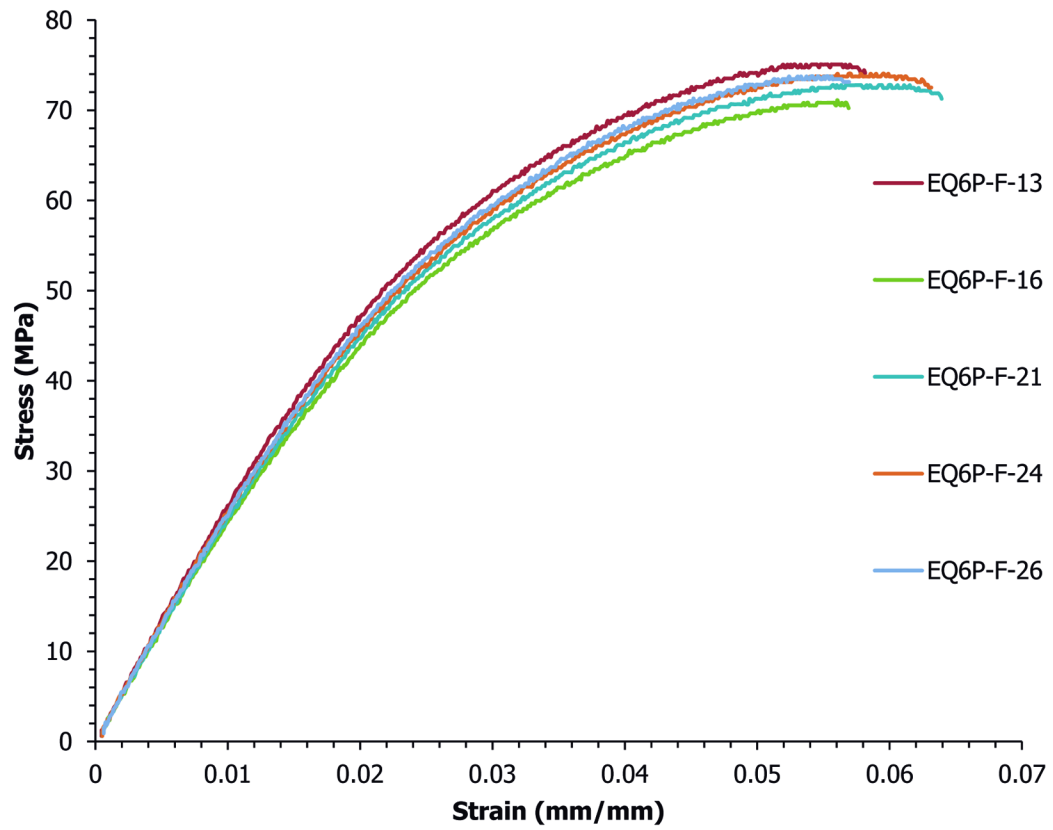


Figure C.27 Flexural results for EQ6P

Table C.27

Flexural test results for 6 wt.% Hyperion FIBRIL™ nanotubes in Dow Polypropylene Semi Crystalline Homopolymer Resin H7012-35RN Injection Molded

Test Date	Sample Number	Flexural maximum Stress (MPa)	Flexural Strain at Maximum Stress (%)	0.1% Offset Yield Flexural Stress (MPa)	Strain at 0.1% Offset Yield Flexural Stress (%)	Flexural Fracture Stress (MPa)	Flexural Strain at Fracture Stress (%)	Flexural Modulus (MPa)
4/27/2009	EQ6P-F-13	75.1	5.53	39.6	1.61	75.1	5.53	2613
4/27/2009	EQ6P-F-16	71.1	5.85	36.7	1.61	71.1	5.85	2445
4/27/2009	EQ6P-F-21	72.8	5.79	43.2	1.91	72.8	5.79	2400
4/27/2009	EQ6P-F-24	74.1	5.99	41.6	1.78	74.1	5.99	2482
4/27/2009	EQ6P-F-26	73.8	5.82	42.1	1.78	73.8	5.82	2501
Average		73.4	5.80	40.6	1.74	73.4	5.80	2488
Standard deviation		1.5	0.17	2.5	0.13	1.5	0.17	80
Number of samples		5	5	5	5	5	5	5

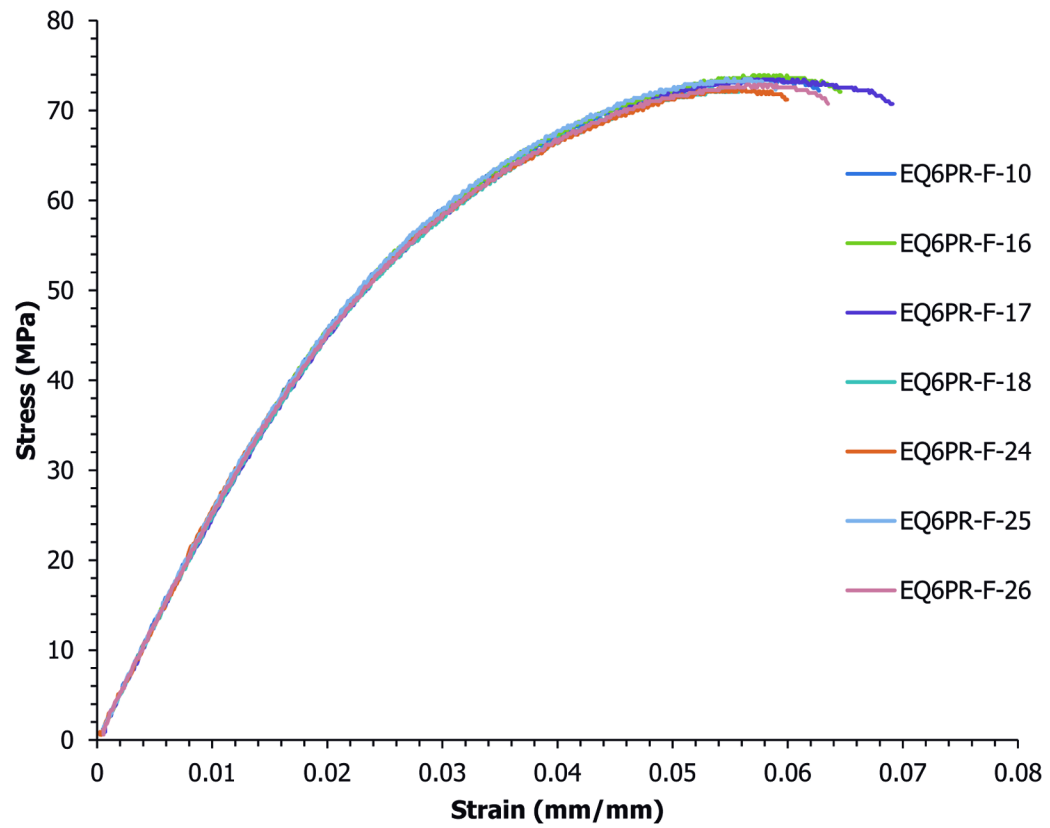


Figure C.28 Flexural results for EQ6PR

Table C.28

Flexural test results for 6 wt.% Hyperion FIBRIL™ nanotubes in Dow Polypropylene Semi Crystalline
Homopolymer Resin H7012-35RN Injection Molded Replicate

Test Date	Sample Number	Flexural maximum Stress (MPa)	Flexural Strain at Maximum Stress (%)	0.1% Offset Yield Flexural Stress (MPa)	Strain at 0.1% Offset Yield Flexural Stress (%)	Flexural Fracture Stress (MPa)	Flexural Strain at Fracture Stress (%)	Flexural Modulus (MPa)
4/27/2009	EQ6PR-F-10	73.7	6.30	38.1	1.60	73.7	6.30	2542
4/27/2009	EQ6PR-F-16	73.9	6.52	38.9	1.65	73.9	6.52	2524
4/27/2009	EQ6PR-F-17	73.5	6.98	45.3	2.04	71.3	6.83	2345
4/27/2009	EQ6PR-F-18	72.4	5.32	40.7	1.77	72.4	5.32	2446
4/27/2009	EQ6PR-F-24	72.4	5.70	37.4	1.57	72.4	5.70	2544
4/27/2009	EQ6PR-F-25	73.5	5.63	40.3	1.71	73.5	5.63	2502
4/27/2009	EQ6PR-F-26	72.9	6.38	40.1	1.73	72.9	6.38	2461
Average		73.2	6.12	40.1	1.73	72.9	6.10	2481
Standard deviation		0.6	0.59	2.6	0.16	0.9	0.55	71
Number of samples		7	7	7	7	7	7	7

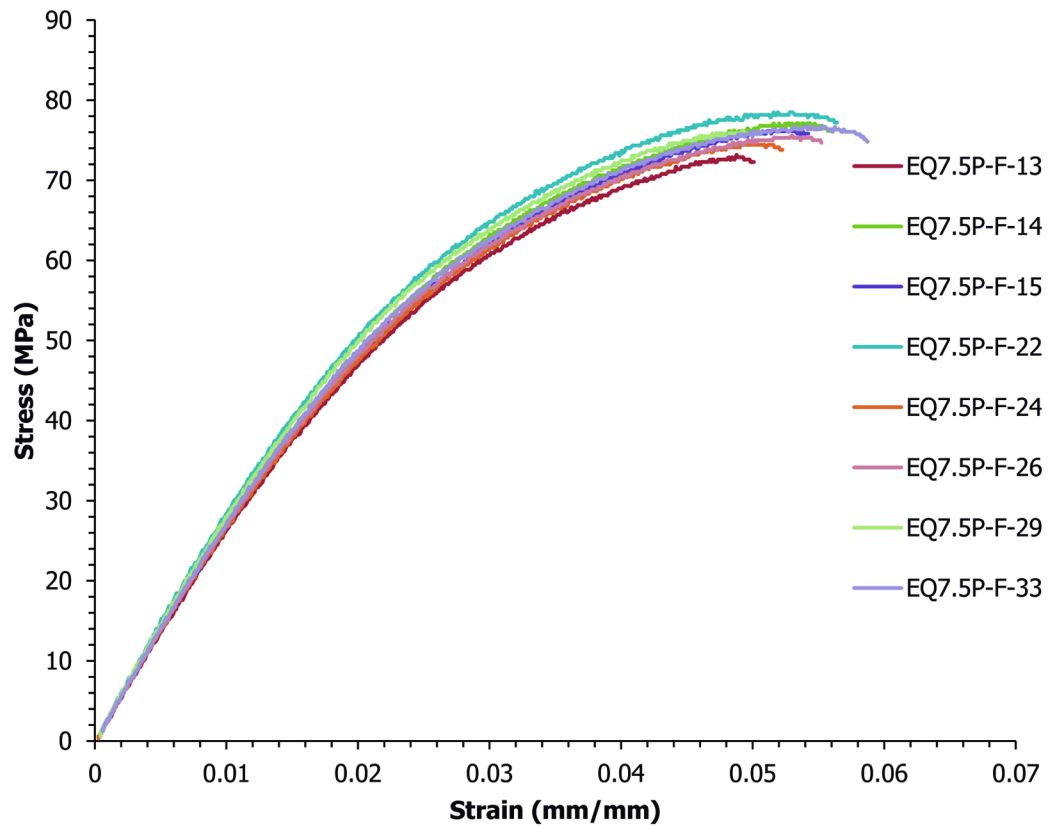


Figure C.29 Flexural results for EQ7.5P

Table C.29

Flexural test results for 7.5 wt.% Hyperion FIBRIL™ nanotubes in Dow Polypropylene Semi Crystalline Homopolymer Resin H7012-35RN Injection Molded

Test Date	Sample Number	Flexural maximum Stress (MPa)	Flexural Strain at Maximum Stress (%)	0.1% Offset Yield Flexural Stress (MPa)	Strain at 0.1% Offset Yield Flexural Stress (%)	Flexural Fracture Stress (MPa)	Flexural Strain at Fracture Stress (%)	Flexural Modulus (MPa)
4/27/2009	EQ7.5P-F-13	73.2	5.10	38.2	1.54	73.2	5.10	2664
4/27/2009	EQ7.5P-F-14	77.1	5.65	38.9	1.52	77.1	5.65	2746
4/27/2009	EQ7.5P-F-15	76.1	5.32	43.0	1.75	76.1	5.32	2619
4/27/2009	EQ7.5P-F-22	78.5	5.70	45.1	1.72	78.5	5.70	2779
4/27/2009	EQ7.5P-F-24	74.4	5.09	40.6	1.64	74.4	5.09	2660
4/27/2009	EQ7.5P-F-26	75.6	5.30	40.9	1.63	75.6	5.30	2686
4/27/2009	EQ7.5P-F-29	76.2	4.51	41.5	1.59	76.2	4.51	2794
4/27/2009	EQ7.5P-F-33	76.7	5.93	41.9	1.65	76.7	5.93	2708
Average		76.0	5.33	41.2	1.63	76.0	5.33	2707
Standard deviation		1.6	0.44	2.2	0.08	1.6	0.44	62
Number of samples		8	8	8	8	8	8	8

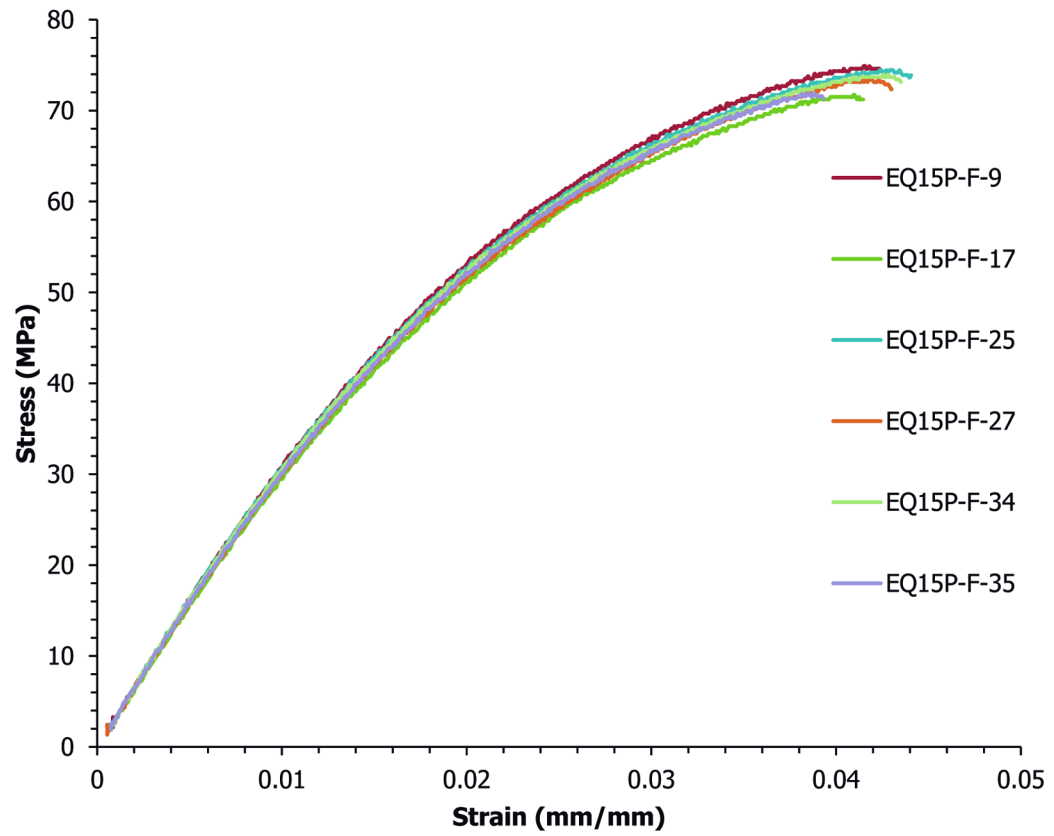


Figure C.30 Flexural results for EQ15P

Table C.30

Flexural test results for 15 wt.% Hyperion FIBRIL™ nanotubes in Dow Polypropylene Semi Crystalline
Homopolymer Resin H7012-35RN Injection Molded

Test Date	Sample Number	Flexural maximum Stress (MPa)	Flexural Strain at Maximum Stress (%)	0.1% Offset Yield Flexural Stress (MPa)	Strain at 0.1% Offset Yield Flexural Stress (%)	Flexural Fracture Stress (MPa)	Flexural Strain at Fracture Stress (%)	Flexural Modulus (MPa)
4/27/2009	EQ15P-F-9	74.9	4.16	39.2	1.34	74.9	4.16	3188
4/27/2009	EQ15P-F-17	71.8	4.20	36.7	1.29	71.8	4.20	3089
4/27/2009	EQ15P-F-25	74.4	4.31	40.9	1.42	74.4	4.31	3105
4/27/2009	EQ15P-F-27	73.4	4.34	39.6	1.39	73.4	4.34	3059
4/27/2009	EQ15P-F-34	74.0	4.37	40.9	1.43	74.0	4.37	3090
4/27/2009	EQ15P-F-35	71.9	3.97	38.5	1.35	71.9	3.97	3105
Average		73.4	4.22	39.3	1.37	73.4	4.22	3106
Standard deviation		1.3	0.15	1.6	0.05	1.3	0.15	43
Number of samples		6	6	6	6	6	6	6

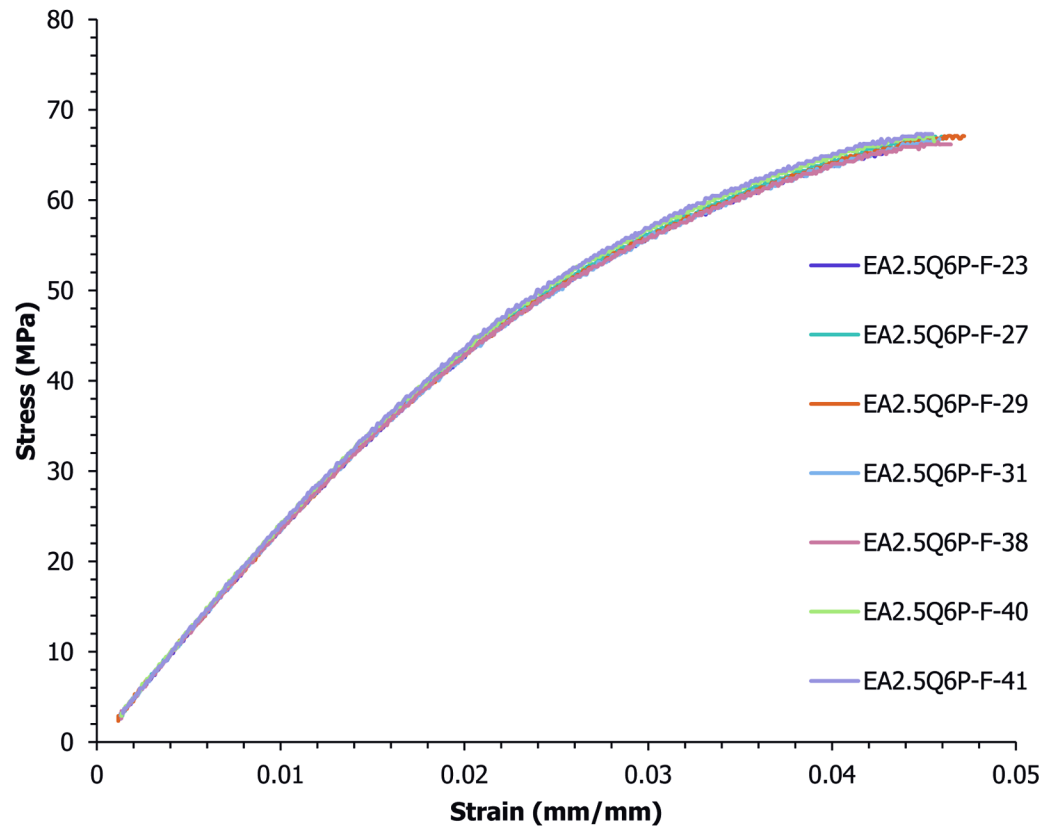


Figure C.31 Flexural results for EA2.5Q6P

Table C.31

Flexural test results for 2.5 wt.% Ketjenblack EC-600 JD and 6 wt.% Hyperion FIBRIL™ nanotubes in
Dow Polypropylene Semi Crystalline Homopolymer Resin H7012-35RN Injection Molded

Test Date	Sample Number	Flexural maximum Stress (MPa)	Flexural Strain at Maximum Stress (%)	0.1% Offset Yield Flexural Stress (MPa)	Strain at 0.1% Offset Yield Flexural Stress (%)	Flexural Fracture Stress (MPa)	Flexural Strain at Fracture Stress (%)	Flexural Modulus (MPa)
4/27/2009	EA2.5Q6P-F-23	65.4	4.30	37.7	1.71	65.4	4.30	2347
4/27/2009	EA2.5Q6P-F-27	67.0	4.63	37.7	1.70	67.0	4.63	2366
4/27/2009	EA2.5Q6P-F-29	67.1	4.65	38.5	1.75	67.1	4.65	2343
4/27/2009	EA2.5Q6P-F-31	66.8	4.62	37.8	1.72	66.8	4.62	2349
4/27/2009	EA2.5Q6P-F-38	66.4	4.65	36.7	1.66	66.4	4.65	2359
4/27/2009	EA2.5Q6P-F-40	67.0	4.43	37.2	1.65	67.0	4.43	2412
4/27/2009	EA2.5Q6P-F-41	67.3	4.49	36.6	1.62	67.3	4.49	2432
Average		66.7	4.54	37.5	1.69	66.7	4.54	2372
Standard deviation		0.7	0.14	0.7	0.05	0.7	0.14	35
Number of samples		7	7	7	7	7	7	7

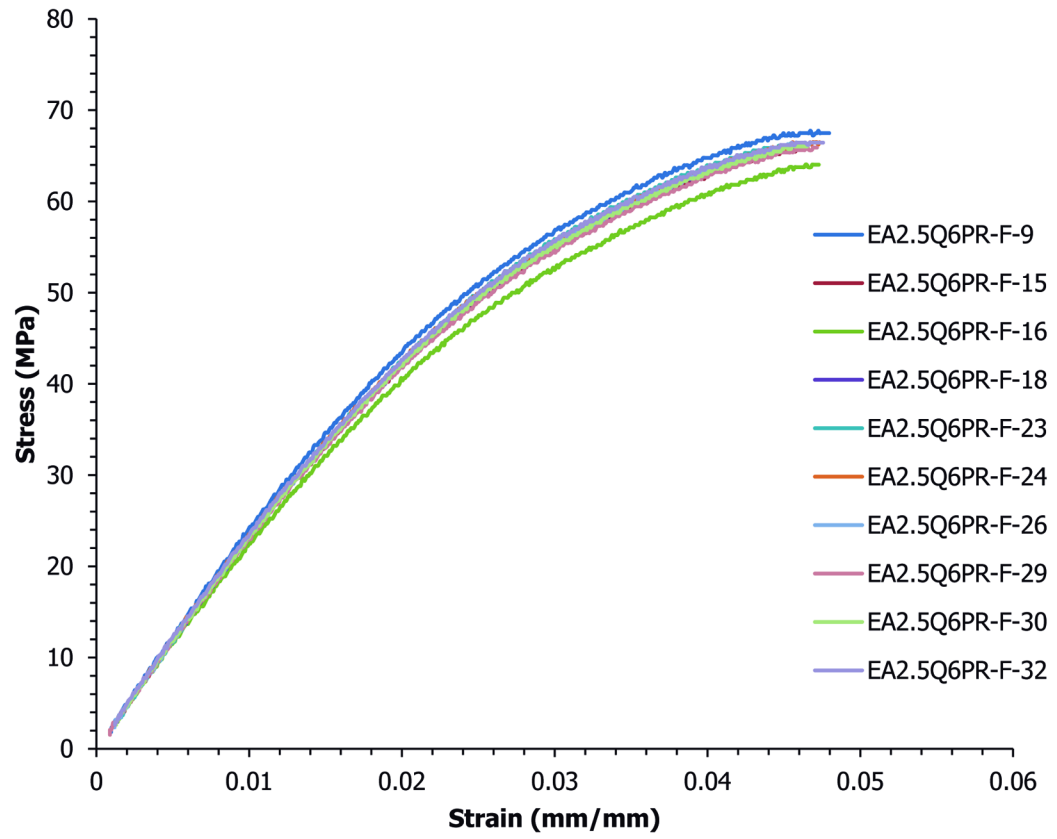


Figure C.32 Flexural results for EA2.5Q6PR

Table C.32

Flexural test results for 2.5 wt.% Ketjenblack EC-600 JD and 6 wt.% Hyperion FIBRIL™ nanotubes in
Dow Polypropylene Semi Crystalline Homopolymer Resin H7012-35RN Injection Molded replicate

Test Date	Sample Number	Flexural maximum Stress (MPa)	Flexural Strain at Maximum Stress (%)	0.1% Offset Yield Flexural Stress (MPa)	Strain at 0.1% Offset Yield Flexural Stress (%)	Flexural Fracture Stress (MPa)	Flexural Strain at Fracture Stress (%)	Flexural Modulus (MPa)
4/27/2009	EA2.5Q6PR-F-9	67.8	4.80	36.3	1.59	67.8	4.80	2434
4/27/2009	EA2.5Q6PR-F-15	65.7	4.18	35.3	1.61	65.7	4.18	2343
4/27/2009	EA2.5Q6PR-F-16	64.3	4.75	33.2	1.57	64.3	4.75	2261
4/27/2009	EA2.5Q6PR-F-18	65.9	4.50	38.3	1.77	65.9	4.50	2299
4/27/2009	EA2.5Q6PR-F-23	66.4	4.56	37.2	1.70	66.4	4.56	2339
4/27/2009	EA2.5Q6PR-F-24	66.5	4.78	37.0	1.68	66.5	4.78	2347
4/27/2009	EA2.5Q6PR-F-26	66.6	4.70	37.1	1.71	66.6	4.70	2318
4/27/2009	EA2.5Q6PR-F-29	65.9	4.77	35.6	1.64	65.9	4.77	2317
4/27/2009	EA2.5Q6PR-F-30	66.3	4.73	37.1	1.71	66.3	4.73	2320
4/27/2009	EA2.5Q6PR-F-32	66.4	4.64	65.9	4.77	66.4	4.64	2358
Average		66.2	4.64	39.3	1.98	66.2	4.64	2334
Standard deviation		0.9	0.19	9.5	0.98	0.9	0.19	45
Number of samples		10	10	10	10	10	10	10

Appendix D: Tensile strength test results

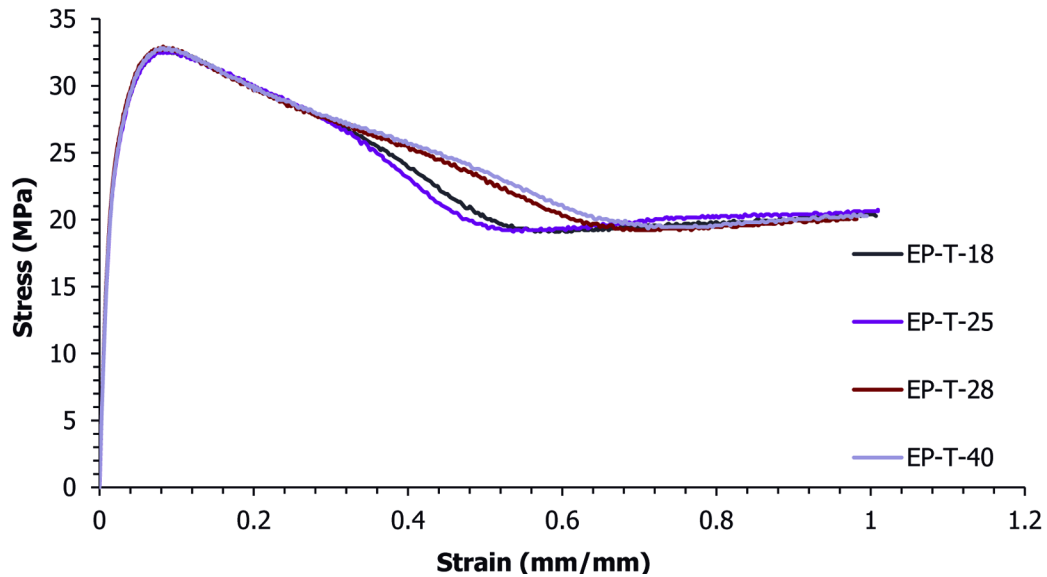


Figure D.1 Tensile results for EP

Table D.1

Tensile test results for Dow Polypropylene Semi Crystalline
Homopolymer Resin H7012-35RN Injection Molded

Test Date	Sample Number	Tensile Ultimate Stress (MPa)	Tensile Strain at Ultimate Stress (%)	Tensile Fracture Stress (MPa)	Tensile Strain at Fracture Stress* (%)	Tensile Modulus (MPa)
5/26/2009	EP-T-18	32.7	9.77	-	>100%	1535
5/26/2009	EP-T-25	32.6	9.11	-	>100%	1469
5/26/2009	EP-T-28	32.9	8.25	-	>100%	1502
5/26/2009	EP-T-30	32.7	8.73	-	>100%	1537
5/26/2009	EP-T-34	32.6	8.59	-	>100%	1484
5/26/2009	EP-T-37	32.8	8.45	-	>100%	1556
5/26/2009	EP-T-40	32.8	8.37	-	>100%	1464
Average		32.7	8.75	-	N/A	1507
Standard deviation		0.1	0.53	-	N/A	36
Number of samples		7	7	7	7	7

*Strain values higher than 100% could not be measured because the strain gage limit was reached.

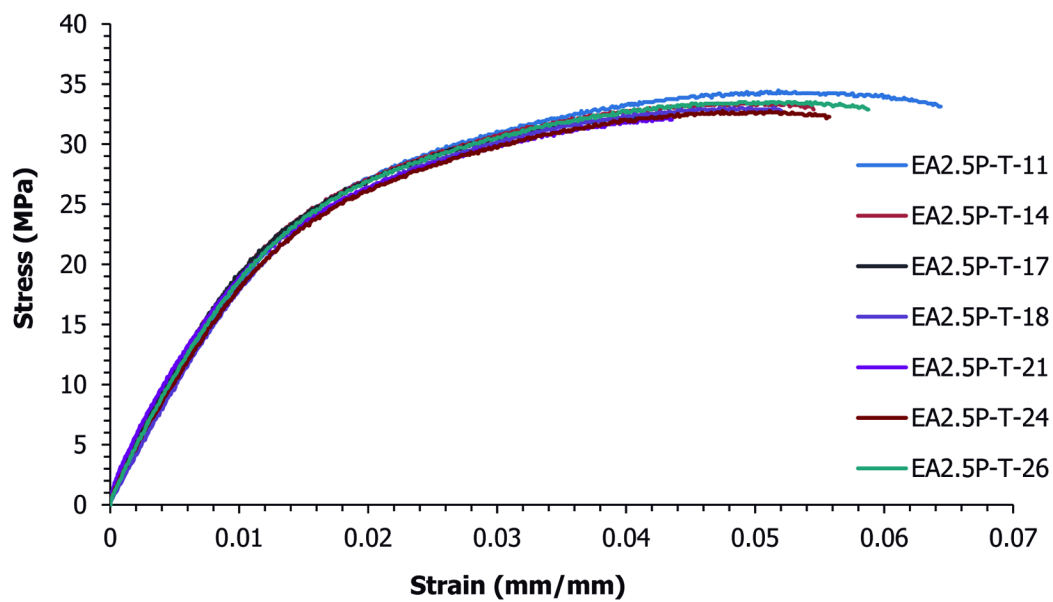


Figure D.2 Tensile results for EA2.5P

Table D.2

Tensile test results for 2.5 wt.% Ketjenblack EC-600 JD in Dow Polypropylene Semi Crystalline Homopolymer Resin H7012-35RN Injection Molded

Test Date	Sample Number	Tensile Ultimate Stress (MPa)	Tensile Strain at Ultimate Stress (%)	Tensile Fracture Stress (MPa)	Tensile Strain at Fracture Stress (%)	Tensile Modulus (MPa)
5/26/2009	EA2.5P-T-11	34.5	5.18	33.1	6.42	1777
5/26/2009	EA2.5P-T-14	33.4	4.91	33.0	5.45	1818
5/26/2009	EA2.5P-T-17	32.5	4.28	32.5	4.34	1863
5/26/2009	EA2.5P-T-18	33.0	4.89	32.9	5.17	1715
5/26/2009	EA2.5P-T-21	32.3	4.32	32.0	4.34	1761
5/26/2009	EA2.5P-T-24	32.8	4.75	32.2	5.63	1686
5/26/2009	EA2.5P-T-26	33.5	4.87	32.9	5.87	1790
Average		33.1	4.74	32.7	5.32	1773
Standard deviation		0.7	0.33	0.4	0.77	60
Number of samples		7	7	7	7	7

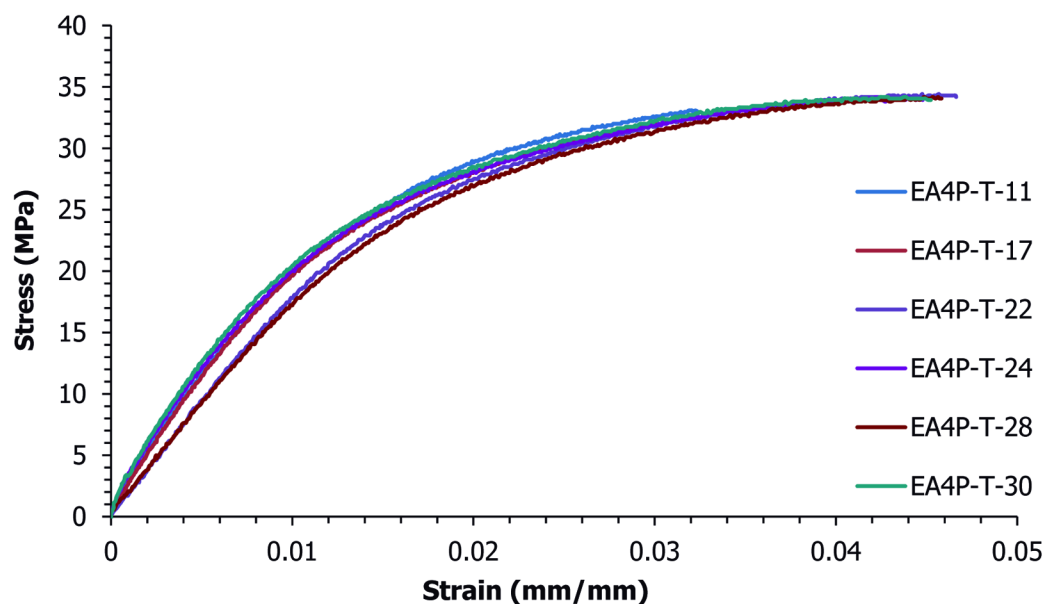


Figure D.3 Tensile results for EA4P

Table D.3

Tensile test results for 4 wt.% Ketjenblack EC-600 JD in Dow Polypropylene Semi Crystalline Homopolymer Resin H7012-35RN Injection Molded

Test Date	Sample Number	Tensile Ultimate Stress (MPa)	Tensile Strain at Ultimate Stress (%)	Tensile Fracture Stress (MPa)	Tensile Strain at Fracture Stress (%)	Tensile Modulus (MPa)
5/26/2009	EA4P-T-11	33.1	3.19	33.1	3.19	2117
5/26/2009	EA4P-T-17	32.4	3.12	32.2	3.13	2136
5/26/2009	EA4P-T-22	34.4	4.57	34.3	4.62	1842
5/26/2009	EA4P-T-24	34.2	4.22	34.1	4.41	2174
5/26/2009	EA4P-T-28	34.2	4.49	34.1	4.58	1760
5/26/2009	EA4P-T-30	34.2	4.27	33.9	4.51	2299
Average		33.7	3.98	33.6	4.07	2054
Standard deviation		0.8	0.65	0.8	0.71	208
Number of samples		6	6	6	6	6

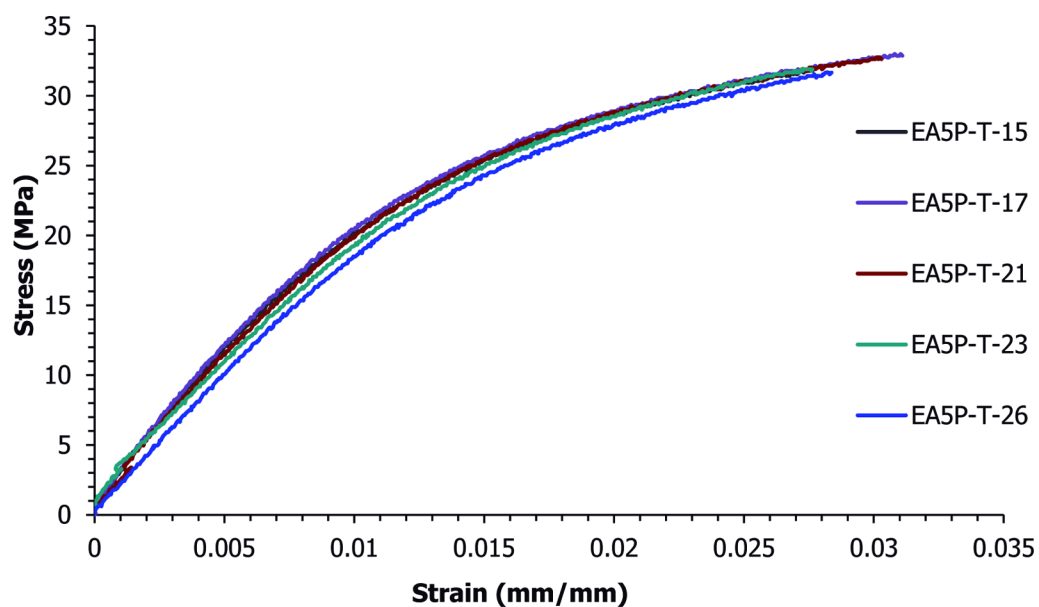


Figure D.4 Tensile results for EA5P

Table D.4

Tensile test results for 5 wt.% Ketjenblack EC-600 JD in Dow Polypropylene Semi Crystalline Homopolymer Resin H7012-35RN Injection Molded

Test Date	Sample Number	Tensile Ultimate Stress (MPa)	Tensile Strain at Ultimate Stress (%)	Tensile Fracture Stress (MPa)	Tensile Strain at Fracture Stress (%)	Tensile Modulus (MPa)
5/26/2009	EA5P-T-15	31.8	2.76	31.8	2.76	2184
5/26/2009	EA5P-T-17	33.0	3.08	33.0	3.08	2234
5/26/2009	EA5P-T-21	32.8	3.05	32.8	3.05	2129
5/26/2009	EA5P-T-23	31.9	2.75	31.9	2.75	1923
5/26/2009	EA5P-T-26	31.8	2.89	31.8	2.89	1921
Average		32.2	2.90	32.2	2.90	2078
Standard deviation		0.6	0.16	0.6	0.16	148
Number of samples		5	5	5	5	5

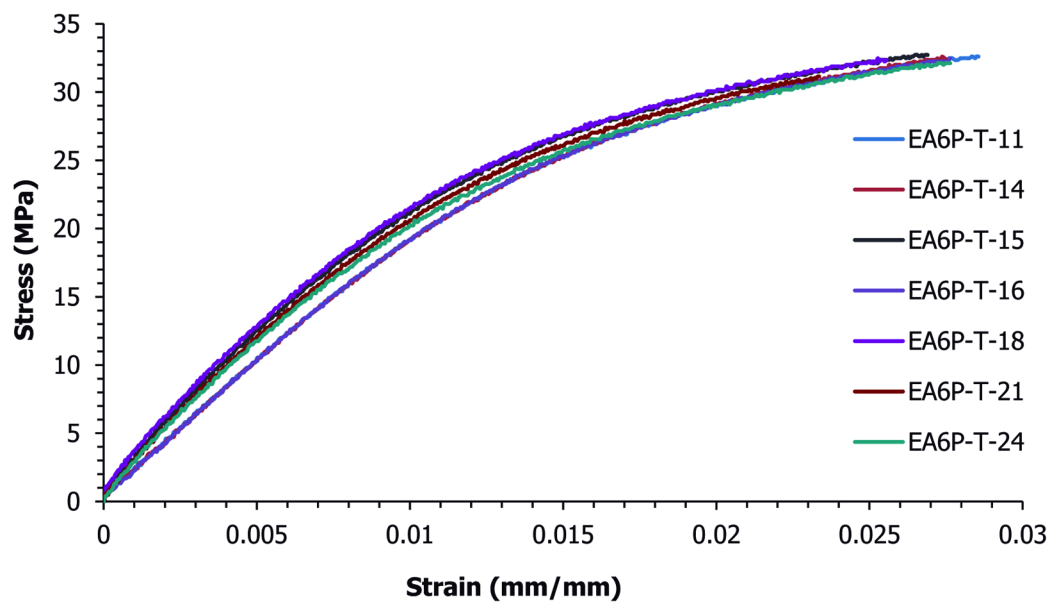


Figure D.5 Tensile results for EA6P

Table D.5

Tensile test results for 6 wt.% Ketjenblack EC-600 JD in Dow Polypropylene Semi Crystalline Homopolymer Resin H7012-35RN Injection Molded

Test Date	Sample Number	Tensile Ultimate Stress (MPa)	Tensile Strain at Ultimate Stress (%)	Tensile Fracture Stress (MPa)	Tensile Strain at Fracture Stress (%)	Tensile Modulus (MPa)
5/26/2009	EA6P-T-11	32.6	2.86	32.6	2.86	1966
5/26/2009	EA6P-T-14	32.6	2.74	32.5	2.73	1974
5/26/2009	EA6P-T-15	32.8	2.69	32.8	2.69	2328
5/26/2009	EA6P-T-16	32.5	2.76	32.5	2.76	1992
5/26/2009	EA6P-T-18	32.5	2.53	32.4	2.54	2351
5/26/2009	EA6P-T-21	31.3	2.36	31.3	2.36	2259
5/26/2009	EA6P-T-24	32.2	2.77	32.2	2.77	2193
Average		32.4	2.67	32.3	2.67	2152
Standard deviation		0.5	0.17	0.5	0.17	171
Number of samples		7	7	7	7	7

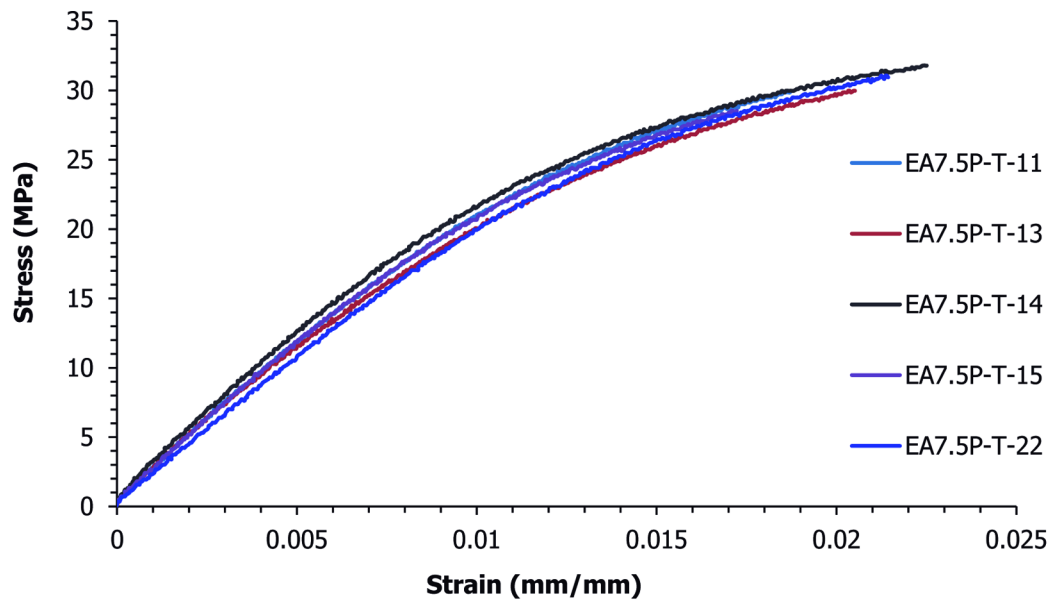


Figure D.6 Tensile results for EA7.5P

Table D.6

Tensile test results for 7.5 wt.% Ketjenblack EC-600 JD in Dow Polypropylene Semi Crystalline Homopolymer Resin H7012-35RN Injection Molded

Test Date	Sample Number	Tensile Ultimate Stress (MPa)	Tensile Strain at Ultimate Stress (%)	Tensile Fracture Stress (MPa)	Tensile Strain at Fracture Stress (%)	Tensile Modulus (MPa)
5/26/2009	EA7.5P-T-11	30.0	1.87	30.0	1.87	2335
5/26/2009	EA7.5P-T-13	30.0	2.03	30.0	2.03	2273
5/26/2009	EA7.5P-T-14	31.8	2.24	31.8	2.24	2369
5/26/2009	EA7.5P-T-15	28.5	1.71	28.5	1.71	2343
5/26/2009	EA7.5P-T-22	31.2	2.17	31.2	2.17	2119
Average		30.3	2.00	30.3	2.00	2288
Standard deviation		1.3	0.22	1.3	0.22	101
Number of samples		5	5	5	5	5

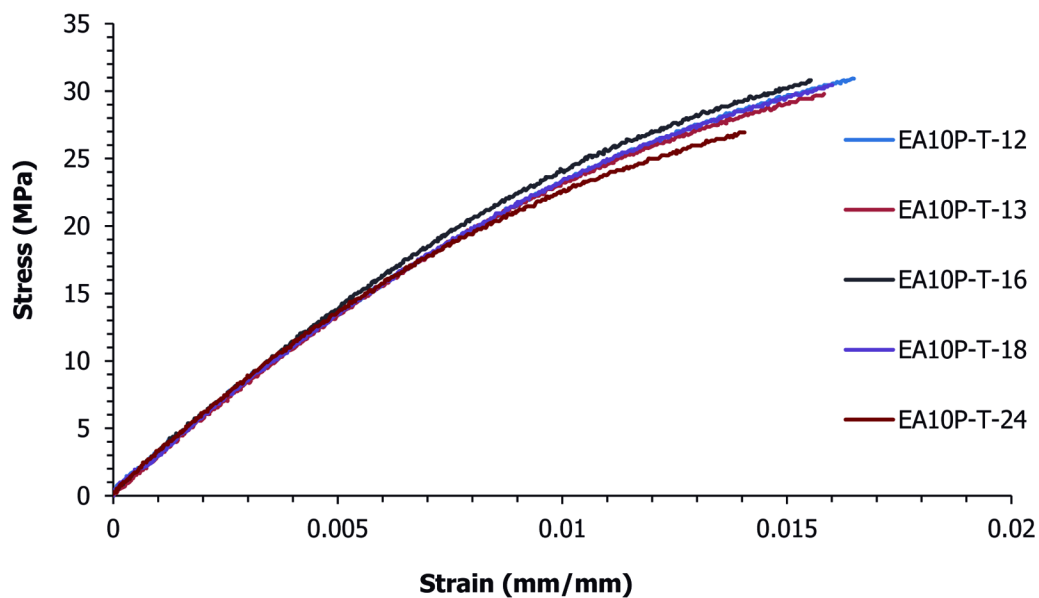


Figure D.7 Tensile results for EA10P

Table D.7

Tensile test results for 10 wt.% Ketjenblack EC-600 JD in Dow Polypropylene Semi Crystalline Homopolymer Resin H7012-35RN Injection Molded

Test Date	Sample Number	Tensile Ultimate Stress (MPa)	Tensile Strain at Ultimate Stress (%)	Tensile Fracture Stress (MPa)	Tensile Strain at Fracture Stress (%)	Tensile Modulus (MPa)
5/26/2009	EA10P-T-12	30.9	1.65	30.9	1.65	2709
5/26/2009	EA10P-T-13	29.8	1.58	29.8	1.58	2945
5/26/2009	EA10P-T-16	30.8	1.55	30.8	1.55	2801
5/26/2009	EA10P-T-18	30.4	1.59	30.4	1.59	2745
5/26/2009	EA10P-T-24	27.1	1.42	26.9	1.41	2851
Average		29.8	1.56	29.8	1.56	2810
Standard deviation		1.6	0.09	1.6	0.09	93
Number of samples		5	5	5	5	5

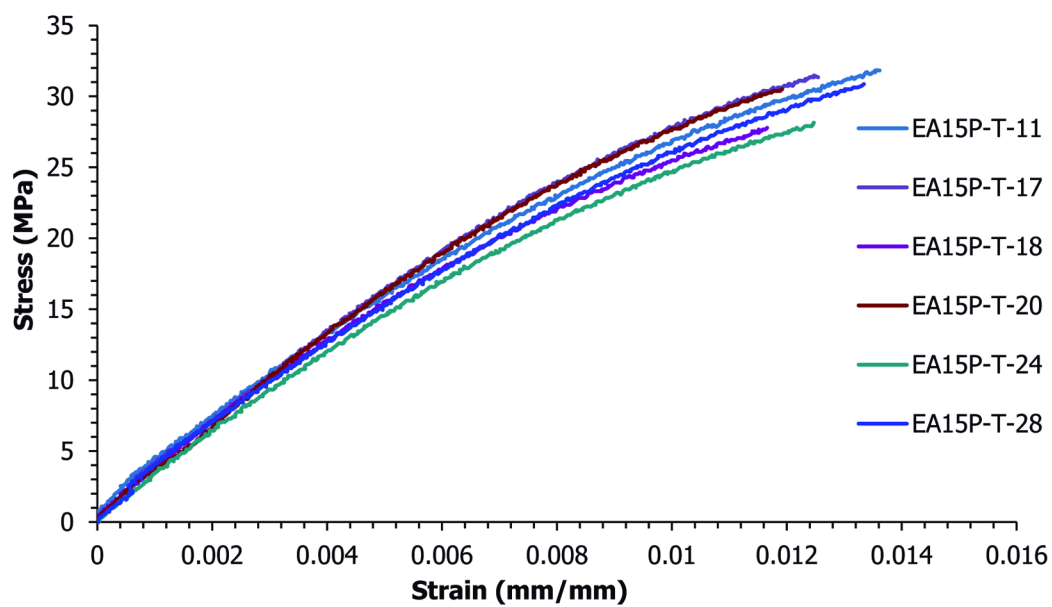


Figure D.8 Tensile results for EA15P

Table D.8

Tensile test results for 15 wt.% Ketjenblack EC-600 JD in Dow Polypropylene Semi Crystalline Homopolymer Resin H7012-35RN Injection Molded

Test Date	Sample Number	Tensile Ultimate Stress (MPa)	Tensile Strain at Ultimate Stress (%)	Tensile Fracture Stress (MPa)	Tensile Strain at Fracture Stress (%)	Tensile Modulus (MPa)
5/26/2009	EA15P-T-11	31.8	1.35	31.8	1.35	3299
5/26/2009	EA15P-T-17	31.5	1.25	31.5	1.25	3300
5/26/2009	EA15P-T-18	27.8	1.17	27.8	1.17	3258
5/26/2009	EA15P-T-20	30.6	1.20	30.6	1.20	3208
5/26/2009	EA15P-T-24	28.1	1.25	28.1	1.25	3119
5/26/2009	EA15P-T-28	31.1	1.35	31.1	1.35	3269
Average		30.2	1.26	30.2	1.26	3242
Standard deviation		1.7	0.08	1.7	0.08	69
Number of samples		6	6	6	6	6

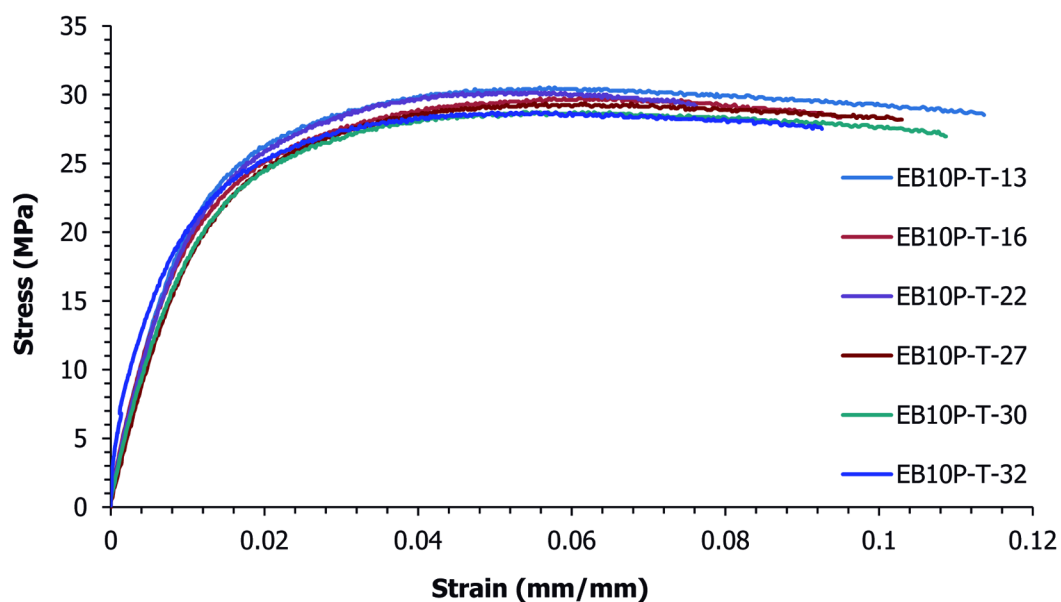


Figure D.9 Tensile results for EB10P

Table D.9

Tensile test results for 10 wt.% Thermocarb TC-300 in Dow Polypropylene Semi Crystalline Homopolymer Resin H7012-35RN Injection Molded

Test Date	Sample Number	Tensile Ultimate Stress (MPa)	Tensile Strain at Ultimate Stress (%)	Tensile Fracture Stress (MPa)	Tensile Strain at Fracture Stress (%)	Tensile Modulus (MPa)
5/27/2009	EB10P-T-13	30.5	5.70	28.7	11.13	2291
5/27/2009	EB10P-T-16	29.7	6.31	28.3	9.46	2159
5/27/2009	EB10P-T-22	30.1	5.22	29.2	7.61	2198
5/27/2009	EB10P-T-27	29.4	5.66	28.1	10.43	1922
5/27/2009	EB10P-T-30	28.7	5.54	27.0	10.86	1932
5/27/2009	EB10P-T-32	28.7	5.35	27.4	9.52	2050
Average		29.5	5.63	28.1	9.84	2092
Standard deviation		0.7	0.38	0.8	1.29	149
Number of samples		6	6	6	6	6

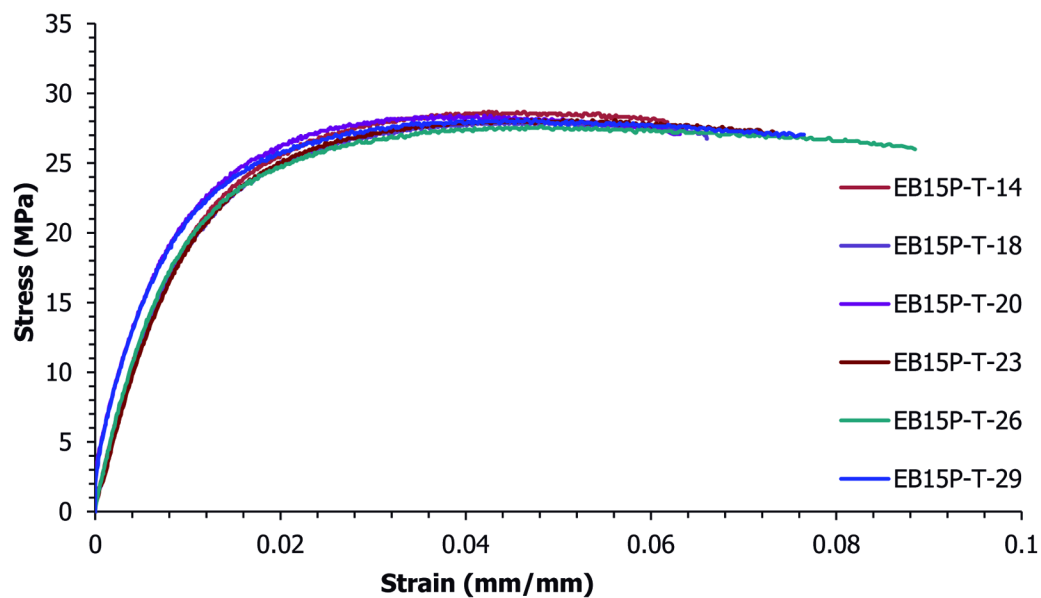


Figure D.10 Tensile results for EB15P

Table D.10

Tensile test results for 15 wt.% Thermocarb TC-300 in Dow Polypropylene Semi Crystalline Homopolymer Resin H7012-35RN Injection Molded

Test Date	Sample Number	Tensile Ultimate Stress (MPa)	Tensile Strain at Ultimate Stress (%)	Tensile Fracture Stress (MPa)	Tensile Strain at Fracture Stress (%)	Tensile Modulus (MPa)
5/27/2009	EB15P-T-14	28.7	4.27	28.0	6.18	2369
5/27/2009	EB15P-T-18	28.0	4.44	26.7	6.60	2492
5/27/2009	EB15P-T-20	28.4	3.93	27.1	6.27	2643
5/27/2009	EB15P-T-23	28.1	4.78	27.0	7.39	2391
5/27/2009	EB15P-T-26	27.6	4.73	26.1	8.77	2678
5/27/2009	EB15P-T-29	28.1	4.43	26.7	7.94	2685
Average		28.2	4.43	26.9	7.19	2543
Standard deviation		0.4	0.31	0.6	1.03	145
Number of samples		6	6	6	6	6

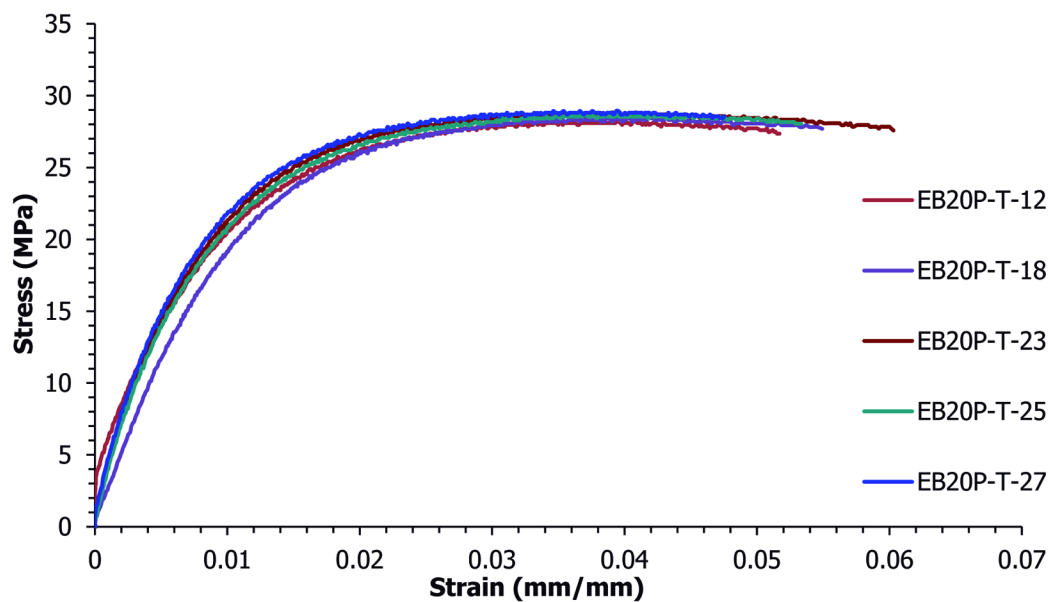


Figure D.11 Tensile results for EB20P

Table D.11

Tensile test results for 20 wt.% Thermocarb TC-300 in Dow Polypropylene Semi Crystalline Homopolymer Resin H7012-35RN Injection Molded

Test Date	Sample Number	Tensile Ultimate Stress (MPa)	Tensile Strain at Ultimate Stress (%)	Tensile Fracture Stress (MPa)	Tensile Strain at Fracture Stress (%)	Tensile Modulus (MPa)
5/27/2009	EB20P-T-12	28.2	3.74	27.4	5.15	2350
5/27/2009	EB20P-T-18	28.4	4.08	27.8	5.42	2337
5/27/2009	EB20P-T-23	28.8	3.74	27.5	6.08	2996
5/27/2009	EB20P-T-25	28.7	3.76	28.0	5.32	3135
5/27/2009	EB20P-T-27	28.9	3.76	28.3	4.82	3420
Average		28.6	3.82	27.8	5.36	2848
Standard deviation		0.3	0.15	0.4	0.47	485
Number of samples		5	5	5	5	5

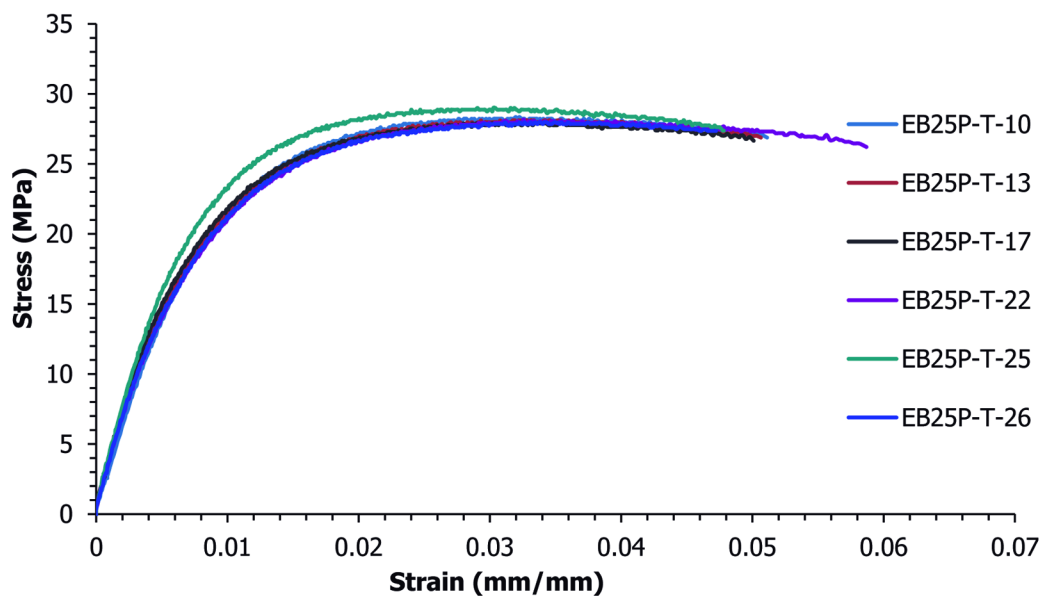


Figure D.12 Tensile results for EB25P

Table D.12

Tensile test results for 25 wt.% Thermocarb TC-300 in Dow Polypropylene Semi Crystalline Homopolymer Resin H7012-35RN Injection Molded

Test Date	Sample Number	Tensile Ultimate Stress (MPa)	Tensile Strain at Ultimate Stress (%)	Tensile Fracture Stress (MPa)	Tensile Strain at Fracture Stress (%)	Tensile Modulus (MPa)
5/27/2009	EB25P-T-10	28.3	3.20	27.0	5.09	2939
5/27/2009	EB25P-T-13	28.1	3.32	27.0	5.02	3284
5/27/2009	EB25P-T-17	28.0	3.21	26.9	4.97	3403
5/27/2009	EB25P-T-22	28.2	3.26	26.5	5.77	3082
5/27/2009	EB25P-T-25	29.0	3.04	27.4	4.77	3508
5/27/2009	EB25P-T-26	28.0	3.44	27.0	4.90	3127
Average		28.3	3.24	27.0	5.09	3224
Standard deviation		0.4	0.13	0.3	0.35	213
Number of samples		6	6	6	6	6

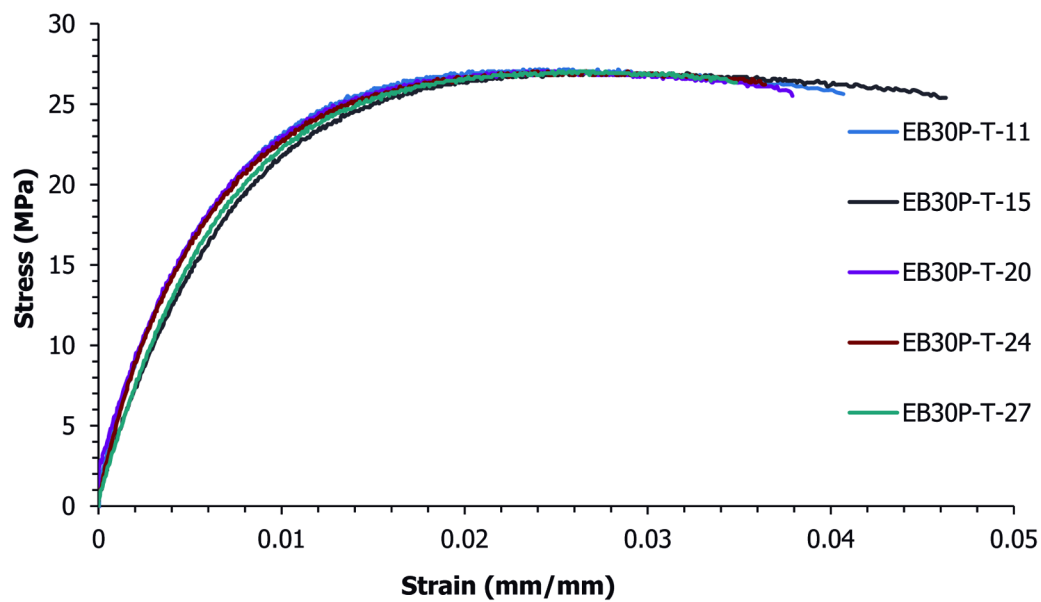


Figure D.13 Tensile results for EB30P

Table D.13

Tensile test results for 30 wt.% Thermocarb TC-300 in Dow Polypropylene Semi Crystalline Homopolymer Resin H7012-35RN Injection Molded

Test Date	Sample Number	Tensile Ultimate Stress (MPa)	Tensile Strain at Ultimate Stress (%)	Tensile Fracture Stress (MPa)	Tensile Strain at Fracture Stress (%)	Tensile Modulus (MPa)
5/27/2009	EB30P-T-11	27.2	2.41	25.8	4.03	3887
5/27/2009	EB30P-T-15	26.9	2.70	25.4	4.61	3194
5/27/2009	EB30P-T-20	27.0	2.43	25.9	3.75	3214
5/27/2009	EB30P-T-24	27.0	2.66	26.1	3.69	4097
5/27/2009	EB30P-T-27	27.0	2.66	26.3	3.47	3376
Average		27.0	2.57	25.9	3.91	3554
Standard deviation		0.1	0.14	0.4	0.44	413
Number of samples		5	5	5	5	5

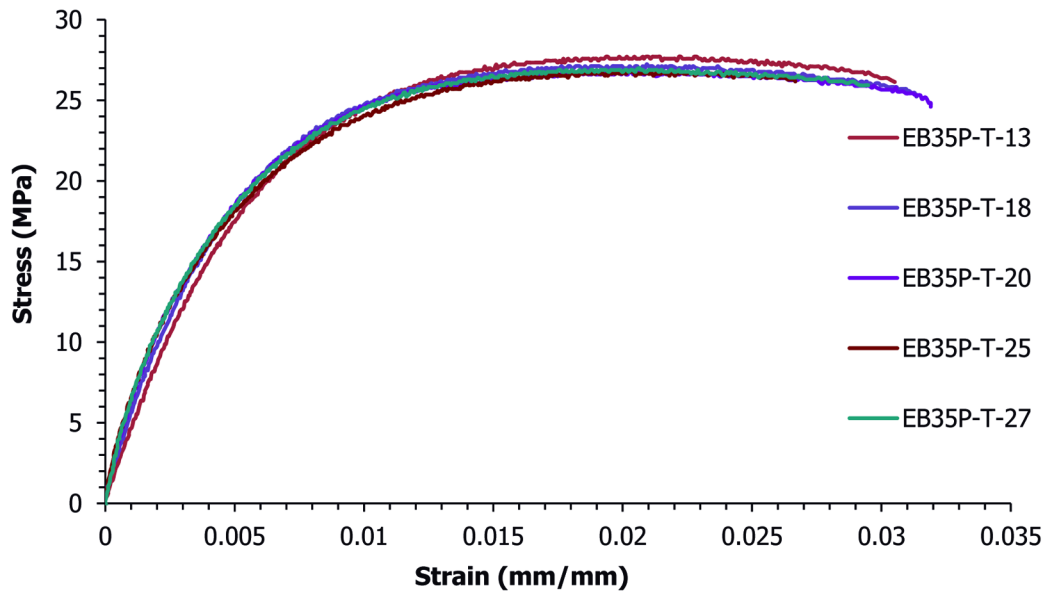


Figure D.14 Tensile results for EB35P

Table D.14

Tensile test results for 35 wt.% Thermocarb TC-300 in Dow Polypropylene Semi Crystalline Homopolymer Resin H7012-35RN Injection Molded

Test Date	Sample Number	Tensile Ultimate Stress (MPa)	Tensile Strain at Ultimate Stress (%)	Tensile Fracture Stress (MPa)	Tensile Strain at Fracture Stress (%)	Tensile Modulus (MPa)
5/27/2009	EB35P-T-13	27.7	2.13	26.3	3.04	4183
5/27/2009	EB35P-T-18	27.2	2.09	25.1	3.14	4766
5/27/2009	EB35P-T-20	26.7	2.06	24.8	3.18	5267
5/27/2009	EB35P-T-25	26.8	1.99	26.2	2.67	5299
5/27/2009	EB35P-T-27	27.0	2.06	25.9	2.92	5469
Average		27.1	2.07	25.7	2.99	4997
Standard deviation		0.4	0.05	0.6	0.21	525
Number of samples		5	5	5	5	5

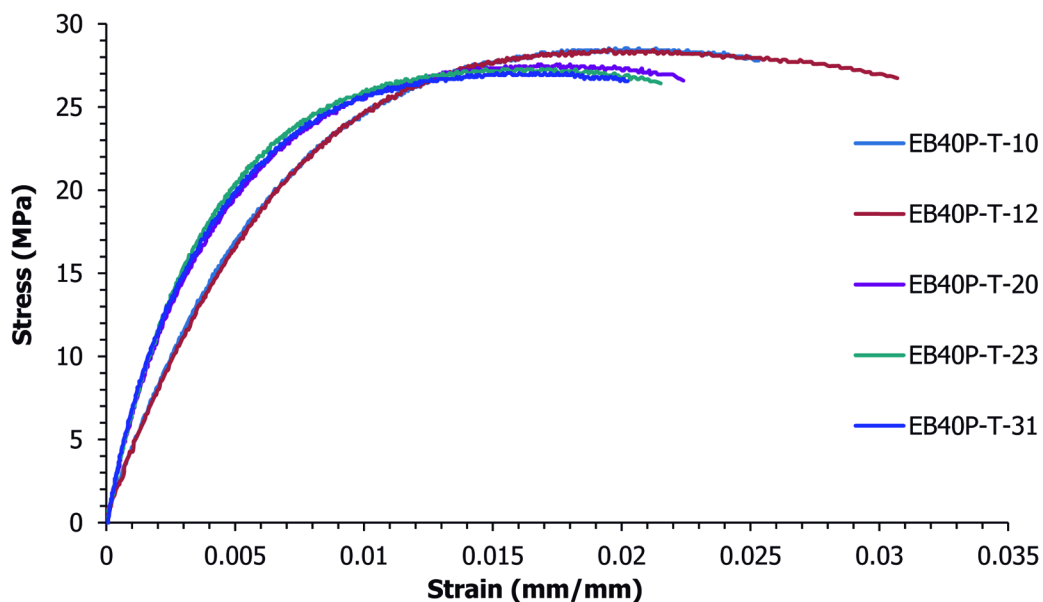


Figure D.15 Tensile results for EB40P

Table D.15

Tensile test results for 40 wt.% Thermocarb TC-300 in Dow Polypropylene Semi Crystalline Homopolymer Resin H7012-35RN Injection Molded

Test Date	Sample Number	Tensile Ultimate Stress (MPa)	Tensile Strain at Ultimate Stress (%)	Tensile Fracture Stress (MPa)	Tensile Strain at Fracture Stress (%)	Tensile Modulus (MPa)
5/27/2009	EB40P-T-10	28.5	2.07	27.8	2.52	3969
5/27/2009	EB40P-T-12	28.4	1.93	26.9	3.03	3754
5/27/2009	EB40P-T-20	27.6	1.75	26.7	2.22	5329
5/27/2009	EB40P-T-23	27.3	1.63	26.5	2.11	6705
5/27/2009	EB40P-T-31	27.0	1.65	26.4	2.05	5916
Average		27.8	1.81	26.9	2.39	5134
Standard deviation		0.7	0.19	0.5	0.40	1263
Number of samples		5	5	5	5	5

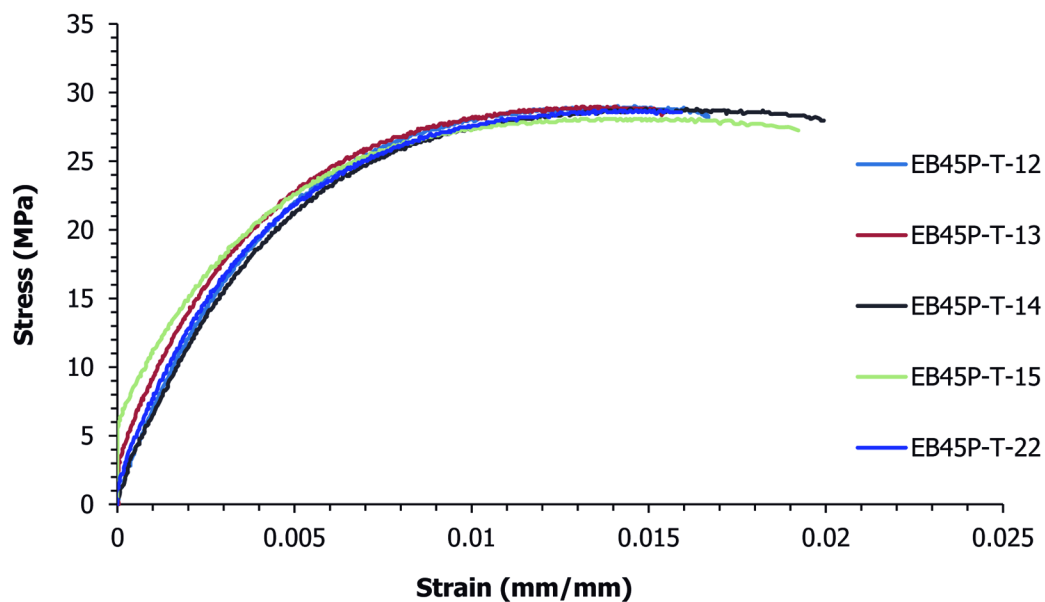


Figure D.16 Tensile results for EB45P

Table D.16

Tensile test results for 45 wt.% Thermocarb TC-300 in Dow Polypropylene Semi Crystalline Homopolymer Resin H7012-35RN Injection Molded

Test Date	Sample Number	Tensile Ultimate Stress (MPa)	Tensile Strain at Ultimate Stress (%)	Tensile Fracture Stress (MPa)	Tensile Strain at Fracture Stress (%)	Tensile Modulus (MPa)
5/27/2009	EB45P-T-12	29.0	1.44	28.2	1.67	6179
5/27/2009	EB45P-T-13	29.0	1.36	28.2	1.54	5735
5/27/2009	EB45P-T-14	28.8	1.47	28.0	1.99	5671
6/9/2009	EB45P-T-15	28.1	1.45	27.5	1.89	5641
5/27/2009	EB45P-T-22	28.7	1.45	28.3	1.61	5528
Average		28.7	1.43	28.0	1.74	5751
Standard deviation		0.4	0.04	0.3	0.19	251
Number of samples		5	5	5	5	5

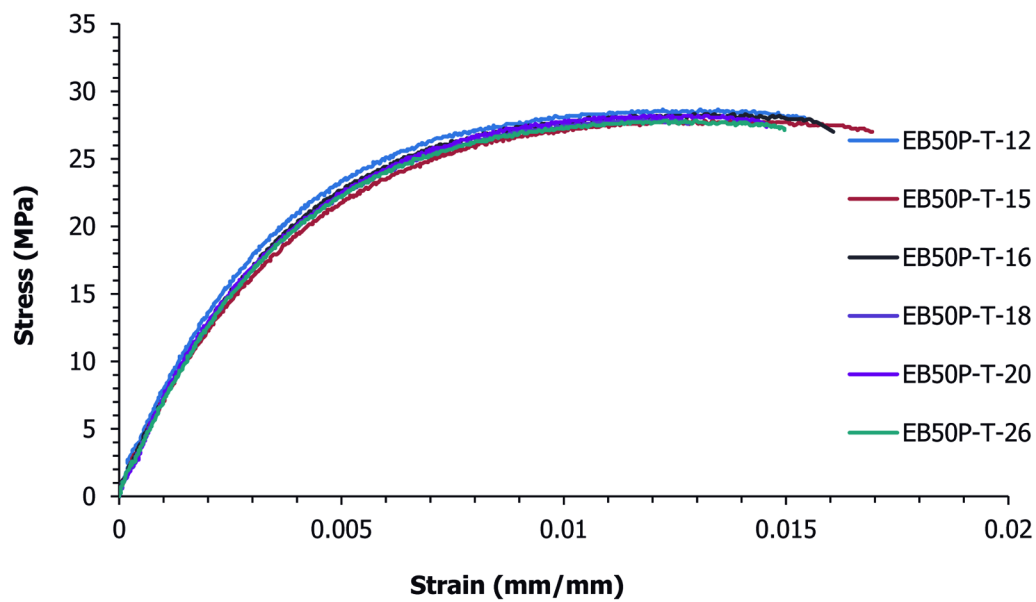


Figure D.17 Tensile results for EB50P

Table D.17

Tensile test results for 50 wt.% Thermcarb TC-300 in Dow Polypropylene Semi Crystalline Homopolymer Resin H7012-35RN Injection Molded

Test Date	Sample Number	Tensile Ultimate Stress (MPa)	Tensile Strain at Ultimate Stress (%)	Tensile Fracture Stress (MPa)	Tensile Strain at Fracture Stress (%)	Tensile Modulus (MPa)
5/27/2009	EB50P-T-12	28.7	1.22	27.7	1.54	7161
5/27/2009	EB50P-T-15	27.8	1.32	26.9	1.70	6434
5/27/2009	EB50P-T-16	28.3	1.32	27.7	1.56	6613
5/27/2009	EB50P-T-18	27.9	1.20	27.6	1.28	6827
5/27/2009	EB50P-T-20	28.2	1.24	27.5	1.45	7013
5/27/2009	EB50P-T-26	27.8	1.25	26.9	1.50	6510
Average		28.1	1.26	27.4	1.50	6760
Standard deviation		0.3	0.05	0.4	0.14	290
Number of samples		6	6	6	6	6

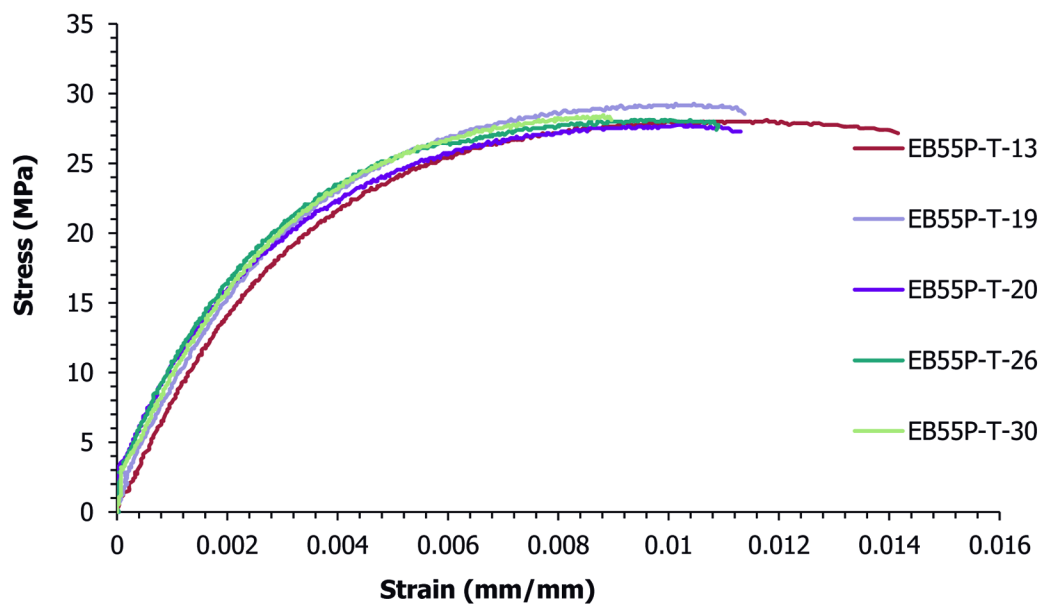


Figure D.18 Tensile results for EB55P

Table D.18

Tensile test results for 55 wt.% Thermocarb TC-300 in Dow Polypropylene Semi Crystalline Homopolymer Resin H7012-35RN Injection Molded

Test Date	Sample Number	Tensile Ultimate Stress (MPa)	Tensile Strain at Ultimate Stress (%)	Tensile Fracture Stress (MPa)	Tensile Strain at Fracture Stress (%)	Tensile Modulus (MPa)
5/27/2009	EB55P-T-13	28.1	1.18	27.4	1.38	7665
6/9/2009	EB55P-T-19	29.3	1.05	28.8	1.13	8279
5/27/2009	EB55P-T-20	27.8	1.02	27.3	1.12	7795
5/27/2009	EB55P-T-26	28.1	0.97	27.6	1.09	9616
5/27/2009	EB55P-T-30	28.5	0.88	28.1	0.90	8632
Average		28.3	1.02	27.8	1.12	8398
Standard deviation		0.6	0.11	0.6	0.17	783
Number of samples		5	5	5	5	5

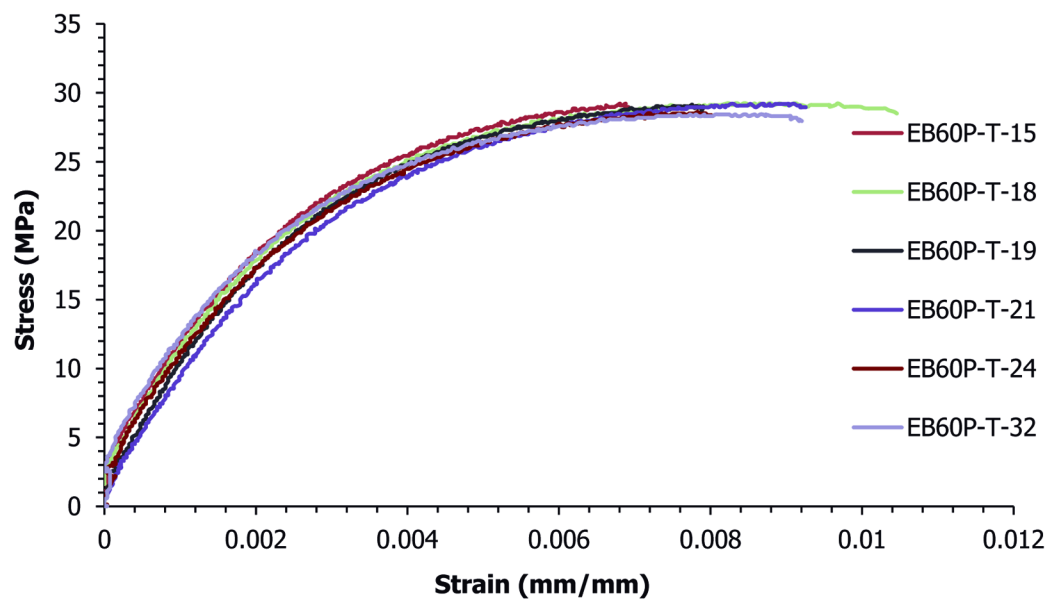


Figure D.19 Tensile results for EB60P

Table D.19

Tensile test results for 60 wt.% Thermocarb TC-300 in Dow Polypropylene Semi Crystalline Homopolymer Resin H7012-35RN Injection Molded

Test Date	Sample Number	Tensile Ultimate Stress (MPa)	Tensile Strain at Ultimate Stress (%)	Tensile Fracture Stress (MPa)	Tensile Strain at Fracture Stress (%)	Tensile Modulus (MPa)
5/27/2009	EB60P-T-15	29.2	0.68	29.0	0.69	8752
6/9/2009	EB60P-T-18	29.2	0.85	28.3	1.05	8998
5/27/2009	EB60P-T-19	29.1	0.78	28.9	0.79	9320
5/27/2009	EB60P-T-21	29.2	0.89	29.0	0.92	8657
5/27/2009	EB60P-T-24	28.6	0.78	28.1	0.80	8411
6/9/2009	EB60P-T-32	28.4	0.81	28.1	0.92	9033
Average		29.0	0.80	28.6	0.86	8862
Standard deviation		0.4	0.07	0.4	0.13	321
Number of samples		6	6	6	6	6

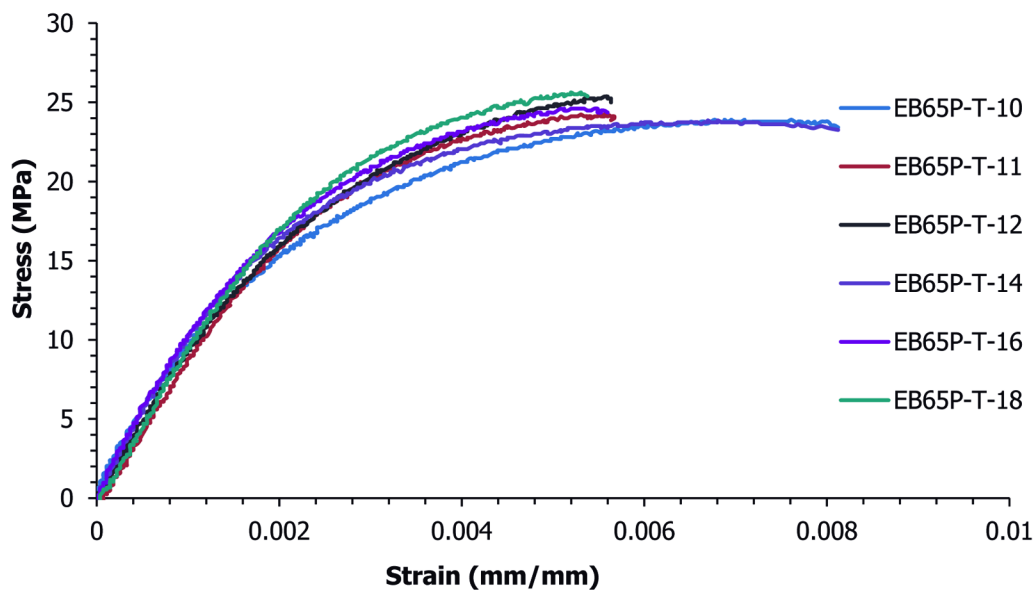


Figure D.20 Tensile results for EB65P

Table D.20

Tensile test results for 65 wt.% Thermocarb TC-300 in Dow Polypropylene Semi Crystalline Homopolymer Resin H7012-35RN Injection Molded

Test Date	Sample Number	Tensile Ultimate Stress (MPa)	Tensile Strain at Ultimate Stress (%)	Tensile Fracture Stress (MPa)	Tensile Strain at Fracture Stress (%)	Tensile Modulus (MPa)
5/27/2009	EB65P-T-10	23.9	0.70	23.5	0.80	10369
5/27/2009	EB65P-T-11	24.2	0.56	24.0	0.57	9627
5/27/2009	EB65P-T-12	25.4	0.56	24.0	0.56	9552
5/27/2009	EB65P-T-14	23.9	0.67	23.4	0.78	10830
5/27/2009	EB65P-T-16	24.6	0.53	24.4	0.55	10656
5/27/2009	EB65P-T-18	25.6	0.52	25.4	0.54	9847
Average		24.6	0.59	24.1	0.63	10147
Standard deviation		0.7	0.08	0.7	0.12	546
Number of samples		6	6	6	6	6

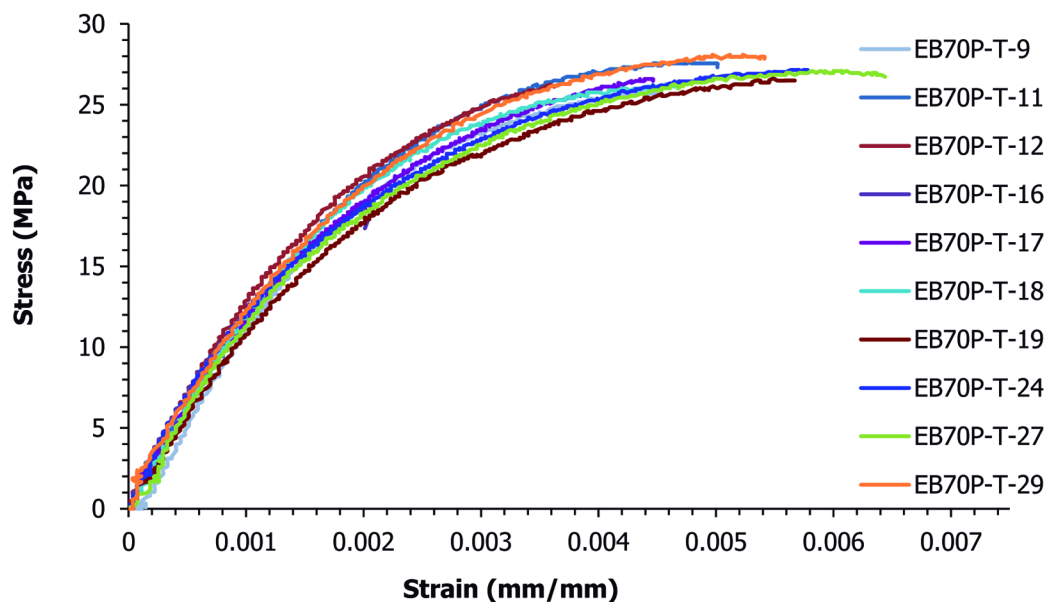


Figure D.21 Tensile results for EB70P

Table D.21

Tensile test results for 70 wt.% Thermocarb TC-300 in Dow Polypropylene Semi Crystalline Homopolymer Resin H7012-35RN Injection Molded

Test Date	Sample Number	Tensile Ultimate Stress (MPa)	Tensile Strain at Ultimate Stress (%)	Tensile Fracture Stress (MPa)	Tensile Strain at Fracture Stress (%)	Tensile Modulus (MPa)
6/9/2009	EB70P-T-9	25.9	0.43	25.8	0.44	12827
5/27/2009	EB70P-T-11	27.7	0.48	27.3	0.50	11433
5/27/2009	EB70P-T-12	26.2	0.36	26.1	0.36	13534
5/27/2009	EB70P-T-16	18.9	0.20	18.8	0.21	13328
5/27/2009	EB70P-T-17	26.6	0.44	26.5	0.45	11570
6/9/2009	EB70P-T-18	26.2	0.46	26.1	0.46	12649
5/27/2009	EB70P-T-19	26.6	0.55	26.5	0.57	11450
5/27/2009	EB70P-T-24	27.1	0.56	27.1	0.59	13577
5/27/2009	EB70P-T-27	27.1	0.60	26.8	0.63	13853
6/9/2009	EB70P-T-29	28.1	0.51	28.0	0.53	11997
Average		26.0	0.46	25.9	0.47	12622
Standard deviation		2.6	0.11	2.6	0.12	948
Number of samples		10	10	10	10	10

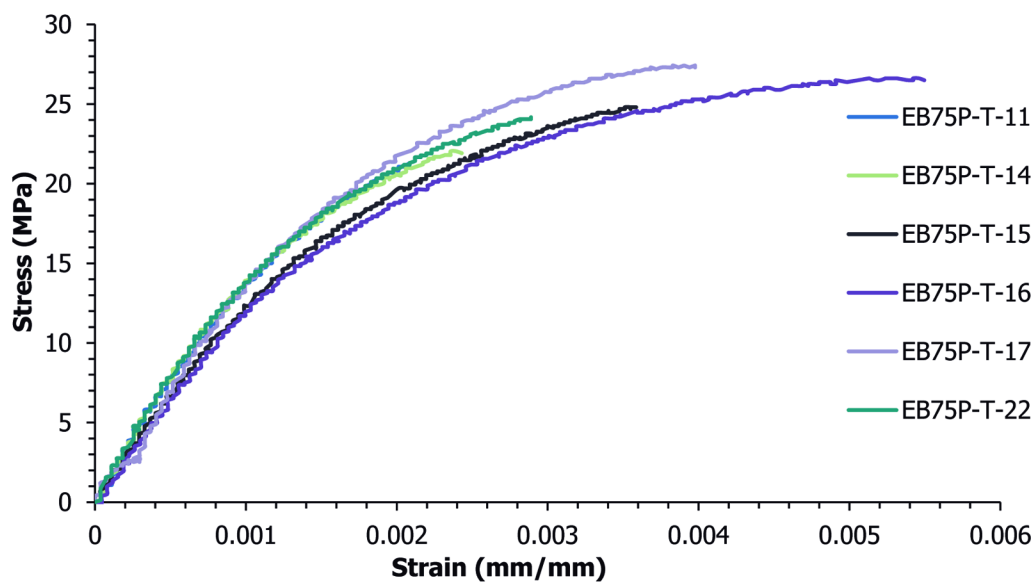


Figure D.22 Tensile results for EB75P

Table D.22

Tensile test results for 75 wt.% Thermocarb TC-300 in Dow Polypropylene Semi Crystalline Homopolymer Resin H7012-35RN Injection Molded

Test Date	Sample Number	Tensile Ultimate Stress (MPa)	Tensile Strain at Ultimate Stress (%)	Tensile Fracture Stress (MPa)	Tensile Strain at Fracture Stress (%)	Tensile Modulus (MPa)
5/27/2009	EB75P-T-11	21.3	0.21	21.3	0.21	16709
6/9/2009	EB75P-T-14	22.0	0.24	21.8	0.24	16206
5/27/2009	EB75P-T-15	24.8	0.35	24.8	0.35	13206
5/27/2009	EB75P-T-16	26.6	0.54	26.6	0.54	13367
6/9/2009	EB75P-T-17	27.4	0.39	27.3	0.40	13973
5/27/2009	EB75P-T-22	24.2	0.29	24.1	0.29	15141
Average		24.4	0.34	24.3	0.34	14767
Standard deviation		2.4	0.12	2.4	0.12	1484
Number of samples		6	6	6	6	6

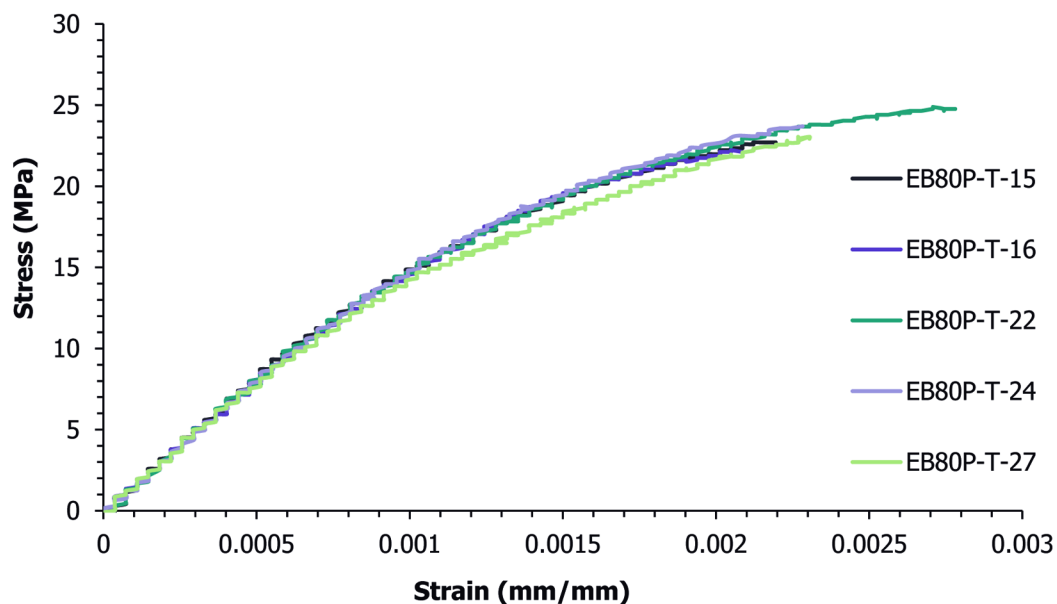


Figure D.23 Tensile results for EB80P

Table D.23

Tensile test results for 80 wt.% Thermocarb TC-300 in Dow Polypropylene Semi Crystalline Homopolymer Resin H7012-35RN Injection Molded

Test Date	Sample Number	Tensile Ultimate Stress (MPa)	Tensile Strain at Ultimate Stress (%)	Tensile Fracture Stress (MPa)	Tensile Strain at Fracture Stress (%)	Tensile Modulus (MPa)
5/27/2009	EB80P-T-15	22.7	0.21	21.9	0.22	16940
5/27/2009	EB80P-T-16	22.2	0.21	21.9	0.21	15946
5/27/2009	EB80P-T-22	24.9	0.27	24.0	0.28	16372
6/9/2009	EB80P-T-24	23.8	0.23	23.7	0.23	16202
5/27/2009	EB80P-T-27	23.0	0.23	23.0	0.23	15693
Average		23.3	0.23	22.9	0.23	16231
Standard deviation		1.0	0.02	1.0	0.03	473
Number of samples		5	5	5	5	5

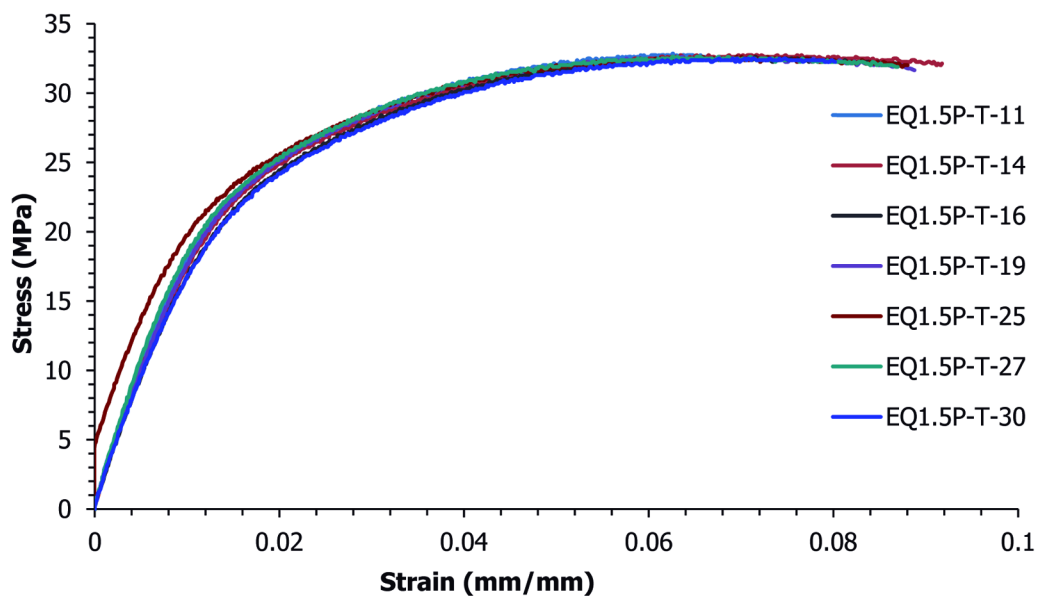


Figure D.24 Tensile results for EQ1.5P

Table D.24

Tensile test results for 1.5 wt.% Hyperion FIBRIL™ nanotubes in Dow Polypropylene Semi Crystalline Homopolymer Resin H7012-35RN Injection Molded

Test Date	Sample Number	Tensile Ultimate Stress (MPa)	Tensile Strain at Ultimate Stress (%)	Tensile Fracture Stress (MPa)	Tensile Strain at Fracture Stress (%)	Tensile Modulus (MPa)
5/26/2009	EQ1.5P-T-11	32.9	6.26	32.6	6.63	1890
5/26/2009	EQ1.5P-T-14	32.7	7.08	32.1	9.18	1807
5/26/2009	EQ1.5P-T-16	32.6	7.15	32.0	8.72	1719
5/26/2009	EQ1.5P-T-19	32.6	6.52	31.8	8.81	1825
5/26/2009	EQ1.5P-T-25	32.6	6.95	31.9	8.95	1735
5/26/2009	EQ1.5P-T-27	32.6	6.76	31.9	8.68	2012
5/26/2009	EQ1.5P-T-30	32.5	7.04	32.1	8.22	1722
Average		32.7	6.82	32.1	8.46	1816
Standard deviation		0.1	0.33	0.3	0.86	107
Number of samples		7	7	7	7	7

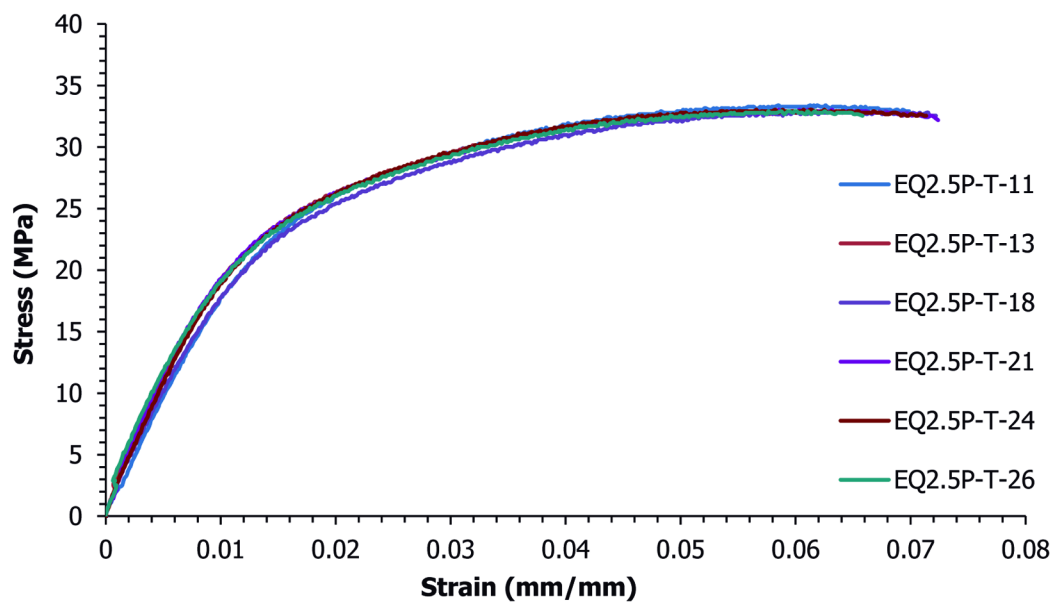


Figure D.25 Tensile results for EQ2.5P

Table D.25

Tensile test results for 2.5 wt.% Hyperion FIBRIL™ nanotubes in Dow Polypropylene Semi Crystalline Homopolymer Resin H7012-35RN Injection Molded

Test Date	Sample Number	Tensile Ultimate Stress (MPa)	Tensile Strain at Ultimate Stress (%)	Tensile Fracture Stress (MPa)	Tensile Strain at Fracture Stress (%)	Tensile Modulus (MPa)
5/26/2009	EQ2.5P-T-11	33.4	6.16	32.9	6.92	1867
5/26/2009	EQ2.5P-T-13	32.8	5.67	32.7	5.83	2052
5/26/2009	EQ2.5P-T-18	32.9	6.33	32.6	7.21	1849
5/26/2009	EQ2.5P-T-21	33.0	6.03	32.6	7.18	2177
5/26/2009	EQ2.5P-T-24	33.0	5.66	32.4	7.24	2026
5/26/2009	EQ2.5P-T-26	32.9	5.87	32.7	6.54	2112
Average		33.0	5.95	32.6	6.82	2014
Standard deviation		0.2	0.27	0.2	0.55	132
Number of samples		6	6	6	6	6

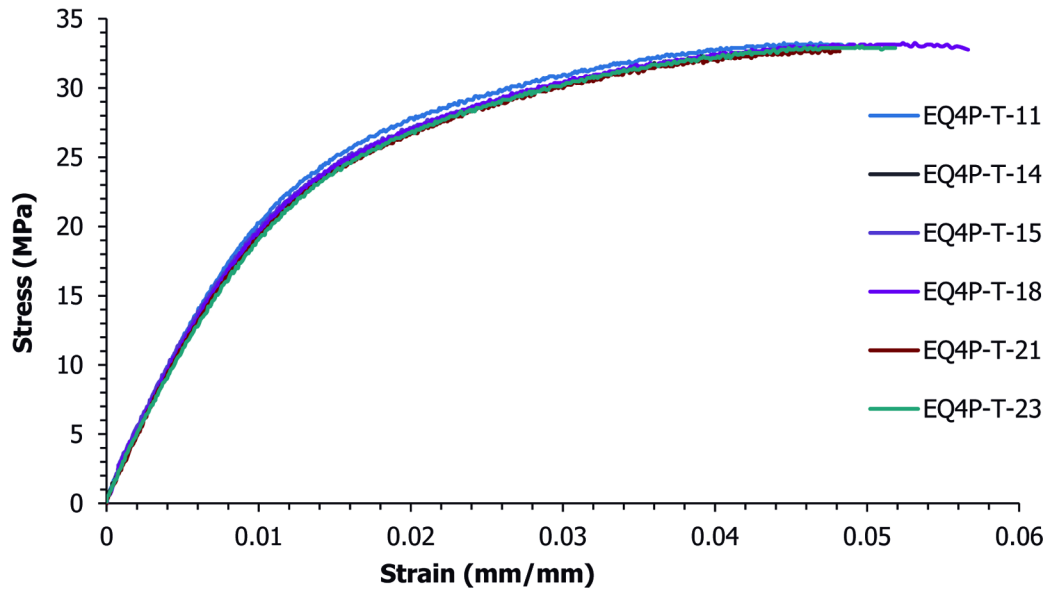


Figure D.26 Tensile results for EQ4P

Table D.26

Tensile test results for 4 wt.% Hyperion FIBRIL™ nanotubes in Dow Polypropylene Semi Crystalline Homopolymer Resin H7012-35RN Injection Molded

Test Date	Sample Number	Tensile Ultimate Stress (MPa)	Tensile Strain at Ultimate Stress (%)	Tensile Fracture Stress (MPa)	Tensile Strain at Fracture Stress (%)	Tensile Modulus (MPa)
5/26/2009	EQ4P-T-11	33.2	4.63	33.1	4.89	2219
5/26/2009	EQ4P-T-14	32.6	4.29	32.5	4.29	2092
5/26/2009	EQ4P-T-15	33.0	4.52	32.8	4.55	2184
5/26/2009	EQ4P-T-18	33.2	5.24	33.0	5.48	2147
5/26/2009	EQ4P-T-21	32.8	4.74	32.5	4.88	2114
5/26/2009	EQ4P-T-23	33.0	4.94	32.9	4.90	2039
Average		33.0	4.72	32.8	4.83	2132
Standard deviation		0.2	0.33	0.2	0.40	65
Number of samples		6	6	6	6	6

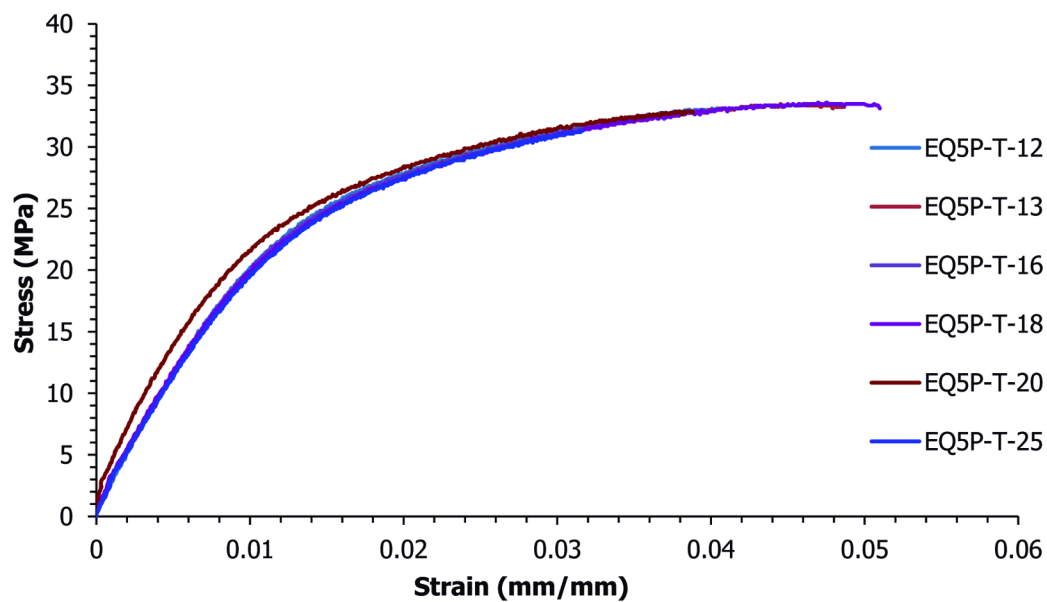


Figure D.27 Tensile results for EQ5P

Table D.27

Tensile test results for 5 wt.% Hyperion FIBRIL™ nanotubes in Dow Polypropylene Semi Crystalline Homopolymer Resin H7012-35RN Injection Molded

Test Date	Sample Number	Tensile Ultimate Stress (MPa)	Tensile Strain at Ultimate Stress (%)	Tensile Fracture Stress (MPa)	Tensile Strain at Fracture Stress (%)	Tensile Modulus (MPa)
5/26/2009	EQ5P-T-12	33.1	4.04	33.0	3.99	2211
5/26/2009	EQ5P-T-13	33.5	4.58	33.2	4.84	2115
5/26/2009	EQ5P-T-16	32.5	3.67	32.5	3.67	2156
5/26/2009	EQ5P-T-18	33.6	4.72	33.4	5.05	2130
5/26/2009	EQ5P-T-20	32.9	3.86	32.8	3.78	2509
5/26/2009	EQ5P-T-25	31.4	3.20	31.4	3.20	2097
Average		32.8	4.01	32.7	4.09	2203
Standard deviation		0.8	0.57	0.7	0.72	155
Number of samples		6	6	6	6	6

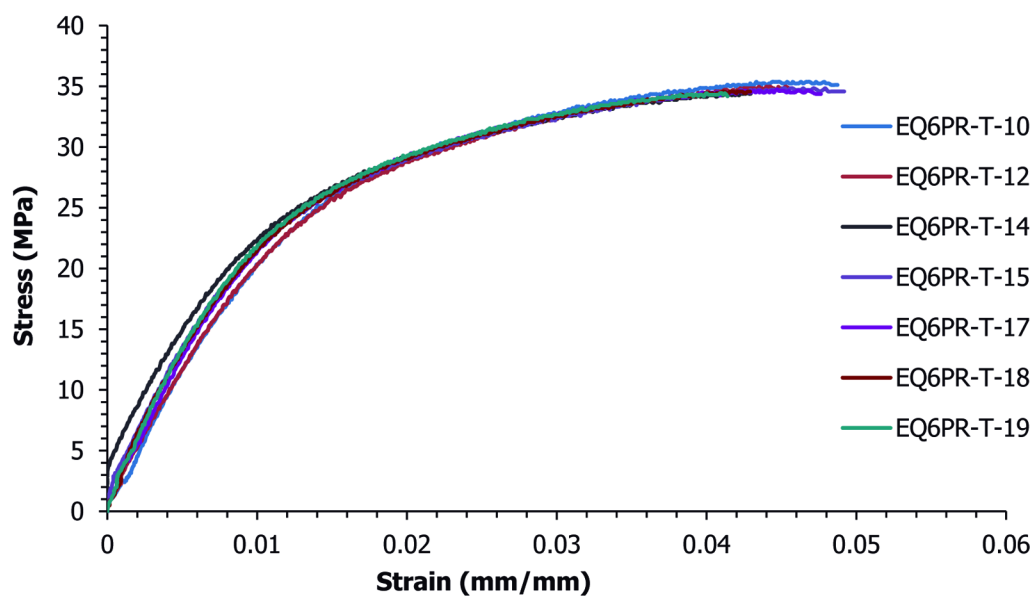


Figure D.28 Tensile results for EQ6PR

Table D.28

Tensile test results for 6 wt.% Hyperion FIBRIL™ nanotubes in Dow Polypropylene Semi Crystalline Homopolymer Resin H7012-35RN Injection Molded Replicate

Test Date	Sample Number	Tensile Ultimate Stress (MPa)	Tensile Strain at Ultimate Stress (%)	Tensile Fracture Stress (MPa)	Tensile Strain at Fracture Stress (%)	Tensile Modulus (MPa)
5/26/2009	EQ6PR-T-10	35.4	4.54	35.1	4.86	2285
5/26/2009	EQ6PR-T-12	35.0	4.42	34.8	4.37	2189
5/26/2009	EQ6PR-T-14	34.5	4.25	34.4	4.18	2193
5/26/2009	EQ6PR-T-15	34.8	4.71	34.6	4.84	2294
5/26/2009	EQ6PR-T-17	34.7	4.47	34.5	4.28	2382
5/26/2009	EQ6PR-T-18	34.6	4.24	34.6	4.24	2557
5/26/2009	EQ6PR-T-19	34.4	4.09	34.2	3.98	2537
Average		34.8	4.39	34.6	4.39	2348
Standard deviation		0.3	0.21	0.3	0.33	151
Number of samples		7	7	7	7	7

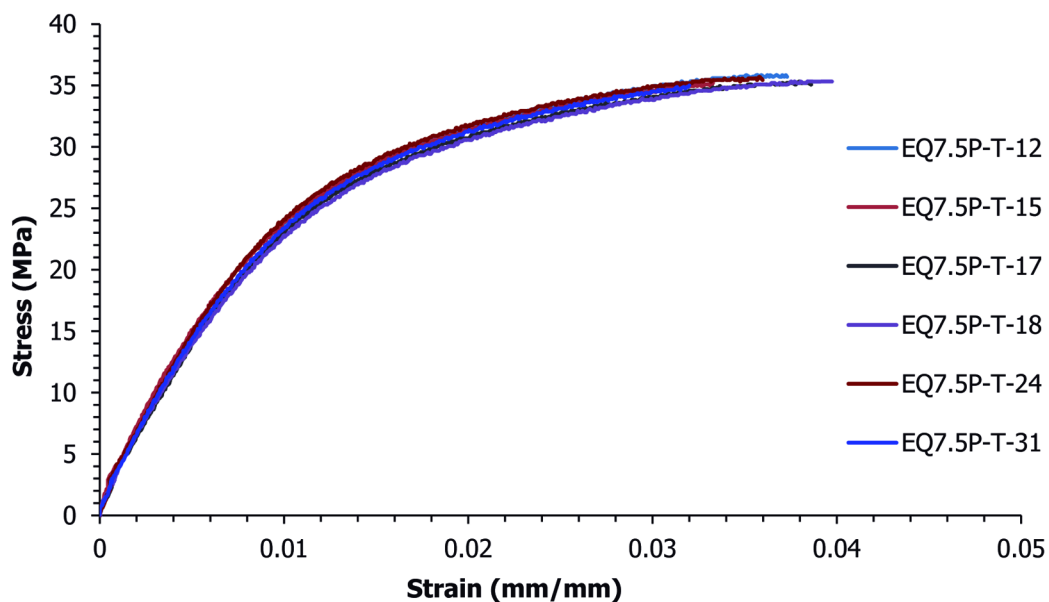


Figure D.29 Tensile results for EQ7.5P

Table D.29

Tensile test results for 7.5 wt.% Hyperion FIBRIL™ nanotubes in Dow Polypropylene Semi Crystalline Homopolymer Resin H7012-35RN Injection Molded

Test Date	Sample Number	Tensile Ultimate Stress (MPa)	Tensile Strain at Ultimate Stress (%)	Tensile Fracture Stress (MPa)	Tensile Strain at Fracture Stress (%)	Tensile Modulus (MPa)
5/26/2009	EQ7.5P-T-12	35.8	3.62	35.8	3.62	2620
5/26/2009	EQ7.5P-T-15	35.2	3.33	35.2	3.33	2854
5/26/2009	EQ7.5P-T-17	35.3	3.80	35.2	3.78	2613
5/26/2009	EQ7.5P-T-18	35.3	3.90	35.3	3.90	2652
5/26/2009	EQ7.5P-T-24	35.7	3.58	35.4	3.63	2841
5/26/2009	EQ7.5P-T-31	35.0	3.22	34.9	3.24	2756
Average		35.4	3.57	35.3	3.58	2723
Standard deviation		0.3	0.26	0.3	0.26	109
Number of samples		6	6	6	6	6

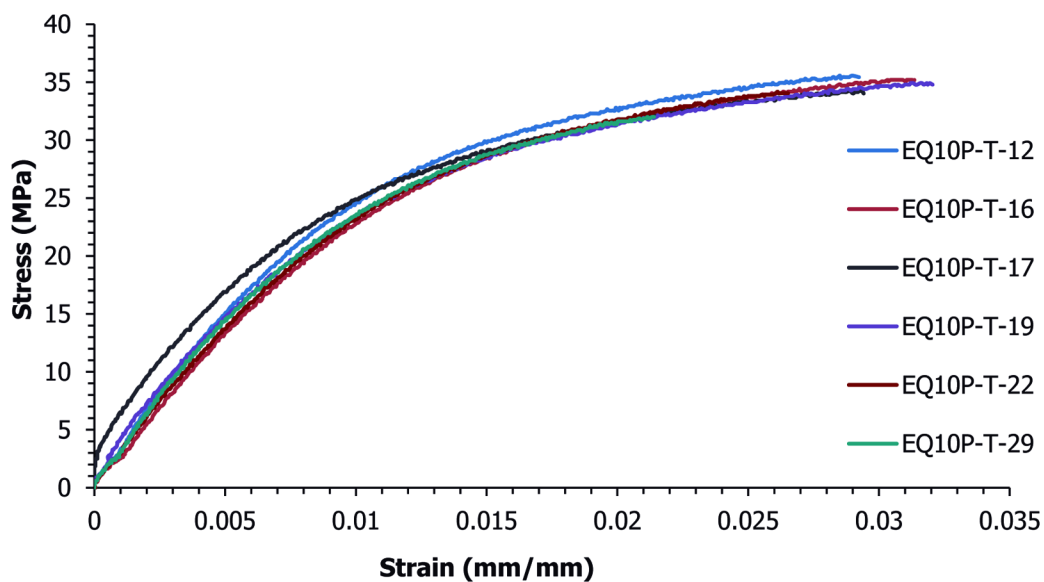


Figure D.30 Tensile results for EQ10P

Table D.30

Tensile test results for 10 wt.% Hyperion FIBRIL™ nanotubes in Dow Polypropylene Semi Crystalline Homopolymer Resin H7012-35RN Injection Molded

Test Date	Sample Number	Tensile Ultimate Stress (MPa)	Tensile Strain at Ultimate Stress (%)	Tensile Fracture Stress (MPa)	Tensile Strain at Fracture Stress (%)	Tensile Modulus (MPa)
5/27/2009	EQ10P-T-12	35.6	2.87	35.6	2.87	3255
5/27/2009	EQ10P-T-16	35.2	3.08	35.2	3.08	2693
5/27/2009	EQ10P-T-17	34.3	2.91	34.2	2.88	3402
5/27/2009	EQ10P-T-19	34.9	3.16	34.9	3.16	3173
5/27/2009	EQ10P-T-22	34.3	2.71	34.3	2.71	2866
5/27/2009	EQ10P-T-29	32.0	2.13	32.0	2.13	3087
Average		34.4	2.81	34.4	2.81	3079
Standard deviation		1.3	0.37	1.3	0.37	260
Number of samples		6	6	6	6	6

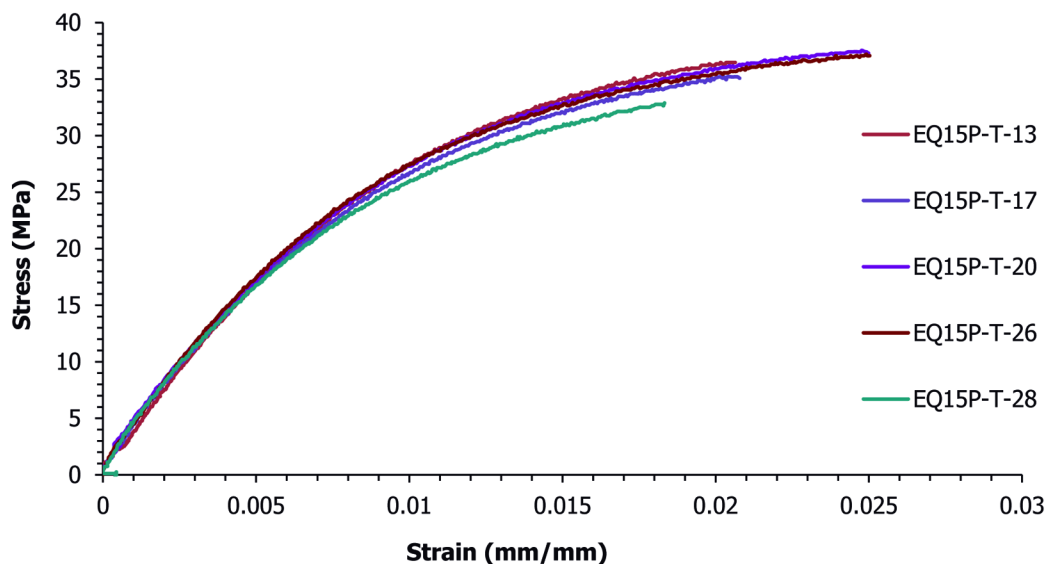


Figure D.31 Tensile results for EQ15P

Table D.31

Tensile test results for 15 wt.% Hyperion FIBRIL™ nanotubes in Dow Polypropylene Semi Crystalline Homopolymer Resin H7012-35RN Injection Molded

Test Date	Sample Number	Tensile Ultimate Stress (MPa)	Tensile Strain at Ultimate Stress (%)	Tensile Fracture Stress (MPa)	Tensile Strain at Fracture Stress (%)	Tensile Modulus (MPa)
5/27/2009	EQ15P-T-13	36.5	2.04	36.5	2.04	3538
5/27/2009	EQ15P-T-17	35.3	2.09	35.3	2.09	3735
5/27/2009	EQ15P-T-20	37.5	2.48	37.4	2.48	3762
5/27/2009	EQ15P-T-26	37.3	2.52	37.2	2.51	3729
5/27/2009	EQ15P-T-28	32.9	1.83	32.9	1.83	3671
Average		35.9	2.19	35.9	2.19	3687
Standard deviation		1.9	0.30	1.8	0.29	90
Number of samples		5	5	5	5	5

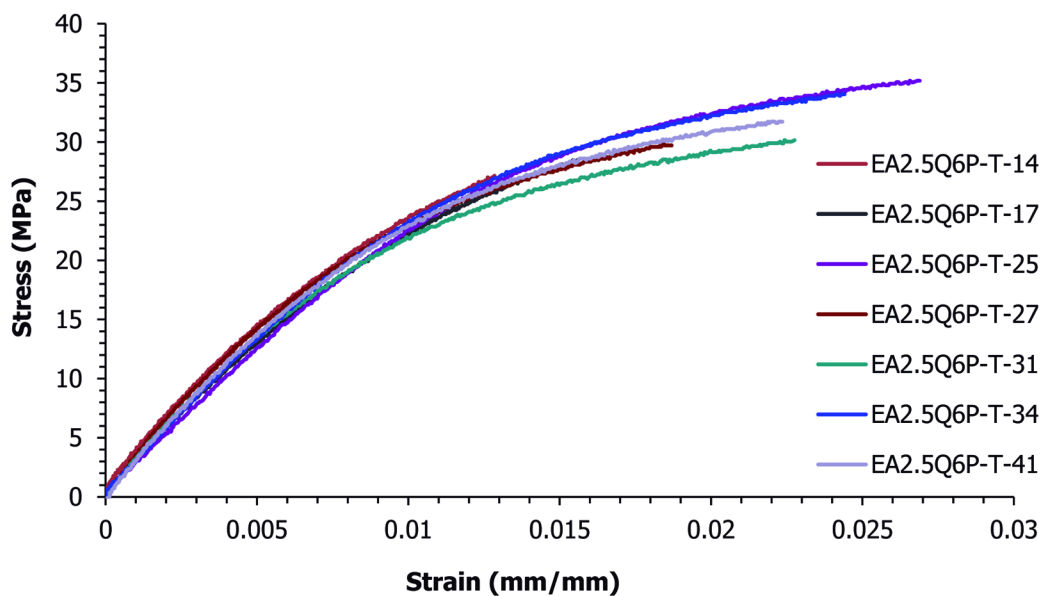


Figure D.32 Tensile results for EA2.5Q6P

Table D.32

Tensile test results for 2.5 wt.% Ketjenblack EC-600 JD and 6 wt.% Hyperion FIBRIL™ nanotubes in Dow Polypropylene Semi Crystalline Homopolymer Resin H7012-35RN Injection Molded

Test Date	Sample Number	Tensile Ultimate Stress (MPa)	Tensile Strain at Ultimate Stress (%)	Tensile Fracture Stress (MPa)	Tensile Strain at Fracture Stress (%)	Tensile Modulus (MPa)
5/27/2009	EA2.5Q6P-T-14	27.1	1.28	27.1	1.28	2981
5/27/2009	EA2.5Q6P-T-17	28.5	1.56	28.5	1.56	2647
5/27/2009	EA2.5Q6P-T-25	35.2	2.69	35.2	2.69	2452
5/27/2009	EA2.5Q6P-T-27	30.0	1.88	30.0	1.88	3226
5/27/2009	EA2.5Q6P-T-31	30.2	2.24	30.2	2.24	3019
5/27/2009	EA2.5Q6P-T-34	34.2	2.46	34.2	2.46	2681
5/27/2009	EA2.5Q6P-T-41	31.7	2.22	31.7	2.22	3245
Average		31.0	2.05	31.0	2.05	2893
Standard deviation		2.9	0.50	2.9	0.50	305
Number of samples		7	7	7	7	7

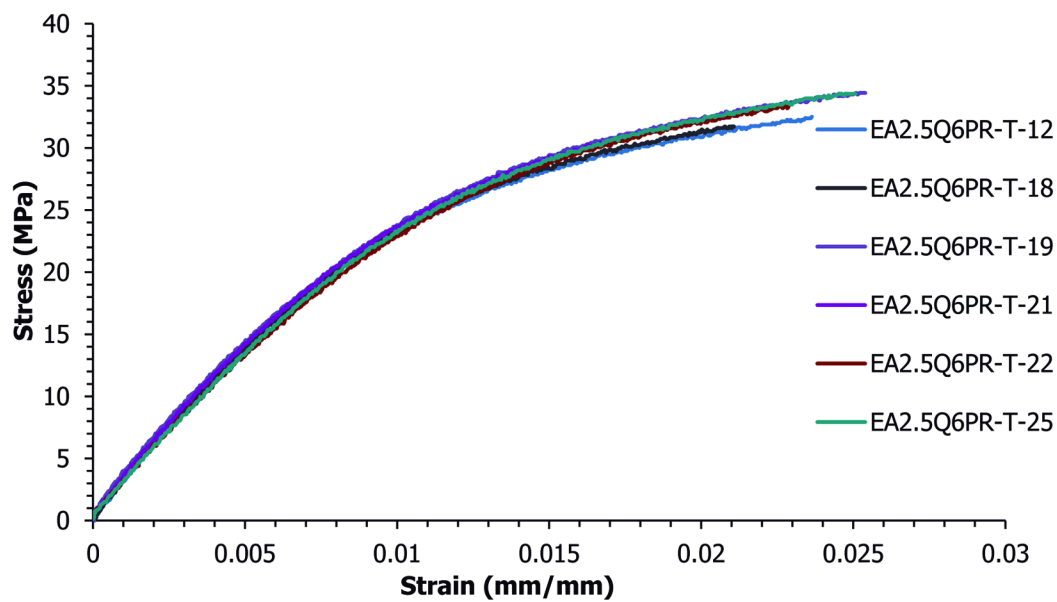


Figure D.33 Tensile results for EA2.5Q6PR

Table D.33

Tensile test results for 2.5 wt.% Ketjenblack EC-600 JD and 6 wt.% Hyperion FIBRIL™ nanotubes in Dow Polypropylene Semi Crystalline Homopolymer Resin H7012-35RN Injection Molded replicate

Test Date	Sample Number	Tensile Ultimate Stress (MPa)	Tensile Strain at Ultimate Stress (%)	Tensile Fracture Stress (MPa)	Tensile Strain at Fracture Stress (%)	Tensile Modulus (MPa)
5/27/2009	EA2.5Q6PR-T-12	32.5	2.36	32.5	2.36	2814
5/27/2009	EA2.5Q6PR-T-18	31.7	2.10	31.7	2.10	2860
5/27/2009	EA2.5Q6PR-T-19	34.4	2.53	34.4	2.53	2971
5/27/2009	EA2.5Q6PR-T-21	32.5	2.08	32.5	2.08	2916
5/27/2009	EA2.5Q6PR-T-22	33.6	2.32	33.6	2.32	2666
5/27/2009	EA2.5Q6PR-T-25	34.5	2.51	34.5	2.51	2680
Average		33.2	2.32	33.2	2.32	2818
Standard deviation		1.1	0.19	1.1	0.19	124
Number of samples		6	6	6	6	6

Appendix E: List of Problem Modules Developed as Supplementary Material for the Textbook "Elementary Principles of Chemical Processes", Third Edition, by R. M. Felder and R. W. Rousseau

Chapter 2: Introduction to Engineering Calculations

- 2.2-1 Conversion of Units
- 2.3-1 Conversion Between Systems of Units
- 2.4-1 Weight and Mass
- 2.5-1 Order-of-Magnitude Estimation
- 2.5-2 Statistical Quality Control
- 2.6-1 Dimensional Homogeneity
- 2.6-2 Dimensional Homogeneity and Dimensionless Groups
- 2.7-1 Fitting a Straight Line to Flowmeter Calibration Data
- 2.7-2 Linear Curve-Fitting of Nonlinear Data
- 2.7-3 Curve Fitting on Semilog and Log Plots

Chapter 3: Processes and Process

- 3.1-1 Mass, Volume, and Density
- 3.1-2 Effect of Temperature on Liquid Density
- 3.3-1 Conversion Between Mass and Moles
- 3.3-2 Conversions Using Mass and Mole Fractions
- 3.3-3 Conversion from a Composition by Mass to a Molar Composition
- 3.3-4 Calculation of an Average Molecular Weight
- 3.3-5 Conversion between Mass, Molar, and Volumetric Flow Rates of a Gas
- 3.4-1 Calculation of a Pressure as a Head of Fluid
- 3.4-3 Pressure Measurement with Manometers
- 3.5-2 Temperature Conversion
- 3.5-3 Temperature Conversion and Dimensional Homogeneity

Chapter 4: Processes and Process Variables

- 4.2-1 The General Balance Equation
- 4.2-2 Material Balances on a Continuous Distillation Process
- 4.2-3 Balances on a Batch Mixing Process
- 4.2-4 Integral Balance on a Semibatch Process
- 4.3-1 Flowchart of an Air Humidification and Oxygenation Process
- 4.3-2 Scale-up of a Separation Process Flowchart
- 4.3-3 Balances on a Mixing Unit
- 4.3-4 Degree of Freedom Analysis
- 4.3-5 Material Balances on a Distillation Column
- 4.4-1 Two-Unit Process
- 4.4-2 An Extraction-Distillation Process
- 4.5-1 Material and Energy Balances on an Air Conditioner
- 4.5-2 An Evaporative Crystallization Process
- 4.6-1 Reaction Stoichiometry
- 4.6-2 Calculation of an Equilibrium Composition
- 4.6-3 Yield and Selectivity in Partial Oxidation of Methane
- 4.7-1 Incomplete Combustion of Methane
- 4.7-2 Product Separation and Recycle in a Steam-Methane Reforming Process
- 4.7-3 Recycle and Purge in the Synthesis of Methanol for use in Direct Methanol Fuel Cells
- 4.8-1 Composition on Wet and Dry Bases
- 4.8-2 Theoretical and Excess Air in Partial Oxidation of Methane
- 4.8-3 Combustion of Methane in a Steam-Methane Reforming Process
- 4.8-4 Combustion of a Hydrocarbon Fuel of Unknown Composition

Chapter 5: Single-Phase Systems

- 5.1-1 Determination of a Solution Density
- 5.2-1 The Ideal Gas Equation of State
- 5.2-2 Conversion from Standard Conditions

5.2-3 Effect of Temperature and Pressure on Volumetric Flow Rates

5.2-4 Standard and True Volumetric Flow Rates

5.2-5 Material Balances on an Evaporator-Compressor

5.3-1 The Truncated Virial Equation of State

5.3-2 The SRK Equation of State

5.3-3 Estimation of Volumes using the SRK Equation of State

5.4-1 Tabulated Compressibility Factors

5.4-2 The Generalized Compressibility Chart

5.4-3 Kay's Rule

Chapter 6: Multiphase Systems

6.1-1 Vapor Pressure Estimation Using the Clausius-Clapeyron Equation

6.3-1 Composition of a Saturated Gas-Vapor System

6.3-2 Material Balances around a Condenser

6.3-3 Relative Humidity

6.4-1 Humidification of Air for Proton Exchange Membrane Fuel Cells

6.4-5 Boiling Point of a Mixture

Chapter 7: Energy and Energy Balances

7.4-2 Energy Balance on a Turbine

7.5-1 Use of Tabulated Enthalpy Data

7.6-1 Energy Balance on a One-Component Process

7.6-2 Energy Balance on a Two-Component Process

7.6-3 Simultaneous Material and Energy Balances

Chapter 8: Balances on Nonreactive Processes

8.1-1 Energy Balance on a Condenser

8.3-1 Evaluation of an Internal Energy Change from Tabulated Heat Capacity

8.3-2 Heating and Cooling of an Ideal Gas

8.3-4 Heat Capacity of a Mixture

8.3-5 Energy Balance on a Gas Cooler

8.3-6 Energy Balance on a Waste Heat Boiler

Chapter 9: Balances on Reactive Processes

9.1-1 Calculation of Heats of Reaction

9.1-2 Evaluation of $\Delta\hat{U}_r$

9.2-1 Hess's Law

9.3-1 Determination of a Heat of Reaction from Heats of Formation

9.4-1 Calculation of a Heat of Reaction from Heats of Combustion

9.5-1 Energy Balance on a Coal Gasification Process

9.5.2 Calculation of Heat of Formation of Woody Biomass

9.5-3 Energy Balance on an Adiabatic Reactor

9.5-4 Simultaneous Material and Energy Balances

9.6-1 Calculation of a Heating Value

9.6-2 Calculation of an Adiabatic Flame Temperature

9.6-3 Ignition Temperature and Flammability Limits

Chapter 11: Balances on Transient Processes

11.1-1 Differential Balances on a Fuel Cell

11.1-2 Hydrogen Balance on a Fuel Tank

11.2-2 Transient Behavior of a Proton-Exchange Membrane Fuel Cell

11.3-1 Startup of a Fuel Cell

11.3-2 Air-Cooling System for a Fuel Cell

**Appendix F: List of Problem Modules Developed as Supplementary
Material for the Textbook "Transport Processes and Separation Process
Principles (Includes Unit Operations)", Fourth Edition, by C. J.
Geankoplis**

Chapter 1: Introduction to Engineering Principles and Units

- 1.3-1 Determination of a Solution Density
- 1.4-1 Gas-Law Constant
- 1.4-2 Composition of a Gas Mixture
- 1.5-3 Combustion of Fuel Gas
- 1.6-1 Pre-heating of Methane and Steam
- 1.6-2 Heating of an Ethanol Solution
- 1.6-3 Calculation of Heat Transfer Rate using Steam Tables
- 1.6-4 Incomplete Combustion of Methane
- 1.6-5 Standard Enthalpy of Reaction
- 1.7-1 Cooling of a Fuel Cell
- 1.7-2 Simultaneous Material and Energy Balances
- 1.7-3 Oxidation of Woody Biomass

Chapter 2: Principles of Momentum Transfer and Overall Balances

- 2.2-3 Conversion of Pressure to Head of a Fluid
- 2.3-1 Diffusivity of Hydrogen inside a Fuel Cell
- 2.5-1 Reynolds Number of Hydrogen flowing into a Fuel Cell
- 2.6-1 Flow of Hydrogen into Fuel Cells
- 2.6-3 Velocity of Hydrogen in Bipolar Plate Channel
- 2.7-1 Energy Balance on Ethanol boiler
- 2.10-1 Methanol Flow in Fuel Cell
- 2.10-2 Use of Friction Factor in Laminar Flow
- 2.10-3 Use of Friction Factor in Turbulent Flow
- 2.10-4 Trial-and-Error Solution to Calculate Pipe Diameter

- 2.10-5 Flow of Gas in Line and Pressure Drop
- 2.10-8 Entry Length for a Fluid in a Rectangular Channel
- 2.11-1 Compressible Flow of a Gas in a Pipe Line
- 2.11-2 Maximum Flow for Compressible Flow of a Gas

Chapter 3: Principles of Momentum Transfer and Applications

- 3.1-3 Surface Area in Packed Bed of Cylinders
- 3.1-4 Pressure Drop and Flow of Gases in Packed Bed
- 3.2-1 Flow Measurement using a Pitot Tube
- 3.3-1 NPSH Available for Pump
- 3.3-2 Calculation of Brake Horsepower of a Pump
- 3.3-3 Brake-kW Power of a Centrifugal Fan
- 3.3-4 Compression of Methane
- 3.8-3 Laminar Flow in a Circular Tube
- 3.11-1 Dimensionless Groups

Chapter 4: Principles of Steady-State Heat Transfer

- 4.1-1 Heat Loss through a Stainless Steel Bipolar Plate
- 4.3-1 Cooling of a Fuel Cell
- 4.3-2 Heat Loss from an Insulated Pipe
- 4.3-3 Heat Loss by Convection and Conduction and Overall U
- 4.3-4 Heat Generation in a Solid-Oxide Fuel Cell
- 4.5-1 Heating of Natural Gas in Steam-Methane Reforming Process
- 4.5-2 Trial-and-Error Solution for Heating of Steam
- 4.5-3 Heating of Ethanol in Reforming Process
- 4.5-4 Heat-Transfer Area and Log Mean Temperature Difference
- 4.5-5 Laminar Heat Transfer and Trial and Error
- 4.6-3 Heating of Steam by a Bank of Tubes in High-Temperature Electrolysis
- 4.7-3 Natural Convection in Bipolar Plate Vertical Channel

- 4.8-2 Steam Condensation in a Fuel Cell
- 4.9-1 Temperature Correction Factor for a Heat Exchanger
- 4.9-2 Effectiveness of Heat Exchanger
- 4.11-1 Radiation in Cylindrical Solid-Oxide Fuel Cell
- 4.15-1 Cooling Channels in Fuel Cell Bipolar Plates

Chapter 5: Principles of Unsteady-State Heat Transfer

- 5.2-1 Cooling of a Cylindrical Solid-Oxide Fuel Cell
- 5.2-2 Total Amount of Heat in Cooling of a Solid-Oxide Fuel Cell
- 5.3-2 Heat Conduction in a Fuel Cell Stack
- 5.3-3 Transient Heat Conduction in a Cylindrical Solid-Oxide Fuel Cell
- 5.3-4 Two-Dimensional Conduction in a Cylindrical Solid-Oxide Fuel Cell
- 5.4-1 Unsteady-State Conduction and the Schmidt Numerical Method
- 5.4-3 Unsteady-State Conduction with Convective Boundary Condition

Chapter 6: Principles of Mass Transfer

- 6.1-1 Molecular Diffusion of Water in Air at the Cathode of a Fuel Cell
- 6.2-1 Equimolar Counterdiffusion at the Cathode Chamber of a Proton-Exchange Membrane Fuel Cell
- 6.2-5 Diffusivity in Steam-Methane Reforming Process
- 6.3-1 Diffusion of Methanol in Water in Direct Methanol Fuel Cells
- 6.3-2 Prediction of Diffusivity of Methanol in Water
- 6.5-1 Diffusion of Hydrogen through Nafion
- 6.5-3 Diffusion of Oxygen through Gas Diffusion Layer

Chapter 7: Principles of Unsteady-State and Convective Mass Transfer

- 7.5-2 Diffusion and Chemical Reaction in the Anode Chamber of a Direct Methanol Fuel Cell
- 7.5-4 Diffusion of CO₂ and O₂ through stagnant Nitrogen in a Solid-Oxide Fuel Cell

Chapter 9: Drying of Process Materials

9.3-1 Humidity from Vapor–Pressure Data

9.3-2 Use of Humidity Chart

9.3-3 Adiabatic Saturation of Feed Air for Proton Exchange Membrane Fuel Cells.

9.3-4 Wet Bulb Temperature and Humidity

Chapter 11: Vapor–Liquid Separation Processes

11.1-1 Use of Raoult’s Law for Methanol–Water Equilibrium Data

11.3-1 Relative Volatility of Methanol–Water Mixture

Chapter 12: Liquid–Liquid and Fluid–Solid Separation Processes

12.3-1 Hydrogen Purification in Pressure Swing Adsorption Process

Appendix G: Permission Letters

Zimbra Collaboration Suite

dlopezga@mtu.edu

Fwd: RE: Permission to use your photomicrograph of
Thermocarb TC-300

jueves, 16 de junio de 2011
11:22:12 a.m.

De: jaking@mtu.edu
Para: dlopezga@mtu.edu

----- Original Message -----

Subject:RE: Permission to use your photomicrograph of Thermocarb TC-300

Date:Wed, 2 Jan 2008 07:05:43 -0500

From:Albert V. Tamashausky <ALBERT@asbury.com>

To:Julie King <jaking@mtu.edu>

Dear Julie,

Please accept this email correspondence as permission to use any micrographs I have supplied to you in the
aforementioned paper. Also, I am happy and very appreciative to see credit given to Asbury Carbons and me in this
paper.

Thank you,

Albert

Albert V. Tamashausky

Director of Technical Services
Asbury Carbons
PO Box 144
405 Old Main Street
Asbury, NJ 08802
908-537-2155

Figure G.1 Email from Asbury Carbons for Figure 3.3

Fwd: permission to use picture miércoles, 06 de mayo de 2009 12:49:08 p.m.

De: jmkeith@mtu.edu

Para: dlopezga@mtu.edu

Daniel - save this email to use in an appendix of your dissertation. We asked permission to use it as Figure 5.2 of your dissertation. Thank you and have a nice day,

jk

Jason M. Keith
Associate Professor
Department of Chemical Engineering
Michigan Technological University
Houghton, MI 49931

Ph: 906-487-2106
Fax: 906-487-3213
email: jmkeith@mtu.edu

----- Forwarded Message -----
From: "Robert Campbell" <Robert.Campbell@netzsch.com>
To: "Jason Keith" <jmkeith@mtu.edu>
Sent: Tuesday, April 14, 2009 12:22:08 PM GMT -05:00 US/Canada Eastern
Subject: RE: permission to use picture

Hi Jason,
It's no problem to use the Figure.

Best Regards,

Robert Campbell
Applications Lab Manager
NETZSCH Instruments, Inc.

BU Analyzing & Testing

Phone: +1 781 272 5353 109
Fax: +1 781 272 5225

e-mail: Robert.Campbell@netzsch.com
www.netzsch-thermal-analysis.com

NETZSCH Instruments, Inc. · 37 North Avenue · Burlington, MA 01803
Phone: +1 781 272 5353 · Fax: +1 781 272 5225 · e-mail: nib@netzsch.com

THIS MESSAGE IS INTENDED ONLY FOR THE USE OF THE PARTY TO WHOM IT IS ADDRESSED AND MAY

Zimbra: dlopezga@mtu.edu

Page 2 of 2

CONTAIN INFORMATION THAT IS PRIVILEGED, CONFIDENTIAL, AND PROTECTED FROM DISCLOSURE UNDER LAW. If you are

not the addressee, or a person authorized to deliver the document to the addressee, you are hereby notified that any review,

disclosure, dissemination, copying, or other action based on the content of this communication is not authorized. If you have

received this document in error, please immediately notify the sender immediately by e-mail or phone.

-----Original Message-----
From: Jason Keith [mailto:jmkeith@mtu.edu]
Sent: Tuesday, April 14, 2009 8:35 AM
To: Campbell, Robert
Subject: permission to use picture

Rob - this is Jason Keith at Michigan Tech. Julie King and I are supervising grad students using the Nanoflash instrument for their research. Eventually they will write their MS thesis and/or PhD dissertations on their work.

You had sent us a report which I have attached. Can we have permission to use Figure 2 from page 4 of this document in their thesis / dissertation? We will not use it in a peer reviewed paper due to space constraints but we would like to use it in the thesis / dissertation.

Thank you, and best regards,

jk

Jason M. Keith
Associate Professor
Department of Chemical Engineering
Michigan Technological University
Houghton, MI 49931

Ph: 906-487-2106
Fax: 906-487-3213
email: jmkeith@mtu.edu

Figure G.2 Email from NETZSCH for Figure 4.4